Role of Scalar Fields in Particle Physics and Cosmology

Abhijit Kumar Saha

A thesis
submitted for the degree of

Doctor of Philosophy

Department of Physics
Indian Institute of Technology Guwahati
Guwahati - 781039, Assam, India

Role of Scalar Fields in Particle Physics and Cosmology

A thesis submitted by

Abhijit Kumar Saha

to

Indian Institute of Technology Guwahati
in partial fulfillment of the requirements
for the award of the degree of
Doctor of Philosophy in Physics

Supervisor

Dr. Arunansu Sil

Department of Physics
Indian Institute of Technology Guwahati
Guwahati - 781039, Assam, India

Declaration

The work in this thesis is based on research carried out at the Department of Physics, Indian Institute of Technology Guwahati, India under the supervision of Dr. Arunansu Sil. No part of this thesis has been submitted elsewhere for award of any other degree or qualification. Works presented in the thesis are entirely my own unless referenced to the contrary in the text.

Signed:

Date:

Certificate

Dr. Arunansu Sil
Associate Professor
Department of Physics, IIT Guwahati
Email: asil@iitg.ac.in

It is certified that the work contained in the thesis entitled **"Role of Scalar Fields in Particle Physics and Cosmology"** by Mr. Abhijit Kumar Saha, a PhD student of the Department of Physics, IIT Guwahati was carried out under my supervision and has not been submitted elsewhere for award of any degree.

Dr. Arunansu Sil

Acknowledgements

I would like to express my greatest appreciation to Dr. Arunansu Sil for his constant support and guidance throughout my PhD tenure. Being my supervisor, he has taught me to remain focused, dedicated and calm in achieving the goal. His observations and comments helped me to think everything in depth. Along with the academic support, he was always there for me to serve regarding anything, anytime. Words are not enough to describe his backing to overcome those hard times. My journey would never be complete without his immense care.

I would like to acknowledge my DC committee members: Prof. Bipul Bhuyan, Dr. Soumitra Nandi and Dr. K.V. Srikanth. I also convey my gratitude to Dr. Subhaditya Bhattacharya and Prof. Jose Wudka who were very kind to collaborate with me. In particular I am grateful to Subhoda for introducing me into the field of dark matter.

I also thank Prof. Palash Baran Pal for having several closed door interesting discussion sessions during his visit to IIT Guwahati. He was very kind to provide me the opportunity to work with him. I also thank Prof. Subhendra Mohanty for his wonderful lectures on Particle Physics and Cosmology during SARC school at BITS, Pilani and his visit to IIT Guwahati. I enjoyed the personal interaction sessions with him.

It is the best time to convey gratefulness to my well wishers including my group members, friends, family members and few other people. I would like to express my deepest respect and gratitude to Bishuda (Dr. Biswajit Karmakar). Very few people come with such golden fate to get senior like him. I also thank Sujoyda (Sujay Shil) for introducing and teaching me the fundamentals of particle physics during my early days of PhD. I thank Rishav and Dr. Amit Dutta Banik for providing me countless academic and non-academic helps.

Here at IITG, I have spent many beautiful, mesmerizing and emotional moments. I thank few of my close local friends Ramiz, Kallol, Sourav, Ashis, Koushik, Sudin, Rahul, Shibananda, Atanu. Their love, care and encouragement helped me to survive in the difficult situations. I am also grateful to Srikrishna, Pankaj, Srimoy, Pulak, Anabilda for playing several important parts during this long journey. I would also like to thank my dear friend cum collaborator Purusottam Ghosh for having many meaningful academic and non-academic discussions. My special thank to Luxmi Machahari from Gauhati University for giving me company during few academic and non-academic trips.

I owe my deepest gratitude to Pranoy for being there always since college days. I convey my heartiest gratitude to Samiran Roy from HRI for his constant inspiration. I am also grateful

to Sushmita Gogoi for providing me motivation and immense mental support during PhD days. I thank Mita Pramanick for tolerating me during the early years of my PhD.

Before I end, I would like to express that I am nothing without my family. I dedicate every seconds of my life to my parents, Ma: Shipra Saha and Baba: Monojit Kumar Saha, my brother: Chandrajit Kumar Saha, my sister: Ruma Das and my loving niece: Mani. Finally I convey my heartiest gratitude to Alolika Mandal for her selfless affection and care.

Abstract

In this thesis we investigate the different kind of roles, scalar fields can serve in the Universe. First we analyze the scalar field's role in guiding successful inflation in the early Universe. For this purpose, we focus on the sneutrino chaotic inflation model (within supesymmetric framework) which is disfavored from recent experimental observations by Planck. We deform the model minimally by coupling the inflation sector with a supersymmetry breaking sector. We find that such a coupling can provide correct magnitude of inflationary observables, consistent with Planck results. At the end of inflation dynamical supersymmetry breaking can be also realized. We also comment on some of the neutrino mass parameters. Next we study the Higgs vacuum stability in presence of chaotic inflation in early Universe. We find that extension of the inflation sector by an additional scalar field is sufficient to achieve successful inflation and absolute stability of the electroweak vacuum. After that, we explore the role of scalar field as a potential dark matter candidate. As low mass range (< 500 GeV) of a scalar dark matter is ruled out from experimental data, we extend the minimal scalar DM model further by an additional scalar field. We find that a mere interaction of this additional scalar field with the dark matter is sufficient in order to revive the scalar DM model in the low mass range. In addition, the extra scalar also helps to establish absolute stability of the EW vacuum in presence of large neutrino Yukawa coupling to generate light neutrino mass in type-I seesaw framework. Then we propose a common origin of primordial inflation and scalar DM in the Universe. In the scenario, it turns out that after the end of inflation, associated global symmetry breaks down, and corresponding Nambu Goldstone bosons can be identified with viable dark matter candidates. Finally we revisit the well known singlet doublet fermionic dark matter model extended by a scalar field. The scalar field serves instrumental role in stabilizing the electroweak vacuum as well as provides interesting features of dark matter phenomenology in view of recent experiments.

List of Publications included in the Thesis:

1. **Abhijit Kumar Saha** and Arunansu Sil, *"A Dynamic modification to Sneutrino Chaotic Inflation"*, **JHEP 1511 (2015) 118** [arXiv:1509.00218 [hep-ph]].

2. **Abhijit Kunar Saha** and Arunansu Sil, *"Higgs Vacuum Stability and Modified Chaotic Inflation"* **Phys. Lett. B765 (2017) 244-250** [arXiv:1608.04919 [hep-ph]].

3. Purusottam Ghosh, **Abhijit Kumar Saha** and Arunansu Sil, *"Electroweak Vacuum Stability in an Extended Framework of Dark Matter and Neutrinos"*, **Phys. Rev. D97 (2018) no.7, 075034** [arXiv:1706.04931 [hep-ph]].

4. Subhaditya Bhattacharya, **Abhijit Kumar Saha**, Arunansu Sil and Jose Wudka, *"Dark Matter as a remnant of SQCD Inflation"*, Preprint - arXiv:1805.03621 [hep-ph].

5. Amit Dutta Banik, **Abhijit Kumar Saha** and Arunansu Sil, *"A scalar assisted singlet doublet fermion dark matter model and electroweak vacuum stability "*, Preprint - arXiv: 1806.08080 [hep-ph], accepted for publication in **Phys. Rev. D**.

Contents

Chapter 1

Introduction

Modern day research in high energy physics aims for a consistent theory to understand the Universe at both microscopic and macroscopic scales. This requires involvement of both particle physics and cosmology. Over the years, remarkable progress has been made both in theoretical and experimental directions in these fields. However there still remain several long standing questions that stimulate us to look beyond the existing theories.

The Standard Model (SM) of particle physics [1–8], developed in early 70's, stands as the most elegant and successful theory of all elementary particles. It accurately explains the three fundamental interactions between all known elementary particles namely electromagnetic, strong and weak forces. The SM of particle physics has been tested very precisely over the decades. So far, all the predictions of the SM are in excellent agreement with the experimental observations. In 2012, the major discovery of Higgs boson by both ATLAS [9] and CMS [10] collaborations at LHC finally ends the search of the SM particle spectrum. However despite its immense success, several theoretical and observational facts like non-zero neutrino mass, absence of viable dark matter candidate, description of matter-antimatter symmetry, Higgs vacuum stability, naturalness issues etc, raise doubts over the validity of the SM as the complete theory of particle physics.

On the other hand cosmology offers us profound description of early Universe and the evolution of it at large scales. The standard theory of cosmology known as the Big Bang cosmology (BBC) [11] is very rich and enormously successful. According to the BBC, the Universe started roughly fourteen billion years ago. Since then, it has been expanding. The theory is based on the assumption that the Universe is isotropic and homogeneous. However

within the standard framework of cosmology, some of the important fundamental issues can not be explained. These are mainly related to horizon and flatness problems of the Universe.

The first hint toward physics beyond the SM comes from neutrinos. Neutrinos are part of the SM lepton family. Neutrinos have ample natural sources: solar neutrinos, atmospheric neutrinos and supernovae neutrinos. The solution to the solar neutrino problem supports the idea of neutrino oscillation phenomena among different flavors [12–15]. This hints towards non-zero tiny neutrino mass which is also experimentally accomplished by the renowned neutrino experiments (Super-Kamioonade, K2K etc. [16–20]) around the globe. However the SM of particle physics predicts neutrinos as massless [21–24].

On the other hand, the form of the SM Higgs potential raises concern about the stability of the electroweak (EW) vacuum . The quartic coupling of the SM Higgs turns negative at some high scale as followed from its running (through renormalization group (RG) equation) [26–38]. This happens due to strong fermionic effect predominantly by top quark Yukawa coupling. This further predicts possible existence of another deeper minimum (other than the EW vacuum) at some high energy scale. Although the present measurements of top mass ($\simeq 173.24 \pm 0.81$ GeV [25]) and Higgs mass ($\simeq 125.09 \pm 0.24$ GeV [25]) indicate the electroweak vacuum as metastable [26–38], presence of additional fields in order to circumvent some of the problems of the SM may lead to an instability. There are other reasons, *e.g.*, inability of the SM to explain mass hierarchies of leptons and quarks, observed baryon symmetry of the Universe etc., to believe that the SM is not the complete theory of nature.

In addition, to the problems discussed above, Cosmic Microwave background radiation (CMBR) [39, 40] provides us precise estimate of the content of the Universe. According to it, the total matter content of the Universe is only 25%. More surprisingly, the ordinary or visible matter constitutes a small fraction (5%) only, while the rest of matter are non-luminous, weakly interacting, popularly known as dark matter (DM). The origin of DM and its nature still remain mystery due to lack of any satisfactory explanation of it within the framework of the SM of particle physics. Furthermore, observation from Cosmic Microwave Background [39, 41, 42] strongly favors for a flat Universe.

Therefore the present situation demands extension of the standard theories of both particle physics and cosmology in order to explore the nature in a more elegant way. Considerable efforts have been made over the years to build a possible guiding theory to unravel these unknown pockets of the Universe. One of the feasible resolutions could be the extension of the SM of particle physics with additional fields as these can serve significant roles in the Universe. For example, it can be argued that rapid accelerated expansion of the early Universe at very early

epoch (called as inflation [43–53]) by a scalar field can explain horizon and flatness problem. Also extension of the SM by scalars/fermions/vector bosons may explain the DM. It can be noted that a scalar extension is arguably the most promising candidate of DM [54–57]. Moreover, they might be useful in explaining other puzzles of the Universe like Higgs vacuum stability [58, 59], naturalness issue in the SM [60, 61], matter-antimatter asymmetry [62, 63] etc. However, one should note that introduction of any new physics eventually demands fine agreement with experimental observations.

The thesis is devoted in studying the extension of the SM of particle physics by additional scalars with an aim to resolve some of the problems described above. Various forms of inflationary models [64], driven by scalar fields have already been explored at large extent. On the other hand scalar DM and Higgs vacuum stability using scalar fields have been studied in detail [65–68, 71–76]. While most of these analyses (involving scalar field extension of SM) focus on individual issues, we feel it is important to study the correlation between two or more such issues, particularly in the light of recent experimental results. Motivated by this, in the thesis, we mainly have tried to connect various apparently uncorrelated events of the Universe like inflation, DM, Higgs vacuum stability, neutrino mass using scalar fields (additional fermionic fields may also be required) by keeping in mind the recent experimental observations. We have shown that indeed the extension of the SM of particle physics with scalar fields could be one of the powerful, plausible and viable guiding theories of the Universe.

Below in Secs. 1.1 and 1.2, we briefly describe the SM of particle physics and Big bang cosmological model. Then we proceed to discuss few important problems associated with the standard theories and probable solutions in Sec. 1.2.1. Thereafter in Sec 1.4 and Sec 1.5, we state the detailed motivation and outline of the thesis. Then we directly move into the Chapters (2-6) representative of the works. Finally a conclusion of the thesis is included in Chapter 7.

1.1 Standard Model of Particle Physics

1.1.1 Basic set up

The SM of particle physics is a quantum field theory which accommodates three of the four fundamental forces of Nature namely strong, weak and electromagnetic ones. The theory turns out to be remarkably successful in describing the Nature at elementary level. Knowledge of the SM is the very basic requirement in studying particle physics. The theory of the SM [3, 4, 6, 7, 77–79] is based on the $SU(3)_C \times SU(2)_L \times U(1)_Y$ gauge symmetry [80, 81] where

"C", "L" and "Y" represent "color", "left-hand chirality" and "weak-hypercharge" respectively. $SU(3)_C$ describes the strong interaction involving the fields charged under this symmetry and mediated by gluons [82–84]. The remaining gauge symmetry $SU(2)_L \times U(1)_Y$ governs the electroweak interactions [85, 86] mediated by three gauge bosons. The particle contents of the SM and their transformation properties (under electroweak symmetry only) are provided in Table 1.1.

Fields			$SU(2)_L$	$U(1)_Y$
Fermions	Leptons (l_L ; e_R)	$\begin{pmatrix}\nu_e\\ e^-\end{pmatrix}_L$; e_R $\begin{pmatrix}\nu_\mu\\ \mu^-\end{pmatrix}_L$; μ_R $\begin{pmatrix}\nu_\tau\\ \tau^-\end{pmatrix}_L$; τ_R	2 ; 1	-1 ; -2
	Quarks (Q_L ; q_R)	$\begin{pmatrix}u\\ d\end{pmatrix}_L$; u_R ; d_R $\begin{pmatrix}c\\ s\end{pmatrix}_L$; c_R ; s_R $\begin{pmatrix}t\\ b\end{pmatrix}_L$; t_R ; b_R	2 ; 1 ; 1	$\frac{1}{3}$; $\frac{4}{3}$; $-\frac{2}{3}$
Scalar		Higgs $H = \begin{pmatrix}H^+\\ H_0\end{pmatrix}$	2	1

TABLE 1.1: Field content of the SM of particle physics. The subscripts L and R represents LH and RH fields.

The fermion sector of the SM consists of (i) leptons (antileptons) and (ii) quarks (anti-quarks). The lepton sector contains three left handed (LH) $SU(2)_L$ doublets (l_L). Each LH doublet is formed by one electrically charged (with $Q = -1$) and another neutral lepton ($Q = 0$) having same lepton quantum numbers. For example e_L and ν_{eL} form a $SU(2)_L$ doublet. The lepton sector also accommodates three right handed partners (e_R) of electrically charged leptons (e_R, μ_R, τ_R) which are singlets under $SU(2)_L$. RH neutrinos do not exist in SM. The quark sector contains six flavored quarks: three up-type: up (u), charm (c) and top (t) and three down-type: down (d), strange (s) and bottom (b). The LH partners of up-type quarks (with $Q = 2/3$) and down-type quarks (with $Q = -1/3$) form a $SU(2)_L$ doublet (Q_L) as displayed in Table 1.1. On the other hand, the RH partners (q_R) of these quarks transform as singlets under $SU(2)_L$. In the scalar sector of the SM there exists only a $SU(2)_L$ doublet known as Higgs (H)

multiplet which is expressed as [80]

$$H = \begin{pmatrix} H^+ \\ H_0 \end{pmatrix}, \tag{1.1}$$

where H^+ and H_0 are the charged and neutral components of the SM Higgs doublet respectively. The SM also involves four gauge bosons: W^a_μ associated with $SU(2)_L$ symmetry (with $a = 1-3$) and B_μ corresponding to $U(1)_Y$ gauge symmetry.

Let us proceed to write the electroweak Lagrangian of the SM invariant under the $SU(2)_L \times U(1)_Y$ gauge symmetry without involving $SU(3)_C$ as

$$\mathcal{L}_{\rm SM} = \mathcal{L}_{\rm F} + \mathcal{L}_{\rm G} + \mathcal{L}_{\rm Y} + \mathcal{L}_H, \tag{1.2}$$

where F, G, Y and H stand for fermion, gauge, Yukawa and scalar (Higgs) part of the Lagrangian respectively. Now $\mathcal{L}_{\rm F}$ is given by [80]

$$\begin{aligned} \mathcal{L}_{\rm F} \; &= \bar{l}_L i\gamma^\mu(\partial_\mu + \frac{1}{2}ig\tau^a W^a_\mu + \frac{1}{2}ig' Y_{l_L} B_\mu) l_L + \bar{e}_R i\gamma^\mu(\partial_\mu + \frac{Y_{e_R}}{2} ig' B_\mu) e_R \\ &+ \bar{Q}_L i\gamma^\mu(\partial_\mu + \frac{1}{2}ig\tau^a W^a_\mu + \frac{1}{2}ig' Y_{Q_L} B_\mu) Q_L + \bar{q}_R i\gamma^\mu(\partial_\mu + \frac{Y_{q_R}}{2} ig' B_\mu) q_R. \end{aligned} \tag{1.3}$$

Note that τ_a are the generators of the $SU(2)_L$ symmetry with a runs from 1-3. Here g and g' are corresponding gauge coupling constants of $SU(2)_L$ and $U(1)_Y$ symmetries respectively. The notation $Y_{l_L}(Y_{e_R})$ and $Y_{Q_L}(Y_{q_R})$ denote the weak hypercharges of LH (RH) lepton and quark doublets (singlets) as mentioned in Table 1.1. The $\mathcal{L}_{\rm G}$ in Eq.(1.2) can be written as [87, 88]

$$-\mathcal{L}_{\rm G} = \frac{1}{4} W^a_{\mu\nu} W^{a,\mu\nu} + \frac{1}{4} B_{\mu\nu} B^{\mu\nu}, \tag{1.4}$$

where $W^a_{\mu\nu} = \partial_\mu W^a_\nu - \partial_\nu W^a_\mu + g\epsilon^{abc} W^b_\mu W^c_\nu$ and $B_{\mu\nu} = \partial_\mu B_\nu - \partial_\nu B_\mu$.

The Yukawa Lagrangian $\mathcal{L}_{\rm Y}$ is written as [89]

$$-\mathcal{L}_{\rm Y} = y_{l_{ij}} \bar{l}_{L_i} H e_{R_j} + y_{u_{ij}} \bar{Q}_{L_i} H Q_{R_j} + y_{d_{ij}} \bar{Q}_{L_i} \tilde{H} Q_{R_j}, \tag{1.5}$$

where $\tilde{H} = i\tau_2 H^*$. $y_{l/u/d}$ represents the Yukawa coupling constants with i, j indices indicating the generation indices. The remaining part of the SM Lagrangian *i.e.* $\mathcal{L}_H$ in Eq.(1.2) is given by

$$\mathcal{L}_H = (D_\mu H)^\dagger (D^\mu H) - V(H); \qquad V(H) = \mu^2 |H|^2 + \frac{\lambda_h}{4} |H|^4, \tag{1.6}$$

where $D_\mu = \partial_\mu + \frac{1}{2}ig\tau^a W^a_\mu + \frac{1}{2}ig'B_\mu$, is the covariant derivative. The λ_h is the Higgs self quartic coupling. Using the conditions $\lambda_h > 0$ and $\mu^2 < 0$ and after minimization of $V(H)$, one can obtain the minima of H as: $\langle H^\dagger H\rangle = \frac{-\mu^2}{2\lambda_h}$. As a consequence, electroweak symmetry gets spontaneously broken [90–93]. In the unitary gauge the Higgs field can be written as

$$H = \begin{pmatrix} 0 \\ \frac{v+h}{\sqrt{2}} \end{pmatrix}. \tag{1.7}$$

where $v = \sqrt{\frac{-\mu^2}{\lambda_h}}$ and h is identified as the physical Higgs field with mass $m_h^2 = 2v^2\lambda_h$.

After the spontaneous breaking of the electroweak symmetry $(SU(2)_L \times U(1)_Y$ to $U(1)_{\rm em})$, the physical gauge fields can be defined as

$$W^\pm_\mu = \frac{1}{\sqrt{2}}(W^1_\mu \mp W^2_\mu), \tag{1.8}$$

$$Z_\mu = \cos\theta_W W^3_\mu - \sin\theta_W B_\mu, \tag{1.9}$$

$$A_\mu = \sin\theta_W W^3_\mu - \cos\theta_W B_\mu, \tag{1.10}$$

where θ_W is known as the Weinberg angle which is defined as

$$\tan\theta_W = \frac{g'}{g}. \tag{1.11}$$

Among these, $W^\pm$ and Z bosons are massive after the spontaneous symmetry breaking with masses $M_W = \frac{gv}{2}$ and $M_Z = \frac{gv}{2\cos\theta_W}$. The other gauge field (A_μ) remains massless and is identified as photon (the gauge boson of the unbroken $U(1)_{\rm em}$). Also, charged leptons and all quarks acquire masses which are obtained through $\mathcal{L}_Y$ and are given by

$$m_{l_{ij}} = y_{l_{ij}}\frac{v}{\sqrt{2}}\ ;\ m_{u_{ij}} = y_{u_{ij}}\frac{v}{\sqrt{2}}\ ;\ m_{d_{ij}} = y_{d_{ij}}\frac{v}{\sqrt{2}}. \tag{1.12}$$

However the neutrinos remain massless due to the absence of RH neutrinos in the set up.

1.1.2 Success and drawbacks of the SM of particle physics

The theoretical predictions of the SM are in impressive agreement with the experimental results. Moreover, the biggest achievement of the SM is to combine the weak and electromagnetic forces in a unified gauge theory named as electroweak theory. The search of the SM particle spectrum has been completed with the grand discovery of the Higgs boson at LHC [9, 10] in 2012. Even then there exist several drawbacks of the SM which we state below pointwise.

- The SM of particle physics does not accommodate any proper candidate for DM. However presence of DM in the Universe is strongly favored by various cosmological signatures.
- Particle physics experiments confirm neutrinos to be massive. However, in the SM they remain massless.
- The EW vacuum stability at high scale is not assured within the SM framework.
- The SM does not provide any sort of explanation on gravitational interaction between fundamental particles which is likely to dominate over other three forces at energy scale of $\mathcal{O}(M_P)$.
- The existing large hierarchy between the fundamental scales does not have any explanation in the SM. For example the electroweak scale is $\mathcal{O}(100)$ GeV, and the value of Planck scale is $\mathcal{O}(10^{19})$ GeV. In addition, in order to have the correct value of Higgs mass, a severe fine tuning is required between the bare mass and the radiatively induced correction. This is known as Higgs mass hierarchy problem which has no theoretical understanding within the SM.
- The masses of the elementary particles and magnitude of various couplings in the Standard Model are determined by fitting to experimentally observed values. the SM is incapable to provide any probable reasons of hierarchies present between the masses of physical fields and magnitude of couplings.
- The SM of particle physics does not have any convincing explanation for the observed amount of baryon asymmetry.

There are few other important shortcomings associated with the SM of particle physics like strong CP problem, cosmological constant problem etc.. All these indicate that introduction of new physics is required beyond this standard framework.

1.2 Salient features of Big Bang Cosmology

After the discussion over the SM of particle physics, here we discuss in brief few important features of the standard cosmological model and some of its related problems. The theory starts with the assumption that Universe is homogeneous and isotropic [11, 94–99]. This assumption is also supported from the observation of CMBR [42]. The dynamics of an isotropic and homogeneous Universe is represented by Friedman-Robertson-Walker (FRW) metric. In comoving

spherical coordinate (r, θ and ϕ), it turns out to be [11]

$$ds^2 = -dt^2 + a(t)^2\Big[\frac{dr^2}{1-kr^2} + r^2(d\theta^2 + \sin^2\theta d\phi^2)\Big], \tag{1.13}$$

where k stands for spatial curvature of the Universe: $k = 0$ corresponds to flat Universe whereas $k < 0$ and $k > 0$ indicate closed and open Universe respectively. The notation, $a(t)$, is termed as scale factor representative of the size of the Universe. Note that we will follow natural units *i.e.* $c = \hbar = k_B = 1$. We also consider t_0 to be the present cosmic time. The form of instantaneous radial physical distance using Eq.(1.13) at time t is provided by

$$R(t) = a(t)\int_0^r \frac{dr}{(1-kr^2)^{\frac{1}{2}}}. \tag{1.14}$$

• **Hubble's law:** The observation of Hubble expansion is one of the important discoveries in support of Big bang cosmology. The Hubbles's law states that all objects in the Universe run away from each other with velocities proportional to their distances. The interpretation of Hubble law of expansion can be simply done through the amount of redshift in the wavelength of a emitted photon from a distant galaxy. Suppose, the emitted wavelength of the photon at time t_1 is λ_1 and the wavelength we received today (t_0) is λ_0. Then the amount of redshift (z_r) is defined by

$$z_r = \frac{\lambda_0 - \lambda_1}{\lambda_1}, \tag{1.15}$$

$$= \frac{a(t_0)}{a(t_1)} - 1. \tag{1.16}$$

Now using Taylor expansion it can be written,

$$a(t_1) = a(t_0)[1 + (t_1 - t_0)H_0 + ...], \tag{1.17}$$

where $H_0 = \frac{\dot{a}(t_0)}{a(t_0)}$, the present expansion rate of the Universe ($H_0 = 100h$km s^{-1}Mpc^{-1} [39, 40]). Then Eq.(1.16) can be rewritten as

$$z_r = \frac{1}{1 + (t_1 - t_0)H_0} \quad \rightarrow (t_0 - t_1)H_0 + ... \tag{1.18}$$

Now in natural unit (velocity of light $c = 1$), physical distance traveled by the photon is simply $(t_0 - t_1)$ identified as l_P. Assuming l_P is not much large, one can find a linear relationship between the amount of redshift and the physical distance measured as $z_r = H_0 l_P$. If one considers to illustrate the redshift of light from distant galaxies in terms of Doppler effect [98],

then $z_r \simeq v_D$, where v_D would be the relative velocity between observer and the source. Then it turns out that $v_D = H_0 d_P$. This is the well known numerical form of the famous Hubble law.

• **Particle horizon:** Maximum comoving distance that light could traverse within a time interval $(t_1 - t_2)$ is called comoving particle horizon. This has to be determined along the null geodesics which implies $dt = a(t)dr$. Then the expression of comoving particle horizon is given by (for a flat Universe $k = 0$) [11],

$$d_H = \int_{t_1}^{t_2} \frac{dt}{a(t)}, \tag{1.19}$$

where $t_1 < t_2$.

• **Friedman equations:** Next we proceed further to discuss Friedman equations. In a Universe governed by FRW metric, the Einstein field equation is taken to be of the form

$$R_\mu^{\ \nu} - \frac{1}{2}\delta_\mu^{\ \nu} R = 8\pi G T_\mu^{\ \nu}, \tag{1.20}$$

where $R_\mu^{\ \nu}$ and R stand out to be Ricci tensor and scalar curvature. The notation $G = 8\pi m_P^{-2}$ is identified as Newton's constant with $m_p \simeq 1.22 \times 10^{19}$ GeV. Using Eq.(1.20) one can obtain Friedman equations provided by,

$$H^2 = \frac{8\pi G}{3}\rho - \frac{k}{a^2}, \tag{1.21}$$

$$\dot{H} + H^2 = -\frac{1}{6M_P^2}(\rho + 3P), \tag{1.22}$$

where $M_P = \frac{m_P}{\sqrt{8\pi}} \simeq 2.4 \times 10^{18}$ GeV is the reduced Planck scale. The energy density and pressure of the Universe are denoted by ρ and P respectively in Eq.(1.22). Note that ρ includes contributions from all the components present in the Universe like matter (ρ_m), radiation (ρ_r) *etc.* $(\rho = \rho_m + \rho_r$ by assuming no vacuum energy is present). Then from Eqs.(1.21,1.22), one can further yield the continuity equation

$$\dot{\rho} + 3H(P + \rho) = 0. \tag{1.23}$$

If we express pressure as a function of energy density, $P = \omega\rho$, Eq.(1.23) can be converted to

$$\rho_i = \rho_{i,0}\left(\frac{a_0}{a}\right)^{3(1+w)}, \tag{1.24}$$

where"0" indicates the present time. For matter dominated (MD), radiation dominated (RD) and vacuum energy dominated (VD) universe, values of ω are 0, 1/3 and -1 respectively. Below

we provide the scale factor dependence of energy (ρ) for different possible states of the Universe which can be obtained from Eqs.(1.23,1.24)

$$\rho \propto \begin{cases} a^{-3} \Rightarrow a(t) \propto t^{2/3}, & \text{Matter dominated} \quad P >> \rho, \\ a^{-4} \Rightarrow a(t) \propto t^{1/2}, & \text{Radiation dominated} \quad P = \frac{1}{3}\rho, \\ a^{0} \Rightarrow a(t) \propto e^{Ht} & \text{Vacuum energy dominated} \quad P = -\rho. \end{cases} \tag{1.25}$$

Now using Eq.(1.21) and (1.24), one can simply find

$$\frac{1}{aH} = \frac{1}{H_0}\left(\frac{a}{a_0}\right)^{\frac{1}{2}(1+3w)}. \tag{1.26}$$

Maximum comoving distance from which light could travel in course of one Hubble expansion time (H^{-1}) is identified as $(aH)^{-1}$. This is also known as *comoving Hubble sphere*. It roughly coincides with the comoving particle horizon (Eq.(1.19)) which tells that regions separated by comoving distance larger than $(aH)^{-1}$ were never in casual contact. Therefore for a MD or RD ($w \geq 0$) expanding Universe, comoving Hubble sphere with radius $(aH)^{-1}$ is always increasing function of time.

• **Different phases of the early Universe:** After the Big bang, the Universe was RD and all particles were relativistic. At a later stage $t \sim 10^{-10}$ sec ($T \sim 100$ GeV), the SM particles acquire masses through EW symmetry breaking. Then around $T \sim 100$ MeV, quarks and gluons form hadrons as strong interactions between them turns important. Subsequently around $T \sim 1$ MeV, Big bang nucleosynthesis occurs where protons and neutrons form nuclei. Then at $T \sim 0.25$ eV after recombination of atoms, photons stream freely in the Universe and decoupling between matter and radiation takes place. Today in CMBR we observe the imprints of the decoupled photons.

1.2.1 Success and shortcomings of the Big Bang Cosmology

The standard Big bang cosmology describes the evolution of our Universe with time. Explanation of observed redshift or Hubble expansion, the idea of nucleosynthesis (formation of nucleus) and thereafter producing the observed abundance of light particles are among the few important successes of Big bang cosmology. Despite the striking success, there remains few puzzles that can not be interpreted within the known theoretical model. Below we briefly mention few such important problems through some theoretical and observational facts of the Universe.

• **Horizon problem:** Observation from CMBR spectrum infers that Universe is amazingly isotropic with average temperature $T_0 = 2.7255 \pm 0.01$ K [39, 40]. Therefore it is expected that CMB photons we receive today from different portions of the Universe were in casual contact. However we find from the standard big bang theory that the Universe has many causally disconnected regions. This means that those regions were outside of the particle horizon or Hubble sphere during the decoupling phase of the Universe. In fact, it can be shown that there are 10^4 number of disconnected patches in the visible Universe [46]. They never communicated before emitting radiations. Question emerges why two apparently causally disconnected regions look similar in CMB observation. This is known as so called Horizon problem [43, 44].

• **Flatness problem:** One of the Friedman equations (Eq.(1.21)) can be translated to

$$\frac{k}{a^2H^2} = \frac{\rho}{\rho_C} - 1, \tag{1.27}$$

$$= \Omega - 1, \tag{1.28}$$

where $\rho_C = \frac{3H^2}{8\pi G}$ from Eq.(1.21), is the critical density of the Universe. CMB observations predicts Ω very close to one ($\Omega \simeq \frac{\rho}{\rho_C} - 1 = \pm 0.02$ [39, 40]). Now Eq.(1.26) suggests that $(\Omega - 1)$ is proportional to $t^{2/3}$ in MD Universe while for RD Universe $(\Omega - 1) \propto t$. Assuming RD Universe, when t was of $\mathcal{O}(1)$ sec (during Big bang nucleosynthesis), $(\Omega - 1)$ turns out to be $\mathcal{O}(10^{-16})$ [47]. And for a little earlier time $t \sim 10^{-11}$ sec (during EW symmetry breaking) it is $\mathcal{O}(10^{-27})$ [47]. This fact suggests energy density of the Universe is extremely fine tuned (close to unity) from very early stage. Cosmologists have termed this puzzle as flatness problem [43, 44].

1.3 Possible resolutions of drawbacks of the Big bang cosmology and the SM of particle physics

1.3.1 Inflation

In this section we will first briefly define the inflation. Subsequently we will see how inflation can resolve horizon and flatness problem. Thereafter we will focus on detailed analysis of inflationary dynamics.

In order to build a proper theory that can explain flatness and horizon problems appropriately, the idea of inflation was proposed by A. Guth around 1980 [43]. The concept behind this postulate is that the Universe went through a rapid accelerated expansion at very early epoch.

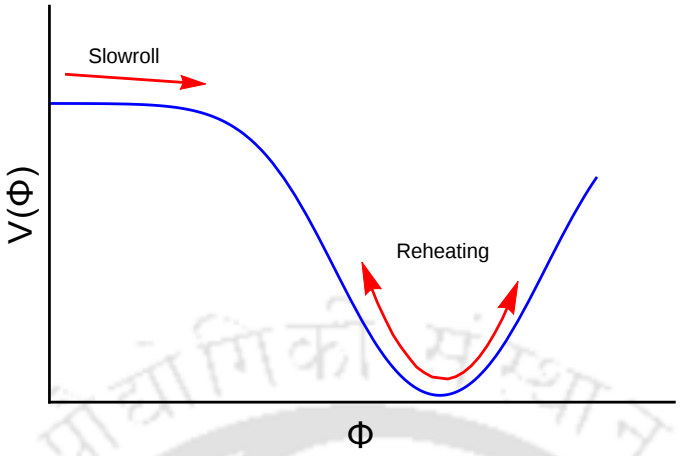

FIGURE 1.1: A schematic presentaion of slow roll inflation.

This implies

$$\ddot{a} > 0 \;\Rightarrow\; \frac{d}{dt}(aH)^{-1} < 0. \tag{1.29}$$

.

• **Resolution of the horizon and flatness problems:** According to Eq.(1.29), during inflation, comoving Hubble radius decreases. Thus provided inflation survives for a sufficient time, two apparently casually disconnected regions at decoupling time, might be inside the comoving Hubble radius or particle horizon at the onset of inflation and hence causally connected. Suppose $(a_i H_i)^{-1}$ indicates the comoving Hubble radius at the beginning of inflation. Then it is expected that observable Universe fits into the comoving Hubble radius at the onset of inflation to solve the horizon problem. Analytically it means that

$$(a_0 H_0)^{-1} < (a_i H_i)^{-1},. \tag{1.30}$$

It can be shown that around 50-60 number of e-folds of inflation ($N_e = \ln\left(\frac{a_e}{a_i}\right)$) are sufficient to solve the horizon problem [43, 44].

Also from Eq.(1.28), it is visible that $\Omega - 1 \propto (aH)^{-2}$. Now during inflationary phase comoving Hubble radius decreases (aH increases). Therefore, before inflation $\Omega - 1$ could be arbitrary. However the sufficient amount of inflation (depending on the number of e-folds) could make it close to unity. Hence it seems natural that the density of the Universe is close one from very early epoch [43, 44]. This provides a possible explanation of the flatness problem in the Universe.

Dynamics of inflation: Let us consider a simple toy model for inflation, driven by a scalar field (Φ), called as inflaton. Then the energy density of the scalar field can be written as

$$\rho_\Phi = \frac{1}{2}\dot{\Phi}^2 + V(\Phi), \tag{1.31}$$

where $V(\Phi)$ is the potential energy density of the inflaton Φ. The equation of motion of Φ is described as

$$\ddot{\Phi} + 3H\dot{\Phi} = -V'(\Phi), \tag{1.32}$$

where $V'(\Phi)$ is the first order differentiation of $V(\Phi)$ w.r.t Φ and $\dot{\Phi}$ represents first order time derivative. This equation determines the time evolution of the inflaton field. Inflation happens when the kinetic energy density is subdominant to the potential energy as depicted in Fig. 1.1. Hence during inflation one can assume $\rho_\Phi \simeq V(\Phi) = const.$ which further implies $H \sim const. \rightarrow a(t) \sim e^{Ht}$. In that case one can ignore the $\ddot{\phi}$ term compared to the friction term $3H\dot{\phi}$ in Eq.(1.32). Then Eq.(1.32) can be reduced to

$$3H\dot{\Phi} = -V'(\Phi), \tag{1.33}$$

$$\Rightarrow \ \dot{\Phi} = -\frac{V''(\Phi)\dot{\Phi}}{3H(\Phi)} + \frac{V'(\Phi)}{3H^2(\Phi)}H'(\Phi)\dot{\Phi}. \tag{1.34}$$

Now applying the condition for having successful inflation $\ddot{\Phi} << 3H\dot{\Phi}$, one can find,

$$\epsilon, \ \eta << 1, \tag{1.35}$$

where ϵ and η are known as the slow roll parameters defined as

$$\epsilon = \frac{M_P^2}{2}\Big[\frac{V'(\Phi)}{V(\Phi)}\Big]^2 \ ; \ \eta = M_P^2\Big[\frac{V''(\Phi)}{V(\Phi)}\Big]. \tag{1.36}$$

Inflation ends when one of the slow roll parameters becomes equal to unity. The number of e-fold of inflation will be provided by

$$N_e = \ln\frac{a(t_e)}{a(t_i)} = -M_P^2\int_{\Phi_i}^{\Phi_f}\frac{V}{V'}d\Phi. \tag{1.37}$$

where t_i denotes the beginning of inflation and t_e corresponds to end of inflation.

Remarkably, the inflation also produces density perturbations which are required for structure formation of the Universe. These density perturbations are caused due to quantum fluctuations of the scalar field driving inflation. In addition, these density inhomogeneities also produce

temperature anisotropies in the CMBR. The scalar perturbation spectrum (P_s) is obtained as [100, 101]

$$P_s = \frac{V(\Phi)}{24\pi^2 M_P^4 \epsilon}. \tag{1.38}$$

The parameter which determines the scale invariance of the scalar perturbation spectrum, known as spectral index n_s given by

$$n_s = 1 - 6\epsilon + 2\eta. \tag{1.39}$$

The experimental value of scalar perturbation spectrum is measured to be $P_S \simeq 2.2 \times 10^{-9}$ [39, 40]. Inflation also creates tensorial fluctuations. The tensor to scalar ratio (r) determines the amount of tensorial perturbation in the CMB spectrum. It is parametrized as [100, 101]

$$r = 16\epsilon, \tag{1.40}$$

where ϵ is one of the slow roll parameters as mentioned in Eq.(1.36). All these parameters (r, n_s and P_s) have to be evaluated at the inflaton value during horizon exit of the relevant cosmological scales. Planck experiment provides a strong upper bound on the value of $r \lesssim 0.11$ [39, 40, 102].

Once inflation terminates after the slow roll, conditions in Eq.(1.36) are violated and the inflaton field (Φ) rolls down rapidly towards the minimum of the potential. Then it starts to oscillate and decays to the SM particles provided it has coupling with the SM fields. At this stage connection between inflation and the SM is of significant importance. Slowly the energy density of Φ gets transferred to the conventional particles. This phase is known as reheating. At this point standard Big Bang era begins. The reheating temperature at the end of inflation is written as [100, 101]

$$T_R \simeq 0.1\sqrt{\Gamma_\Phi M_P}, \tag{1.41}$$

where Γ_Φ is the total decay width of inflaton Φ.

Now as an exercise, let us clarify how to calculate the inflationary observables for a given inflationary potential. For this purpose, let us choose the chaotic inflation model [52, 103, 104]. It is probably the simplest kind of slow roll inflationary model. The potential of such a framework is given by

$$V = \frac{1}{2} m_\Phi^2 \Phi^2, \tag{1.42}$$

where Φ is the inflaton and m_Φ is the mass of the inflaton. The slow roll parameters can be obtained as using Eq.(1.36)

$$\epsilon = \eta = 2\Big(\frac{M_P}{\Phi}\Big). \tag{1.43}$$

For inflation to occur it requires $\epsilon, \eta << 1$. This clearly states that during inflation the value of Φ has to be larger than M_P *i.e.* super-Planckian. Due to its super-Planckian value, this model falls into large scale inflation model category. Now the number of e-folds can be obtained by Eq.(1.37)

$$N_e = \frac{\Phi_*^2}{4M_P^2} - \frac{1}{2}, \tag{1.44}$$

where Φ_* is the value of inflaton at horizon exit. The value of Φ_* can be obtained as a function of number of e-fold through $\Phi_* \simeq 2M_P\sqrt{N_e}$. For $N_e = 55 - 60$, it turns out that $\Phi^* \simeq (13.5 - 15.5)M_P$. The magnitude of $m_\Phi \simeq 10^{12}$ GeV can be computed in order to match the experimental the value of scalar perturbation spectrum (P_s). This model provides scalar to tensor ratio r=0.13 and $n_s = 0.967$ for $N_e = 60$. Thus the model is in tension with the Planck observation which provides a strong upper limit $r \lesssim 0.11$ [102]. We will unfold a possible way to revive this model in Chapter 2.

1.3.2 Dark Matter

In this section we will provide a brief review [105–110] on the presence of DM in the Universe. We first shed light on the evidences of DM from various astrophysical and cosmological observations. Thereafter we speak about possible candidates of DM. Then we discuss the production mechanism of DM specifically the freeze-out mechanism. Next, we go through the dark matter detection techniques. Finally as an exercise we will review the scalar DM phenomenology.

1.3.2.1 Evidence of DM

There are numerous evidences of existence of DM in the Universe. Below we comment on some of the important evidences which support presence of DM in the Universe.

The most spectacular and earliest evidence of DM is the nature of the observed flat rotation curves of spiral galaxies [111–113]. Suppose in a spiral galaxy, a star of mass m at distance r from the origin of the galaxy is rotating with velocity $v(r)$. Now one can apply the Virial theorem, which states that the mean kinetic energy is equal to minus half of the mean potential

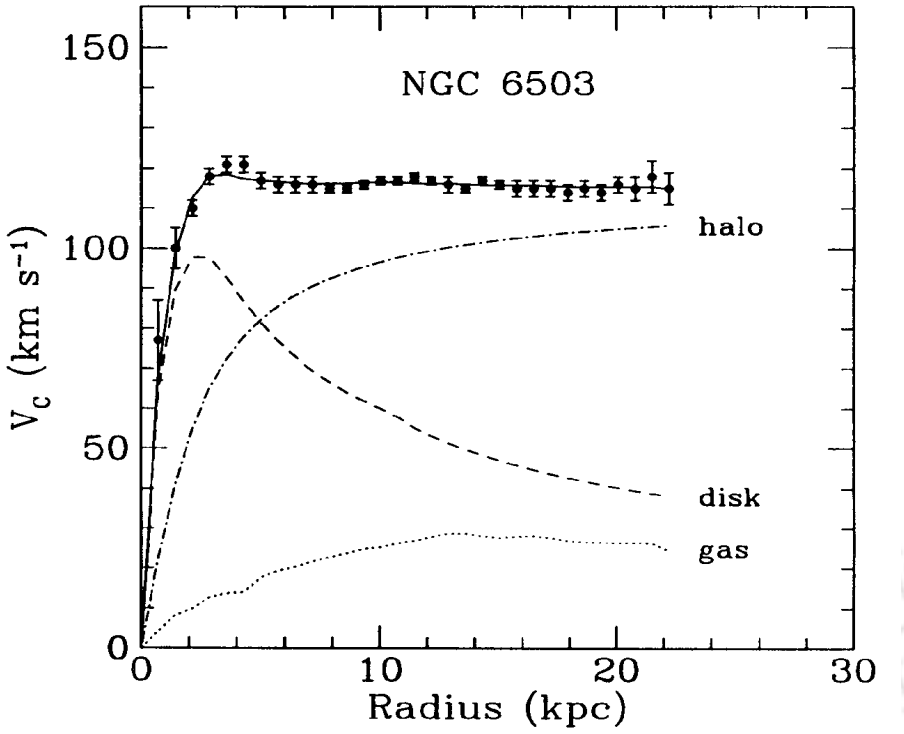

FIGURE 1.2: Galactic rotation curve for NGC 6503 shows the possible presence of the dark matter (halo) along with baryonic matter components required to match the data. The figure has been borrowed from [114].

energy. The concentrated mass in a spherical volume element of radius r and matter density $\rho(r)$ is $M(r) = \frac{4}{3}\pi r^3 \rho$. Hence in this spiral system, the Virial theorem can be mathematically portrayed as,

$$\frac{1}{2}mv^2(r) = -\frac{1}{2}\frac{GM(r)m}{r} \tag{1.45}$$

$$\Rightarrow\ v(r) \propto r, \tag{1.46}$$

where G is the gravitational constant. Now if $M(r)$ is constant, the dependence of $v(r)$ on r will be modified to

$$\Rightarrow\ v(r) \propto r^{-1/2}. \tag{1.47}$$

Therefore for small values of r near the origin, velocity of star rises linearly with radial distance r which is consistent with the observation. However if we move further from the visible part of the galaxy, v is expected to fall as $r^{-1/2}$. However, it is very surprising to note that, the observation from rare stars or gas cloud predicts that $v \simeq$ constant for regions far from the origin

(outside the visible region) of the spiral galaxy. This strange behaviour of galactic rotational velocity was first forecasted by Fritz Zwicky in 1933. This observation is consistent only when $M(r) \propto r$ as evident from Eq.(1.45). Hence, it strongly hints towards the presence of some massive unexplored kind of gravitating matter (see Fig. 1.2).

Another powerful tool to study the presence of dark matter in the Universe is gravitational lensing [115–120]. According to the Einstein's general theory of relativity, light can bend in presence of bulk of matter. In gravitational lensing, rays coming from the distant galaxy gets distorted when it passes through the bulk of of matter and reach to the observer. Here, the pile of matter acts as a lens and as a consequence, the bending of light occurs. Therefore, any observer behind the detector could see the distorted or multiple images of the source. From the distortion patterns in the image sample, one can compute the density distribution of matter content of the galaxy which provides the lensing effect through gravitational effect. The observation from several lensing clusters such as Abell 2281, Bergmann, Petrosian reveals the astonishing presence of large amounts of DM in these clusters (see [121, 122] for details).

In addition, observation from Bullet cluster [121, 122] strongly favors DM hypothesis. Using X-ray spectroscopy and gravitational lensing method, amount of luminous and non-luminous matter density can be estimated inside the cluster. And from observation, presence of large amount of non-luminous object has been found. The CMB analysis also reveals that most of the matter in the Universe is composed of non-baryonic DM. The present value of DM relic density in present Universe according to CMB analysis is [39]

$$0.1175 \leq \Omega_{\rm DM} h^2 \leq 0.1219. \tag{1.48}$$

1.3.2.2 Feasible DM candidates

A viable DM candidate should hold the following properties.

• DM particle has to be electrically neutral. Otherwise they will annihilate to photon and would be easily detected.

• It interacts weakly with the ordinary matter.

• DM has to be stable or long-lived particle in cosmological time scale.

One of the major mystery of DM hypothesis is the nature of DM particles. They might decouple while in (ultra)relativistic (hot/warm) or non-relativistic (cold) state. Generally it is believed that DM's are weakly interacting and termed as weakly interacting massive particle

(WIMP). WIMPSs have been massively studied over the years and typically they are searched in the form of missing energy at particle colliders. However with the recent progress, various forms of DM have also been proposed. Among them, feebly interacting DM (FIMP [125, 126]) and strongly self interacting DM (SIMP [127–132]) are being explored.

It turns out no SM particle can account for DM including light neutrinos. Present bound on sum of the masses from Planck experiment[39] rules out the possibility for the SM neutrinos to account for correct DM relic abundance. Therefore to build a proper DM model, one has to go beyond the SM framework with new sets of additional fields to accommodate the DM candidate. Among probable candidates of DM, bosons (scalars [54–57] or vector bosons [133–135]) and fermions [136–138] are well motivated and investigated largely. In addition, gauge bosons or pseudo Nambu Goldstone bosons [139–157] originating from a gauged or global symmetry are also gaining attention. In one of the well motivated popular BSM framework *i.e.* supersymmetry (SUSY), the lightest supersymmteric particle (LSP) [158–161] (neutralino or gravitino) is a very attractive dark matter candidate. DM can also be identified with the axion [162–177] in the Peccei-Quinn extended SM which is required to resolve the strong CP problem [178, 179]. However irrespective of the identity, it is important to understand the dynamics of dark matter evolution through Boltzman equation.

1.3.2.3 Boltzman equation

Before we describe the DM evolution through different phases of the Universe, let us define energy density (ρ) and entropy density (s) of the Universe. The energy density of all species in thermal equilibrium can be well approximated by the contribution of relativistic species [11]. The simplified expression for energy density is given by [11]

$$\rho = \frac{\pi^2}{30} g^* T^4, \tag{1.49}$$

where g^*s are the number of effective massless degrees of freedom (dof) provided by

$$g^* = \sum_{\text{bosons}} g_i \Big(\frac{T_i}{T}\Big)^4 + \frac{7}{8} \sum_{\text{fermions}} g_i \Big(\frac{T_i}{T}\Big)^4 \tag{1.50}$$

where g_i is the number of dof of individual species and T_i indicates the temperature of i'th species of fermions or bosons. On the other hand, entropy density (s) in an expanding Universe is an important quantity to measure. Similar to ρ, s is also dominated by the contributions of

relativistic dofs which can be approximated as [11]

$$s = \frac{2\pi^2}{45} g_s^* T^3, \tag{1.51}$$

where g_s^* is the entropy dof given by,

$$g_s^* = \sum_{\text{bosons}} g_i \Big(\frac{T_i}{T}\Big)^3 + \frac{7}{8} \sum_{\text{fermions}} g_i \Big(\frac{T_i}{T}\Big)^3. \tag{1.52}$$

Therefore, both g^* and g_s^* are functions of time. As for most of the time in the early Universe, maximum number of species had uniform temperature, it can be approximated that $g^* \simeq g_s^*$ [11].

The evolution of any particle, suppose X, in Universe is governed by the Boltzman equation. This is generally written as

$$\hat{L}(f) = \hat{C}(f), \tag{1.53}$$

where $\hat{C}$ is the collision operator and $\hat{L}$ is the Liouville operator [11]. $f \to f(x^\mu, p^\mu)$ is the phase space distribution of the concerned particle X. According to FRW model, the Universe is spatially flat and homogeneous which corresponds, $f(x^\mu, p^\mu) \to f(E, t)$. Thereafter the number density of the X particle can be obtained as

$$n_X(t) = \frac{g}{(2\pi)^3} \int d^3p f(E, t), \tag{1.54}$$

where g is the number of dof of X particle. Now one can find the simplified form of the Boltzman equation using the standard form of Liouville operator [11]. The evolution of number density of the particle $6n_X$ therefore reads,

$$\frac{dn_X}{dt} + 3Hn_X = \frac{g}{(2\pi)^3} \int \frac{\hat{C}(f)}{E} d^3p. \tag{1.55}$$

A generalized collision process of X particle with other species can be identified as $X + a_1 + a_2 + ... \leftrightarrow i_1 + i_2 + i_3 + ...$ Then the R.H.S of Eq.(1.55) can be converted to [11]

$$\begin{aligned}\frac{g}{(2\pi)^3} \int \frac{\hat{C}(f)}{E} d^3p = &- \int d\Pi_X d\Pi_{a_1} d\Pi_{a_2} ... d\Pi_{i_1} d\Pi_{i_2} d\Pi_{i_3} .. (2\pi)^4 \delta^4(p_X + p_{a_1} + p_{a_2} .. - p_{i_1} - p_{i_2} - p_{i_3} ...) \\ &\times \Big[|\mathcal{M}|^2_{X+a_1+a_2+... \to i_1+i_2+i_3+...} f_X f_{a_1} f_{a_2} .. (1 \pm f_{i_1})(1 \pm f_{i_2}) .. \\ &- |\mathcal{M}|^2_{i_1+i_2+i_3+... \to X+a_1+a_2+...} f_{i_1} f_{i_2} .. (1 \pm f_{a_1})(1 \pm f_{a_2})(1 \pm f_X) ... \Big],\end{aligned} \tag{1.56}$$

where f_{i_n} is the phase space density of n'th species and $d\Pi_j = g_j \frac{d^3p}{(2\pi)^3 2E}$. The "+" sign applies for bosons while "$-$" applies to fermions. We will use Maxwell-Boltzman distribution statistics for all the particle species in oder to simplify the Boltzman equation further.

Freeze out mechanism: According to freeze-out mechanism, the particle we are concerned with (X) was in thermal equilibrium at early Universe. Later as the Universe cools down, its interaction rate with thermal plasma (Γ_X) slowly declines. The condition $\Gamma_X \sim H$ (H is the expansion rate of the Universe) determines the decoupling point of X from thermal plasma and then the relic abundance of DM freezes out.

Suppose X is stable (or long lived) in cosmological time scale and hence could be a viable DM candidate. At early stage, X was in thermal equilibrium with other particles in the thermal plasma. Hence during that time annihilation and inverse annihilation processes of X *e.g.* $XX \leftrightarrow YY$ were active where Y represents the other particles in the thermal plasma. Let us also consider X has no decay mode. During thermal equilibrium, phase space distribution for any species (f_{i_n}) can be written as following Maxwell Boltzman distribution,

$$f_{i_n} = e^{-\frac{E_{i_n}}{T}}. \tag{1.57}$$

We define the number density of X during thermal equilibrium $n_X \simeq n_X^{\rm eq}$. We also use some standard redefinitions of variables $x = \frac{m_X}{T}$, $Y_X = \frac{n_X}{s}$ where s is the entropy density (Eq.(1.51)) of the Universe. In that case after few intermediate steps [11], the Eq.(1.55) can be simplified to the conventional form,

$$\frac{dY_X}{dx} = -\frac{\langle\sigma v\rangle s}{Hx}(Y_X^2 - Y_X^{\rm eq^2}), \tag{1.58}$$

where $Y_X^{\rm eq} = \frac{n_X^{\rm eq}}{s}$ and $\langle\sigma v\rangle$ is thermally averaged interaction cross section of X which is related with the interaction rate of X as $\Gamma_X = n_X \sigma v$. The parameter v is identified as the relative velocity between two DM particles in the centre of mass frame ($XX \leftrightarrow YY$). To obtain Eq.(1.58) from Eq.(1.55) the change of variable from time t to x has been performed using $T \propto \frac{1}{t}$.

Now in the relativistic ($x << 3$) and non-relativistic limit ($x << 3$) one can obtain from Eq.(1.54),

$$Y_X^{\rm eq} = 0.145 \frac{g}{g_s^*} x^{3/2} e^{-x} \quad \text{for} \quad x >> 3, \tag{1.59}$$

$$= 0.278 \frac{g_{\rm eff}}{g_s^*} \quad \text{for} \quad x << 3, \tag{1.60}$$

where $g_{\rm eff} = g$ for bosons and $\frac{3g}{4}$ for fermions. The value of x at which $\Gamma_X = H$, is the freeze out value conventionally denoted by x_f.

Note that, Eq.(1.58) is not solvable analytically. It requires to invoke some physics intuition to simplify Eq.(1.58). The L.H.S. of Eq.(1.58) is proportional to $\mathcal{O}(Y_X)$, while R.H.S. is of $\frac{\Xi}{x^2}\mathcal{O}(Y_X^2)$ with $\Xi >> 1$ as we will shortly see. Hence for $x << 1$, the factor $(Y_X^2 - Y_X^{\rm eq^2})$ in R.H.S of Eq.(1.58) must have been very small. Then we can safely assume $Y_X \sim Y_X^{\rm eq}$ during relativistic regime. On the other hand for $x >> 1$, $Y_X^{\rm eq}$ falls as e^{-x}. Therefore in view of Eq.(1.58), Y_X should stop following $Y_X^{\rm eq}$ during non-relativistic regime.

Freezeout may occur when X is in both (a) relativistic and (b) non-relativistic regimes. Below we discuss the related phenomenology of these.

(a) In this case X decouples from thermal plasma during relativistic regime. The particles which decouples at relativistic mode is known as "hot relic". For this type of particles, we can approximate $Y_X(x_f) \simeq Y_X^{\rm eq}$=constant where x_f denotes the decoupling point of X. (see Eq.(1.60) where $x_f >> 3$). Hence at present Universe the value of Y_X would be

$$Y_X^{\infty} \simeq 0.278 \frac{g_{\rm eff}}{g_s^*}. \tag{1.61}$$

Therefore, present energy density of relic X can be obtained as

$$\rho_X^0 \;=\; s_0 Y_X^{\infty} m_X \;\simeq\; 3\times 10^3 \Big(\frac{m_X}{\rm eV}\Big)\frac{g_{\rm eff}(x_f)}{g_s^*(x_f)}{\rm cm}^{-3}, \tag{1.62}$$

where $s_0 \simeq 3000$ cm^{-3} is the present entropy density. Then the relic abundance of X particle ($\Omega_X = \frac{\rho}{\rho_C}$) will be provided as

$$\Omega_X h^2 \simeq 7.9\times 10^{-2}\Big(\frac{g_{\rm eff}(x_f)}{g_s^*(x_f)}\Big)\Big(\frac{m_X}{\rm eV}\Big), \tag{1.63}$$

where $\rho_C = 1.88h^2 \times 10^{-29}$ gm cm^{-3} is the critical density of the Universe [39]. One can wonder whether light neutrinos in the SM could be a DM candidate. They decouple at temperature $x_f \sim \mathcal{O}$ (1 MeV). Then considering three generations of neutrinos, roughly $g_s^*(x_f) = g^*(x_f) = 10.75$ and $g_{\rm eff} = 3\times\Big(\frac{3}{4}\Big)$. Hence, to satisfy the correct relic abundance of DM, $\Omega_{X=\nu_l} \simeq 0.11$, neutrino mass should satisfy $m_{X=\nu_l} \simeq 0.95$ eV using Eq.(1.63). However the recent Planck [39] and WMAP [124] data put a stringent upper limit on sum of the neutrino masses as $\sum_i m_{\nu_i} < 0.22$ eV. It confirms that neutrinos in the SM can not provide correct relic abundance of DM.

(b) The species which decouples at non-relativistic regime is often called as"cold relic". Theoretically velocity dependence of annihilation cross section can be parametrized as

$$\langle \sigma v \rangle \propto v^p, \tag{1.64}$$

where $p = 0$ corresponds to s-wave annihilation while $p = 2$ indicates p-wave annihilation. Now as $v \propto T^{1/2}$, it is possible to write $\langle \sigma v \rangle$ as

$$\langle \sigma v \rangle = \sigma_0 x^{-n}, \tag{1.65}$$

where $n = \frac{p}{2}$.

The Boltzman equation of Eq.(1.58) can be further reduced to

$$\frac{dY_X}{dx} = -\Xi x^{-n-2}(Y^2 - Y_X^{\mathrm{eq}^2}), \tag{1.66}$$

where $\Xi = \frac{2\pi^2}{75.15}\frac{g_s^*}{\sqrt{g^*}} m_P \sigma_0 m_X$ and we have also used $H = 1.67\sqrt{g^*}\frac{T^2}{m_P}$. Now in order to find the relic density of X, let us attempt to solve Eq.(1.66) analytically. First we assume $\langle \sigma v \rangle$ has only s-wave contribution ($n = 0$).

$$\frac{dY_X}{dx} = -\frac{\Xi}{x^2}(Y^2 - Y_X^{\mathrm{eq}^2}), \tag{1.67}$$

After freeze out, it is also safe to consider $Y >> Y_X^{\mathrm{eq}}$. Therefore, Eq.(1.66) turns out to be,

$$\frac{dY_X}{dx} = -\frac{\Xi}{x^2} Y_X^2. \tag{1.68}$$

The solution is obtained by differentiating both sides of Eq.(1.68) from $x = x_f$ to $x = \infty$ yielding.

$$Y_X^{\infty} = \frac{x_f}{\Xi}. \tag{1.69}$$

In Fig. 1.3, general behaviour of Y_X has been shown. It can be viewed that after certain value of $x = x_f$, Y_X stops following Y_X^{eq} and after sometime it freezes out. Now it is very trivial to calculate the relic abundance of X as

$$\Omega_X = \frac{\rho_X}{\rho_C}, \tag{1.70}$$

$$= \frac{s_0 Y_X^{\infty} m_X}{\rho_C}, \tag{1.71}$$

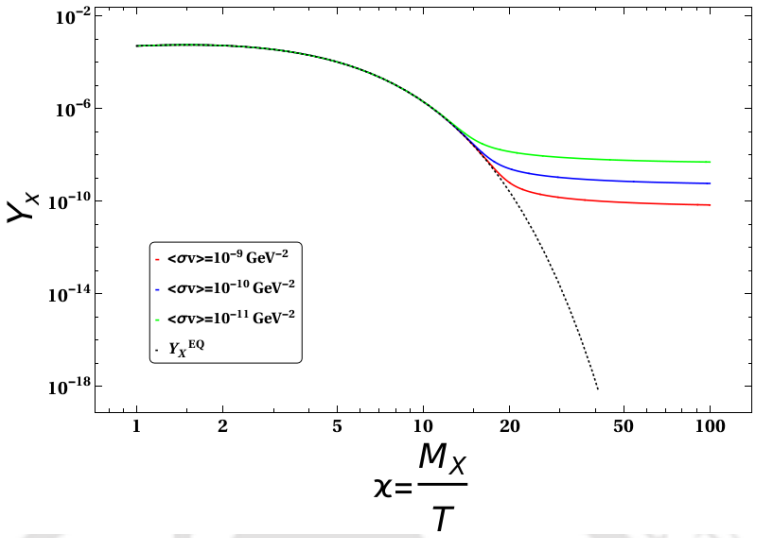

FIGURE 1.3: Evolution of Y_X as a function of $x = \frac{m_X}{T}$ in freeze out scenario [160] considering different magnitudes of interaction cross section of X field. We also show the evolution of $Y_X^{\rm EQ}$.

where $\rho_C = 1.88h^2 \times 10^{-29}$ gm cm^{-3} is the critical density of the Universe and $s_0 \simeq 3000$ cm^{-3} is present entropy density [39]. Putting the values of ρ_C, s_0 and substituting Y_X^{∞} in Eq.(1.71) we find,

$$\Omega_X h^2 \simeq 1.07 \times 10^9 \frac{x_f}{(g_s^*/g_*^{1/2}) m_P \sigma_0} \text{GeV}^{-1}. \tag{1.72}$$

As an example, assuming $g_s^* = g_* \simeq 100$ and $x_f \simeq 20$, we can obtain an estimate of Ω_X as

$$\Omega_X h^2 = \frac{2 \times 10^{-10} \text{GeV}^{-2}}{\langle \sigma v \rangle}, \tag{1.73}$$

where we substitute σ_0 by $\langle \sigma v \rangle$ from Eq.(1.65) Hence to achieve correct order of relic abundance ~ 0.1, $\langle \sigma v \rangle$ has to be around 10^{-9} GeV^{-2}. This is the order of weak scale interaction. Hence, any massive particle having this order of interaction cross section can satisfy the relic abundance bound. Theoretically, these kind of weakly interacting DM candidates are commonly categorized as WIMP.

Freeze in: Recently another kind of dark matter production mechanism is proposed known as feebly interacting massive particle (FIMP) [125, 126]. In this scenario, due to very weak coupling, the DM never stays in thermal equilibrium. Initial density of DM is assumed to be zero, and at later epoch it can be produced thermally (annihilation) or non thermally (decay from some heavier particles).

Suppose X is the DM candidate which is having interaction with two other particles B_1 and B_2 with $m_{B_1} > m_{B_2}$. Then the $B_1 \to B_2 + X$ process governs the freeze in of DM. In this case the collision factor ($\hat{C}(f)$) of Boltzman equation (Eq.(1.55)) turns out to be

$$\begin{aligned}\frac{g}{2\pi^3}\int \frac{\hat{C}(f)}{E}d^3p = -\int d\Pi_X d\Pi_{B_1} d\Pi_{B_2}(2\pi)^4\delta^4(p_{B_1} - p_X - p_{B_2}) \\ \times \Big[|\mathcal{M}|^2_{B_1\to B_2+X} f_{B_1}(1 \pm f_X)(1 \pm f_{B_2}) \\ - |\mathcal{M}|^2_{B_1\to X+B_2} f_{B_1}(1 \pm f_X)(1 \pm f_{B_2})...\Big]. \end{aligned} \tag{1.74}$$

To solve the Boltzman equation one needs to make few important assumptions: (i) initial abundance of X particle is zero ($f_X = 0$), (ii) dilute gas limit *i.e.* $f_2 \pm 1 \simeq f_1 \pm 1 = 1$, (iii) the other two particle are in thermal equilibrium $f_1 = e^{-\frac{E_1}{T}}$, $f_2 = e^{-\frac{E_2}{T}}$. Next to obtain the relic abundance of X particle in this case, one has to solve Eq.(1.55) using Eq.(1.74). We will not discuss it further since our focus in the thesis will be mainly on the freeze out scenario. We refer Refs. [125, 126] for further study on FIMP mechanism.

1.3.2.4 Detection of DM

Detection of DM is the one of the major challenges in modern era of particle physics and cosmology experiments. To know the nature of DM in the Universe, we must capture DM signals in laboratory. Below we some techniques which are used to detect DM.

Direct detection: In direct detection (DD) method, [180, 181] flux of DM is expected to pass through the detector and interact with nucleons inside the nuclei. The detectors measure the recoil energy of nucleon which is dependent upon the interaction cross section of DM-nucleon scattering. It is obvious that the probability of DM-nucleon scattering increases with the size of the target and the local volume of the DM. The spin independent (SI) DD cross section is written as [182]

$$\sigma^{\rm SI}_{\rm DD} = \frac{4\mu_D^2}{\pi}\Big(Z\alpha_P + (A-Z)\alpha_N\Big), \tag{1.75}$$

where A is the mass number of the target nuclei where Z and N are the total number of proton and neutrons respectively. The effective couplings of DM with the nucleon (protons and neutrons) have been expressed in terms of α_P and α_N. The reduced mass of DM and nucleon has been denoted by $\mu_D = \frac{m_{\rm DM} m_N}{m_N + m_{DM}}$.

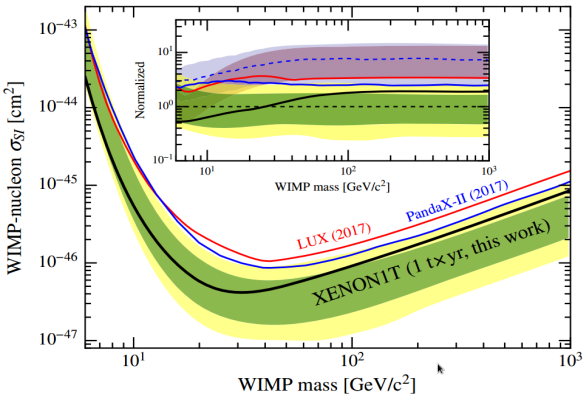

FIGURE 1.4: Recently predicted upper limit on SI DD cross section ($\sigma_{\rm SI}$) from XENON 1T [183, 184] (thick black line) has been shown. Previous results from LUX [185] and PandaX-II [186] are also plotted for comparison purpose. This image has been borrowed from [184].

On the other hand the spin dependent (SD) DD cross section can be obtained as [182]

$$\sigma^{\rm SD}_{\rm DD} = \frac{32\mu_D^2 G_F^2}{\pi}\frac{J+1}{J}(\alpha_P\langle S_P\rangle + \alpha_n\langle S_N\rangle)^2, \tag{1.76}$$

where $\langle S_{P,N}\rangle$ are the expectation values of proton and neutron spin operator. J represents the spin of the target nuclei. Currently lot of experiments are going on around the globe in search of DM through this DD method. Few important such ongoing experiments, XENON [183, 184], LUX [185], PANDA [186]. Till now, no positive signal has been observed yet. Hence, the experiments only poses strong upper bound on the DD cross section of DM.

Indirect detection: There is another popular scheme [187–189] to look for DM signal via its direct decay or annihilation to SM particles. It may happen that, somewhere in the Universe DM density is high (DM can be captured locally due to strong gravitation pull by some heavy volume like galactic center). In those dense region dark matter may annihilate into some particles and their in turn decay produces a flux of photons, electrons, protons, positrons, antiprotons and/or (anti-)neutrinos. This can cause excess in photon, positron or neutrinos flux in the Universe. Experiments like PAMELA [193], Fermi-LAT [194] etc. try to detect such excesses in order to confirm the presence of DM.

1.3.2.5 Real scalar singlet dark matter

One of the appealing and decent possibilities to accommodate WIMP type DM is to extend the SM of particle physics with a real gauge singlet scalar ϕ [54–56]. The stability of the DM

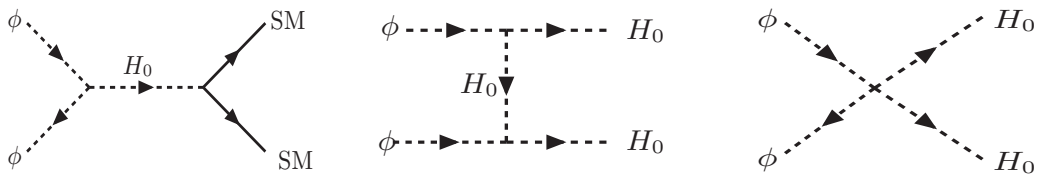

FIGURE 1.5: Feynman diagrams of scalar singlet DM annihilaton to the SM particles.

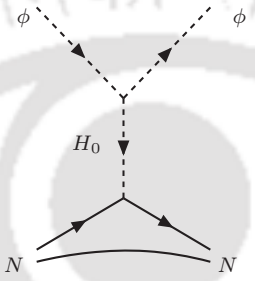

FIGURE 1.6: Feynman diagram for DD process of scalar singlet DM.

candidate can be ensured by imposing a Z_2 symmetry under which the DM candidate transforms non-trivially. The DM interacts with the SM Higgs doublet (H) only. Let us write the scalar potential

$$V = V_H + V_\phi + V_{\phi H}, \tag{1.77}$$

where $V_\phi = m_\phi^2\phi^2 + \frac{\lambda_\phi}{4}\phi^4$ and $V_{\phi H} = \frac{1}{2}\lambda_{\phi H}\phi^2|H|^2$. The DM ϕ annihilates to all the SM particles mediated by the SM Higgs field as shown in Fig. 1.5. The DM mass is obtained as $m_{\rm DM}^2 = m_\phi^2 + \frac{\lambda_{\phi H}}{2}v^2$. The Higgs portal coupling of DM ($\lambda_{\phi H}$) and its mass (m_ϕ) are the only two free parameters in this scenario. The involvement of mere two parameters make this particular set up quite predictive and hence popular. The relic abundance will be determined by Eq.(1.71). Now using the relic abundance constraint in Eq.(1.48) one can find correlation between the two parameters m_ϕ and $\lambda_{\phi H}$. In addition, one can also determine the cross section of SI direct detection process as portrayed in Fig. 1.6. The scalar DM-nucleon cross section is given by [56]

$$\sigma_{\phi N}^{\rm SI} = \frac{\lambda_{\phi H}^2 v^2 |C_N|^2}{4\pi}\Big(\frac{\mu_r^2}{m_{\rm DM}^2 m_h^4}\Big), \tag{1.78}$$

where $m_h \simeq 125.09$ GeV is the SM Higgs mass, v=246 GeV, $\mu_r = \frac{m_N m_{\rm DM}}{m_N + m_{\rm DM}}$ and C_N is the coupling between the SM Higgs and nucleon having magnitude 340 MeV/v [56]. As a numerical example, for $m_{\rm DM} = 500$ GeV, $\lambda_{\phi H}$ has to be 0.145 to satisfy the correct relic abundance. On the other hand with $m_{\rm DM} = 500$ GeV and $\lambda_{\phi H} = 0.145$, the SI DD cross section turns out to be $\sim 10^{-46}$ cm^2. In Fig. 1.7 (left panel), we have shown the relic density satisfied contour in $m_{\rm DM} - \lambda_{\phi H}$ plane.

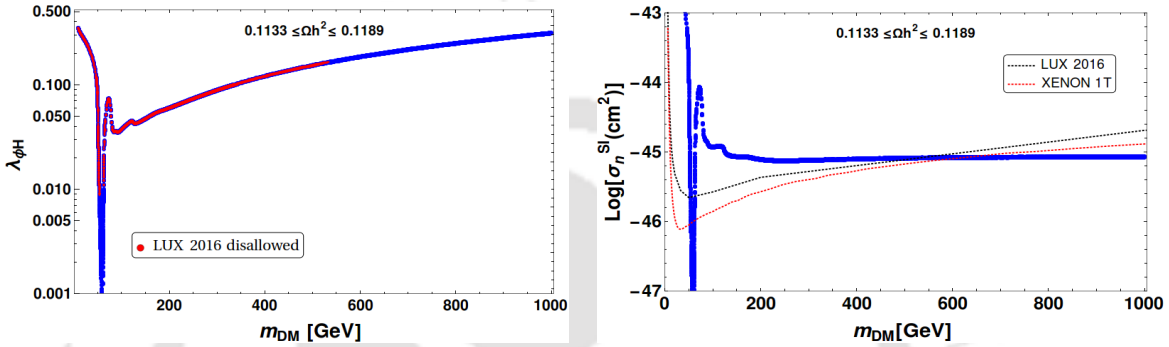

FIGURE 1.7: [Left panel:] Relic density satisfied contour in $m_{\rm DM} - \lambda_{\phi H}$ plane. [Right panel:] SI DD cross section vs $m_{\rm DM}$ has been plotted for all relic satisfied points in left panel.

The right panel of Fig. 1.7 shows the estimate of SI direct detection cross section for different values of mass of the DM using for all the relic abundance satisfied points in the left panel. The bounds on DD cross section from XENON [183], LUX [185], PANDA [186] have been used to constrain the model. As it is seen, the experimental bounds clearly disfavors the minimal version of scalar singlet Higgs portal DM model for $m_{\rm DM} \lesssim 500$ GeV. In order to rescue this particular set up from being ruled out, extension is required which we will discuss in Chapter 4. In addition, we will also see that in presence of scalar DM the Higgs vacuum stability scenario turns interesting.

1.3.3 Neutrino Mass

In this section, we discuss few aspects of neutrino physics, specifically physics behind non-zero neutrino mass as it is going to be involved in some of our studies. First we will speak about neutrino oscillation and Pontecorvo-Nakagawa-Sakata (PMNS) matrix. Then we will focus on generation of neutrino mass via seesaw mechanism.

The physics associated with neutrino masses and mixing is a major domain of current particle physics research. First proposed by Pauli in 1930 and discovered by Chadwick in

1932, research on neutrino has passed long time with developments in both experimental and theoretical frontiers. After decades of detailed study, we really have gained lot of knowledge on this elusive particle like their absolute mass scale, mixing pattern etc (see [190–192] for review) with impressive accuracy. However there are many unsolved issues like nature of neutrinos (Dirac or Majorana), hierarchy of neutrino masses and magnitude of CP violation in the lepton sector etc.

Neutrinos are massless in the Standard Model due to the absence of right handed neutrinos. However, neutrino oscillation is one such phenomena which contradicts with this massless nature of neutrinos. The first convincing evidence of neutrino oscillation phenomena was found at the Super-Kamiokande experiment [17], Japan in 1998. Later it has been verified in several experiments worldwide like Sudbury Neutrino Observatory (SNO) [18], K2K [19], KamLAND [20] etc. It also indicates towards mixing between three generations of neutrino flavor states (*i.e.* ν_e, ν_μ and ν_τ). Hence flavor eigenstates and mass eigenstates of neutrinos are different. In addition, the smoking gun evidences for neutrino oscillation directly points towards non-zero mass of neutrinos with an urgent requirement of extension of the Standard Model.

PMNS matrix: The mixing between the neutrino flavor and mass eigenstates can be expressed as

$$\nu_{\alpha L} = U_\nu \nu_{jL}, \tag{1.79}$$

where α and j are the respective flavor and mass indices and run as e, μ, τ and 1, 2, 3 respectively. Note that the charged lepton mass matrix (m_l) in the SM is provided by $Y_l \bar{l}_L H e_R$ term in the Yukawa Lagrangian as defined in Eq.(1.12). Now to diagonalize m_l, a bi-unitary transformation is required:

$$m_l = U_l m_l^{\text{diag}} V_l^\dagger, \tag{1.80}$$

where we have redefined the SM charged lepton fields as $l_L \to U_l l_L$ and $e_R \to V_l e_R$. Next, considering the neutrino oscillation among flavor states, the charge current interaction originating from Eq.(1.3), using Eq.(1.79) and Eq.(1.84), can be obtained as,

$$-\mathcal{L}_{CC} = \frac{g}{\sqrt{2}} \sum_{\alpha,j} \bar{l}_{L,\alpha} \gamma^\mu \left(U_l^\dagger U_\nu \right)_{\alpha j} \nu_{jL} W_\mu^- \; + \; h.c., \tag{1.81}$$

where g is the $SU(2)_L$ gauge coupling. The unitary matrix $U_{PMNS} = U_l^\dagger U_\nu$ is popularly known as Pontecorvo-Nakagawa-Sakata (PMNS) matrix.

Next, let us comment on parametrization of U_{PMNS}. For 3 generation of neutrinos, U_{PMNS} is a 3×3 unitary matrix. It can be described by 9 independent real elements. Now, among the 9 parameters, 3 are mixing angles and other 6 are phases. However out of 6 phases, only one phase is physically relevant. This phase is commonly called as Dirac phase. For Majorona nature of neutrinos, there exists additional two CP violating phases. Hence, generally a U_{PMNS} matrix is conventionally parametrized as

$$\begin{aligned} U_{PMNS} &= \begin{pmatrix} 1 & 0 & 0 \\ 0 & c_{23} & s_{23} \\ 0 & -s_{23} & c_{23} \end{pmatrix} \begin{pmatrix} c_{13} & 0 & s_{13}e^{-i\delta} \\ 0 & 1 & 0 \\ -s_{13}e^{i\delta} & 0 & c_{23} \end{pmatrix} \begin{pmatrix} c_{12} & s_{12} & 0 \\ -s_{12} & c_{12} & 0 \\ 0 & 0 & 1 \end{pmatrix} \mathcal{R}, \\ &= \begin{pmatrix} c_{12}c_{13} & s_{12}c_{13} & s_{13}e^{-i\delta} \\ -s_{12}c_{23} - c_{12}s_{13}s_{23}e^{i\delta} & c_{12}c_{23} - s_{12}s_{13}s_{23}e^{i\delta} & c_{13}s_{23} \\ s_{12}s_{23} - c_{12}S_{13}c_{23}e^{i\delta} & c_{12}s_{23} - s_{12}s_{13}c_{23}e^{i\delta} & c_{13}c_{23} \end{pmatrix} \mathcal{R}, \end{aligned} \tag{1.82}$$

where $c_{ij} = \cos\theta_{ij}$, $s_{ij} = \sin\theta_{ij}$, δ represents the CP violating Dirac phase. $\mathcal{R}$ is a diagonal matrix containing two Majorona phases α_{21} and α_{31}, *i.e.* $\mathcal{R}$=diag$(1, e^{i\alpha_{21}/2}, e^{i\alpha_{31}/2})$. The present experimental status of neutrino mass parameters and mixing angles are listed below [199–201]:

$$\Delta m^2_{21} = (7.11 - 8.18) \times 10^{-5}\ \text{eV}^2, \quad |\Delta m_{31}|^2 = (2.30 - 2.65) \times 10^{-3}\ \text{eV}^2 \tag{1.83}$$

$$\sin^2\theta_{12} = 0.278 - 0.375, \quad \sin^2\theta_{23} = 0.392 - 0.643, \quad \sin^2\theta_{13} = 0.0177 - 0.0294. \tag{1.84}$$

Type-I seesaw mechanism: One of the most simple and renowned process to generate neutrino mass is Type-I seesaw [21, 195–197]. In this case, the SM is extended by three SM gauge singlet RH Majorona Neutrinos (N_{R_i} with $i = 1 - 3$). The Lagrangian for neutrino mass is written as

$$-\mathcal{L}_{\text{seesaw}} = Y_\nu \bar{\psi}_L \tilde{H} N_R + \frac{1}{2} M_R \bar{N^C_R} N_R + h.c.. \tag{1.85}$$

After electroweak symmetry breaking, one can obtain

$$-\mathcal{L}_{\text{Type-I}} = m_D \overline{\nu_L} N_R + \frac{1}{2} M_R \overline{N^c_R} N_R + h.c.. \tag{1.86}$$

In Eq.(1.86), $m_D = Y_\nu v$ is the Dirac mass matrix for the neutrinos where Y_D is the coupling matrix. M_R is the symmetric mass matrix for the Majorana neutrinos. In the basis (ν_L, N^c_R),

the effective neutrino mass matrix can be written as

$$M_\nu = \begin{pmatrix} 0 & m_D^T \\ m_D & M_R \end{pmatrix}. \tag{1.87}$$

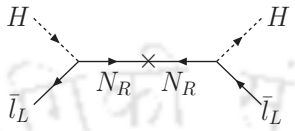

FIGURE 1.8: Feynman diagram for Type-I seesaw.

For three generations of neutrinos, each entries in Eq.(1.87) are 3×3 matrices. Assuming m_D to be much lighter than M_R ($m_D << M_R$), after block diagonalisation, mass matrices for light and heavy neutrinos can be expressed as

$$m_\nu^I \simeq -m_D^T M_R^{-1} m_D \quad \text{and} \quad M_{\text{heavy}} \simeq M_R. \tag{1.88}$$

Hence from Eq.(1.88) it is easy to explain the smallness of the light neutrinos, provided M_R is sufficiently large. This is commonly known as type-I seesaw mechanism of neutrino mass generation. A typical Feynman diagram for such mass generation is portrayed in Fig. 1.8. As an example, from Eq.(1.88), to yield neutrino mass of the order of 0.1 eV assuming $Y_D \sim \mathcal{O}(1)$, the required value of RH neutrino mass is $M_R \sim 10^{14}$ GeV. Although there are several other mechanism of generating neutrino mass such as Type-II seesaw [22, 23], Type-III seesaw [24] and radiative generation [198], we employ mainly Type-I seesaw in the thesis.

1.3.4 Higgs Vacuum Stability

This section is devoted to the discussion on EW vacuum stability in the SM. The stability of the SM Higgs vacuum depends on the running of Higgs quartic coupling λ_h. With the present measured value of Higgs mass $\sim 125.09 \pm 0.24$ GeV [25] and top mass $\sim 173.24 \pm 0.81$ GeV [25] by LHC, λ_h turns negative at high energy scale $\Lambda_I^{\text{SM}} \sim 10^{9-10}$ Ge. This implies that there may exist another deeper minimum at some high scale. However in cosmological context this does not sound legitimate [202–218]. During ination the Higgs eld is expected to receive a typical uctuation with amplitude of $\mathcal{O}(H_{\text{Inf}})$ where $H_{\text{Inf}}$is the Hubble scale during ination. So there is a possibility that it can be driven from the EW vacuum toward the unstable part of the Higgs

potential provided $H_{\rm Inf} > \Lambda_I^{\rm SM}$ which is satised by most of the large eld ination models Below we discuss the fate of Higgs vacuum in the SM considering 3σ uncertainty of top mass.

1.3.4.1 Higgs Vacuum Stability in Standard Model

The tree level Higgs potential in the SM as narrated in Eq.(1.6)

$$V(H) = \mu_H^2|H^2| + \frac{\lambda_h}{4}|H|^4. \tag{1.89}$$

At high energy ($H_0 >> v$ in Eq.(1.7)), one can safely ignore the quadratic term in $V(H)$. Now for a correct description of Higgs potential we should consider the higher order loop contributions [219–221]. Particles which have coupling with the SM Higgs will enter into the loop and contribute to the correction of the Higgs potential. Therefore, the effective Higgs potential with the approximation $H_) >> v$, can be written as

$$V^{\rm eff}(H) = \frac{\lambda_h^{\rm eff}}{4} H_0^4, \tag{1.90}$$

where $\lambda_h^{\rm eff}$ includes contribution of higher order loop correction in the SM Higgs potential which is read as [34, 219–221]

$$\lambda_h^{\rm eff} = e^{4\Gamma(h)}\Big[\lambda_h(\mu = H_0) + \lambda_h^1(\mu = h) + ..\Big], \tag{1.91}$$

where $\Gamma(h) = \int_{m_t}^{h} \gamma(\mu) d\ln\mu$, γ the anomalous dimension of Higgs field [34]. The one loop correction to the self coupling of Higgs field is given by [34, 219–221]

$$\begin{aligned}\lambda_h^1 =& \frac{1}{(4\pi)^2}\Big[\frac{3g_2^4}{8}\Big(\ln\frac{g_2^4}{4} - \frac{5}{6} + 2\Gamma\Big) + \frac{3}{16}(g_2^2+g_1^2)^2\Big(\ln\frac{g_2^2+g_1^2}{4} - \frac{5}{6} + 2\Gamma\Big) \\ & - 3y_t^4\Big(\ln\frac{y_t^2}{2} - \frac{3}{2} + 2\Gamma\Big) + 3\lambda_h^2(4\ln\lambda_h - 6 + 3\ln 3 + 8\Gamma)\Big].\end{aligned} \tag{1.92}$$

In addition we also have to perform the renormalization group (RG) running of the SM couplings. Among all the fermionic couplings, top Yukawa coupling y_t turns out to be the dominant one. Now for the purpose of RG running, evaluation of initial values of coupling constants is required. To find their values at m_t, one has to consider various threshold corrections at different mass scales. This has been rigorously worked out in Ref [34]. Below we provide the initial values of all the SM couplings as function of m_t (top mass), m_h (Higgs mass) and strong

coupling constant (α_s) at $\mu = m_t$ energy scale.

$$g_1(\mu = m_t) = 0.35761 + 0.00011\Big(\frac{m_t}{\text{GeV}} - 173.10\Big) - 0.00021\frac{M_W - 80.384\ \text{GeV}}{0.014\ \text{GeV}}, \tag{1.93}$$

$$g_2(\mu = m_t) = 0.64822 + 0.00004\Big(\frac{m_t}{\text{GeV}} - 173.10\Big) - 0.00011\frac{M_W - 80.384\ \text{GeV}}{0.014\ \text{GeV}}, \tag{1.94}$$

$$g_3(\mu = m_t) = 1.16449 + 0.0005\Big(\frac{m_t}{\text{GeV}} - 173.10\Big) - 0.00011\frac{M_W - 80.384\ \text{GeV}}{0.014\ \text{GeV}} + 0.0031\Big(\frac{\alpha_3 - 0.1184}{0.0007}\Big) \tag{1.95}$$

$$\lambda_h(\mu = m_t) = 0.12711 + 0.00206\Big(\frac{M_{H_0}}{\text{GeV}} - 125.66\Big) - 0.00004\Big(\frac{m_t}{\text{GeV}} - 173.10\Big), \tag{1.96}$$

$$y(\mu = m_t) = 0.93558 - 0.00550\Big(\frac{m_t}{\text{GeV}} - 173.10\Big) - 0.00042\frac{\alpha_3(M_Z) - 0.1184}{0.0007} - 0.00042\frac{M_W - 80.384\ \text{GeV}}{0.014\ \text{GeV}}. \tag{1.97}$$

Next in order to study the running, one should employ RG equations of all the SM couplings [34, 222–226] at three loop. Below we present one loop RG equations of relevant SM couplings.

$$\beta_{g_1}^{\text{SM}} = \frac{1}{16\pi^2}\Big\{-\frac{41}{6}g_1^3\Big\}, \tag{1.98}$$

$$\beta_{g_2}^{\text{SM}} = \frac{1}{16\pi^2}\Big\{-\frac{19}{6}g_2^3\Big\}, \tag{1.99}$$

$$\beta_{g_3}^{\text{SM}} = \frac{1}{16\pi^2}\Big\{-7g_3^3\Big\}, \tag{1.100}$$

$$\beta_{\lambda_h}^{\text{SM}} = \frac{1}{16\pi^2}\Big\{24\lambda_h^2 + 12y_t^2\lambda_h - 9\lambda_h\Big(\frac{g_1^2}{3} + g_2^2\Big) - 6y_t^4 + \frac{9}{8}\Big(\frac{g_1^4}{3} + g_2^4 + \frac{2}{3}g_1^2g_2^2\Big)\Big\}, \tag{1.101}$$

$$\beta_{y_t}^{\text{SM}} = \frac{1}{16\pi^2}\Big\{\frac{9}{2}y_t^3 + \Big(-\frac{17}{12}g_1^2 - \frac{9}{4}g_2^2 - 8g_3^2\Big)y_t\Big\} \tag{1.102}$$

where $\beta_{C_i} = \frac{dC_i}{dt}$ and $t = \ln\mu$. The stability condition of electroweak vacuum is $\lambda_h(\mu) > 0$ for any energy scale. Using this criteria the stability region has been presented by light green color in left panel of Fig. 1.9. On the other hand, if there exists another deeper minimum other than the EW one, the estimate of the tunneling probability P_T of the EW vacuum to the second minimum is essential. The Universe will be in metastable state only provided the decay time of EW vacuum is longer than the age of the Universe. The tunneling probability is given by [30, 34],

$$P_T = T_U^4\mu_B^4 e^{-\frac{8\pi^2}{3|\lambda_H(\mu_B)|}}. \tag{1.103}$$

where T_U is the age of the Universe. μ_B is the scale at which probability is maximized, determined from $\beta_{\lambda_H} = 0$. Hence for metastable Universe requires [30, 34]

$$\lambda_H(\mu_B) \; > \; \frac{-0.065}{1 - \ln\left(\frac{v}{\mu_B}\right)}. \tag{1.104}$$

As noted in [34], for $\mu_B > M_P$, one can safely consider $\lambda_H(\mu_B) = \lambda_H(M_P)$. This condition has been plotted in Fig. 1.9 with solid red line. Hence pink colored region below the solid red line is considered to be the instable region. Therefore, using Eqs.(1.93-1.97) and Eqs.(1.98-1.102) one can attain the RG evolutions of the relevant couplings.

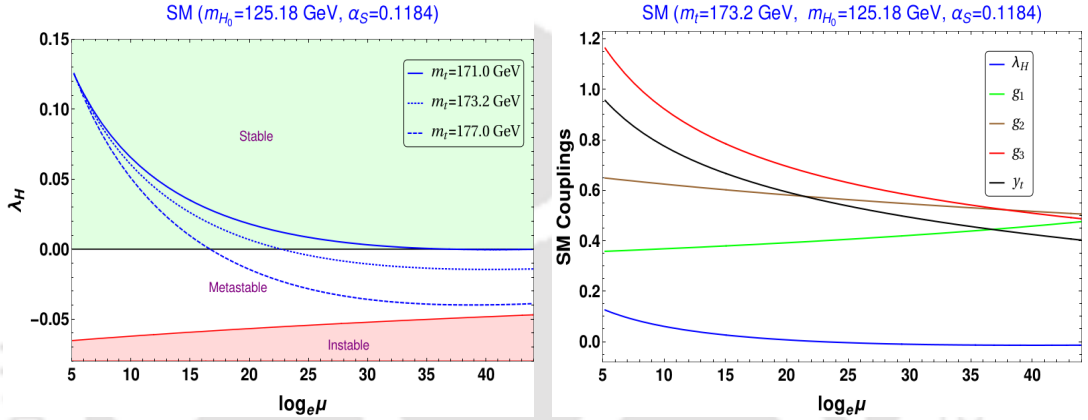

FIGURE 1.9: Running of λ_h as a function of energy scale μ for [left panel:] for varying m_t with fixed $m_{H_0} = 125.18$ GeV and [righ panel] for varying m_{H_0} with $m_t = 173.2$ GeV

In left panel of Fig. 1.9, we display the running of λ_h with energy scale μ. As initial value of y_t is of $\mathcal{O}(1)$ (see Eq.(1.96)), fermionic effect dominates in Eq.(1.101) which brings down λ_h from the initial value in tis RG running. As a consequence, λ_h turns negative at $\mu \sim 10^{10} = \Lambda_I^{\rm SM}$ GeV for $m_t = 173.2$ GeV with $m_{H_0} = 125.18$ GeV in Fig. 1.9 (left panel). If we consider somewhat a lower value of top mass, initial value y_t will be lesser than the earlier case. Therefore it is obvious that for $m_t = 171$ GeV, the instability energy scale Λ_I becomes larger than $\Lambda_I^{\rm SM}$ as viewed in Fig. 1.9 (left panel). On the other hand for a higher m_t, it turns out that $\Lambda_I < \Lambda_I^{\rm SM}$. In Fig. 1.9 (right panel) running of all the SM couplings have been shown.

Hence, from the discussion, it is quite prominent that any theoretical model having large fermionic couplings with the SM Higgs are dangerous in view of stability of EW vacuum, One ideal way to achieve absolute vacuum stability is to introduce additional scalars [58, 59] in the

theory. In Chapter 3, Chapter 4 and Chapter 6 we will discuss in detail the role of scalars in EW vacuum stability.

1.4 Role of scalar fields in the Universe

So far, we have focused in explaining some of the serious drawbacks of the SM of particle physics and Big bang cosmology and possible resolutions of them. We will address these issues in several possible extensions of the SM of particle physics primarily by scalar fields. Below we state few expected roles that additional scalar can serve in beyond the SM (BSM) framework.

• It is well known that inflaton, responsible for the rapid exponential expansion in early universe is a scalar field. The scalar potential if sufficiently flat could lead the successful inflation.

• Scalar field is one of the robust candidate of Dark matter. The scalar DM phenomenology has been covered at a large extent in literature [54–57, 65–68, 71–76].

• In addition, scalar fields turns out to be instrumental in achieving Higgs vacuum stability [58, 59]

• Scalars can be connected to the origin of light neutrino mass in a BSM framework governed by $U(1)_{B-L}$ symmetry and extended by additional fermions (RH neutrinos [227]).

Therefore, it is comprehensible from the earlier discussions that presence of one or more additional scalars in the Universe might be sufficient in circumventing many of the unexplained issues with the standard theory. In the thesis, Our emphasis will be to connect or correlate two or more puzzles in a single framework involving scalar fields.

1.5 Outline of the thesis

Our aim in Chapter 2 is to establish a successful model to realize chaotic inflation in a BSM framework. We have included supersymmetry, one of the most familiar and logical BSM theory to achieve that. We also predict on dynamical supersymmetry breaking and some of the neutrino parameters at the end of inflation. Chapter 3 deals with the Higgs vacuum stability issue in presence of large scale inflation (modeled by additional scalar fields). In Chapter 4, we have analyzed scalar DM phenomenology in a set up consists of two extra scalars and RH neutrinos. In Chapter 5, we attempted to find a common origin for successful inflation with DM (scalar) in a supersymmetric framework. Chapter 6 have been dedicated to study fermionic

DM phenomenology and Higgs vacuum stability assisted by a scalar field. Finally we conclude on Chapter 7.

Chapter 2

Modified sneutrino chaotic inflation and dynamical Supersymmetry breaking

2.1 Introduction

In our first work (based on [228]), we have studied the role of scalar fields in realizing inflation in the early Universe. As we discussed in Sec. 1.2.1, a chaotic inflation represented by a SM singlet scalar field provides a minimal and most elegant picture of inflation. However it would be even more interesting if such a scalar field has connection with particle physics set up. The extremely flat potential of such a scalar field as demanded by inflationary requirement, turns out to be difficult to achieve as this flatness can be destroyed by radiative corrections. Supersymmetry can play a key role in this regard. In [229–233], it was shown that the inflaton can be the scalar partner of the RH neutrino superfield. This is called sneutrino chaotic inflation. In this way, the inflaton has a direct relation with other BSM physics, as RH neutrinos are crucial to have neutrino mass through type-I seesaw. Also in the framework, there exists a close proximity of the mass parameter involved in chaotic inflation with mass scales of RH neutrino superfields which suggests that the sneutrino can naturally play the role of inflaton. However such a simple realization is ruled out from Planck result.

Here in this work our primary motivation was to deform the original sneutrino chaotic inflation in such a way so as to keep its prediction consistent with observation. In achieving this goal we have found that a coupling between the neutrino sector and a supersymmetry

breaking sector can naturally provide such deformation. Since supersymmetry has to broken (as no superpartners are seen so far), such a set up turns out to be quite natural. The work involves a strongly coupled supersymmetric gauge sector (known as SQCD). Before we go to the details of our work, we provide below a brief introduction to supersymmetry and its breaking which serves as a guide to understand some of the argument we used later.

2.1.1 A brief introduction to Supersymmetry

There are several motivations behind introducing supersymmetry. One of the strongest motivation is related to the fact that it provides a solution to the hierarchy problem [234–238]. It is known that the quantum corrections drag the mass parameter associated with the SM Higgs field to a very high value close to the cut off scale of the theory. This is known as hierarchy problem. The problem is even more prominent when the SM Higgs couples to any new physics. On the other hand, fermions in the SM are protected by the chiral symmetry and gauge boson masses are so by the presence of gauge symmetry. Introduction of supersymmetry can alleviate this problem. As it is a special kind of symmetry which connects the properties of a fermion to that of a scalar (and vice versa), the same chiral symmetry protecting fermion's mass is also responsible to protect scalar's mass. Apart from this, within supersymmetric framework, gauge coupling unify at high scale. It also provides a natural candidate of dark matter.

• **Supersymmetry algebra:** Supersymmetry (for review see [239–248]) is an extended version of Poincare symmetry. In addition to generators of Poincare symmetry ($M^{\mu\nu}$ for Lorentz booss and rotations and P^{μ} for translations), the supersymmetry includes fermionic generator (Q) which relates fermionic and bosonic states:

$$Q|\text{fermion}\rangle = |\text{boson}\rangle, \quad Q|\text{boson}\rangle = |\text{fermion}\rangle, \tag{2.1}$$

where Q is a spin-$\frac{1}{2}$ operator. In four dimensional space time, they can be considered as Weyl spinors. According to the standard definition, the fermionic generators are taken to be of the form Q_α and $\bar{Q}_{\dot{\alpha}}$ with $\alpha, \dot{\alpha} = 1, 2$ are the Lorentz spinor indices. They satisfy the following commutation and anti-commutation relations [248].

$$\begin{aligned} \{Q_\alpha, \bar{Q}_{\dot{\beta}}\} &= 2\sigma^{\mu}_{\alpha\dot{\beta}} P_\mu, \\ \{Q_\alpha, Q_\beta\} &= \{\bar{Q}_{\dot{\beta}}, \bar{Q}_{\dot{\beta}}\} = 0 \\ [Q_\alpha, P_\mu] &= [\bar{Q}_{\dot{\beta}}, P_\mu] = 0, \end{aligned} \tag{2.2}$$

where σ is the pauli matrix and P_μ represents the generator of translation symmetry.

• **Superspace and Superfields:** Before entering into the supersymmetric field theory and Lagrangian formalism, we need to build the idea of superspace. Superspace is obtained by extending the 4-component spacetime coordinates (x_μ) with four fermionic coordinates. The additional fermionic coordinates are labelled by Grassmann variables. Hence any point in superspace is defined by [248]

$$x^\mu,\ \theta^\alpha,\ \bar{\theta}_{\dot{\alpha}}, \tag{2.3}$$

where $\alpha\ , \dot{\alpha} = 1, 2$ are Lorentz indices. The new fermionic coordinates satisfy anti commutation relations

$$\{\theta_\alpha, \bar{\theta}_{\dot{\beta}}\} = \{\theta_\alpha, \theta_\beta\} = \{\bar{\theta}_{\dot{\alpha}}, \bar{\theta}_{\dot{\beta}}\} = 0. \tag{2.4}$$

Let us also define the integral over superspace [248]

$$\begin{aligned}
&\int d\theta = \int d\bar{\theta} = \int d\theta\bar{\theta} = \int d\bar{\theta}\theta = 0,\\
&\int d\theta^\alpha\theta_\beta = \delta^\alpha_\beta,\ \ \int d\bar{\theta}_{\dot{\alpha}}\bar{\theta}^{\dot{\beta}} = \delta^{\dot{\beta}}_{\dot{\alpha}},\\
&\int d^2\theta\theta^2 = \int d^2\bar{\theta}\bar{\theta}^2,\\
&\int d^4\theta\theta^2\bar{\theta}^2 = 1.
\end{aligned} \tag{2.5}$$

At this stage, it is also important to mention that the supercharges ($Q_\alpha,\ \bar{Q}_{\dot{\alpha}}$) are differential operators in superspace [248].

$$Q_\alpha = \frac{\partial}{\partial\theta^\alpha} - i\sigma^\mu_{\alpha\dot{\alpha}}\bar{\theta}^{\dot{\alpha}}\partial_\mu,\ \bar{Q}_{\dot{\alpha}} = -\frac{\partial}{\partial\bar{\theta}^{\dot{\alpha}}} + i\theta^\alpha\sigma^\mu_{\alpha\dot{\alpha}}\partial_\mu, \tag{2.6}$$

where $P_\mu = -i\partial_\mu$ is the momentum operator in bosonic space. Now we can write the general expression of a superfield which depends on superspace coordinates.

$$\begin{aligned}
\Phi(x_\mu, \theta, \bar{\theta}) =& \phi(x_\mu) + \theta\eta(x_\mu) + \bar{\theta}\chi^\dagger(x_\mu) + \bar{\theta}\bar{\sigma}^\mu\theta V_\mu(x_\mu)\\
&+ \theta^2F(x_\mu) + \bar{\theta}^2\bar{F}(x_\mu) + \theta^2\bar{\theta}\bar{\lambda}(x_\mu) + \bar{\theta}^2\theta C(x_\mu) + \theta^2\bar{\theta}^2D(x_\mu).
\end{aligned} \tag{2.7}$$

As evident from Eq.(2.7), a general superfield contains four complex scalar fields ($\phi,\ F,\ \bar{F},\ D$), four Weyl spinors ($\eta,\ \chi^\dagger,\ \bar{\lambda},\ C$) and one vector field ($V_\mu$). From Eq.(2.7), one can also obtain the form of chiral superfield using the constraints $\bar{D}_{\dot{\alpha}}\Phi = 0$ and $D_\alpha\Phi^\dagger = 0$ where $\bar{D}_{\dot{\alpha}}$ and D_α

are covariant derivatives in superspace defined by [248]

$$D_\alpha = \frac{\partial}{\partial\theta_\alpha} - i\sigma^\mu_{\alpha\dot{\alpha}}\bar{\theta}^{\dot{\alpha}}\frac{\partial}{\partial_\mu}, \quad \bar{D}_{\dot{\alpha}} = -\frac{\partial}{\partial\bar{\theta}^{\dot{\alpha}}} + i\theta^\alpha\sigma^\mu_{\alpha\dot{\alpha}}\frac{\partial}{\partial_\mu}. \tag{2.8}$$

The standard expression for chiral superfield turns out to be [248]

$$\Phi = \phi(x) - i\theta\sigma^\mu\bar{\theta}\partial_\mu\phi(x) - \frac{1}{4}\theta^2\bar{\theta}^2\partial^2\phi(x) + \sqrt{2}\theta\eta + \frac{i}{\sqrt{2}}\theta^2\partial_\mu\eta\sigma^\mu\bar{\theta} + \sqrt{2}\theta^2F(x). \tag{2.9}$$

Hence we see from Eq.(2.9) that the chiral superfield contains two complex scalars (ϕ and the auxiliary field F) and a Weyl spinor, known as supersymmetric chiral multiplet. This also explores one of the most important features supersymmetry theory that any supermultiplet contains equal number of bosonic and fermionic degrees of freedom ($n_B = n_F$). Similarly there exists other forms of supermultiplet like gauge supermultiplets and vector supermultiplets.

• **SUSY Lagrangian:** The Lagrangian for a general supersymmetric theory involving only chiral multiplets is conventionally written as [248]

$$\mathcal{L} = \int d^4\theta K(\Phi) + \int d^2\theta W(\Phi) + \int d^2\bar{\theta}\bar{W}(\Phi^\dagger), \tag{2.10}$$

where $K(\Phi)$ is a real function of the chiral field Φ_i known as Kähler potential which provides the kinetic term of Φ. The minimal form of Kähler potential can be expressed as $K(\Phi_i) = \Phi^\dagger\Phi$. The function $W(\Phi)$ is known as superpotential of the theory which provides the mass term and interaction Lagrangian of the theory. Note that superpotential is a holomorphic function of Φ. Provided $W(\Phi)$ is known, the F-term scalar potential of a supersymmetric theory is written as

$$V_F = |F_\Phi|^2 = \left|\frac{\partial W(\Phi)}{\partial\Phi}\right|^2. \tag{2.11}$$

If the theory is protected by a gauge theory, then there will be another contribution to the scalar potential which reads as

$$V_D = \frac{1}{2}\sum_\alpha D^\alpha D^\alpha = \frac{1}{2}\sum_\alpha g_\alpha^2(\Phi^* T^\alpha\Phi)^2, \tag{2.12}$$

where g_α and T^α are the gauge coupling constant and generators of the corresponding gauge symmetry of Φ. V_D is called as D-term potential.

• **Supersymmetry breaking:** Existence of exact supersymmetry in the Universe implies that all properties, except the spin, of particles in a supermultiplet have to be uniform including

masses of the individual components. However, supersymmetry cannot be the governing symmetry of the Nature. Else we should already observe SUSY particles at collider experiments. Therefore supersymmetry has to be broken at some high energy scale such that the superpartners are heavier than the SM particles to a great extent.

In order to construct a proper model of spontaneous supersymmetry breaking, the guiding principle should be the vacuum energy state $|0\rangle$ is not invariant under supersymmetry transformations, *i.e.* $Q_\alpha|0\rangle \neq 0$ and $Q^\dagger_{\dot{\alpha}}|0\rangle \neq 0$. It turns out that the supersymmtetric Hamiltonian (H_S) is a function of these generators:

$$H_S = \frac{1}{4}(Q_1 Q_1^\dagger + Q_1^\dagger Q_1 + Q_2 Q_2^\dagger + Q_2^\dagger Q_2). \tag{2.13}$$

Hence the SUSY breaking criteria can be expressed in terms of the Hamiltonian as $\langle 0|H_S|0\rangle > 0$ This implies that for a supersymmetric model if F and D term vanish, supersymmetry at ground will be preserved having $V_S = V_F + V_D = 0$. On contrary, inability to find simultaneous solutions of all Φ_i's considering $F_{\Phi_i} = 0$ and $D^\alpha = 0$, directly hints towards spontaneous breakdown of supersymmetry. For the moment let us focus on F-term supersymmetry breaking. Below as an exercise we present a simple example of F-term supersymmetry breaking (named as O'Raifeartaigh model [249]) for illustration purpose. Let us write the superpotential below

$$W_O = -\kappa_1\phi_1 + m\phi_2\phi_3 + \kappa_2\phi_1\phi_3^2, \tag{2.14}$$

assuming all ϕ_i's are gauge singlet. The superpotential has a additional global symmetry ($U(1)_R$) with R-charges of $\phi_{1,2,3}$ are two, two and zero respectively. The scalar potential can be otained as

$$V_S = |F_{\phi_1}|^2 + |F_{\phi_2}|^2 + |F_{\phi_3}|^2, \tag{2.15}$$

where

$$F_{\phi_1} = \kappa_1 - \kappa_2\tilde{\phi}_3^2, \quad F_{\phi_2} = -m\tilde{\phi}_3, \quad F_{\phi_3} = -m\tilde{\phi}_2 - 2\kappa_2\tilde{\phi}_1\tilde{\phi}_3, \tag{2.16}$$

where $\tilde{\phi}_i$ is the scalar partner of ϕ_i supermultiplet. Note that, there is no simultaneous solution for $F_{\phi_1} = 0$ and $F_{\phi_2} = 0$. Therefore supersymmetry is spontaneouly broken. One can find the minima of the relevant fields by minimizing the V_S. The minimum of V_S turns out to be at $\tilde{\phi}_2 = \tilde{\phi}_3 = 0$ while value of $\tilde{\phi}_1$ remains undetermined. Hence the vacuum has nonzero energy with with $V_S = \kappa_1^2$. The ϕ_1 field direction is identified as a "flat direction". This can be lifted by taking into account quantum loop corrections.

One important observation is the correlation of R-symmetry and spontaneous supersymmetry breaking. The renowned Nelson-Seiberg theorem [250] states any theory having spontaneous supersymmetry breaking minimum, must be protected by an exact $U(1)_R$ symmetry. However for metastable supersymmetry breaking, $U(1)_R$ could be an approximated symmetry [251–258] with an explicit $U(1)_R$ breaking term in the superpotential W_O [259]. In addition, the common well motivated perception behind supersymmetry breaking is that it occurs in a separate hidden sector other than the visible world. The effect of supersymmetry breaking is mediated to the visible sector. There are few well known mediation mechanisms: (i) gravity mediated or Planck scale mediated, (ii) gauge mediated and (iii) anamoly mediated. However it is very challenging task to predict the supesymmetry breaking scale. Theoretically it could be arbitrary. Any theory where supersymmetry breaks dynamically [260–262] would be very appealing. This means the supersymmetry breaking scale can be naturally generated from the strong coupling scale of the theory through small exponential suppression [260].

Now, as the inflationary energy scale is close to M_P, one should consider the local version of SUSY, *i.e.* Supergravity. The first hurdle one has to deal generally to accommodate inflation in supergravity framework is the famous η problem. This is caused by the field value of the inflaton (χ) during inflation, which exceeds the reduced Planck scale $M_P \simeq 2.4 \times 10^{18}$ GeV as in case of chaotic inflation. Thereby it could spoil the required degree of flatness of the inflationary potential through the Planck-suppressed operators. In [263–268], chaotic inflation model with shift symmetric Kähler potential associated with the inflaton field was proposed to cure this problem. Another interesting aspect of a supersymmetric model of inflation is its relation with supersymmetry breaking. From the completeness point of view, a supersymmetric structure of an inflationary scenario demands a realization of supersymmetry breaking at the end of inflation. Though during inflation, the vacuum energy responsible for inflation breaks supersymmetry (at a large scale of order of energy scale of inflation), as the inflaton field finally rolls down to a global supersymmetric minimum, it reduces to zero vacuum energy, and thereby no residual supersymmetry breaking remains.

2.1.2 Preface of the work

Therefore our purpose is two fold; one is to modify the standard sneutrino chaotic inflation so as to satisfy the PLANCK 2015 [39, 102] results and other is to accommodate supersymmetry breaking at the end of inflation. We consider two sectors namely (i) the inflation sector and (ii) the supersymmetry breaking sector. As earlier mentioned, the inflation sector is part of the neutrino sector consisting of three RH neutrino superfields. There will be a role for another

sneutrino during inflation, which will be unfolded as we proceed. We identify the scalar field responsible for inflation to be associated with one of these three fields. The scalar potential resembles the standard chaotic inflation in the supergravity framework assisted with the shift symmetric Kähler potential. The superpotential involving the RH neutrino responsible for inflation breaks this shift symmetry softly. We have argued the smallness associated with this shift symmetry breaking parameter by introducing a spurion field. In this excercise, we also consider discrete symmetries to forbid unwanted terms. For the supersymmetry breaking sector, we consider the Intriligator-Seiberg-Shih (ISS) model [256] of breaking supersymmetry dynamically in a metastable vacuum. This sector is described by a supersymmetric gauge theory and henceforth called the SQCD sector [269–276]. These two sectors can have a gravitational coupling which in turn provides a dynamical deformation of the standard chaotic inflation. Again the coupling strength between these two sectors can be naturally obtained through another spurion. As the inflaton field approaches its minimum once the inflation is over, this interaction term becomes insignificant and finally the two sectors are effectively decoupled. However the hidden SQCD sector fields stabilize in metastable vacuum, hence supersymmetry breaking is achieved as a remnant of inflation. Earlier attempts in connecting the inflation and ISS type supersymmetry breaking can be found in [277–280]. A global $U(1)_R$ symmetry plays a pivotal role in shaping the ISS model of dynamic supersymmetry breaking. Once the supersymmetry is broken in the hidden SQCD sector, the effective supersymmetry breaking scale in the Standard Model sector is assumed here to be developed by the gauge mediation mechanism. To materialize this, the ISS model requires a modification for breaking $U(1)_R$. In this context we follow the proposal in [281] and show that this can easily be adopted in our set-up. Furthermore, as the RH neutrino superfields are part of the inflation sector, which obeys the same $U(1)_R$ symmetry, their $U(1)_R$ charges are already fixed. The same RH neutrinos also contribute to the light neutrino mass matrix through type-I seesaw mechanism. We find that the $U(1)_R$ charges of various fields involved along with their charges under the discrete symmetries imposed can actually predict an inverted hierarchy of neutrino masses. We provide an estimate of reheating temperature in this context and also comment on leptogenesis.

Below in section 2.2, we briefly discuss the standard chaotic inflation in the supergravity framework. Then we will discuss about the ISS model of dynamic supersymmetry breaking in section 2.3 followed by the role of interaction term between the two sectors in section 2.4. The dynamics of the fields during and after inflation are discussed in section 2.5 and 2.7 respectively. The prediction for this modified chaotic inflation are presented in section 2.6. In section 2.8, we have shown that a deformation to the SQCD sector can be achieved which is related to the $U(1)_R$ symmetry breaking. In section 2.9, we discuss the implication of neutrino masses and

mixing that comes out of the present set-up. We comment on the reheating temperature and leptogenesis in section 2.10. Finally we conclude in section 2.11.

2.2 Standard sneutrino chaotic inflation in supergravity

We start this section by reviewing some of the features of the standard chaotic inflation in supergravity where the scalar partner of a RH neutrino (say N_1 among the three RH superfields $N_{i=1,2,3}$ involved in type-I seesaw for generating light neutrino mass) serves the role of inflaton. Sneutrino chaotic inflation[229, 230, 232, 233] gains much attention from the perspective of particle physics involvement. Mass of the inflaton and in turn mass of that particular RH neutrino (in the supersymmetric limit) can be fixed by the magnitude of curvature perturbation spectrum in this theory. In $\mathcal{N} = 1$ SUGRA, the superpotential is considered to be

$$W_N = mN_1N_2, \tag{2.17}$$

along with the Kähler Potential[1]

$$K_N = |N_2|^2 - \frac{(N_1 - N_1^\dagger)^2}{2}. \tag{2.18}$$

Note that a shift symmetry, $N_1 \to N_1 + \mathrm{C}$, where C is real having mass dimension unity, is imposed on the Kähler potential, whereas the superpotential breaks it. Thus the parameter m can be regarded as a shift-symmetry breaking parameter.

The parameter m being much smaller than M_P, the term in the superpotential W_N would be natural in 't Hooft's sense [282] of increased symmetry in the limit $m \to 0$. The smallness associated with m can be explained with the introduction of a spurion field z_1 as shown in [264]. Also the higher order shift symmetry breaking terms involving N_1 can be controlled in an elegant way through the introduction of z_1. Suppose the spurion field z_1 transforms under the shift symmetry as,

$$z_1 \to \frac{N_1}{N_1 + C} z_1, \tag{2.19}$$

hence $N_1 z_1$ combination remains shift symmetric. At this stage, a discussion on $U(1)_R$ symmetry is pertinent. There exists a global $U(1)_R$ symmetry under which the superpotential W has 2 units of R-charges. However note that with the presence of shift symmetric Kähler potential involving N_1, N_1 can not possess a global $U(1)_R$ charge. Therefore N_2 should carry R-charge 2, while R-charges of N_1 and z_1 are zero. Furthermore, we consider a Z_2 symmetry under which

[1] K_N also involves $|N_3|^2$, which we do not put here for simplifying our discussion.

only N_1 and N_2 are odd. Combining the shift symmetry, $U(1)_R$ and the Z_2, we can write the general superpotential for W_N as

$$W_N^g = [z_1 N_1 + a_3 (z_1 N_1)^3 + ...] N_2. \tag{2.20}$$

As the z_1 gets a vacuum expectation value (vev) $\sim m$ which is small compared to M_P, we can argue that the shift symmetry is softly broken. Simultaneously the higher order terms (with coefficient $a_i \sim \mathcal{O}(1)$) are negligibly small and hence we are essentially left with our working superpotential W_N in Eq.(2.17).

The importance of having this shift symmetry can be understood as discussed below. F-term scalar potential is calculated using the following standard expression,

$$V_F = e^{\frac{K}{M_P^2}} \Big[D_i W K^{-1}_{ij^*} D_{j^*} W^* - 3 \frac{|W|^2}{M_P^2} \Big], \tag{2.21}$$

where $D_i W = \frac{\partial W}{\partial f_i} + K_i / M_P^2$ and the subscript i labels a superfield f_i. Due to the imposed shift symmetry on N_1, the Kähler potential (or e^{K/M_P^2}) depends only on the imaginary component of N_1. The real component of N_1 therefore can be considered to be the inflaton (hereafter denoted by χ). Its absence in the Kähler potential allows it to acquire super-Planckian value during inflation, which is a characteristic of large field inflation models. Assuming that during inflation, all other fields (including N_2 as well) except the inflaton are stabilized at origin[2], the inflationary potential becomes $V_\chi = \frac{1}{2} m^2 \chi^2$.

We have already discussed earlier (in Sec. 1.3.1) that in view of the recent PLANCK update [39, 102], this minimal model is almost outside the 2σ region of $n_s - r$ plot. So a modification of the minimal model is of utmost importance. As we have mentioned before, there has been some suggestions toward this [283–287]. In this work, our approach to accommodate chaotic inflation within the present experimental limit is to couple it with the supersymmetry breaking sector. This coupling serves as a dynamic modification to the minimal chaotic inflation. To discuss it in detail, in the following section we present a brief summary of the ISS model of dynamical supersymmetry breaking.

[2]Particularly for N_2, this can be ensured by adding a non-canonical term in the Kähler as $\xi |N_2|^4 / \left[2 M_P^2\right]$ with $\xi \sim 1$ [263].

2.3 SQCD sector and supersymmetry breaking in a metastable vacuum

It is evident from the F-terms (in particular $F_{N_2} = mN_1$) of W_N in Eq.(2.17) that during inflation, supersymmetry is broken at a very high scale since the inflaton [288] (χ field $\equiv$ real part of N_1) takes a non-zero super-Planckian value. However once the inflation is over, the χ field finally acquires a field-value zero ($\chi = 0$ is the global minimum) as evident from the minimization of the potential $V_\chi = m^2\chi^2/2$. Hence there is no supersymmetry breaking associated with this minimum. It is expected that there should be a small amount of supersymmetry breaking left at the end of inflation so that an effective supersymmetry breaking in the supersymmetric version of the Standard model or its extension can be introduced. In this work, we consider the inflation sector to be assisted by a separate hidden sector responsible for supersymmetry breaking[3]. We consider the hidden sector to be described by a supersymmetric gauge theory similar to the one considered in the ISS model of dynamic supersymmetry breaking [259]. Recently a proposal [289, 290] of generating chaotic potential for a strongly interacting supersymmetry gauge theory is analysed which leads to a fractional chaotic inflation. However in our approach we consider the SQCD sector to provide a deformation to the sneutrino contribution to the minimal chaotic inflation, and at the end of inflation, this serves as the hidden sector of the supersymmetry breaking. The effective supersymmetric breaking in the standard supersymmetric gauge and matter sector (MSSM or its extension) requires a mediation mechanism from this hidden sector. Here it is considered to be the gauge mediation.

The ISS model is described by the $\mathcal{N} = 1$ supersymmetric $SU(N_C)$ gauge theory (called the electric theory) with N_f flavors of quarks (Q) and antiquarks ($\tilde{Q}$). Λ is the strong coupling scale of this theory. Below this scale Λ, the theory is described by its magnetic dual $SU(N = N_f - N_C)$ gauge theory with N_f flavors of magnetic quarks $q_i^c, \tilde{q}_i^c$ (with $i = 1....N_f$ and $c = 1....N$). It is interesting to note that this theory is IR free, provided $N_C + 1 \leq N_f < \frac{3}{2}N_C$. The elegance of the ISS model lies in its UV completion of the theory. There also exists a $N_f \times N_f$ gauge singlet meson field $\Phi = Q\tilde{Q}/\Lambda$. With the introduction of quark mass term in the electric theory ($SU(N_c)$ gauge theory),

$$W_e = m_Q \mathrm{Tr} Q\tilde{Q}, \tag{2.22}$$

with $m_Q < \Lambda$, the IR free magnetic theory becomes

$$W_{ISS} = h\mathrm{Tr}(q\Phi\tilde{q}) - h\mu^2\mathrm{Tr}(\Phi), \tag{2.23}$$

[3]Another approach to accommodate supersymmetry breaking after chaotic inflation is exercised in [288] with an introduction of a Polonyi field.

along with the dynamical superpotential

$$W_{dyn} = N\Big(h^{N_f}\frac{\det\Phi}{\Lambda^{N_f-3N}}\Big)^{\frac{1}{N}}. \tag{2.24}$$

where $h \sim \mathcal{O}(1)$ and $\mu << \Lambda$ and by duality $\mu^2 = m_Q\Lambda$. Note that there exists a $U(1)_R$ symmetry under which W_{ISS} and hence Φ carry R-charge of 2-units. R charge of $Q\bar{Q}$ combination turns out to be two as well from the relation $\Phi = Q\tilde{Q}/\Lambda$. However the R symmetry is explicitly broken by the W_{dyn} term. All the fields in this sector are considered to be even under the Z_2 symmetry considered. The Kähler potential is considered to be canonical in both electric and magnetic theories. It is shown in [256] that there exists a local minimum given by

$$\langle q\rangle = \langle\tilde{q}^T\rangle = \mu\begin{pmatrix} 1_N \\ 0_{N_f-N}\end{pmatrix},\ \langle\Phi\rangle = 0, \tag{2.25}$$

with vacuum energy $V_{ISS} = N_c|h^2\mu^4|$. Supersymmetry is broken in this minimum by the rank condition. Note that W_{dyn} is almost negligible around $\Phi = 0$. The interplay between second term in Eq.(2.23) and the W_{dyn} suggests an existence of a SUSY preserving vacuum at

$$\langle q\rangle = \langle\tilde{q}^T\rangle = 0,\ \langle\Phi\rangle = \frac{\mu}{h}(\epsilon^{\frac{N_f-3N}{N_c}})^{-1}1_{N_f}, \tag{2.26}$$

where $\epsilon = \frac{\mu}{\Lambda}$ and the corresponding vacuum energy $V_0 = 0$. With $\epsilon << 1$, it was shown in [256] that the local minima in Eq.(2.25) is a metastable one.

2.4 Interaction between neutrino and SQCD sectors

We consider W_N as the superpotential describing the inflation with N_1 playing the role of inflaton. In this section our endeavor is to couple the inflaton with the SQCD sector. We assume that the two sectors can communicate with each other only through gravity. The lowest dimensional operator consistent with the set-up is therefore given by,

$$W_{\rm Int} = \beta\frac{N_1^2{\rm Tr}(Q\tilde{Q})}{M_P}, \tag{2.27}$$

where β is a coupling constant. We consider β to be much less than unity. Similar to W_{ISS}, $W_{\rm Int}$ also respects the $U(1)_R$ and hence linear in ${\rm Tr}(Q\tilde{Q})$ having R-charge 2. Among N_1 and N_2, it is therefore the N_1 field only which can couple (N_2 carries 2 units of R-charge) with the ISS sector. Since the interaction between the two sectors are assumed to be mediated by gravity only, the interaction term is expected to be M_P suppressed. Hence $W_{\rm Int}$ in Eq.(2.27) serves as

the minimal description of the interaction between the two sectors. Being a shift-symmetry breaking parameter, the origin of β can be explained with the introduction of another spurion field z_2 which transforms as $z_2 \to \frac{N_1^2}{(N_1+C)^2} z_2$. We consider z_2 to be even under the Z_2 symmetry and it does not carry any R charge. On the other hand, $Q\tilde{Q}$ combination is even under Z_2. We introduce another discrete symmetry Z_4 under which z_2 carries a charge i as well as $Q\tilde{Q}$ carrying charge $-i$. Hence m_Q also carries a Z_4 charge i as seen from Eq.(2.22). Application of this symmetry forbids dangerous term like $\frac{(z_2 N_1^2) z_1 N_1 N_2}{M_P^3}$. Hence a superpotential involving $z_1 N_1^2$ can be obtained as

$$W_{\rm Int} = \frac{{\rm Tr}(Q\tilde{Q})}{M_P}\Big[\frac{z_2 N_1^2}{M_P} + b_5 \frac{(z_2 N_1^2)^5}{M_P^1 2} + ...\Big], \tag{2.28}$$

where b_5 corresponds to respective coupling. Terms involving quadratic, cubic, and quartic powers of $(z_2 N_1^2)$ are not allowed from the Z_4 charge assignment as considered[4]. Therefore β is obtained through $\beta = \langle z_2 \rangle / M_P$. Note that with $\beta \sim 10^{-3}$ (as we will get soon), terms with b_5 and higher orders are negligibly small.

Note that this interaction term in addition to the quark mass term m_Q present in W_e (see Eq.(2.22)), generates an effective mass for the electric quarks, $m'_Q = \beta \frac{N_1^2}{M_P} + m_Q$. Here we are particularly interested in the case when the effective mass of the quarks, m'_Q, becomes larger than the cut-off scale Λ, *i.e.* when $m'_Q >> \Lambda$. Since m_Q is considered to be less than Λ in the ISS set-up, this situation can be achieved when the inflaton field N_1 satisfies, $N_1 > [\Lambda M_P/\beta]^{1/2}$. These heavy quarks can then be integrated out [259] to form an effective theory with a field dependent dynamical scale, $\Lambda_{\rm eff}(N_1)$. As all the quarks are getting large masses, the effective theory becomes a pure gauge theory with no flavors. $\Lambda_{\rm eff}$, can be determined by the standard scale matching of the gauge couplings of two theories at an energy scale $E = m'_Q$. With g_{N_c,N_f} and $g_{N_c,0}$ are the gauge couplings of the $SU(N_c)$ gauge theory with N_f flavors of quarks $(Q, \tilde{Q})$ $(E > m'_Q)$ and pure gauge theory with $N_f = 0$ $(E < m'_Q)$ respectively, the condition $g_{N_c,N_f}(m'_Q) = g_{N_c,0}(m'_Q)$ gives

$$\Big(\frac{m'_Q}{\Lambda}\Big)^b = \Big(\frac{m'_Q}{\Lambda_{\rm eff}}\Big)^{b_{eff}}, \tag{2.29}$$

where $b = 3N_c - N_f$ and $b_{eff} = 3N_c$ are the respective beta functions of gauge couplings of the two theories. Λ_{eff} in our set up turns out to be

$$\Lambda_{\rm eff} \simeq \Big(\frac{\beta N_1^2}{M_P}\Big)^{(1-p)} \Lambda^p, \tag{2.30}$$

[4]With this new Z_4 symmetry, term like $\frac{(z_2 N_1^2) z_1 N_1 N_2}{M_P^9}$ will be allowed in $W_{\rm Int}$. However contribution of this term will be negligibly small.

where $p = \frac{b}{b_{\rm eff}}$ and m'_Q is mostly dominated by $\frac{\beta N_1^2}{M_P}$ term (*i.e.* when $N_1 >> [\Lambda M_P/\beta]^{1/2}$ and m_Q being much smaller than Λ can be neglected). As all the flavors are integrated out, the superpotential describing the effective theory is generated via gaugino condensation and is given by[259]

$$W_{\rm Int}^{\rm eff} = N_c \Lambda_{\rm eff}^3 = N_c \Big(\beta \frac{N_1^2}{M_P}\Big)^{3(1-p)} \Lambda^{3p}. \tag{2.31}$$

Below we study the impact of this term on inflation governed by W_N.

2.5 Modified chaotic potential and its implications to inflationary dynamics

Here we will study the inflationary dynamics based on the superpotential,

$$W_{\rm Inf} = W_N + W_{\rm Int}^{\rm eff} = m N_1 N_2 + N_c \Big(\frac{\beta N_1^2}{M_P}\Big)^{3(1-p)} \Lambda^{3p}, \tag{2.32}$$

when $N_1 >> [\Lambda M_P/\beta]^{1/2}$. Note that it indicates a modification of the chaotic inflationary potential V_χ obtained from W_N only. In this section, we will study the outcome of this modified superpotential in terms of prediction of parameters involved in inflation. Depending upon p, the superpotential may contain fractional powers of N_1. In Ref [291], superpotential with non-integer power of superfields has been studied. It is shown there that the form of Kähler potential remains same irrespective of integer or non-integer power of superfields involved in the superpotential.

The Kähler potential is considered to be the same as K_N in Eq.(2.18). We can write

$$N_1 = \frac{\chi + i\eta}{\sqrt{2}} \text{ and } N_2 = \frac{\sigma + i\delta}{\sqrt{2}}. \tag{2.33}$$

As discussed in section 2.2, we choose χ, the real component of N_1, as inflaton. Using Eq.(2.18,2.21) and Eq.(2.32), the scalar potential involving χ and σ is given by

$$\begin{aligned} V_{\rm Inf}(\tilde{\chi}, \tilde{\sigma}) = M_P^4 e^{\tilde{\sigma}^2/2} \Big[& \frac{\tilde{m}^2 \tilde{\sigma}^2}{2} + \frac{\tilde{m}^2 \tilde{\chi}^2}{2} \Big(1 - \frac{\tilde{\sigma}^2}{2} + \frac{\tilde{\sigma}^4}{4}\Big) \\ & + 3(1-p) A \tilde{\chi}^{5-6p} \tilde{\sigma} + A \tilde{\chi}^{7-6p} \Big(- \frac{\tilde{\sigma}}{2} + \frac{\tilde{\sigma}^3}{8}\Big) \\ & + \frac{9}{2\tilde{m}^2}(1-p)^2 A^2 \tilde{\chi}^{10-12p} + \frac{A^2}{2\tilde{m}^2} \tilde{\chi}^{12-12p} \Big(- \frac{3}{8} + \frac{\tilde{\sigma}^2}{16}\Big) \Big], \end{aligned} \tag{2.34}$$

where $A = \frac{\beta^{3(1-p)}\tilde{m}N_c\tilde{\Lambda}^{3p}}{2^{1-3p}}$ and tilde indicates that the corresponding variable or parameter is scaled in terms of M_P, *e.g.* $\tilde{\sigma} = \frac{\sigma}{M_P}$. We follow this notation throughout this section only. As the electric quarks degrees of freedom $(Q, \tilde{Q})$ are integrated out we will not consider quarks anymore, as long as $N_1 >> \sqrt{\frac{\Lambda M_P}{\beta}}$. Now one can wonder what happened to other two fields η and δ. Due to the presence of e^K factor in the scalar potential V_F the effective mass of η during inflation will be large compared to inflaton mass($m_\eta^2 \sim 6H_{\rm Inf}^2 + m^2$) and hence it will quickly settle down to origin. We have checked numerically that the other field δ also settles at origin during inflation, having mass more than the Hubble.

In this case, dynamics of inflation belongs to $\tilde{\chi} - \tilde{\sigma}$ plane. Note that in case of standard chaotic inflation as discussed in section 2.2, the $\tilde{\sigma}$ field is considered to be at origin during inflation. Contrary to that, the dynamic modification of the scalar potential governed by $W_{\rm Int}^{\rm eff}$ forces the $\tilde{\sigma}$ field to have a nonzero vacuum expectation value in our case. Similar type of scenarios are discussed in [233, 283]. In order to get $\langle\tilde{\sigma}\rangle$ in terms of $\tilde{\chi}$, derivative of the scalar potential with respect to $\tilde{\sigma}$ and yields

$$\begin{aligned}\frac{\partial V_{\rm Inf}}{\partial\tilde{\sigma}} = e^{\frac{\tilde{\sigma}^2}{2}}\Big[&-\frac{A\tilde{\chi}^{5-6p}}{2}(\tilde{\chi}^2 - 6 + 6p) + \tilde{\sigma}\Big\{\tilde{m}^2 + \tilde{\chi}^{10-12p}\frac{A^2}{2\tilde{m}^2}\Big(9 - 18p + 9p^2 - \frac{\tilde{\chi}^2}{4}\Big)\Big\} \\ &+\tilde{\sigma}^2\Big\{A\tilde{\chi}^{5-6p}\Big(3 - 3p - \frac{\tilde{\chi}^2}{8}\Big)\Big\} + \tilde{\sigma}^3\Big\{\frac{\tilde{m}^2}{2}\Big(1 + \frac{\tilde{\chi}^2}{2}\Big) + \frac{\tilde{\chi}^{12-12p}}{32}\frac{A^2}{\tilde{m}^2}\Big\} \\ &+\tilde{\sigma}^4\Big\{\tilde{\chi}^{7-6p}\frac{A}{8}\Big\} + \tilde{\sigma}^5\Big\{\frac{\tilde{\chi}^2\tilde{m}^2}{8}\Big\}\Big]. \quad (2.35)\end{aligned}$$

In order to minimize the scalar potential, we equate the above expression to zero (*i.e.* $\frac{\partial V_{\rm Inf}(\tilde{\chi},\tilde{\sigma})}{\partial\tilde{\sigma}}$=0). It reduces to a fifth order polynomial equation in $\tilde{\sigma}$. At this point we consider a specific value of p $(= 1 - \frac{N_f}{3N_c})$, the choice of which is guided by the construction of the ISS framework and a possible realization of $U(1)_R$ breaking through baryon deformation as we will discuss in section 2.8. Comparing the relative magnitudes of the terms involved in the fifth order polynomial and considering $\tilde{\sigma}$ to be sub-Planckian, we solve the equation for $\tilde{\sigma}$ in a perturbative way, the details of which is given in Appendix A.1. Once $\langle\tilde{\sigma}\rangle$ is obtained in terms of $\tilde{\chi}$, we replace $\tilde{\sigma}$ by its VEV in Eq.(2.34) and potential responsible for inflation now becomes function of $\tilde{\chi}$ only. Due to its very complicated functional dependence on $\tilde{\chi}$, we have not presented $V_{\rm Inf}$ here. Instead in Fig. 2.1 we have depicted the potential $V(\tilde{\chi})$ in terms of $\tilde{\chi}$ for $p = 4/7$ (indicated by dashed line). Note that this potential is indeed flatter compared to the standard sneutrino chaotic inflation potential [232], indicated in Fig. 2.1 by the solid line. For completeness a shift symmetry breaking parameter (α) in the Kähler potential can also be introduced. The modified Kähler

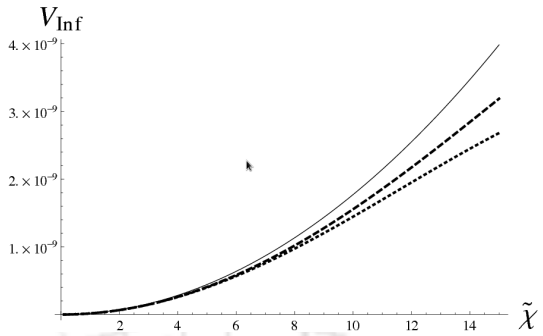

FIGURE 2.1: Examples of inflation potential ($V_{\rm Inf}$) against $\tilde{\chi}$ are presented. The solid, large-dashed and small-dashed curves represent (I) minimal chaotic potential with $V_{\rm Inf}(\tilde{\chi}) = \frac{1}{2}\tilde{m}^2\tilde{\chi}^2$, (II) modified $V_{\rm Inf}(\tilde{\chi})$ obtained from our set-up with $\alpha = 0$ and (III) modified $V_{\rm Inf}(\tilde{\chi})$ with $\alpha = 7 \times 10^{-4}$ respectively.

potential will look like as

$$K = K_N - \alpha\frac{(N_1 + N_1^\dagger)^2}{2}, \tag{2.36}$$

with $\alpha << 1$. The scalar potential in Eq.(2.34) will be modified and takes a further complicated form. In this case we obtain the scalar potential as a function of $\tilde{\chi}$ in a similar way. In Fig. (2.1) we also plot $V_{\rm Inf}(\tilde{\chi})$ including the nonzero value of $\alpha\{\sim 7 \times 10^{-4}\}$ represented by dashed line. It is to be noted that introduction of α makes the shape of $V_{\rm Inf}(\tilde{\chi})$ even flatter.

2.6 Results

End of inflation occurs when slow roll parameters become unity *i.e.* $\epsilon, \eta \simeq 1$. Solving the equalities we find inflaton field value at the end of inflation $\chi_{end} \simeq \sqrt{2}M_P$. Now it is visible from $V_{\rm Inf}(\chi, \sigma)$ and Eq.(2.35) that we are left with two free parameters m and Λ once p is fixed. The value of β is taken to be $\mathcal{O}(10^{-3})$ so that it satisfies $\Lambda < m'_Q < M_P$. We have performed a scan over these parameters to estimate values of n_s and r using Eq.(1.36). Few of our findings are tabulated in Table 2.1. We find m is mostly restricted by the value of curvature perturbation, while Λ helps decreasing r. We consider m to be below Λ. Also, we consider

Λ	m	χ^*	r	n_s
8.90×10^{-4}	5.75×10^{-6}	14.95	0.099	0.965
1.05×10^{-3}	5.47×10^{-6}	14.55	0.079	0.961
1.18×10^{-3}	4.91×10^{-6}	13.92	0.052	0.954

TABLE 2.1: Predictions for r, n_s and χ^* are provided for sets of values of parameters m, Λ involved in $V_{\rm Inf}$. The dataset corresponds to $N_e = 60$, $\alpha = 0$, $p = 4/7$, $\beta = 1.5 \times 10^{-3}$ and values of (m, Λ, χ^*) are in M_P unit.

effects of non-zero α which is provided in Table 2.2.

α	m	χ^*	r	n_s
0.0003	5.390×10^{-6}	14.271	0.069	0.960
0.0005	5.300×10^{-6}	14.067	0.063	0.959
0.0007	5.156×10^{-6}	13.841	0.055	0.957

TABLE 2.2: Predictions for r, n_s and χ^* are provided for sets of values of parameters m and Λ involved in $V_{\rm Inf}$. The dataset corresponds to $N_e = 60$, $\Lambda = 1.05 \times 10^{-3} M_P$, $p = 4/7$, $\beta = 1.5 \times 10^{-3}$ and values of (m, χ^*) are in M_P unit.

We find from Table 2.1 that corresponding to $\Lambda = 1.05 \times 10^{-3} M_P$, values of $r \sim 0.079$ and $n_s \sim 0.96$ can be achieved with $m \sim 5.5 \times 10^{-6} M_P$. To compare, with the same Λ, a somewhat lower value of $r \sim 0.069$ and $n_s \sim 0.96$ are obtained with $m = 5.5 \times 10^{-6} M_P$ and $\alpha = 0.0003$. In obtaining Table 2.2, we have kept $\frac{\alpha \chi^2}{M_P^2} << 1$. In Fig. 2.2, we indicate the respective points of Table 2.1 by black dots and note that those points fall within the 2σ allowed range of $n_s - r$ plot from PLANCK 2015 [39, 102] safely. The solid line for $N_e = 60$ indicates the possible set of points (including the ones from Table 2.1) that describe n_s and r for different values of Λ.

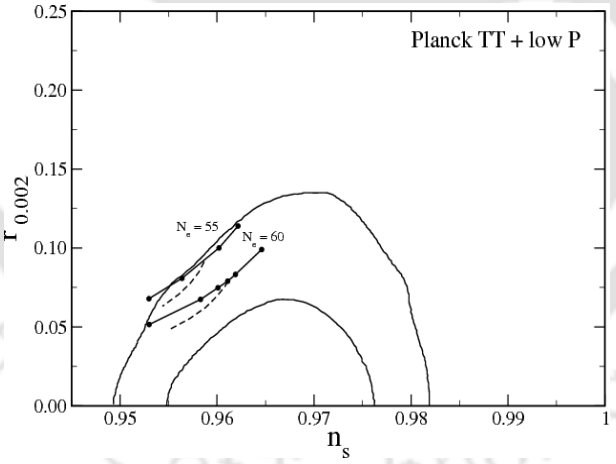

FIGURE 2.2: Predictions for n_s and r as obtained including dataset from the modified chaotic inflation model (from Table 2.1) indicated by dark dots for $N_e = 60$. A solid line joining them represents the prediction of n_s and r while Λ is varied. Similar predictions for $N_e = 55$ are also included. The dashed lines correspond to the predictions by varying α while value of Λ is fixed at $1.1 \times 10^{-3} M_P$ (for $N_e = 55$) and $1.05 \times 10^{-3} M_P$ (for $N_e = 60$).

Similarly the other solid line corresponds to the set of points for $N_e = 55$. The dashed lines describe the effect of introducing α. Now we can have an estimate of the mass of the δ field (m_δ) during inflation. For $\Lambda = 1.05 \times 10^{-3} M_P$, $m = 5.5 \times 10^{-6} M_P$ we found numerically $\frac{m_\delta}{H_{\rm Inf}} =\sim 1.2$ during inflation. This ensures δ field to be stabilized at origin. On the other hand, $\frac{m_\sigma}{H_{\rm Inf}}$ is found

to be ~ 2.5 which indicates that the fluctuation of σ-field about $\langle\sigma\rangle$ (in terms of χ) is almost negligible.

2.7 Dynamics after inflation

Once the inflation is over, the field χ rolls down along the path as shown in Fig. 2.1 and $\langle\sigma\rangle$ also follows its VEV which is χ dependent. Note that at the end of inflation, N_1 still satisfies $N_1 >> \sqrt{\frac{\Lambda M_P}{\beta}}$ condition. However once $N_1 < \Lambda$ is realized, we need to relook into the term responsible for dynamic modification of chaotic inflation. As in this situation $m'_Q << \Lambda$, the electric quarks $(Q, \tilde{Q})$ can not be integrated out anymore and we can use the magnetic dual description of the ISS sector similar to Eq.(2.23) and (2.24). Therefore the superpotential for the ISS, describing the magnetic dual theory and the RH neutrino becomes

$$W_m = h\mathrm{Tr}(q\Phi\tilde{q}) - h\mu^2\mathrm{Tr}\Phi - \frac{\beta N_1^2\mathrm{Tr}(\Phi)\Lambda}{M_P} + mN_1N_2. \tag{2.37}$$

To discuss what happens to the N_1 and the fields involved in SUSY breaking sector, let us calculate the F-terms as follows

$$F_{\Phi_{ij}} = h\tilde{q}_c^i q_j^c - \Big(h\mu^2 + \frac{\beta\Lambda N_1^2}{M_P}\Big)\delta_{ij}, \tag{2.38}$$

$$F_{q_i} = h\Phi_j^i\tilde{q}^j;\ F_{\tilde{q}^j} = hq_i\Phi_j^i, \tag{2.39}$$

$$F_{N_1} = -\frac{2\beta\Lambda}{M_P}N_1 Tr(\Phi) + mN_2, \tag{2.40}$$

$$F_{N_2} = mN_1. \tag{2.41}$$

Similar to the original ISS model, here also all the F-terms can not be set to zero simultaneously and hence the supersymmetry breaking is realized. The scalar potential becomes

$$\begin{aligned} V = (N_f - N_c)|hq\tilde{q} - h\mu^2 - \frac{\beta N_1^2\Lambda}{M_P}|^2 + N_c|h\mu^2 + \frac{\beta N_1^2\Lambda}{M_P}|^2 \\ +|hq\Phi|^2 + |h\Phi\tilde{q}|^2 + |mN_2 - \frac{2\beta N_1\mathrm{Tr}(\Phi)\Lambda}{M_P}|^2 + m^2|N_1|^2. \end{aligned} \tag{2.42}$$

Supergravity corrections are not included in this potential as below the scale Λ, the SUGRA corrections become negligible. As long as N_1 remains nonzero, the minimum of q, $\tilde{q}$, Φ and N_2 are given by

$$\langle q\rangle = \langle\tilde{q}\rangle = \sqrt{\mu^2 + \frac{\beta\Lambda N_1^2}{hM_P}}\begin{pmatrix} 1_{N_f-N_c} \\ 0_{N_c}\end{pmatrix},\ \langle\Phi\rangle = 0,\ \langle N_2\rangle = 0. \tag{2.43}$$

A point related to $\langle\Phi\rangle$ is pertinent here. In the ISS set-up, a classical flat direction is present in a smaller subspace of Φ which is essentially lifted by the ColemanWeinberg (CW) [256] correction and $\langle\Phi\rangle = 0$ is achieved. In our set-up there exists a supergravity influenced mass $\sim \frac{m^2 N_1^2}{M_P^2}$ for all the components of Φ once a canonical Kähler potential is assumed. This helps Φ to settle at origin. However once N_1 moves to its own minimum which is at $N_1 = 0$, this induced mass term vanishes and at that stage, CW correction becomes important to lift the flatness. For our purpose, we consider $\langle\Phi\rangle$ to be at zero which serves as the local minimum of the theory.

We will now concentrate on the potential involving N_1. Assuming all other fields are stabilized at their VEV (with $\langle N_2\rangle = 0$ as $\langle\Phi\rangle = 0$) the scalar potential involving N_1 becomes

$$V_{N_1} = N_c|h\mu^2 + \frac{\beta N_1^2 \Lambda}{M_P}|^2 + m^2|N_1|^2. \tag{2.44}$$

Splitting N_1 into real and imaginary components we get

$$\begin{aligned} V_{N_1}(\chi,\eta) =& N_c h^2|\mu|^4 + (\chi^4 + \eta^4 + 2\chi^2\eta^2)\frac{N_c\Lambda^2\beta^2}{4M_P^2} + \\ & \eta^2(\frac{m^2}{2} - \frac{hN_c\beta\mu^2\Lambda}{M_P}) + \chi^2(\frac{m^2}{2} + \frac{hN_c\beta\mu^2\Lambda}{M_P}). \end{aligned} \tag{2.45}$$

By equating $\frac{\partial V(\chi,\eta)}{\partial\eta}$ with zero, we find $\langle\eta\rangle = 0$ provided $m^2 > \frac{2hN_c\beta\mu^2\Lambda}{M_P}$. This condition is easily satisfied in our analysis for the allowed range of m, Λ and N_c with the observation that μ can be at most $\sim 10^{12}$ GeV for gravity mediated supersymmetry breaking and $h \sim \mathcal{O}(1)$. In case of gauge mediatioin μ can be even smaller. Therefore setting $\eta = 0$ Eq.(2.45) becomes

$$V_\chi = N_c h^2|\mu|^4 + \chi^4\frac{N_c\beta^2\Lambda^2}{4M_P^2} + \chi^2(\frac{m^2}{2} + \frac{hN_c\beta\mu^2\Lambda}{M_P}). \tag{2.46}$$

It clearly shows that $\chi = 0$ is the minimum of the potential with the vacuum energy $V_0 = N_c h^2|\mu|^4$. So when N_1 settles to zero and reheats, the SQCD sector is essentially decoupled as $W_{\rm Int}$ vanishes with $N_1 = 0$. At this stage the ISS sector stands for the supersymmetry breaking in the metastable minima described by Eq.(2.25) and $\langle\chi\rangle = 0$. Reheat will depend on the coupling of N_1 with other SM fields.

2.8 Dynamical breaking of $U(1)_R$

In the construction of the ISS picture of realizing supersymmetry breaking dynamically, $U(1)_R$ symmetry plays an important role. The superpotential W carries R-charge of two units. The

Φ field being linear in the superpotential must also carry the R-charge 2 and it is not broken as $\langle\Phi\rangle = 0$. A lot of exercises have been performed to achieve R-symmetry breaking in order to give mass to the gauginos. One such interesting approach is through the baryon deformation of W_m suggested by [281]. In [281] the authors considered the superpotential (for the magnetic theory)

$$W = \Phi_{ij} q_i \tilde{q}_j - \mu^2 \Phi_{ij} + m_q \epsilon^r_a \epsilon^s_b q^a_r q^b_s, \tag{2.47}$$

with $N_f = 7$ and $N_c = 5$, where $r,\ s = 1, 2$ and $i,\ j = 1, .., 7$. R-charges of q, $\tilde{q}$ and Φ are provided in Table 2.3 and reason behind this choice is elaborated in Appendix A.2. With the specific choice of N_f and N_c, the last term is a singlet under the gauge group in the magnetic theory. It represents the baryon deformation, introduction of which shifts the $\langle\Phi\rangle$ to a nonzero value $\sim m_q$ and thereby breaking R-symmetry spontaneously. In realizing this set-up it was assumed the associated global symmetry $SU(N_f = 7)$ is broken down to $SU(5) \times SU(2)$ and the $SU(5)$ after gauging can therefore be identified with the parent of the Standard Model gauge group. We follow this suggestion for breaking the $U(1)_R$ and argue that this approach and the conclusion of [281] are effectively unaltered by the additional interaction between the SQCD-sector and the inflation sector. In view of Eq.(2.47), the charges of q, $\tilde{q}$ and Φ under the discrete symmetries introduced in our framework are provided in Table 2.3.

Fields	q	$\tilde{q}$	Φ
$U(1)_R$	1	-1	2
Z_2	1	1	1
Z_4	1	$-i$	$-i$
Z'_4	1	1	1

TABLE 2.3: $U(1)_R$, Z_2, Z_4 and Z'_4 charges of various fields involved in the modified ISS model.

With the introduction of the additional interaction term ($W_{\rm Int}$), we can define an effective μ_{eff} in the superpotential with $\mu^2_{eff} = \mu^2 + \Lambda \frac{N_1^2}{M_P}$. We find the minimal choice as in [281] $N_f = 7$ and $N_c = 5$, does not provide enough modification (or flatness) in terms of the inflaton potential. So we have chosen $N_f = 9$ and $N_c = 7$ so that the gaug group in the magnetic theory remains $SU(2)$ as in [281]. The global symmetry $SU(9)$ is expected to be broken into $SU(2) \times SU(7)$ explicitly. Taking both these modifications into account, we expect the conclusions of [281] are essentially remain unchanged, *i.e.* $\langle\Phi\rangle$ is shifted by an amount $\sim m_q \sim \mathcal{O}(\mu)$ and hence gauginos become massive. The detailed discussion of the $U(1)_R$ breaking is beyond the scope of this paper. Note that this sort of mechanism for breaking $U(1)_R$ holds for $\mu \geq 10^5$ TeV as found in [281]. The upper limit on μ can be $\sim 10^{12}$ GeV, where gravity mediation dominates

over gauge mediation. This range of μ is consistent in satisfying $m^2 > \frac{2N_c\beta\mu^2\Lambda}{M_P}$ relation also which keeps the $\langle\eta\rangle$ at origin as discussed in section 2.7.

2.9 Neutrino masses and mixing

We will discuss reheating and generation of light neutrino masses through the superpotential

$$W = W_m + m_3 N_3^2 + h_{i\alpha} N_i L_\alpha H_u. \tag{2.48}$$

W_m is as described in Eq.(2.37). The second and third terms represent the mass term for the third RH neutrino and the neutrino Yukawa couplings with all three RH neutrinos respectively. Note that the superpotential respects the $U(1)_R$ symmetry and therefore the choice of R-charges of the $SU(2)_L$ lepton doublets further restricts the Yukawa interaction terms.

Fields	N_1	N_2	N_3	L_1	L_2	L_3	$H_{u,d}$	z_1	z_2	z_3
$U(1)_R$	0	2	1	2	0	0	0	0	0	0
Z_2	-1	-1	1	1	-1	-1	1	1	1	-1
Z_4	1	1	1	1	1	1	1	1	i	1
Z_4'	1	1	1	$-i$	1	1	1	1	1	i

TABLE 2.4: $U(1)_R$, Z_2, Z_4 and Z_4' charges of the RH neutrinos, Higgses and Lepton doublets.

With one such typical choice of R-charges (only) specified in Table-2.4, the allowed Yukawa terms are given by,

$$W_Y \supset h_{11} N_1 L_1 H_u + h_{22} N_2 L_2 H_u + h_{23} N_2 L_3 H_u. \tag{2.49}$$

The coefficient h_{11} can be explained through the vev of another spurion z_3 which transforms similar to z_1 under shift symmetry while odd under the Z_2 symmetry considered. With a term in the superpotential $(y_1 z_3 N_1 L_1 H_u)/M_P$ then generates $h_{11} = y_1\langle z_3\rangle/M_P$. Here we incorporate another discrete symmetry Z_4' under which z_3 has charge i and L_1 carries $-i$. All the other fields transform trivially under Z_4' as seen from Table 2.4. The new Z_4' helps to disallow the unwanted terms[5] like $\frac{(z_3 N_1) z_1 N_1 N_2}{M_P^2}$ and $\frac{z_3 N_1 \mathrm{Tr} Q\bar{Q}}{M_P}$.

[5]Even with the new Z_4', $\frac{(z_3 N_1)^4 z_1 N_1 N_2}{M_P^8}$ term will be allowed, however this term turns out to be very small.

The superpotential in Eq.(2.37) and Eq.(2.48) and W_Y in Eq.(2.49) determine the structure of the RH neutrino mass matrix and the Dirac neutrino mass matrix as

$$M_R = \begin{pmatrix} \varepsilon_m & m & 0 \\ m & 0 & 0 \\ 0 & 0 & m_3 \end{pmatrix} \; ; m_D = \langle H_u \rangle \begin{pmatrix} h_{11} & 0 & 0 \\ 0 & h_{22} & h_{23} \\ 0 & 0 & 0 \end{pmatrix}, \tag{2.50}$$

with $\varepsilon_m = \frac{\beta\langle\Phi\rangle\Lambda}{M_P} << m$. Here we have incorporated the $\langle\Phi\rangle$ related to the deformation as discussed in section 2.8.

Light neutrino mass-matrix can therefore be obtained from the type-I seesaw [21] contribution $m_\nu = m_D^T \frac{1}{M_R} m_D$ and is given by

$$m_\nu = \frac{\langle H_u \rangle^2}{m} \begin{pmatrix} 0 & h_{11}h_{22} & h_{11}h_{23} \\ h_{11}h_{22} & -\frac{\varepsilon_m h_{22}^2}{m} & -\frac{\varepsilon_m h_{22}h_{23}}{m} \\ h_{11}h_{23} & -\frac{\varepsilon_m h_{22}h_{23}}{m} & -\frac{\varepsilon_m h_{22}^2}{m} \end{pmatrix}. \tag{2.51}$$

Note that all the terms involving ε_m/m are much smaller compared to the 12(21) and 13(31) entries of m_ν. Once the terms proportional to ε_m/m are set to zero, m_ν coincides with the neutrino mass matrix proposed in [292] leading to an inverted hierarchical spectrum of light neutrinos. The above texture of m_ν in Eq.(2.51) then predicts

$$m_{\nu_1} \simeq m_{\nu_2} \simeq \sqrt{2}\frac{\kappa h_{11} v_u^2}{m}; \; m_{\nu_3} \simeq \frac{\kappa^2 v_u^2}{2m}\left(\frac{\varepsilon_m}{m}\right), \tag{2.52}$$

$$\Delta m_{12}^2 \simeq \frac{\kappa^3 h_{11} v_u^4}{m^2}\left(\frac{\varepsilon_m}{m}\right) \text{ and } \Delta m_{23}^2 \simeq \frac{2\kappa^2 h_{11}^2 v_u^4}{m^2}, \tag{2.53}$$

where $h_{22} \simeq h_{23} = \kappa$ is assumed for simplicity and $\langle H_u \rangle = v_u$. It also indicates a bi-maximal mixing pattern in solar and atmospheric sectors along with $\theta_{13} \simeq \frac{\varepsilon_m}{m}\frac{\kappa}{h_{11}}$.

Now as m is essentially determined from the inflation part in our scenario, we find h_{11} of order $\sim \mathcal{O}(10^{-2})$ to get correct magnitude of $\Delta m_{23}^2 \simeq 2.5 \times 10^{-3}$ eV^2 [293] with $v_u = 174$ GeV and $\kappa = 1$. At first sight it is tantalizing to note that with $\frac{\varepsilon_m}{m} << 1$ and we could also accommodate Δm_{12}^2 ($\simeq 7 \times 10^{-5}$ eV^2 [293]). However $\frac{\varepsilon_m}{m} \simeq \frac{\beta\Lambda}{m}\frac{\mathrm{Tr}\langle\Phi\rangle}{M_P} \sim \frac{\mu}{M_P} \leq \mathcal{O}(10^{-6})$ and it turns out to be too small (a value of $\frac{\varepsilon_m}{m} \sim 10^{-2}$ could fulfill the requirement) to explain the solar splitting correctly. Therefore small but relatively larger entries are required in place of $\left(\frac{\varepsilon_m}{m}\right)$ terms in m_ν [294]. A possible source of these terms could arise in our case from higher order R-symmetry breaking terms. The mixing angles θ_{12}, θ_{13} can be corrected from the contribution in the charged lepton sector. We do not explore this possibility in detail here. It could as well

be the effect of renormalization group evolutions as pointed out by [294], or even other sources (*e.g.* type-II contribution as in [295]) of neutrino mass.

2.10 Reheating

As soon as Hubble parameter becomes less than the mass of the inflaton, N_1 starts to oscillate around its minimum and universe reheats. The estimate of h helps us determining the reheat temperature. The decay of N_1 is governed through the W in Eq.(2.48). The decay width therefore is estimated to be

$$\Gamma_{N_1} = \frac{(2\kappa^2 + h_{11}^2)}{8\pi} m, \tag{2.54}$$

neglecting the effect of ε_m term. The corresponding reheat temperature is obtained as

$$T_{RH} = \Big(\frac{45}{2\pi^2 g_*}\Big)^{1/4} \sqrt{\Gamma_{N_1} M_P} \simeq 4 \times 10^{14} \text{ GeV}, \tag{2.55}$$

where $m \sim 10^{-6} M_P$ is considered and $\kappa \sim \mathcal{O}(1)$, as obtained from the discussion of the previous section. Such a high reheating temperature poses a threat in terms of over abundance of thermally produced gravitinos[6]. Their abundance is mostly proportional to the reheat temperature [298],

$$Y_{3/2} \simeq 2 \times 10^{-9} \Big(\frac{T_{RH}}{10^{13} \text{ GeV}}\Big), \tag{2.56}$$

where $Y_{3/2} = \frac{n_{3/2}}{s}$ with $n_{3/2}$ as the number density of gravitinos and s is the entropy density. These gravitinos, if massive, then decays into the lightest supersymmetric particles (LSP) and can destroy the predictions of primordial abundance of light elements. On the other hand, if gravitino is the LSP, the reheating temperature can not be as high as mentioned in our work. This problem can be circumvented if the gravitinos are superlight, *e.g.* $m_{3/2} \sim 16$ eV [299]. Such a gravitino can be accommodated in the gauge mediated supersymmetry breaking. In our set-up, μ is the scale which in turn predicts the gravitino mass through $m_{3/2} \simeq \frac{\mu^2}{\sqrt{3} M_P}$. Therefore with $\mu \sim 10^5$ GeV, such a light gravitino mass can be obtained. Another way to circumvent this gravitino problem is through the late time entropy production [300]. Apart from these possibilities one interesting observation by [301] could be of help in this regard. The author in [301] have shown that once the messenger mass scale (in case of gauge mediation of supersymmetry breaking) falls below the reheat temperature, the relic abundance of thermally produced gravitinos becomes insensitive to T_{RH} and a large $T_{RH} \sim 10^{13-14}$ GeV can be realized.

[6]Note that the chaotic inflation is free from gravitino problem indeed for the non-thermal decay of inflaton [296, 297].

Finally we make brief comments on leptogenesis in the present scenario. Considering $m_3 << m$, N_3 would contribute mostly for the lepton asymmetry production. The CP asymmetry generated can be estimated as [302]

$$\epsilon_3 = \frac{3}{8\pi v_u^2} \frac{1}{(\hat{m}_D^\dagger \hat{m}_D)_{33}} \sum_{i=1,2} \mathrm{Im}[(\hat{m}_D^\dagger \hat{m}_D)_{i3}^2] \frac{m_3}{m}. \tag{2.57}$$

Here $\hat{m_D}$ represents the rotated Dirac mass matrix in the basis where M_R is diagonal. It is found that CP-asymmetry exactly vanishes in this case. We expect this can be cured with the introduction of higher order $U(1)_R$ symmetry breaking terms which could be introduced into m_D and M_R[7]. Then similar to [303], a non-zero lepton asymmetry through the decay of N_3 can be realized.

2.11 Chapter Summary

We have considered the superpartner of a right-handed neutrino as playing the role of inflaton. Although a minimal chaotic inflation scenario out of this consideration is a well studied subject, its simplest form is almost outside the 2σ region of recent $n_s - r$ plot by PLANCK 2015. We have shown in this work, that a mere coupling with the SQCD sector responsible for supersymmetry breaking can be considered as a deformation to the minimal version of the chaotic inflation. Such a deformation results in a successful entry of the chaotic inflation into the latest $n_s - r$ plot. Apart from this, the construction also ensures that a remnant supersymmetry breaking is realized at the end of inflation. The global $U(1)_R$ symmetry plays important role in constructing the superpotential for both the RH neutrino as well as SQCD sector. We have shown that the shift-symmetry breaking terms in the set up can be accommodated in an elegant way by introducing spurions. Their introduction, although ad hoc, can not only explain the size of the symmetry breaking but also provide a prescription for operators involving the RH neutrino superfields (responsible for inflation) in the superpotential. With the help of the R-symmetry and the discrete symmetries introduced, we are able to show that light neutrino masses and mixing resulted from the set-up can accommodate the recent available data nicely, predicting an inverted hierarchy for light neutrinos. However there still exists a scope for further study in terms of leptogenesis through the R-symmetry breaking terms.

[7] We have already mentioned about this possibility of inclusion of such (small) term in the previous section, that can correct the Δm_{12}^2 and the lepton mixing angles.

Chapter 3

EW vacuum stability and chaotic Inflation

3.1 Introduction

In the previous chapter we have studied the dynamics of successful chaotic inflation model in supersymmetric framework, where scalar partner of a superfield serve the role of inflaton. Here, in this chapter (based on [304]) we will study non-supersymmetric version of chaotic inflation and how the vacuum stability problem gets affected in presence of the inflation. To accommodate chaotic inflation scenario in a non-supersymmetric framework, one has to extend the SM by an additional scalar field (ϕ). However as stated in Sec. 1.3.1, the minimal form of chaotic inflation [52] with quadratic potential ($V_\phi = \frac{1}{2}m^2\phi^2$) is disfavored by the Planck observations [39]. We have already explored one possible direction in Chapter 2 to save the model from being ruled out. There also exist several other elegant proposals [233, 265, 266, 283, 305–307]. The main idea is to flatten the chaotic inflationary potential dynamically to certain extent so that it can predict correct values of spectral index (n_s) and scalar to tensor ratio (r). One particular approach [283] seems interesting in this context where involvement of a second SM singlet scalar field χ (apart from the one, ϕ, responsible for chaotic inflation) is assumed. The effect of this additional scalar (χ) is to modify the quadratic potential V_ϕ to some extent.

On the other hand, the chaotic inflation (specifically large scale inflation models) model is also not favored in view of the uncertainty over the stability of EW vacuum. The fluctuations of the Higgs field during inflation might turn dangerous [203, 205, 208, 209, 308] for metastable Higgs vacuum. This is already mentioned in beginning of Sec. 1.3.4.1. However if the effective

mass of the Higgs boson can be made sufficiently large during inflation ($m_h^{\rm eff} > H_{\rm Inf}$), the Higgs field will naturally evolve to origin and the problem can be evaded. This large effective mass term can be generated through Higgs-inflaton interaction as suggested in [309] and the dangerous effect on Higgs vacuum stability during inflation could be avoided. Once the inflation is over, this field can then fall in the EW minimum as this minimum is close to the origin.

In view of the stability of EW vacuum issue, here (based on [304]) we investigate the possibility of using the extra scalar field (χ) of the inflation system (which modifies the chaotic inflation) to take part in resolving the Higgs vacuum stability problem both during and after inflation. During inflation, the Higgs field receives a large Hubble induced mass through its coupling with the χ field, the effect of which is to stabilize the Higgs field at origin and thereby getting rid of any kind of fluctuation during inflation. This ensures that even if the Higgs quartic coupling becomes negative at some scale Λ_I (called the instability scale), the Higgs field does not move into region beyond Λ_I during inflation. After inflation, the effective Hubble induced mass of the Higgs field decreases. So during the oscillatory phase of the inflaton field and afterwards, this can pose a threat as now the Higgs field can take values beyond Λ_I and rolls towards the unstable part of the Higgs potential [207, 310]. This instability issue can be avoided if the Higgs quartic coupling remains positive until a very large scale, *e.g.* at least upto the inflation scale. It is shown in [58, 59, 311–313] that involvement of a scalar field can indeed modify the stability condition of electroweak vacuum in the SM provided this singlet field acquires a large vacuum expectation value and couples with the SM Higgs at tree level. In our scenario, the χ field of the inflaton system may get a large vacuum expectation value which turns out to be unconstrained from inflationary point of view. Its coupling with the SM Higgs can induce a tree level shift in λ_h through the threshold correction at a scale below which this scalar would be integrated out. Hence the involvement of a second scalar in the inflaton system turns out to be effective not only in keeping the chaotic inflation in the right ballpark of the existing data from Planck 2015, but also resolves the SM vacuum instability problem by keeping the Higgs quartic coupling positive upto very high scale (even upto M_P).

Previously, connecting the inflaton and the Higgs sector to solve the vacuum stability problem has been extensively studied in [314]. They have considered hilltop and quartic inflations where inflaton itself plays the role of this singlet as at the end of inflation, the inflaton field gets a large vev. Below its mass scale the inflaton can be integrated out and the higgs quartic coupling gets a shift. The energy scale where this threshold effect occurs is therefore fixed by the inflaton mass m. Our approach however differs from [314]. Instead of hilltop or quartic inflation, here we employ the chaotic inflation with potential $V_\phi = m^2\phi^2/2$ where ϕ is the inflaton field. Following [283] we introduce another scalar field χ, the coupling of which with ϕ

provides the required modification so that the inflationary predictions fall within the allowed $n_s - r$ region by Planck 2015 [39]. In this scenario ϕ gets super-Planckian field value during inflation as in case of standard chaotic inflation. However once the inflation is over, the field ϕ is expected to oscillate about its potential minimum (which is at $\phi = 0$) and decays into the SM particles thereby reheating the universe. In [283], the χ field also has the potential minimum at $\chi = 0$. Here we suggest a modification where the χ field has a large vev (v_χ). It is found that the size of the vev is essentially unconstrained from inflation data. On the other hand this field can play important role in studying the Higgs vacuum stability issue. Apart from inflation, moduli fields [310] and the scalar singlet(s) involved in dark matter [65, 68–71, 73, 76, 315], neutrinos [227, 316–320, 322–326, 346, 347] can have effect on the Higgs vacuum stability in many different ways.

Below in Sec. 3.2 we first describe the inflation model. Then in Sec. 3.3, we state the predictions of the proposed inflationary set up. In the subsequent section, we perform the EW vacuum stability analysis in presence of the inflation. Thereafter in Sec. 3.4 we discuss about the possible reheating mechanism in post inflationary era. Finally we conclude in Sec. 3.6.

3.2 Inflation Model

Following the recent proposal in [283], we consider a variant of the above potential

$$V_{\rm I} = \frac{1}{2}m^2\phi^2 - \frac{c_1}{2}\phi^2(\chi^2 - v_\chi^2) + \frac{\lambda_\chi}{4}(\chi^2 - v_\chi^2)^2, \tag{3.1}$$

where m, c_1, λ_χ and v_χ are real and positive parameters. χ is another SM singlet scalar field which helps flattening the quadratic part of the potential involving ϕ. We assume a Z_2 symmetry under which ϕ and χ fields are odd and hence they appear quadratically in the potential. The vev of the χ field in its global minimum is v_χ. As it will turn out v_χ does not have almost any impact on the inflationary predictions[1]. Note that we have not considered the higher order terms involving ϕ, *e.g.* ϕ^4. The effect of those terms would be destructive in terms of the flatness of the potential. Therefore coefficients associated with those higher order terms in ϕ are assumed to be negligibly small[2].

[1] The sole purpose of introducing a χ vev is to contribute in the Higgs quartic coupling λ_h through threshold effect.

[2] Their absence or smallness can be argued in terms of shift symmetry of the ϕ field [328] where m serves as the shift symmetry breaking parameter.

Similar to the original chaotic inflation model with V_ϕ, here also during inflation the ϕ field takes super-Planckian value. The potential is such that the χ field receives a negative mass-squared term which depends on the field value of ϕ during inflation. Therefore χ acquires a large field value due to its coupling (through c_1 term) with the ϕ field

$$\langle\chi\rangle = \left(v_\chi^2 + \frac{c_1}{\lambda_\chi}\phi^2\right)^{1/2} \simeq \sqrt{\frac{c_1}{\lambda_\chi}}\phi = \chi_{\rm I}, \tag{3.2}$$

$\chi_{\rm I}$ is however considered to be sub-Planckian which implies $\frac{c_1}{\lambda_\chi} << 1$. Note that along the ϕ direction, V_I has a minimum at $\phi = 0$. Therefore after the slow roll period is over, the ϕ field should evolve toward its minimum. Eventually with smaller field value of ϕ, $\langle\chi\rangle$ also decreases as evident from Eq.(3.2). When ϕ finally reaches at origin, $\langle\chi\rangle$ is shifted to v_χ. The magnitude of v_χ is assumed to be below m ($v_\chi < m$) so that it does not disturb predictions [283] of the modified chaotic inflation model.

As long as the field χ is stucked at $\chi_{\rm I}$ during inflation, its mass is found to satisfy

$$m_\chi^2(\phi) = \frac{\partial^2 V}{\partial\chi^2}\Big|_{\langle\chi\rangle} = 2c_1\phi^2 + 2\lambda_\chi v_\chi^2. \tag{3.3}$$

It is to be noted that due to the super-Planckian field value of ϕ at the beginning and during inflation, $m_\chi^2(\phi)$ turns out to be (with suitable c_1 and λ_χ as we will see) greater than $H_{\rm Inf}^2 \simeq \frac{m^2\phi^2}{6M_P^2}$. Hence χ is expected to be stabilized at $\chi_{\rm I}$ quickly. We can therefore integrate out the heavy field χ as compared to the ϕ field having smaller mass and write down the effective potential during inflation in terms of ϕ only as given by

$$V_{\rm Inf} \simeq \frac{1}{2}m^2\phi^2 - \frac{c_1^2}{4\lambda_\chi}\phi^4, \tag{3.4}$$

$$= M_P^4\left[\frac{1}{2}\tilde{m}^2\tilde{\phi}^2\left(1-\alpha\tilde{\phi}^2\right)\right]. \tag{3.5}$$

For convenience the notations $\tilde{m}$ and $\tilde{\phi}$ are used to express m and ϕ in terms of M_P unit respectively. We will describe our findings in M_P unit in the rest of our discussion involving inflation. The parameter α is defined as $\alpha = \frac{c_1^2}{2\lambda_\chi\tilde{m}^2}$. We assume $\alpha\tilde{\phi}^2 << 1$ so that this correction term does not deform the standard chaotic inflation model much.

The slow roll parameters are obtained from the standard definitions as given by

$$\epsilon = \frac{1}{2}\Big(\frac{V'_{\rm Inf}}{V_{\rm Inf}}\Big)^2 = \frac{2}{\tilde{\phi}^2}\Big[\frac{1-2\alpha\tilde{\phi}^2}{1-\alpha\tilde{\phi}^2}\Big]^2,\ \eta = \frac{V''_{\rm Inf}}{V_{\rm Inf}} = \frac{2}{\tilde{\phi}^2}\Big[\frac{1-6\alpha\tilde{\phi}^2}{1-\alpha\tilde{\phi}^2}\Big]. \tag{3.6}$$

The number of e-foldings is given by

$$N_e = \int_{\tilde{\phi}_{end}}^{\tilde{\phi}^*} \frac{\tilde{\phi}\left(1-\alpha\tilde{\phi}^2\right)}{2(1-2\alpha\tilde{\phi}^2)} d\tilde{\phi}, \tag{3.7}$$

where $\tilde{\phi}^*$ and $\tilde{\phi}_{end}$ correspond to the field values at the point of horizon exit and end of inflaton (triggered by $\epsilon, \eta \leq 1$) respectively. The spectral index and tensor to scalar ratio are given by $n_s = 1 - 6\epsilon + 2\eta$ and $r = 16\epsilon$. The curvature perturbation is defined as

$$P_s = \frac{V_{\rm Inf}}{24\pi^2\epsilon} = \frac{\tilde{m}^2\tilde{\phi}^4}{96\pi^2}\frac{(1-\alpha\tilde{\phi}^2)^3}{(1-2\alpha\tilde{\phi}^2)^2}. \tag{3.8}$$

Observational value of P_s is found to be 2.2×10^{-9} at the pivot scale $k^* \sim 0.05$ Mpc^{-1} [39].

$\tilde{m}$	α	n_s	r
5.83×10^{-6}	7×10^{-4}	0.966	0.097
5.72×10^{-6}	9×10^{-4}	0.964	0.086
5.59×10^{-6}	1.1×10^{-3}	0.962	0.076
5.42×10^{-6}	1.3×10^{-3}	0.959	0.066

TABLE 3.1: Inflationary predictions for n_s and r for different values of α with $N_e = 60$.

3.3 Inflationary Predictions

We perform a scan over the parameters m and α involved in Eq.(3.5) so as to obtain r and n_s within the allowed range of Planck 2015 [39]. We take N_e as 60. Few of our findings for n_s and r in terms of the parameters m and α are provided in the Table 3.1. In Fig.3.1 we show our predictions for n_s and r by four dark dots joined by a line. The dark dots represent the four sets of parameters mentioned in Table 3.1. Along the line joining these, the parameter α is varied and correspondingly the magnitude of $\tilde{m}$ is adjusted mildly (as seen from Table 3.1) in order to keep the curvature perturbation unchanged. The 1σ and 2σ contours from the Planck 2015 [39] are also depicted as reference in Fig.3.1. As an example with $\alpha \sim 7 \times 10^{-4}$ and $N_e = 60$, we find $\tilde{\phi}^* \simeq 14.85$ (inflaton field value at horizon exit) and $\tilde{\phi}_{end} \simeq \sqrt{2}$ (field value at the end of inflation). Hence the slow roll parameters ϵ and η can be obtained at $\tilde{\phi} = \tilde{\phi}^*$ and we can determine n_s and r. The parameter m is fixed by the required value of curvature perturbation $P_s = 2.2 \times 10^{-9}$ [39]. $\tilde{m}$ is found to be 5.83×10^{-6} for the above values of α and N_e. As

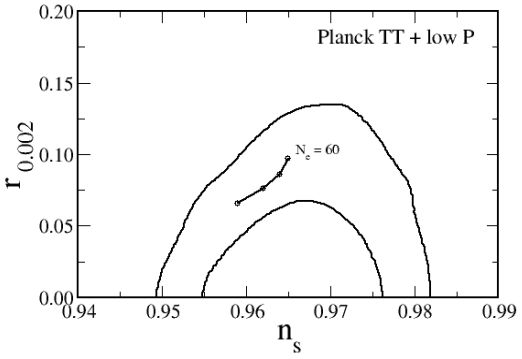

FIGURE 3.1: Predictions for n_s and r (shown in Table 3.1) as obtained from the deformed version of standard chaotic inflation are indicated by dark dots with $N_e = 60$. A solid line joining them represents the predictions for n_s and r while α is varied. 1σ and 2σ contours of $n_s - r$ as obtained from Planck 2015 data [39] are included for reference.

expected we obtain a smaller value of $r \sim 0.097$ compared to the standard chaotic inflation with $r \sim 0.133$ (and $n_s \simeq 0.966$) as seen from Table 3.1 (first set).

Let us now proceed to determine the allowed range of parameters c_1 and λ_χ from estimate of α and m we found above. For this purpose, we first summarize the relevant points already discussed. Specifically, during inflation:(i) $m_\chi^2 > H_{\rm Inf}^2$,which indicates $c_1/\tilde{m}^2 > 1/12$ or equivalently $\lambda_\chi > \frac{\tilde{m}^2}{288\alpha}$. (ii) We assume χ field as sub-Planckian at the onset of inflation and afterwards. Hence $\tilde{\chi}_{\rm I} \simeq (c_1/\lambda_\chi)\tilde{\phi} < 1$. (iii) As explained below in Eq.(6) we consider $\alpha\tilde{\phi}^2 < 1$.(iv) However note that this term should be sufficiently large so as to produce significant (at least ten percent) change in r as compared to the minimal chaotic inflation. Ten percent or more reduction of r can be achieved with $\alpha\tilde{\phi}^2 \geq 0.05$. Therefore α is bounded by the inequality $0.05 \leq \alpha\tilde{\phi}^2 < 1$. Note that one can find $\tilde{\phi}^*(\alpha)$ (as function of α) by solving $N_e = 60$ for a specific choice of α. Using the fact that we only keep terms of the order $\alpha\tilde{\phi}^2$ (i.e neglecting higher order terms), a suitable upper value of $\alpha\tilde{\phi}^2$ can be chosen as $\alpha\tilde{\phi}^2 < 0.4$. Then plugging $\tilde{\phi}^*$ as a function of α, we obtain $2.7 \times 10^{-4} \leq \alpha \leq 2.5 \times 10^{-3}$ as shown in Fig. 3.2. To be concrete for the sake of discussion we choose a particular value of α within this range, say $\alpha = 7 \times 10^{-4}$ (see the first set of Table 1). One such α corresponds to a particular $\tilde{m}$ value through Eq.(3.8) to have $P_s = 2.2 \times 10^{-9}$ while $\tilde{\phi}^*$ is replaced by $\alpha-$dependence. Hence condition (i) can be translated as $\lambda_\chi > 1.68 \times 10^{-10}$ for $\alpha = 7 \times 10^{-4}$. (v) An upper bound of λ_χ can be set from the requirement that involves the initial condition problem. Note that the universe during the inflation is expected to be dominated by the ϕ field and hence $\lambda_\chi\chi^4/4$ term should be sub-dominated compared to $(1/2)m^2\phi^2$ while initial $\tilde{\phi}^*$ can be large enough during the Planckian time and $\tilde{\chi}^*$ (initial value of χ before inflation starts) should remain sub-Planckian. For example considering

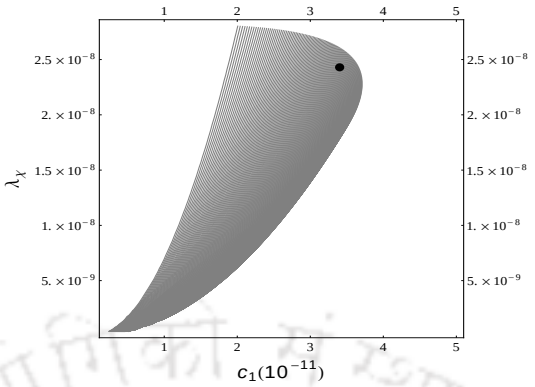

FIGURE 3.2: Allowed region of c_1 (in unit of 10^{-11}) and λ_χ is indicated by the shadowed region where the constraints [(i)-(v)] are included . The black dot represents the reference value of $c_1 \simeq \tilde{m}^2 = 3.39 \times 10^{-11}$ and $\lambda_\chi \simeq 2.43 \times 10^{-8}$. α satisfies $2.7 \times 10^{-4} < \alpha < 2.5 \times 10^{-3}$.

$\tilde{\phi}^* \simeq 16$ and $\tilde{\chi}^* \simeq 0.9$, we have $\lambda_\chi < 2.7 \times 10^{-8}$ such that $\lambda_\chi \tilde{\chi}^4/4 < (1/2)\tilde{m}^2\tilde{\phi}^2$. So λ_χ is restricted by $1.67 \times 10^{-10} < \lambda_\chi < 2.7 \times 10^{-8}$. From this we note that a choice $c_1 = \tilde{m}^2$ falls in the right ballpark which corresponds to $\lambda_\chi = (c_1/2\alpha) = 2.43 \times 10^{-8}$. Considering the range of α as obtained, the allowed parameter space for c_1 and λ_χ are shown in Fig.3.2 where the point corresponding to $c_1 = \tilde{m}^2$ and $\lambda_\chi = 2.43 \times 10^{-8}$ is denoted by a dark dot.

3.4 Study of EW Vacuum Stability

We now turn our attention to the other part of the model which involves the SM Higgs doublet H and its interaction with the inflation sector. The relevant tree level potential is given by

$$V_{\rm II} = \lambda_H\Big(H^\dagger H - \frac{v^2}{2}\Big)^2 + \frac{\lambda_{\chi H}}{2}(\chi^2 - v_\chi^2)\Big(H^\dagger H - \frac{v^2}{2}\Big) + \frac{\lambda_{\phi H}}{2}\phi^2\Big(H^\dagger H - \frac{v^2}{2}\Big). \tag{3.9}$$

As discussed earlier we expect the threshold effect on the running of the Higgs quartic coupling to appear from its interaction with the χ field through its large vev v_χ. For simplicity we drop the last term involving interaction between H and inflaton ϕ for the rest of our discussion by assuming $\lambda_{\phi H}$ as vanishingly small. The presence of $\lambda_{\chi H}$ coupling ensures that during inflation H settles at origin as it receives a large mass term proportional to ϕ as given by $m_H^{\rm eff} \sim [c_1\lambda_{\chi H}/(2\lambda_\chi)]^{1/2}\,\phi$ (using Eq.(3.2)) compared to the Hubble term $H_{\rm Inf}$ (with $\lambda_{\chi H} >> \lambda_\chi$ and neglecting v). So we can disregard any kind of fluctuation of the Higgs field during inflation. Eventually the effective potential during inflation is described by ϕ alone as in Eq. (3.5) (after χ being integrated out and setting H field at zero). However once the inflation is over, ϕ field starts to oscillate about its minimum at $\phi = 0$ with large amplitude (initially) and hence $m_H^{\rm eff}$

starts changing rapidly as well. The Higgs field is then expected not to stay at origin and could be anywhere in the field space [207, 310]. Hence the Higgs instability problem (provided λ_h turns negative in some energy scale Λ_I) may appear if Higgs field takes value beyond Λ_I. The true minimum of the Higgs potential at $H = v$ develops at a later stage when oscillation of the ϕ is over and it settles at origin while χ stays at v_χ. Below we discuss how we can avoid this instability problem after inflation. To explore the stability of the Higgs potential after inflation we need to consider the λ_χ term from Eq.(3.1) as well. The part of the entire potential $V_{\rm I} + V_{\rm II}$ relevant to discuss the vacuum stability issue is therefore given by

$$V_0 = \lambda_H\Big(H^\dagger H - \frac{v^2}{2}\Big)^2 + \frac{\lambda_{\chi H}}{2}(\chi^2 - v_\chi^2)\Big(H^\dagger H - \frac{v^2}{2}\Big) + \frac{\lambda_\chi}{4}(\chi^2 - v_\chi^2)^2. \tag{3.10}$$

The minimum of V_0 is given by

$$\langle H^\dagger H\rangle = \frac{v^2}{2},\ \langle\chi\rangle = v_\chi, \tag{3.11}$$

where we have considered λ_H, $\lambda_\chi > 0$. Note that the above minimum of V_0 (the EW minimum) corresponds to vanishing vacuum energy *i.e.* $V_0^{\rm EW} = 0$. Now in order to maintain the stability of the potential, V_0 should remain positive ($V_0 > 0$) even when the fields involved (χ and H) are away from their respective values at the EW minimum. Since the couplings depend on the renormalization scale μ ($\sim$ field value) we must ensure $\lambda_\chi(\mu)$, $\lambda_H(\mu) > 0$ in order to avoid any deeper minimum (lower than the $V_0^{\rm EW}$) away from the EW one.

In order to study the running of all the couplings under consideration, we consider the renormalization group (RG) equations for them. Below we provide the RG equations for λ_H, $\lambda_{\chi H}$ and λ_χ [58] as

$$\frac{d\lambda_H}{dt} = \beta_{\lambda_H}^{SM} + \frac{1}{16\pi^2}\frac{\lambda_{\chi H}^2}{2}, \tag{3.12}$$

$$\frac{d\lambda_{\chi H}}{dt} = \frac{1}{16\pi^2}\Big\{12\lambda_H\lambda_{\chi H} + 8\lambda_\chi\lambda_{\chi H} + 4\lambda_{\chi H}^2 + 6y_t^2\lambda_{\chi H} - \frac{3}{2}g_1^2\lambda_{\chi H} - \frac{9}{2}g_2^2\lambda_{\chi H}\Big\}, \tag{3.13}$$

$$\frac{d\lambda_\chi}{dt} = \frac{1}{16\pi^2}\Big\{20\lambda_\chi^2 + 2\lambda_{\chi H}^2\Big\}. \tag{3.14}$$

$\beta_{\lambda_H}^{SM}$is the three loop β-function for the Higgs quartic coupling [58] in SM, which is corrected by the one-loop contribution in presence of the χ field. The RG equation for two new physics parameters $\lambda_{\chi H}$ and λ_χ are kept at one loop. The presence of the χ field is therefore expected to modify the stability conditions above its mass m_χ.

Apart from the modified running of the Higgs quartic coupling, vacuum stability is also affected by the presence of the threshold correction from the heavy χ field which carries a large

vev. The mass of the χ field is given by $m_\chi = \sqrt{2\lambda_\chi} v_\chi$ (following from Eq.(3.3)), the heavy field χ can be integrated out below m_χ. By solving the equation of motion of χ field we have

$$\chi^2 \simeq v_\chi^2 - \frac{\lambda_{\chi H}}{\lambda_\chi}\Big(H^\dagger H - \frac{v^2}{2}\Big). \tag{3.15}$$

Hence below the scale m_χ, the effective potential of V_0 becomes

$$V_0^{\rm eff} \simeq \lambda_h\Big(H^\dagger H - \frac{v^2}{2}\Big)^2, \text{ with } \lambda_h(m_\chi) = \Big[\lambda_H - \frac{\lambda_{\chi H}^2}{4\lambda_\chi}\Big]_{m_\chi}, \tag{3.16}$$

where Eq.(3.15) is used to replace χ into Eq.(3.10). Therefore below m_χ, λ_h corresponds to the SM Higgs quartic coupling and above m_χ it gets a positive shift $\delta\lambda = \frac{\lambda_{\chi H}^2}{4\lambda_\chi}$. This could obviously help in delaying the Higgs quartic coupling to become negative provided m_χ is below the SM instability scale, *i.e.* $m_\chi < \Lambda_I^{\rm SM}$. In this analysis, we investigate the parameter space for which the Higgs quartic coupling remains positive upto the scale M_P. This however depends upon m_χ and $\delta\lambda$. Note that λ_χ involved in both m_χ and $\delta\lambda$ which is somewhat restricted from inflation (see Fig.3.2). On the other hand v_χ is not restricted from inflation. We will have an estimate of v_χ by requiring $m_\chi < \Lambda_I^{\rm SM}$ (using a specific λ_χ value corresponding to set-1 of Table 1.) We also consider $\delta\lambda \sim \lambda_h(m_\chi)$ to avoid un-naturalness in the amount of shift. This consideration in turn fixes $\lambda_{\chi H}$.

From the above discussion, it is clear that with suitable choice of parameters involved, the Higgs quartic coupling can remain positive till a very high scale beyond Λ_I^{SM}, say upto the $H_{\rm Inf}$ or even until M_P. As we have discussed before, the H field stays at origin during inflation and after inflation (during the oscillatory phase of the ϕ field) it can be randomly placed. However λ_h being positive untill a very large scale (even beyond the inflationary scale), the Higgs potential has only a single minimum at $\langle H\rangle = v$. Hence once the oscillation period of the ϕ field is over, the H field naturally enters into the electroweak vacuum and electroweak symmetry is broken subsequently. At this stage the Higgs field can be redefined as $H^T = \begin{pmatrix} 0 & \frac{v+\zeta}{\sqrt{2}}\end{pmatrix}$ using the unitary gauge. Now setting $\phi = 0$ and $\chi = v_\chi$, we find the mass-squared matrix involving χ and ζ as

$$\mathcal{M}^2 = \begin{pmatrix} 2\lambda_H v^2 & \lambda_{\chi H} v v_\chi \\ \lambda_{\chi H} v v_\chi & 2\lambda_\chi v_\chi^2 \end{pmatrix}, \tag{3.17}$$

which followed from Eq.(3.10). The diagonalization of this mass-squared matrix yields one light and one heavy scalars. The masses associated with the light and heavy eigenstates are given by

$$m_{h,h_H} = \Big[\lambda_H v^2 + \lambda_\chi v_\chi^2 \mp \sqrt{\Big(\lambda_H v^2 - \lambda_\chi v_\chi^2\Big)^2 + \lambda_{\chi H}^2 v^2 v_\chi^2}\Big]^{1/2}, \tag{3.18}$$

where h and h_H correspond to light and heavy Higgses respectively. In the limit of small mixing angle $\theta = \left[\frac{1}{2}\tan^{-1}\frac{\lambda_{\chi H} v_\chi v}{\lambda_H v^2 - \lambda_\chi v_\chi^2}\right]$, m_h becomes of order $\sim \sqrt{2}v\left(\lambda_H - \frac{\lambda_{\chi H}^2}{4\lambda_\chi}\right)$ with $\lambda_\chi v_\chi^2 >> \lambda_H v^2$. In order to avoid the unwanted negative value of m_h, the extra stability condition $4\lambda_\chi\lambda_H > \lambda_{\chi H}^2$ should be maintained (with $\lambda_{\chi H} > 0$). However it is pointed out in [58] that it is sufficient that this condition should be satisfied for a short interval around m_χ for $\lambda_{\chi H} > 0$. However for $\lambda_{\chi H} < 0$, this extra stability condition becomes $2\sqrt{\lambda_\chi(\mu)\lambda_H(\mu)} + \lambda_{\chi H}(\mu) > 0$. As found in [58], it is difficult to achieve the absolute stability of V_0 till M_P in this case. We restrict ourselves into the case $\lambda_{\chi H} > 0$ for the present work.

Scale (μ)	y_t	g_1	g_2	g_3	λ_h
m_t	0.93668	0.357632	0.648228	1.166508	0.127102

TABLE 3.2: Values of couplings in SM at $m_t = 173.3$ GeV for $m_t = 173.3$ GeV, $m_h = 125.66$ GeV and $\alpha_s = 0.1184$.

Next we proceed to analyze the RG running of all the relevant couplings present in the set up from $\mu = m_t$ to M_P energy scale. For $\mu < m_\chi$, as the χ field would be integrated out, we should only consider the RG evolution of the SM couplings. The initial values of all the SM couplings at m_t energy scale can be determined through Eqs.(1.97-1.101). As an example we tabulize the initial values of the top quark Yukawa coupling (y_t), gauge couplings (g_i) and Higgs quartic coupling (λ_h) considering $m_t = 173.3$ GeV, $m_h = 125.66$ GeV and $\alpha_s = 0.1184$ in Table 3.2.

Scale(μ)	λ_χ	$\lambda_{\chi H}$	y_t	g_1	g_2	g_3	λ_H
m_χ	2.38×10^{-8}	3.66×10^{-5}	0.59523	0.386864	0.58822	0.72327	0.0278
M_P	2.45×10^{-8}	3.56×10^{-5}	0.39112	0.467056	0.509155	0.49591	$\mathcal{O}(10^{-5})$

TABLE 3.3: Values of couplings at m_χ and M_P for $m_\chi = 8 \times 10^7$ GeV and $m_t = 173.3$ GeV, $m_h = 125.66$ GeV and $\alpha_s = 0.1184$.

For energy scale $\mu > m_\chi$, two other couplings λ_χ and $\lambda_{\chi H}$ will appear as in Eq.(3.10). As discussed earlier, we already have an estimate of λ_χ to have successful results in inflation sector with $c_1 = \tilde{m}^2$. We consider the corresponding value of $\lambda_\chi = 2.43 \times 10^{-8}$ at inflation scale $\Lambda_{\rm Inf} \sim V_{\rm Inf}^{1/4} \simeq 10^{16}$ GeV. The initial value of λ_χ should be fixed at m_χ (remains same at m_t) in such a way that it can reproduce $\lambda_\chi(\Lambda_{\rm Inf})$ correctly through its RG equation in Eq.(3.14). $\lambda_{\chi H}$ (m_χ) is chosen to achieve a natural enhancement $\delta\lambda \sim \lambda_h(m_\chi)$ at m_χ. Hereafter above m_χ,

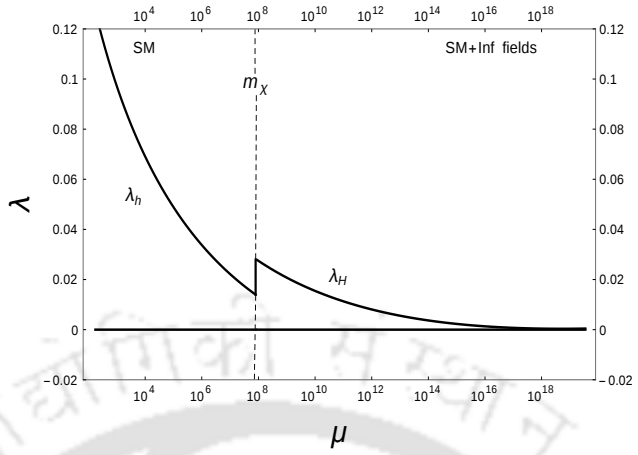

FIGURE 3.3: Running of Higgs quartic coupling till M_P for $\lambda_{\chi H}(m_\chi) = 3.66 \times 10^{-5}, \lambda_\chi(m_\chi) = 2.38 \times 10^{-8}$ with $m_\chi = 8 \times 10^7$ GeV.

the Higgs quartic coupling λ_H is governed through the modified RG equation[3] as in Eq.(3.12). Note that even if λ_χ is known it does not fix $m_\chi (= \sqrt{2\lambda_\chi} v_\chi)$ completely. Therefore we can vary v_χ to have $m_\chi < \Lambda_I^{\rm SM}$.

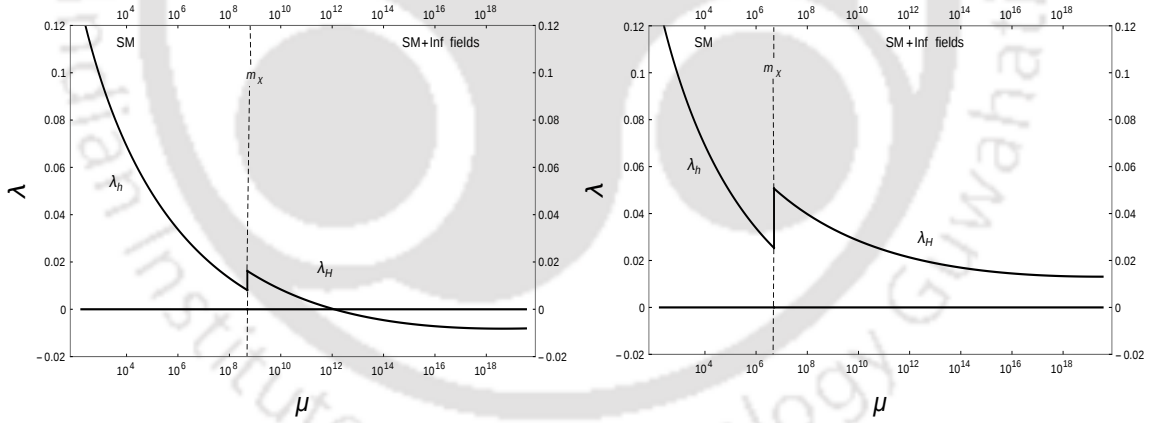

FIGURE 3.4: Running of Higgs quartic coupling till M_P for [left panel:] $m_\chi (= 5 \times 10^8$ GeV$) > m_C$, [right panel:] $m_\chi (= 5 \times 10^6$ GeV$) < m_C$. We consider $\delta\lambda = \lambda_h(m_\chi)$ which corresponds to the choice for (a) $\lambda_{\chi H}(m_\chi) = 2.8 \times 10^{-5}$, $\lambda_\chi(m_\chi) = 2.4 \times 10^{-8}$ and (b) $\lambda_{\chi H}(m_\chi) = 4.88 \times 10^{-5}, \lambda_\chi(m_\chi) = 2.35 \times 10^{-8}$ respectively.

With the above mentioned scheme, we study the running of the Higgs quartic coupling for different m_χ satisfying $m_\chi < \Lambda_I^{\rm SM}$. We find that with $m_\chi = 8 \times 10^7$ GeV, λ_H becomes vanishingly small at M_P (hence the new instability scale Λ_I becomes $\sim M_P$) as shown in Fig.3.3. We specify

[3]It can be noted that such a $\lambda_{\chi H}$ does not alter the running of λ_χ much.

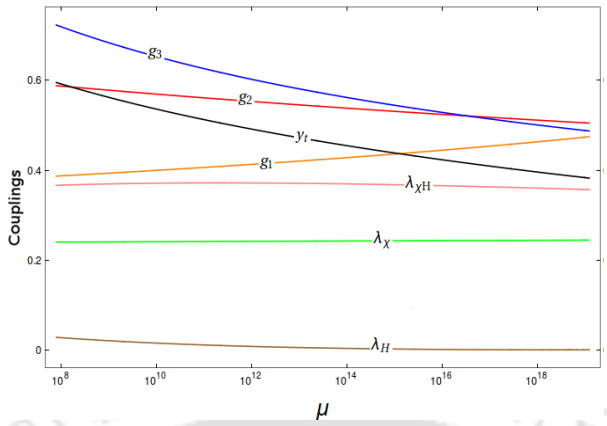

FIGURE 3.5: Running of the couplings $g_{i=1,2,3}$, y_t, λ_H, $\lambda_{\chi H}$ (in unit of 10^{-4}) and λ_χ (in unit of 10^{-7}) in SM+Inflation scenario from $m_\chi = m_C \sim 8 \times 10^7$ GeV to M_P.

the corresponding m_χ value as $m_C (= 8 \times 10^7$ GeV). The value of all the relevant couplings at m_χ and M_P are provided in Table 3.3. It is then observed that in order to keep

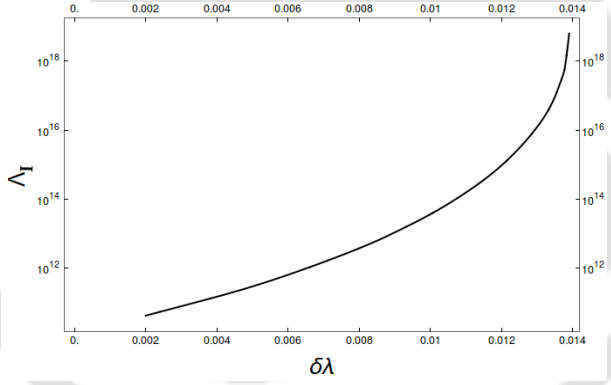

FIGURE 3.6: Variation of instability scale Λ_I with change of $\delta\lambda$ where $m_\chi = m_C \simeq 8 \times 10^7$ GeV.

the Higgs quartic coupling positive all the way upto M_P, we should ensure $m_\chi < m_C$. For example with $m_\chi = 5 \times 10^8$ GeV ($> m_c$) we see λ_H becomes negative at scale $\sim 10^{12}$ GeV as shown in left panel of Fig.3.4. On the other hand in right panel of Fig.3.4 it is seen that λ_H remains positive till M_P for $m_\chi \sim 5 \times 10^6$ GeV $< m_C$. In doing so we consider the amount of positive shift at m_χ to be defined with $\delta\lambda \sim \lambda_h(m_\chi)$. In Fig.3.6 we provide the variation of instability scale Λ_I (which is atmost $\sim M_P$ for $m_\chi = m_C$ case) in SM+Inflation extension if we relax this assumption by changing $\delta\lambda$ arbitrarily. To give a feeling about how other couplings

are changing with μ, we plot running of gauge couplings $g_{i=1,2,3}$, top quark yukawa coupling y_t, λ_χ, λ_H and $\lambda_{\chi H}$ in Fig.3.5 with $m_\chi = m_C = 8 \times 10^7$ GeV.

3.5 Reheating after Inflation

For completeness we now comment on reheating in the present set-up. Once the inflation ends, the inflaton ϕ will oscillate around the minimum at $\phi = 0$. The decay of ϕ would then proceed provided it interacts with the SM fields. Here we do not attempt to discuss it in details. Instead we only mention about the possibilities. The details will be discussed elsewhere in a future study. We may consider terms in the Lagrangian as

$$-\mathcal{L}_{int} = y_\phi \phi N N + y_\nu \bar{L} \tilde{H} N, \tag{3.19}$$

where N is the right handed (RH) neutrino and L is the SM lepton doublet. y_ϕ, y_ν are the respective couplings. Note that the first term is an explicit Z_2 breaking term and hence y_ϕ is expected to be small in the present set-up[4]. The corresponding reheat temperature is then found to be $T_r \simeq y_\phi \sqrt{\frac{mM_P}{8\pi}} \sim 10^{15} y_\phi$ GeV where we have used $m = 1.4 \times 10^{13}$ GeV from set-1, Table 1. A further decay of RH neutrinos into L and H can be responsible for leptogenesis [329–333]. The term $y_\phi \phi N N$ can not however provide the mass of the RH neutrinos as $\langle \phi \rangle = 0$. A mass term like $M_N N N$ has to be present. If we turn our attention to the other field χ involved in the inflation sector, we note that this field will oscillate about $\langle \chi \rangle$ at the end of inflation. The decays of it can proceed via $\chi \to hh$ with $\Gamma_\chi = \frac{\lambda_{\chi H}^2 m_\chi}{256\pi\lambda_\chi}$. Then two cases may arise; (i) $\Gamma_\phi << \Gamma_\chi$: in this case the χ field will decay very fast. However reheat of universe will finish much later after χ field decay. So any radiation energy density produced by χ will be strongly diluted during the matter dominated phase governed by the oscillations of ϕ. (ii) $\Gamma_\phi >> \Gamma_\chi$: note that energy density of the χ field is much less than that of ϕ and universe will reheat once decay of ϕ field is completed. Hence the completion of the inflaton decay into radiation, when Hubble becomes of order Γ_χ, χ field will decay to radiation. So the remnant radiation in this case will be a mixture of ϕ and χ products.

3.6 Chapter Summary

The discovery of the Higgs boson and the precise determination of its mass at LHC provide us an estimate of the Higgs quartic coupling in the SM. However the high scale behavior of

[4] y_ϕ and y_ν should be sufficiently small so that it does not contribute to RG evolutions of all other couplings.

this coupling, whether or not it becomes negative, poses plethora of questions in terms of the stabilization of the electroweak minimum. Though the present data favours the metastability of this vacuum, it is very much dependent on the precision of the top mass measurement. Furthermore inflation in the early universe provides additional threat as it can shift the Higgs field during inflation into the unwanted part of the Higgs potential and hence metastability can also be questioned. As a resolution to this, we propose introduction of the inflation sector consisting of two scalar fields ϕ and χ and their interaction with the SM Higgs. While ϕ is playing the role of the inflaton having the potential $m^2\phi^2/2$, the other field χ provides a deviation in terms of prediction of the spectral index and tensor to scalar ratio so has to be consistent with the Planck 2015 data. The Higgs field is stabilized at origin having a mass larger ($\sim 100H_{\rm Inf}^2$) than the Hubble during inflation with negligible or no fluctuation. After inflation however this problem of Higgs instability may be appear if the Higgs quartic coupling becomes negative at some scale. We have shown that the χ-Higgs coupling can have profound effect in the running of Higgs quartic coupling considering the positive shift through the threshold effect at a scale m_χ. It turns out the quartic coupling of the χ field is restricted to achieve successful inflation. This in turn constrain the other new physics parameters space if we want to make the Higgs potential completely stable upto M_P. We have also commented on the possible reheating scenario in brief. The vev of the χ field breaks the Z_2 symmetry which may spontaneously lead to domain wall problem. An explicit Z_2- symmetry breaking term or gauging the symmetry would help in resolving the issue. As an extension of our present set-up, one can possibly consider a $U(1)_{B-L}$ embedding of the entire framework where the neutrino masses and several other related aspects like effect of gauge bosons on running etc. can be simultaneously addressed.

Chapter 4

EW vacuum stability in presence of dark Matter and RH neutrinos

4.1 Introduction

The scalar fields in the Universe might be present in form of DM also. The phenomenology of real scalar singlet DM model [54, 55, 334–340] is discussed in Sec. 1.3.2.5. Although the scenario is very rich and elegant, it demands attention in view of recent experimental constraints. In particular, present experiments, LUX [185] and XENON1T [183], strongly disfavor the model below $m_{\rm DM} < 500$ GeV except the resonance region. The bound on Higgs invisible decay width further constrain the model for $m_{\rm DM} < 62.5$ GeV [341]. Although excluded, the low mass scalar DM would be an interesting region of search for several ongoing and future direct [183–185] and indirect experiments [188]. On the other hand, scalar DM serves important role in Higgs vacuum stability. It's presence in an extended framework of SM can shift the instability scale (Λ_I) toward larger value compared to the SM one ($\Lambda_I > \Lambda_I^{\rm SM}$) [65, 66, 68, 69, 71, 73, 342].

In addition, to accommodate non-zero neutrino mass via type-I seesaw mechanism, one can extend SM with three right handed(RH) neutrinos. This is already elaborated in Sec 1.3.3. The presence of the neutrino Yukawa coupling affects the running of the Higgs quartic coupling similar to the top Yukawa coupling. In fact with neutrino Yukawa coupling, Y_ν, of $\mathcal{O}(1)$, Λ_I could be lower than $\Lambda_I^{\rm SM}$ [76, 227, 316, 317, 324, 343–348], that might lead to an unstable Universe. The situation does not alter much even if one includes scalar singlet DM ($m_{\rm DM} \leq 500$ GeV) in this framework [69, 72, 76, 349–351]. So the combined framework of RH neutrinos and

scalar singlet DM excludes a significant range of DM mass (< 500 GeV) while keeping the EW vacuum on the verge of being unstable.

With an endeavour to make the EW vacuum absolutely stable upto the Planck scale M_P, in a scenario that can accommodate both the DM and massive neutrinos with large Y_ν (in type-I seesaw) and simultaneously to reopen the window for lighter scalar singlet DM mass (< 500 GeV), in this chapter (based on [67]) we incorporate two SM real singlet scalars and three SM singlet RH neutrinos in this work.

Similar models to address DM phenomenology involving additional scalars (without involving RH neutrinos) have been studied [66, 352–356], however with different motivations. Our set up also differs from them in terms of inclusion of light neutrino mass through type-I seesaw. The proposed model has several important ingredients which are mentioned below along with their importance.

- One of the additional SM singlet scalars is our DM candidate whose stability is achieved with an unbroken Z_2 symmetry.
- The other scalar would acquire a nonzero vacuum expectation value (vev). This field has two fold contributions in our analysis: (i) it affects the running of the SM Higgs quartic coupling and (ii) the dark matter phenomenology becomes more involved due to its mixing with the SM Higgs and the DM.
- The set up also contains three RH neutrinos in order to generate non-zero light neutrino mass through type-I seesaw mechanism. Therefore, along with the contributions from the additional scalar fields, neutrino Yukawa coupling, Y_ν, is also involved in studying the running of the Higgs quartic coupling.

We observe that the presence of the scalar[1] with non-zero vev affects the DM phenomenology in such a way that $m_{\rm DM}$ less than 500 GeV becomes perfectly allowed mass range considering the recent XENON-1T result [183], which otherwise was excluded from the DM direct search results [357]. We also include XENON-nT [183] prediction to further constrain our model. On the other hand, we find that the SM Higgs quartic coupling may remain positive till M_P (or upto some other scale higher than $\Lambda_I^{\rm SM}$) even in presence of large Y_ν, thanks to the involvement of the scalar with non-zero vev. We therefore identify the relevant parameter space (in terms of stability, metastability and instability regions) of the model which can allow large Y_ν (with

[1]This scalar perhaps can be identified with moduli/inflaton fields [58, 304, 310, 314, 358] or messenger field [70] connecting SM and any hidden sector.

different mass scales of RH neutrinos) and scalar DM below 500 GeV. Bounds from other related aspects, *e.g.* lepton flavor violating decays, neutrinoless double beta decay etc., are also considered. The set-up therefore demands rich phenomenology what we present in the following sections.

The chapter is organized as follows. In section 4.2, we discuss the set-up of our model and in section 4.3, we include the constraints on our model parameters. Then in the subsequent sections 4.4 and 4.5, we discuss the DM phenomenology and vacuum stability respectively in the context of our model. In section 4.6, we discuss connection of the model with other observables. Finally we conclude in section 4.7.

4.2 The Model

As mentioned in the introduction, we aim to study how the EW vacuum can be made stable in a model that would successfully accommodate a scalar DM and neutrino mass. For this purpose, we extend the SM by introducing two SM singlet scalar fields, ϕ and χ, and three right-handed neutrinos, $N_{i=1,2,3}$. We have also imposed a discrete symmetry, $Z_2 \times Z_2'$. The field ϕ is odd (even) under Z_2 (Z_2') and χ is even (odd) under Z_2 (Z_2') while all other fields are even under both Z_2 and Z_2'. There exists a non-zero vev associated with the χ field. The unbroken Z_2 ensures the stability of our dark matter candidate ϕ. On the other hand, the inclusion of Z_2' simplifies the scalar potential in the set-up[2]. The RH neutrinos are included in order to incorporate the light neutrino mass through type-I seesaw mechanism.

The scalar potential involving ϕ, χ and the SM Higgs doublet (H) is given by

$$V = V_{\rm I} + V_{\rm II} + V_{\rm III} + V_{\rm H}, \tag{4.1}$$

where

$$\begin{aligned} V_{\rm I} &= \frac{1}{2}\mu_\phi^2\phi^2 + \frac{1}{4!}\lambda_\phi\phi^4 + \frac{1}{2}\lambda_{\phi H}\phi^2 H^\dagger H; \\ V_{\rm II} &= -\frac{1}{2}\mu_\chi^2\chi^2 + \frac{\lambda_\chi}{4!}\chi^4 + \frac{\lambda_{\chi H}}{2}\chi^2|H|^2; \\ V_{\rm III} &= \frac{1}{4}\lambda_{\chi\phi}\phi^2\chi^2, \quad \text{and} \quad V_{\rm H} = -\mu_H^2 H^\dagger H + \lambda_H (H^\dagger H)^2. \end{aligned}$$

[2]A spontaneous breaking of discrete symmetry may lead to cosmological domain wall problem [359]. To circumvent it, one may introduce explicit Z_2' breaking term in higher order which does not affect our analysis.

The relevant part of the Lagrangian responsible for neutrino mass is given by

$$-\mathcal{L}_\nu = Y_{\nu_{ij}} \bar{l_{Li}} \tilde{H} N_j + \frac{1}{2} M_{N\,ij} N_i N_j,$$

where l_{Li} are the left-handed lepton doublets, M_N is the Majorona mass matrix of the RH neutrinos. This leads to the light neutrino mass, $m_\nu = Y_\nu^T {M_N}^{-1} Y_\nu \frac{v^2}{2}$ with $v = 246$ GeV as the vacuum expectation value of the SM Higgs. Minimization of the potential V leads to the following vevs of χ and H^0 (the neutral component of H), as given by

$$v_\chi^2 = 6\frac{2\mu_\chi^2\lambda_H - \mu_H^2\lambda_{\chi H}}{2\lambda_H\lambda_\chi - 3\lambda_{\chi H}^2}, \tag{4.2}$$

$$v^2 = 2\frac{\mu_H^2\lambda_\chi - 3\mu_\chi^2\lambda_{\chi H}}{2\lambda_H\lambda_\chi - 3\lambda_{\chi H}^2}. \tag{4.3}$$

So after χ gets the vev and electroweak symmetry is broken, the mixing between H^0 and χ will take place and new mass or physical eigenstates, H_1 and H_2, will be formed. The two physical eigenstates are related with H^0 and χ by

$$\begin{aligned} H_1 &= H^0\cos\theta - \chi\sin\theta, \\ H_2 &= H^0\sin\theta + \chi\cos\theta, \end{aligned} \tag{4.4}$$

where the mixing angle θ is defined by

$$\tan 2\theta = \frac{\lambda_{\chi H} v v_\chi}{-\lambda_H v^2 + \frac{\lambda_\chi v_\chi^2}{6}}. \tag{4.5}$$

Similarly the mass eigenvalues of these physical Higgses are found to be

$$m_{H_1}^2 = \frac{\lambda_\chi}{6}v_\chi^2(1-\sec 2\theta) + \lambda_H v^2(1+\sec 2\theta), \tag{4.6}$$

$$m_{H_2}^2 = \frac{\lambda_\chi}{6}v_\chi^2(1+\sec 2\theta) + \lambda_H v^2(1-\sec 2\theta). \tag{4.7}$$

Using Eqs.(6.16,6.17,6.18), the couplings λ_H, λ_χ and $\lambda_{\chi H}$ can be expressed in terms of the masses of the physical eigenstates H_1 and H_2, the vevs (v, v_χ) and the mixing angle θ as

$$\lambda_H = \frac{m_{H_1}^2}{4v^2}(1+\cos 2\theta) + \frac{m_{H_2}^2}{4v^2}(1-\cos 2\theta), \tag{4.8}$$

$$\lambda_\chi = \frac{3m_{H_1}^2}{2v_\chi^2}(1-\cos 2\theta) + \frac{3m_{H_2}^2}{2v_\chi^2}(1+\cos 2\theta), \tag{4.9}$$

$$\lambda_{\chi H} = \sin 2\theta \Big(\frac{m^2_{H_2} - m^2_{H_1}}{2vv_\chi} \Big). \tag{4.10}$$

Among H_1 and H_2, one of them would be the Higgs discovered at LHC. The other Higgs can be heavier or lighter than the SM Higgs. Below we proceed to discuss the constraints to be imposed on the couplings and mass parameters of the model before studying the DM phenomenology and vacuum stability in the subsequent sections.

4.3 Constraints

Here we put together the constraints (both theoretical and experimental) that we will take into account to find the parameter space of our model.

- In order to keep the entire potential stable, one needs to maintain the following conditions involving the couplings present in V (considering all couplings as real)

$$\begin{aligned}
&\mathbf{ST}_{1,2,3}\mathbf{:}\ \lambda_H > 0,\ \lambda_\chi > 0,\ \lambda_\phi > 0,\\
&\mathbf{ST}_{4,5,6}\mathbf{:}\ \lambda_{\chi H} + \sqrt{\frac{2}{3}\lambda_H\lambda_\chi} > 0,\ \lambda_{\phi H} + \sqrt{\frac{2}{3}\lambda_H\lambda_\phi} > 0,\ 3\lambda_{\chi\phi} + \sqrt{\lambda_\chi\lambda_\phi} > 0,\\
&\mathbf{ST}_{7}\mathbf{:}\ \sqrt{\lambda_H\lambda_\chi\lambda_\phi} + \lambda_{\chi H}\sqrt{\frac{3}{2}\lambda_\chi} + 3\lambda_{\phi H}\sqrt{\lambda_H} + 3\lambda_{\chi\phi}\sqrt{\lambda_H},\\
&\qquad + 3\Big[\Big(\lambda_{\chi H} + \sqrt{\frac{2}{3}\lambda_H\lambda_\chi}\Big)\Big(\lambda_{\phi H} + \sqrt{\frac{2}{3}\lambda_H\lambda_\phi}\Big)\Big(\lambda_{\chi\phi} + \frac{1}{3}\sqrt{\lambda_\phi\lambda_\chi}\Big)\Big]^{1/2} > 0,
\end{aligned} \tag{4.11}$$

  which followed from the co-positivity of the mass-squared matrix involving H, χ and ϕ [360, 361].

- In addition, the perturbative unitarity associated with the S matrix corresponding to $2 \to 2$ scattering processes involving all two particles initial and final states [362, 363] are considered. In the specific model under study, there are eleven neutral and four singly charged combinations of two-particle initial/final states. The details are provided in Appendix B.1. It turns out that the some of the scalar couplings of Eq.(4.1) are bounded by

$$\lambda_H\ < 4\pi, \quad \lambda_{\phi H}\ < 8\pi, \quad \lambda_{\chi H}\ < 8\pi, \quad \lambda_{\chi\phi}\ < 8\pi. \tag{4.12}$$

  The other scalar couplings are restricted (in form of combinations among them) from the condition that the roots of a polynomial equation should be less than 16π (see Eq.(B.9) of Appendix B.1).

- To maintain the perturbativity of all the couplings, we impose the condition that the scalar couplings should remain below 4π while Yukawa couplings are less than $\sqrt{4\pi}$ till M_P. An upper bound on $\tan\beta(= v/v_\chi)$ follows from the perturbativity of λ_χ [364] with a specific choice of m_{H_2}.

- Turning into the constraints obtained from experiments, we note that the observed signal strength of the 125 GeV Higgs boson at LHC [365–370] provides a limit on $\sin\theta$ as, $|\sin\theta| \lesssim 0.36$ with $m_{H_2} \gtrsim 150$ GeV. The analysis in [371] shows that $\sin\theta$ is restricted significantly ($|\sin\theta| \lesssim 0.3$) by the direct Higgs searches at colliders [365–369] and combined Higgs signal strength [459] for 150 GeV $< m_{H_2} <$ 300 GeV while for 300 GeV $< m_{H_2} <$ 800 GeV, it is the NLO contribution to the W boson mass [364] which restricts $\sin\theta$ in a more stipulated range. Corrections to the electroweak precision observables through the S, T, U parameters turn out to be less dominant compared to the limits obtained from W boson mass correction [364]. For our purpose, we consider $\sin\theta \lesssim 0.3$ for the analysis.

Apart from these, we impose the constraints on Y_ν from lepton flavor violating decays. Also phenomenological limits obtained on the scalar couplings involved in order to satisfy the relic density ($0.1175 \leq \Omega h^2 \leq 0.1219$) [41] and direct search limits [183] by our dark matter candidate ϕ are considered when stability of the EW minimum is investigated.

4.4 Dark matter phenomenology

Let us now move to the relic density estimate in our set-up with the extra scalar χ and compare the phenomenology with the simplest scalar DM scenario in the light of the mixing between the SM Higgs and χ. Using Eq.(6.15) and inserting them into the SM Lagrangian along with the ones mentioned in Eq.(4.1), we obtain the following list of interaction vertices involving two Higgses (H_1 and H_2), dark matter field (ϕ) and several other SM fields.

$$
\begin{aligned}
H_1 f\bar{f}, H_2 f\bar{f} &: \frac{m_f}{v}\cos\theta, \frac{m_f}{v}\sin\theta \\
H_1 ZZ, H_2 ZZ &: \frac{2m_Z^2}{v}\cos\theta g^{\mu\nu}, \frac{2m_Z^2}{v}\sin\theta g^{\mu\nu} \\
H_1 W^+W^-, H_2 W^+W^- &: \frac{2m_W^2}{v}\cos\theta g^{\mu\nu}, \frac{2m_W^2}{v}\sin\theta g^{\mu\nu} \\
\phi\phi H_1 &: -v_\chi \lambda_{\chi\phi}\sin\theta + v\lambda_{\phi H}\cos\theta \equiv \lambda_1 \\
\phi\phi H_2 &: v_\chi \lambda_{\chi\phi}\cos\theta + v\lambda_{\phi H}\sin\theta \equiv \lambda_2
\end{aligned}
$$

$$
\begin{aligned}
\phi\phi H_1H_1 &: \lambda_{\phi H}\cos^2\theta + \lambda_{\chi\phi}\sin^2\theta \\
\phi\phi H_2H_2 &: \lambda_{\phi H}\sin^2\theta + \lambda_{\chi\phi}\cos^2\theta \\
\phi\phi H_1H_2 &: (\lambda_{\phi H} - \lambda_{\chi\phi})\sin\theta\cos\theta \\
H_1H_1H_1 &: [6v\lambda_H\cos^3\theta - 3v_\chi\lambda_{\chi H}\cos^2\theta\sin\theta + 3v\lambda_{\chi H}\cos\theta\sin^2\theta - v_\chi\lambda_\chi\sin^3\theta] \\
H_2H_2H_2 &: [6v\lambda_H\sin^3\theta + 3v_\chi\lambda_{\chi H}\cos\theta\sin^2\theta + 3v\lambda_{\chi H}\cos^2\theta\sin\theta + v_\chi\lambda_\chi\cos^3\theta] \\
H_1H_1H_2 &: [2v(3\lambda_H - \lambda_{\chi H})\cos^2\theta\sin\theta + v\lambda_{\chi H}\sin^3\theta + v_\chi(\lambda_\chi - 2\lambda_{\chi H})\cos\theta\sin^2\theta \\
&\quad + v_\chi\lambda_{\chi H}\cos^3\theta] \\
H_1H_2H_2 &: [2v(3\lambda_H - \lambda_{\chi H})\cos\theta\sin^2\theta + v\lambda_{\chi H}\cos^3\theta - v_\chi(\lambda_\chi - 2\lambda_{\chi H})\cos^2\theta\sin\theta \\
&\quad - v_\chi\lambda_{\chi H}\sin^3\theta].
\end{aligned}
\tag{4.13}
$$

Following Eq.(6.25) we draw the Feynman diagrams for DM annihilation channels into the SM particles and to the second Higgs in Fig.4.1.

It is expected that the DM candidate is in thermal equilibrium with the SM degrees of freedom in the early universe. We therefore proceed to evaluate their abundance through the standard freeze-out mechanism. The Boltzmann equation,

$$\dot{n}_\phi + 3\mathrm{H}n_\phi = -\langle\sigma v_{\phi\phi}\rangle\left(n_\phi^2 - n_\phi^{eq2}\right), \tag{4.14}$$

is employed for this purpose, where n_ϕ is the number density of the dark matter ϕ, H is the Hubble parameter, $\langle\sigma v_{\phi\phi}\rangle$ represents the total annihilation cross-section as given by $\langle\sigma v_{\phi\phi}\rangle = \langle\sigma v_{\phi\phi\to SM,SM}\rangle + \langle\sigma v_{\phi\phi\to H_1H_2}\rangle + \langle\sigma v_{\phi\phi\to H_2H_2}\rangle$. We consider here the RH neutrinos to be massive enough compared to the DM mass. So RH neutrinos do not participate in DM phenomenology. We have then used the MicrOmega package [372] to evaluate the final relic abundance of DM. We have the following parameters in our set-up,

$$\{m_{H_1}, m_{H_2}, m_{\mathrm{DM}}, \sin\theta, \lambda_{\chi\phi}, \lambda_{\phi H}, v, \tan\beta, \lambda_\phi\}. \tag{4.15}$$

The parameters v_χ is involved in the definition of $\tan\beta = v/v_\chi$. Parameters $(\lambda_H, \lambda_\chi, \lambda_{\chi H})$ can be written in terms of other parameters as shown in Eqs.(6.19,4.9,6.21). Among all the parameters in Eq.(4.15), λ_ϕ does not play any significant role in DM analysis.

We first assume H_1 as the Higgs discovered at LHC *i.e.* m_{H_1} ∼125.09 GeV [293] and the other Higgs is the heavier one ($m_{H_2} > m_{H_1}$). It would be appealing in view of LHC accessibility to keep m_{H_2} below 1 TeV. In this case limits on $\sin\theta, \tan\beta$ are applicable as discussed in Section 4.3 depending on specific value of m_{H_2} [371]. Now in this regime (where m_{H_2} is not too heavy,

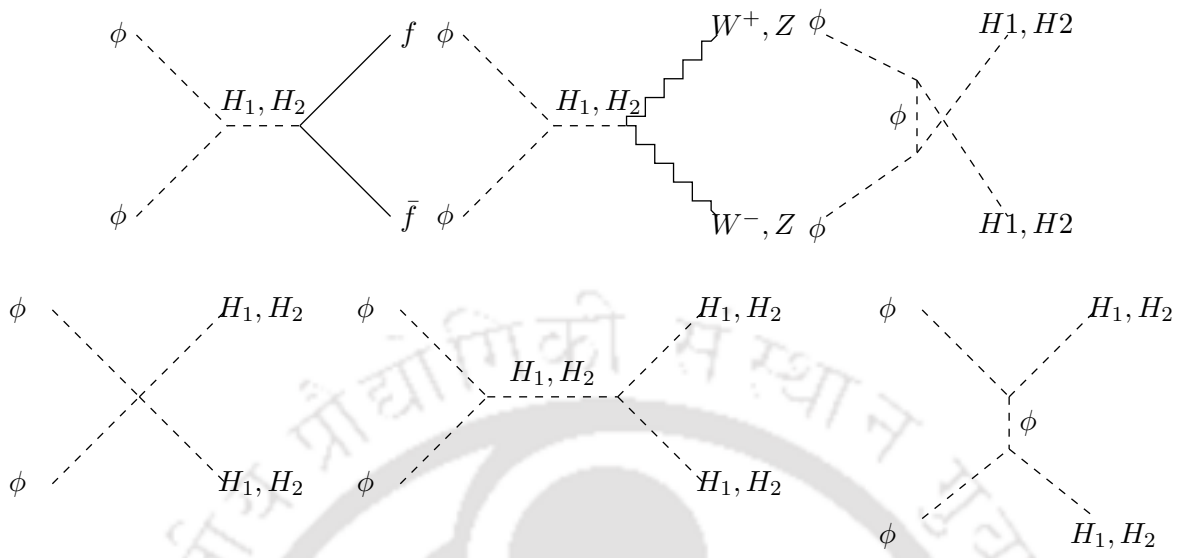

FIGURE 4.1: Diagrams contributing to $\phi\phi$ annihilation to the SM particles and the other Higgs.

in particular $m_{H_2} < 1$ TeV), $\sin\theta$ is bounded by $\sin\theta \lesssim 0.3$ [371] and we have taken here a conservative choice by fixing $\sin\theta = 0.2$. Note that in the small $\sin\theta$ approximation, H_1 is mostly dominated by the SM Higgs doublet H. In this limit the second term in Eq.(6.19) effectively provides the threshold correction to λ_H [58, 59, 312] which helps in achieving vacuum stability as we will see later. Furthermore considering this threshold effect to be equal or less than the first term in Eq.(6.19) (*i.e.* approximately the SM value of λ_H), we obtain an upper bound on m_{H_2} as $m_{H_2} < \frac{m_{H_1}}{\tan\theta}$. Therefore in case with $m_{H_2} > m_{H_1}$, our working regime of m_{H_2} can be considered within $\frac{m_{H_1}}{\tan\theta} > m_{H_2} > m_{H_1}$. We take m_{H_2} to be 300 GeV for our analysis.

Note that with small θ, λ_χ almost coincides with the second term in Eq.(4.9). It is quite natural to keep the magnitude of a coupling below unity to maintain the perturbativity limit for all energy scales including its running. Hence with the demand $\lambda_\chi < 1$, one finds $v_\chi > \sqrt{3}m_{H_2}$. To show it numerically, let us choose $\sin\theta = 0.2$, then we obtain 125 GeV $< m_{H_2} <$ 620 GeV. Therefore with $m_{H_2} = 300$ GeV, a lower limit on $v_\chi \geq 520$ GeV can be set. We consider v_χ to be 800 GeV so that $\tan\beta$ turns out to be 0.307.

On the other hand, if we consider the other Higgs to be lighter than the one discovered at LHC, we identify m_{H_2} to be the one found at LHC and hence $m_{H_1} \leq 125$ GeV. Then Eq.(6.15) suggests $\sin\theta \to 1$ as the complete decoupling limit of the second Higgs. Following the analysis in [313, 371, 373–376], we infer that most of the parameter space except for a very narrow region both in terms of mixing angle ($\sin\theta \sim 0.9$) and mass of the lighter Higgs ($m_{H_1} \sim 85 - 100$)

GeV, is excluded from LEP and LHC searches. Such a range is not suitable for our purpose

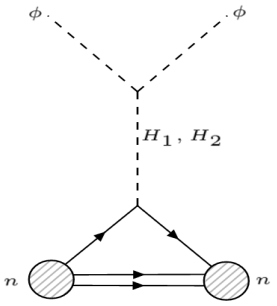

FIGURE 4.2: Feynman diagram for DM Direct Detection.

as can bee seen from Eq.(6.19). In this large $\sin\theta$ limit, λ_H gets the dominant contribution from the second term in Eq.(6.19) where the first term serves the purpose of threshold effect on λ_H. However m_{H_1} being smaller than m_{H_2} (the SM like Higgs), this effect would not be sufficient to enhance λ_H such that its positivity till M_P can be ensured. Therefore we discard the scenario $m_{H_1} < m_{H_2}$ (SM like Higgs) from our discussion. Hence the DM phenomenology basically depends on $m_{\rm DM}, \sin\theta, \lambda_{\chi\phi}$ and $\lambda_{\phi H}$.

In a direct detection experiment, the DM scatters with the nucleon through the exchange of H_1 and H_2 as shown schematically in Fig.4.2 . The resulting spin-independent cross-section of DM-nucleon elastic scattering is given by [66] :

$$\sigma_n^{SI} = \frac{f_n^2 \mu_n^2 m_n^2}{4\pi v^2 m_{\rm DM}^2}\Big[\frac{\lambda_1 \cos\theta}{m_{H_1}^2} + \frac{\lambda_2 \sin\theta}{m_{H_2}^2}\Big]^2, \tag{4.16}$$

where $\mu_n = \frac{m_n m_{\rm DM}}{m_n + m_{\rm DM}}$, $f_n = 0.284$ [377, 378]. The couplings appeared as λ_1, λ_2 are specified in the list of vertices in Eq.(6.25). Below we discuss how we can estimate the relevant parameters (λ_{ϕ_H},$\lambda_{\chi\phi}$ and $m_{\rm DM}$) from relic density and direct search limits. For this purpose, we consider $m_{H_2} = 300$ GeV and $v_\chi = 800$ GeV as reference values, unless otherwise mentioned.

4.4.1 DM mass in region R1: [150 GeV $< m_{\rm DM} \leq$ 500 GeV]

In this region any decay mode of H_1 and H_2 into DM is kinematically forbidden following our consideration for $m_{H_2} = 300$ GeV. As stated before, we consider m_{H_1} to be the SM like Higgs discovered at LHC, with $v_\chi = 800$ GeV and $\tan\beta$ is fixed at 0.307. Therefore in order to satisfy the relic density $\Omega h^2 = 0.1161 \pm 0.0028$ [41], we first scan over $\lambda_{\phi H}$ and $\lambda_{\chi\phi}$ for different ranges of dark matter mass where $\sin\theta$ is kept fixed at 0.2. The allowed range of parameter space

contributing to the relic abundance satisfying the correct relic density is indicated on $\lambda_{\phi H} - \lambda_{\chi\phi}$ plane in Fig.4.3 (in the top left panel), where different coloured patches indicate different ranges of $m_{\rm DM}$. In the upper-right plot of Fig.4.3, the corresponding direct search cross sections for the relic density satisfied points obtained from the upper left plot (including the variation of $\lambda_{\phi H}, \lambda_{\chi\phi}$) are provided. It can be clearly seen that many of these points lie below the LUX 2016 [185] experimental limit for a wide range of dark matter mass (indicated by the colors depicted in the inset of Fig.4.3, upper left panel).

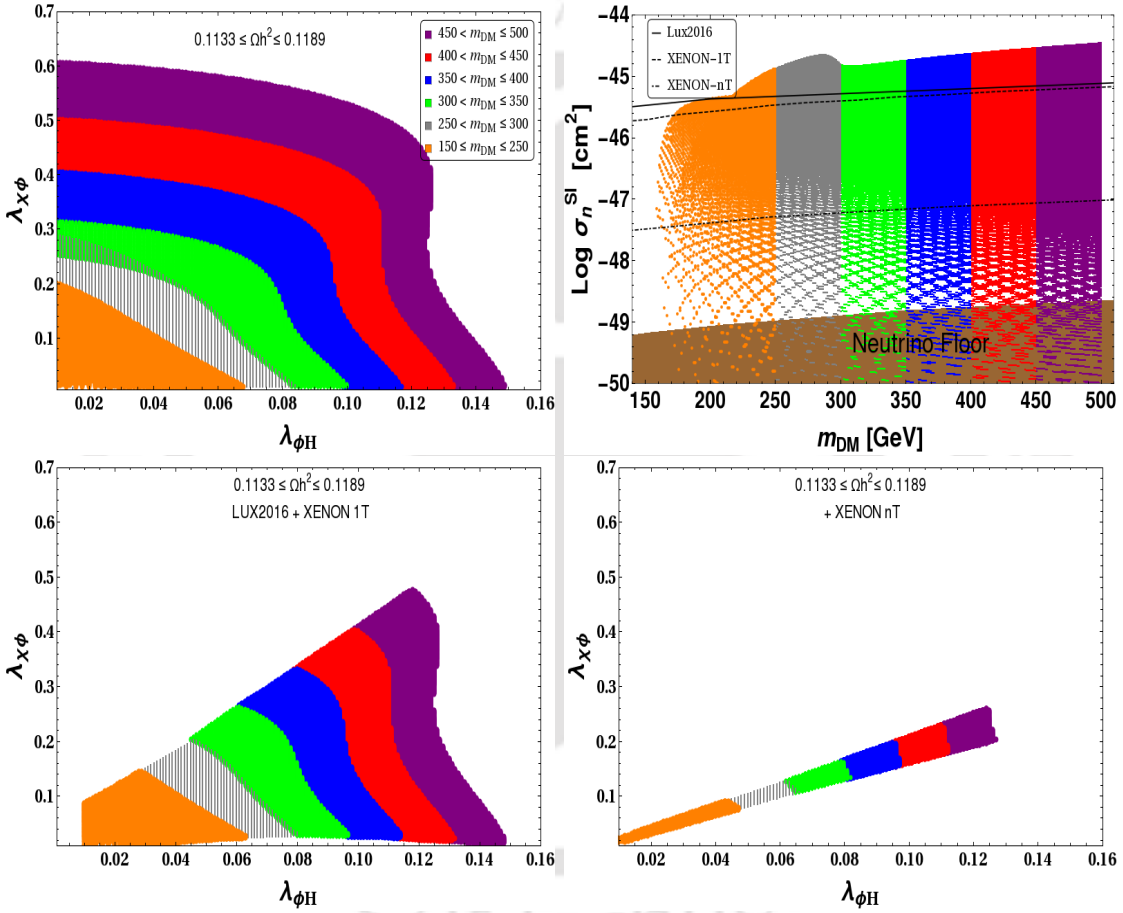

FIGURE 4.3: Top left: Allowed points on $\lambda_{\phi H}$-$\lambda_{\chi\phi}$ plane for DM having mass $150 < m_{\rm DM} < 500$ GeV to satisfy correct order of relic density. Top right: Spin independent nucleon cross section of DM has been plotted against the DM mass. Bottom panel: The top left plot has been constrained using recent LUX 2016 [185], Xenon 1T [183] limits to produce bottom-left figure and Xenon nT [379] predictions to get bottom-right figure.

From the top left panel of Fig.4.3, the relic density contour plot (with a particular $m_{\rm DM}$) in $\lambda_{\chi\phi}$-$\lambda_{\phi H}$ plane shows that there exists a range of $\lambda_{\phi H}$ for which the plot is (almost) insensitive to the change in $\lambda_{\chi\phi}$. This becomes more prominent for plots associated with higher dark matter mass. In particular, the contour line satisfying the correct relic density with $m_{\rm DM} = 500$ GeV

depicts a sharp variation in $\lambda_{\chi\phi}$ (below 0.4) with almost no variation of $\lambda_{\phi H}$ around 0.13. We now discuss the reason behind such a behaviour. We note that for $\lambda_{\phi H} > 0.13$, the total annihilation cross section satisfying the relic density is mostly dominated by the $\phi\phi \to$ SM, SM process, specifically $\phi\phi \to WW, ZZ$ dominate. In our scenario, $\phi\phi \to WW, ZZ$ processes are mediated by both the Higgses, H_1 and H_2. Although $\lambda_{\chi\phi}$ is involved in the vertices characterizing these processes, it turns out that once both the H_1, H_2 contributions are taken into account, the $\lambda_{\chi\phi}$ dependence is effectively canceled leaving the $\phi\phi \to WW, ZZ$ annihilation almost independent of $\lambda_{\chi\phi}$. Hence $\phi\phi \to$ SM, SM depends mostly on $\lambda_{\phi H}$. The other processes like $\phi\phi \to H_1H_2(H_2H_2)$ are subdominant (these are allowed provided $m_{\rm DM} > 212.5(300)$ GeV) in this region with large $\lambda_{\phi H}$. Then the total cross section $\langle\sigma v_{\phi\phi}\rangle$ and hence the relic density contour line becomes insensitive to the change in $\lambda_{\chi\phi}$ as long as it remains below 0.4 while $\lambda_{\phi H} > 0.13$. This is evident in the top left panel of Fig.4.3. Similar effects are seen in case of lower $m_{\rm DM}$ (< 500 GeV) as well.

Once we keep on decreasing $\lambda_{\phi H}$ below 0.13, it turns out that $\phi\phi \to$ SM, SM becomes less important compared to the $\phi\phi \to H_2H_2$ (in particular the t channel) with $\lambda_{\chi\phi}$ beyond 0.4 (in case of $m_{\rm DM} = 500$ GeV). Note that the plot shows the insensitiveness related to $\lambda_{\phi H}$ in this low $\lambda_{\phi H}$ region for obvious reason. Similar results follow with $m_{\rm DM} < 300$ GeV also, where $\phi\phi \to H_1H_2$ provides the dominant contribution in $\langle\sigma v_{\phi\phi}\rangle$. Based on our discussion so far we note that for $\lambda_{\chi\phi} >> \lambda_{\phi H}$ the channels with Higgses in the final states contribute more to total $\langle\sigma v_{\phi\phi}\rangle$. On the other hand for low values of $\lambda_{\chi\phi}$ (although comparable to $\lambda_{\phi H}$), the model resembles the usual Higgs portal dark matter scenario where W bosons in the final state dominate. To summarize,

- 150 **GeV** $< m_{\rm DM} <$ 212.5 **GeV:** For low $\lambda_{\chi\phi}$, $\phi\phi \to W^+W^-$ dominates. However for large $\lambda_{\chi\phi}$, $\phi\phi \to H_1H_1$ becomes the main annihilation channel.
- 212.5 **GeV** $< m_{\rm DM} <$ 300 **GeV:** New annihilation process $\phi\phi \to H_1H_2$ opens up. This with $\phi\phi \to H_1H_1$ contribute dominantly for large $\lambda_{\chi\phi}$. Otherwise the channels with SM particles in final states dominate.
- 300 **GeV** $< m_{\rm DM} <$ 500 **GeV:** The annihilation channel $\phi\phi \to H_2H_2$ opens up in addition to H_1H_1 and H_1H_2 in the final states. Their relative contributions to total $\langle\sigma v_{\phi\phi}\rangle$ again depend on the value of $\lambda_{\chi\phi}$.

In the top left panel of Fig.4.3, we also note the existence of a small overlapped region when $\lambda_{\phi H} << \lambda_{\chi\phi}$ for the dark matter mass regions between 280-300 GeV and 300-310 GeV. This has been further clarified in Fig.4.4, where we note that relic density contour lines with

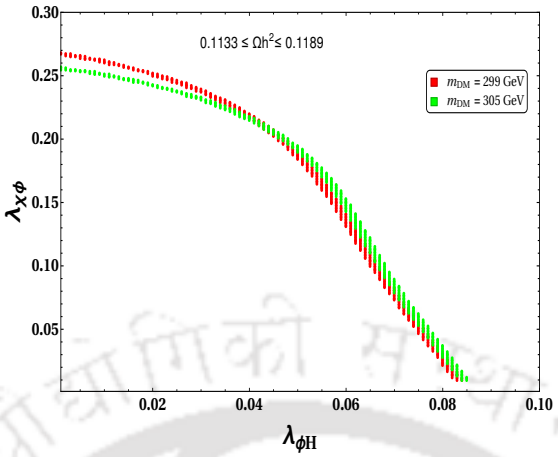

FIGURE 4.4: DM relic density contour lines in $\lambda_{\phi H}$-$\lambda_{\chi\phi}$ plane with $m_{\rm DM} = 299$ (red), 305 GeV (green).

$m_{\rm DM} = 299$ GeV and $m_{\rm DM} = 305$ GeV intersect each other around $\lambda_{\phi H} \sim 0.05$ and $\lambda_{\chi\phi} \sim 0.21$. Note that when DM mass $m_{\rm DM} \geq m_{H_2} = 300$ GeV, in addition to the $\phi\phi \to SM, SM$ and $\phi\phi \to H_1 H_2$ annihilation processes, $\phi\phi \to H_2 H_2$ opens up and contribute to the total annihilation cross section (this new channel can be realized through both H_1 and H_2 mediation). Then total annihilation cross section will be enhanced for $m_{\rm DM} > 300$ GeV case, *i.e* $\langle\sigma v_{\phi\phi}\rangle = \langle\sigma v\rangle_{\phi\phi\to SM,SM} + \langle\sigma v\rangle_{\phi\phi\to H_1,H_2} + \langle\sigma v\rangle_{\phi\phi\to H_2,H_2}$ becomes large compared to the 280 GeV $< m_{\rm DM} < 300$ GeV mass range where $\langle\sigma v\rangle_{\phi\phi\to H_2 H_2}$ is not present. This enhancement has to be nullified in order to realize the correct relic density and this is achieved by reducing $\lambda_{\chi\phi}$ compared to its required value for a fixed $\lambda_{\phi H}$ and $m_{\rm DM}$ in 280 GeV $\leq m_{\rm DM} < 300$ region. Note that in view of our previous discussion, we already understand that $\phi\phi \to H_2 H_2$ becomes important compared to $\phi\phi \to$ SM, SM process in the region with $\lambda_{\chi\phi} >> \lambda_{\phi H}$. Hence the two mass regions (below and above 300 GeV) overlap in $\lambda_{\phi H} - \lambda_{\chi\phi}$ plane as seen in the top left panel of Fig.4.3 as well in Fig.4.4. The total annihilation cross section of DM depends on its mass also. However the small mass differences between the two overlapped regions have very mild effect on $\langle\sigma v\rangle_{\rm Tot}$. Similar effect should be observed below and above $m_{\rm DM} \sim (m_{H_1} + m_{H_2})/2 = 212.5$ GeV as $\phi\phi \to H_1 H_2$ opens up there. However we find that around the $m_{\rm DM} = 212.5$ GeV, even with $\lambda_{\chi\phi} >> \lambda_{\phi H}$, the contribution from this particular channel to $\langle\sigma v\rangle_{\rm Tot}$ is negligible as compared to $\phi\phi \to$ SM SM contribution and hence we do not observe any such overlapped region there.

In the top right panel of Fig. 4.3 we provide the spin-independent (SI) direct detection (DD) cross sections corresponding to the points in the left panel satisfying relic density data having different range of dark matter masses as indicated by the colored patches. We further

put the LUX 2016[185], XENON 1T[183] and nT (expected) lines on it. As known, for a lowerer cross section, it reaches the neutrino floor where signals from DM can not be distinguished from that of neutrino. We find that the scenario works with reasonable values of the parameters, *i.e.* not with any un-naturally small or large values of couplings. Note that once we use the XENON 1T [183] and projected XENON nT [379] limits on the scattering cross section, we would obtain more restricted region of parameter space for $\lambda_{\phi H} - \lambda_{\chi\phi}$ as shown in left (with XENON 1T [183]) and right (with XENON nT [379]) figures of the bottom panel. From the plot with XENON-nT prediction, we find that the scenario works even with reasonably large values of $\lambda_{\phi H}$, $\lambda_{\chi\phi}$ required for satisfying the relic density, although they are comparable to each other. This is because of the fact that to keep the direct detection cross section relatively small (even smaller than the XENON nT), it requires a cancellation between $\lambda_{\phi H}$ and $\lambda_{\chi\phi}$ as can be seen from Eq.(4.16) in conjugation with definition of λ_1 and λ_2 for a specific $\sin\theta = 0.2$ value. Such a cancellation is not that important for plots with LUX 2016 [185] or XENON 1T [183] results and hence showing a wider region of parameter space for $\lambda_{\chi\phi}$ and $\lambda_{\phi H}$.

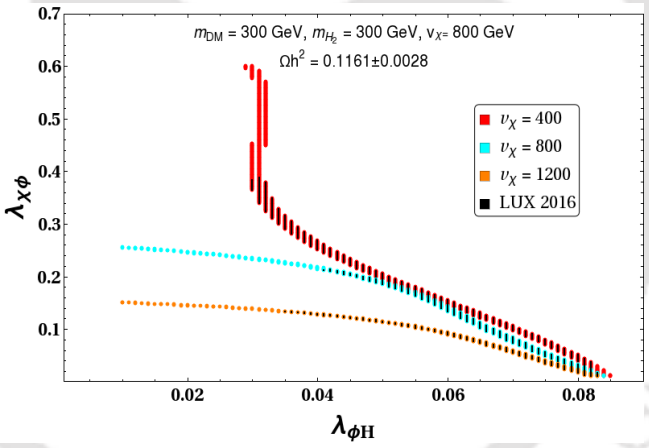

FIGURE 4.5: Allowed parameter space to satisfy correct relic abundance in $\lambda_{\phi H} - \lambda_{\chi\phi}$ plane with different v_χ for $m_{\rm DM} = 300$ GeV . Other parameters $m_{H_2} = 300$ GeV and and $\sin\theta = 0.2$ have been kept fixed. The LUX 2016 [185] allowed region are also accommodated (solid black region) in the figures.

It can be concluded from upper panel of Fig.4.3 that the presence of additional singlet scalar field χ helps in reducing the magnitude of $\lambda_{\phi H}$ that was required (say $\lambda^0_{\phi H}$) to produce correct relic density in minimal form of singlet scalar DM or in other words it dilutes the pressure on $\lambda_{\phi H}$ to produce correct relic density and to satisfy DD cross section simultaneously. For illustrative purpose, let us choose a dark matter mass with 500 GeV. From Fig. 1.7, we found that in order to satisfy the relic density, we need to have a $\lambda^0_{\phi H} \sim 0.15$ which can even be 0.02 in case with large $\lambda_{\chi\phi} \sim 0.6$. Similarly we notice that for $m_{\rm DM} = 300$ GeV, $\lambda^0_{\phi H}$ was 0.086 in

order to produce correct relic density which however was excluded from direct search point of view. This conclusion changes in presence of $\lambda_{\chi\phi}$ as we can see from Fig.4.3, (left panel) that $m_{\rm DM} = 300$ GeV can produce correct relic density and evade the direct search limit with smaller $\lambda_{\phi H}$: $0.065 - 0.086$. This is possible in presence of nonzero $\lambda_{\chi H}$ and small $\sin\theta(\sim 0.2$ here) which redistribute the previously obtained value of $\lambda^0_{\phi H}$ into $\lambda_{\phi H}$ and $\lambda_{\chi\phi}$ while simultaneously brings the direct search cross section less than the experimental limit due to its association with $\sin\theta$ (see the definition of λ_1 and λ_1).

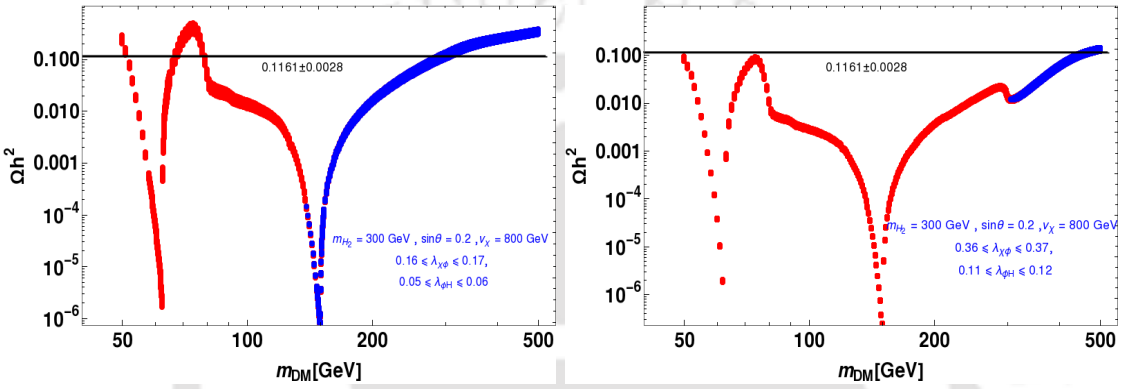

FIGURE 4.6: Relic density vs $m_{\rm DM}$ plot in the combined set up of SM+DM+RH neutrinos and χ field for two different specified range of of $\lambda_{\phi H}$ and $\lambda_{\chi\phi}$ as mentioned within the inset of figures. Two resonances are clearly visible at $m_{\rm DM} = m_{H_1}/2$ and $m_{H_2}/2$ respectively Blue patch represents the favoured region by LUX 2016 direct detection cross section limit whereas red patch is excluded by LUX 2016.

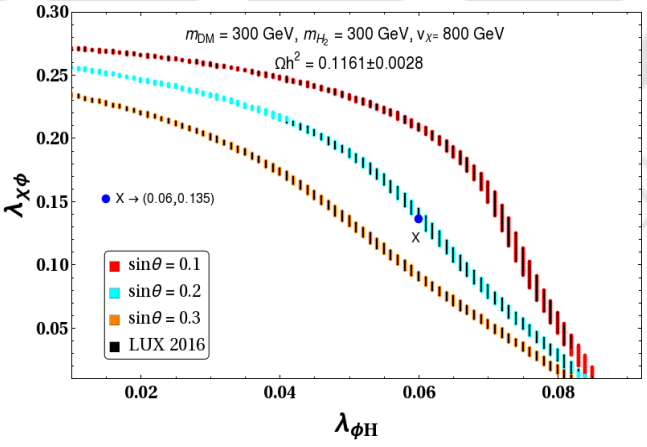

FIGURE 4.7: Allowed parameter space to satisfy correct relic abundance in $\lambda_{\phi H} - \lambda_{\chi\phi}$ plane with different values of $\sin\theta$ for $m_{\rm DM} = 300$ GeV. Other parameters $m_{H_2} = 300$ GeV and $v_\chi = 800$ GeV have been kept fixed. The LUX 2016 [185] allowed region are also accommodated (solid black region) in the figures. The blue dot point denoted by X in right panel will be used as a reference point for study on Higgs vacuum stability.

In Fig.4.6 (left panel), we show the relic density versus $m_{\rm DM}$ plot with our chosen set of parameters, $\{m_{H_2} = 300$ GeV ,$m_{H_1} = 125.09$ GeV, $\tan\beta = 0.307$, $\sin\theta = 0.2\}$ while varying $\lambda_{\chi H}$ and $\lambda_{\phi H}$ within $0.16 \leq \lambda_{\chi\phi} \leq 0.17$ and $0.05 \leq \lambda_{\phi H} \leq 0.06$. Similarly in right panel, we provide the relic density vs $m_{\rm DM}$ plot for a different range of $\lambda_{\chi H}$ and $\lambda_{\phi H}$. We note that there are two resonance regions, one at $m_{H_1}/2$ for the SM like Higgs and other at $m_{H_2}/2$ with heavy Higgs[3] mass at 300 GeV. In left panel for DM heavier than 150 GeV, we find $m_{\rm DM} \sim 300$ GeV can correctly produce the relic density in the observed range and simultaneously evade the DD limit set by LUX 2016 [185]. This result is consistent with the plot in Fig.4.3. Similarly $m_{\rm DM} \sim 500$ GeV is in the acceptable range, which is in line with observation in Fig.4.3. In the left panel of Fig.4.6 we also have another region of DM mass$\sim$ 75 GeV having correct relic abundance however discarded by LUX 2016. The region was not incorporated in top left panel of Fig.4.3 as we have started with $m_{\rm DM}$ bigger than 150 GeV only. The possibility of having dark matter lighter than 150 GeV in the present scenario will be discussed in the next subsection. Since in obtaining the Fig.4.3, we have fixed $\sin\theta, \tan\beta$ and m_{H_2}, below in Fig.4.5 and 4.7, we provide the expected range of two couplings $\lambda_{\chi H}$ and $\lambda_{\phi H}$ when $\sin\theta, \tan\beta$ are varied for dark matter mass $m_{\rm DM} = 300$ GeV . We find the variation is little sensitive with the change of both v_χ and $\sin\theta$. As v_χ or $\sin\theta$ increases for $m_{\rm DM} = 300$ GeV, it requires less $\lambda_{\chi\phi}$ for a particular $\lambda_{\phi H}$ to satisfy the relic density. We have also applied the LUX 2016[185] DD cross section limit in those plots and are indicated by solid black patches. In Fig.4.7, one dark blue dot has been put on the $\sin\theta = 0.2$ contour which will be used in study of Higgs vacuum stability as a reference point.

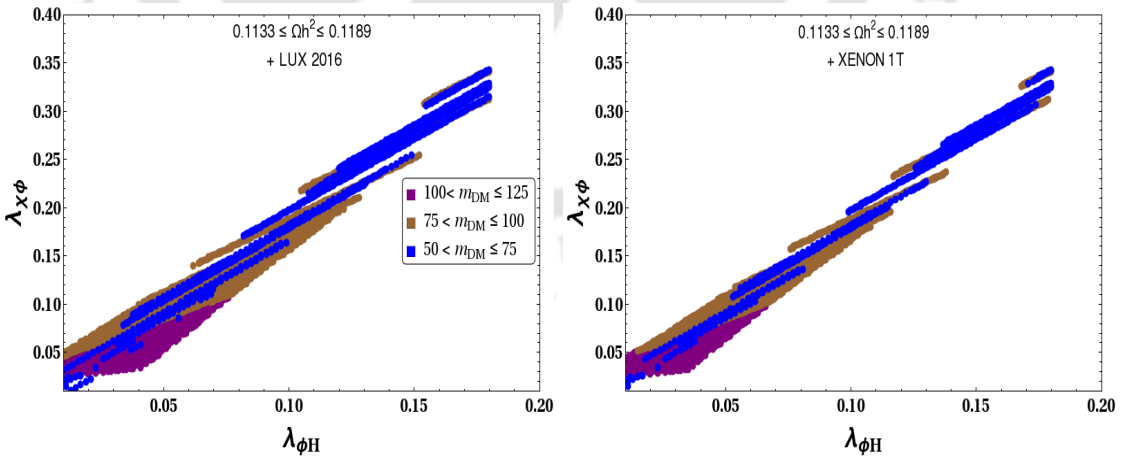

FIGURE 4.8: Relic density satisfied points in $\lambda_{\phi H} - \lambda_{\chi\phi}$ plane for $m_{\rm DM} < 150$ GeV with DD cross section consistent with [left panel] LUX 2016 [185] and [right panel] XENON 1T limit [183]. Benchmark points: $m_{H_2} = 300$ GeV, $v_\chi = 800$ GeV, $\sin\theta = 0.2$.

[3]As expected, it would be always possible to satisfy the relic density and DD limits within this region.

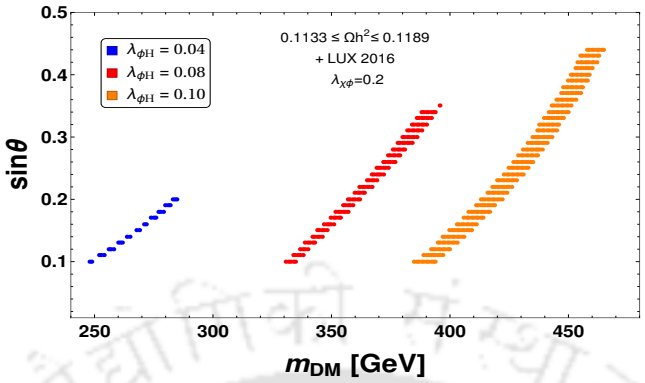

FIGURE 4.9: $m_{\rm DM}$ vs $\sin\theta$ plot for a fixed $\lambda_{\chi\phi}$ and $\lambda_{\phi H}$ as mentioned in the figure to satisfy the correct relic abundance and direct detection cross section consistent with LUX 2016 limit. Values of other parameters: $m_{H_2} = 300$ GeV, $\lambda_{\chi\phi} = 0.2$ and $v_\chi = 800$ GeV.

4.4.2 DM mass in region R2: ($m_{\rm DM} < 150$ GeV)

Here we briefly discuss the DM phenomenology in the low mass region $m_{\rm DM} < \frac{m_{H_2}}{2} = 150$ GeV. In this region, the decay process of heavy higgs to DM ($H_2 \to \phi\phi$) will be active. For further low $m_{\rm DM} < m_{H_1}/2 \simeq 62.5$, both $H_2 \to \phi\phi$ and $H_1 \to \phi\phi$ decay modes will be present.

We perform a scan over the $\lambda_{\phi H} - \lambda_{\chi\phi}$ region to find the correct relic density satisfied parameter space with allowed direct detection cross section from LUX 2016 [185] and XENON 1T experiments [183]. The results are shown in Fig.4.8, left and right panels where DD limits from LUX 2016 [left panel] and XENON 1T [right panel] are considered separately. In doing these plots, we have considered different mass ranges as indicated by different colors. The color codes are depicted within the inset of each figures. We note that the required $\lambda_{\chi\phi}$, $\lambda_{\phi H}$ values are almost in the similar range as obtained in Fig.4.3. We also note that there exists a resonance region through H_1 near $m_{\rm DM} \sim 63$ GeV, indicated by the blue patch. In this resonance region, the relic density becomes insensitive to the coupling and hence the blue patch is extended over the entire region of $\lambda_{\chi\phi}$, $\lambda_{\phi H}$ in the Fig.4.8.

Finally we attempt to estimate the $\sin\theta$ required to provide the correct amount of modification over the minimal version of a real singlet DM having interaction with the SM Higgs only in order to revive the 'below 500 GeV' DM into picture. In other words, the amount of $\sin\theta$ should be enough to satisfy correct relic abundance and DD cross section limits of LUX 2016 [185] and XENON 1T [183] for this particular mass range. To do the analysis, we fix $\lambda_{\chi\phi} \sim 0.2$ while three different values of $\lambda_{\phi H}$ at 0.04, 0.08 and 0.10 are considered for the study. We then

provide the $\sin\theta$ versus $m_{\rm DM}$ plot in Fig.4.9 which is consistent with relic density and LUX 2016 limits. We infer that a sizable value of $\sin\theta$ is required for this. With $\lambda_{\phi H} = 0.1$, we have noted earlier from Fig. 1.7 that it alone reproduces the desired relic density with a 330 GeV dark matter, although excluded by LUX 2016 limits. Now we observe from Fig. 4.9 that in order to make this as a viable DM mass, we need to have a $\sin\theta = \mathcal{O}(0.1)$ with $\lambda_{\phi H} = 0.1$. Such a moderate value of $\sin\theta$ is compatible with LEP and LHC results. A larger value of $\sin\theta \sim \mathcal{O}(0.3)$ with $\lambda_{\phi H} = 0.1$ can accommodate DM mass around 440 GeV as seen from the Fig. 4.9. Similarly, we indicate that with $\lambda_{\phi H} = 0.08[0.04]$ (for which DM mass $\sim$ 270 GeV and 110 GeV satisfy the relic density as seen from Fig. 1.7), $\sin\theta$ variation covers a range of DM mass $\sim$ 330-370 GeV [240-290 GeV] provided we restrict ourselves upto $\sin\theta = 0.3$.

4.5 Vacuum stability

In this section, we will discuss how the EW vacuum stability can be achieved in our model. For clarification purpose and a comparative study of it, we first discuss how the presence of different ingredients (three RH neutrinos, DM and extra scalar χ) can affect the running of the Higgs quartic coupling when added one after other. We first comment on the inclusion of the RH neutrinos and investigate the running of λ_H. Then we study how the involvement of the scalar singlet DM field ϕ can alter the conclusion. Finally we discuss the result corresponding to our set-up, *i.e.* including the χ field as well.

In doing this analysis, the absolute stability of the Higgs vacuum is ensured by $\lambda_H(\mu) > 0$ for any energy scale μ where the EW minimum of the scalar potential is the global minimum. However there may exist another minimum which is deeper than the EW one. In that case, we need to investigate whether the EW vacuum remains metastable or it turns into a unstable vacuum. The metastability criteria is provided in Eq.(1.107).

Before proceeding further, some discussion on the involvement of light neutrino mass in the context of vacuum stability is pertinent here. As stated before, the light neutrino mass is generated through type-I seesaw for which three RH neutrinos are included in the set up. We now describe the strategy that we adopt here in order to study their impact on RG evolution. For simplicity, the RH neutrino mass matrix M_N is considered to be diagonal with degenerate entries, *i.e.* $M_{i=1,2,3} = M_R$. As we will see, it is $\mathrm{Tr}[Y_\nu^\dagger Y_\nu]$ which enters in the β function of the relevant couplings. In order to extract the information on Y_ν, we employ the type-I mass formula $m_\nu = Y_\nu^T Y_\nu \frac{v^2}{2M_R}$. Naively one would expect that large Yukawas are possible only with very large RH neutrino masses. For example with $M_R \sim 10^{14}$ GeV, Y_ν comes out to be 0.3 in

order to obtain $m_\nu \simeq 0.05$ eV. Contrary to our naive expectation, it can be shown that even with smaller M_R one can achieve large values of $\mathrm{Tr}[Y_\nu^\dagger Y_\nu]$ once a special flavor structure of Y_ν is considered[348]. Note that we aim to study the EW vacuum stability in presence of large value of $\mathrm{Tr}[Y_\nu^\dagger Y_\nu]$. For this purpose, we use the parametrization by [380] and write Y_ν as

$$Y_\nu = \sqrt{2}\frac{\sqrt{M_R}}{v}\mathcal{R}\sqrt{m_\nu^d}\; U_{\rm PMNS}^\dagger, \tag{4.17}$$

where m_ν^d is the diagonal light neutrino mass matrix and $U_{\rm PMNS}$ is the unitary matrix diagonalizing the neutrino mass matrix m_ν such that $m_\nu = U_{\rm PMNS}^* m_\nu^d U_{\rm PMNS}^\dagger$. Here $\mathcal{R}$ represents a complex orthogonal matrix which can be written as $\mathcal{R} = O\exp(i\mathcal{A})$ with O as real orthogonal and $\mathcal{A}$ as real antisymmetric matrices respectively. Hence one gets

$$\mathrm{Tr}[Y_\nu^\dagger Y_\nu] = \frac{2M_R}{v^2}\mathrm{Tr}\Big[\sqrt{m_\nu^d}e^{2i\mathcal{A}}\sqrt{m_\nu^d}\Big]. \tag{4.18}$$

Note that the real antisymmetric matrix $\mathcal{A}$ does not appear in the seesaw expression for $m_\nu = \frac{Y_\nu^T Y_\nu v^2}{2M_R}$. Therefore with any suitable choice of $\mathcal{A}$, it would actually be possible to have sizeable Yukawas even with light M_R and hence this can affect the RG evolution of λ_H significantly. As an example, let us consider magnitude of all the entries of $\mathcal{A}$ to be equal, say a with all diagonal entries as zero. Then with $M_R = 1$ TeV, $\mathrm{Tr}[Y_\nu^\dagger Y_\nu]$ can be as large as 1 with $a = 8.1$ [380, 381]. Below we specify the details of Higgs vacuum stability in presence of RH neutrinos only.

4.5.1 Higgs vacuum stability with right-handed neutrinos

In presence of the RH neutrino Yukawa coupling Y_ν, the renormalization group (RG) equation of the SM couplings will be modified [382]. Below we present the one loop beta functions of Higgs quartic coupling λ_H, top quark Yukawa coupling y_t and neutrino Yukawa coupling Y_ν,

$$\frac{d\lambda_H}{d\ln\mu} = \frac{1}{16\pi^2}\{\beta_{\lambda_H}^{SM} + \beta_{\lambda_H}^{\rm I}\} \text{ with } \beta_{\lambda_H}^{\rm I} = 4\lambda_H\mathrm{Tr}[Y_\nu^\dagger Y_\nu] - 2\mathrm{Tr}[(Y_\nu^\dagger Y_\nu)^2]\,, \tag{4.19}$$

$$\frac{dy_t}{d\ln\mu} = \frac{1}{16\pi^2}\{\beta_{y_t}^{SM} + \beta_{y_t}^{\rm I}\} \text{ with } \beta_{y_t}^{\rm I} = \mathrm{Tr}[Y_\nu^\dagger Y_\nu]y_t, \tag{4.20}$$

$$\frac{d\mathrm{Tr}[Y_\nu^\dagger Y_\nu]}{d\ln\mu} = \frac{1}{16\pi^2}\beta_{\mathrm{Tr}[Y_\nu^\dagger Y_\nu]}^{\rm I} = \frac{1}{16\pi^2}\Big\{(6y_t^2 + 2\mathrm{Tr}[Y_\nu^\dagger Y_\nu] - \frac{3}{2}g_1^2 - \frac{9}{2}g_2^2)\mathrm{Tr}[Y_\nu^\dagger Y_\nu] + 3\mathrm{Tr}[(Y_\nu^\dagger Y_\nu)^2]\Big\}, \tag{4.21}$$

where $\beta_{\lambda_H}^{SM}$ and $\beta_{y_t}^{SM}$ represent the β functions of λ_H and y_t respectively in SM. The Y_ν dependence is to be evaluated in accordance with the type-I seesaw expression, $m_\nu = Y_\nu^T Y_\nu \frac{v^2}{M_R}$. Also with large a (elements of $\mathcal{A}$), it is found [348] that $\mathrm{Tr}[(Y_\nu^\dagger Y_\nu)^2] \simeq \mathrm{Tr}[Y_\nu^\dagger Y_\nu]^2$ and we

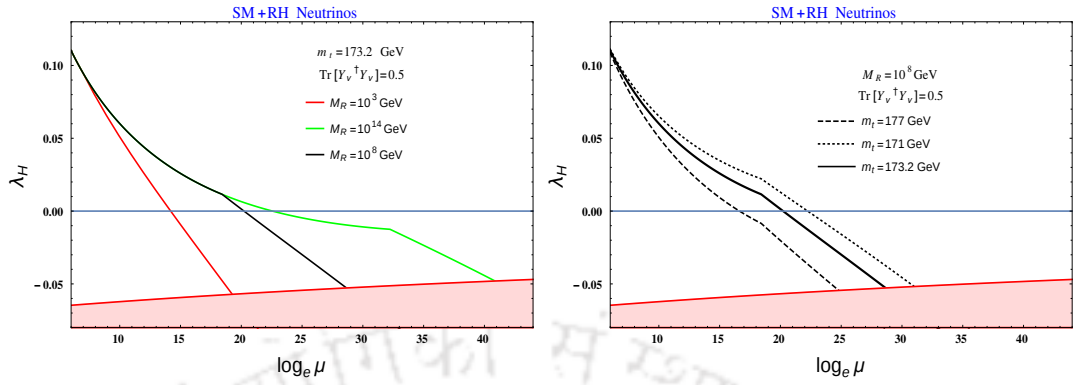

FIGURE 4.10: RG running of λ_H with energy scale μ in SM + RH neutrinos;[Left panel]: different RH neutrino mass scales M_R are considered with fixed $m_t = 173.2$ GeV, [Right panel]: different top masses are considered with $M_R = 10^8$ GeV.

will be using this approximated relation in obtaining the running of the couplings through Eqs.(4.19,4.20,4.21). Here we have used the best fit values of neutrino oscillation parameters for normal hierarchy [383, 384]. We have also considered the mass of lightest neutrino to be zero.

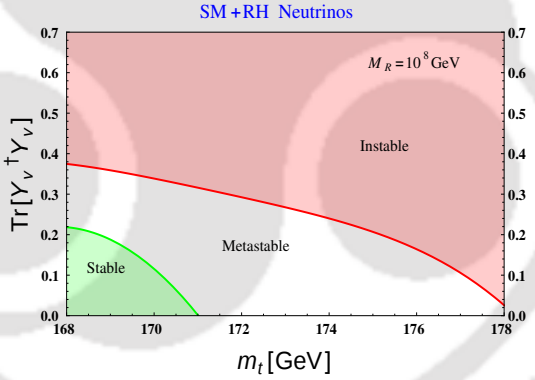

FIGURE 4.11: Region plot for m_t-Tr$[Y_\nu^\dagger Y_\nu]$ in the SM, extended with RH neutrinos having degenerate mass $M_R = 10^8$ GeV. The plane is divided into three categories (i) absolute stability, (ii) metastability and (iii) instability.

Note that just like the top quark Yukawa coupling, the neutrino Dirac Yukawa is having a similar impact on the Higgs quartic coupling, in particular with large Y_ν. Also the top quark Yukawa would have a contribution dependent on Y_ν. This has been studied in several works [76, 227, 317, 324, 343–348]. We summarize here the results with some benchmark values of RH neutrino masses. These will be useful for a comparative study with the results specific to our model. In Fig.4.10 (left panel), we have plotted running of the Higgs quartic coupling λ_H against energy scale μ till M_P for different choices of $M_R = 10^3, 10^8$ and 10^{14} GeV with Tr$[Y_\nu^\dagger Y_\nu] = 0.5$ denoted by red, black and green solid lines respectively. The pink shaded portion

represents the instability region given by the inequality [30] $\lambda_H \leq -0.065/[1 - 0.01\ln\left(\frac{v}{\mu}\right)]$. As expected, we find that the Higgs quartic coupling enters into the instability region well before the Planck scale. In the right panel of Fig.4.10, the effect of choosing different m_t within the

Scale	y_t	g_1	g_2	g_3	λ_H
$\mu = m_t$	0.93610	0.357606	0.648216	1.16655	0.125932

TABLE 4.1: Values of the relevant SM couplings (top-quark Yukawa y_t, gauge couplings g_i and λ_H) at energy scale $\mu = m_t = 173.2$ GeV with $m_h = 125.09$ GeV and $\alpha_S(m_Z) = 0.1184$.

present 2σ uncertainty is shown for a fixed $M_R = 10^8$ GeV. The black solid, dashed and dotted lines represent the λ_H running with m_t as 173.2 GeV, 177 GeV and 171 GeV respectively. In doing this analysis, we fix the initial values of all the SM couplings [34] as given in Table 6.3 at an energy scale $\mu = m_t$. Here we consider $m_h = 125.09$ GeV, $m_t = 173.2$ GeV and $\alpha_s = 0.1184$. In Fig.4.11, we have shown a region plot for $\mathrm{Tr}[Y_\nu^\dagger Y_\nu]$ and m_t with fixed M_R at 10^8 GeV in terms of stability (λ_H remains positive all the way upto M_P), metastability and instability of the EW vacuum of the SM. The top quark mass is varied between 168 GeV to 178 GeV. The region in which EW vacuum is stable is indicated by green and the metastable region is indicated by white patches. The instability region is denoted with pink shaded part. It can be noted that the result coincides with the one obtained in [343]. We aim to discuss the change obtained over this diagram in the context of our model.

4.5.2 Higgs vacuum stability from Higgs Portal DM and RH neutrinos

Here we discuss the vacuum stability scenario in presence of both the scalar DM (ϕ) and three RH neutrinos (N). In that case, effective scalar potential becomes $V_{\rm I} + V_H$ only. Note that the DM phenomenology is essentially unaffected from the inclusion of the heavy RH neutrinos with the assumption $M_R >> m_{\rm DM}$. On the other hand combining Eq.(4.19,4.20,4.21), we obtain the corresponding beta functions for the couplings as provided below;

$$\frac{d\lambda_H}{dt} = \frac{1}{16\pi^2}\{\beta^{SM}_{\lambda_H} + \beta^{\rm I}_{\lambda_H} + \beta^{\rm II}_{\lambda_H}\} \text{ where } \beta^{\rm II}_{\lambda_H} = \frac{\lambda^2_{\phi H}}{2}, \tag{4.22}$$

$$\frac{d\lambda_{\phi H}}{dt} = \frac{1}{16\pi^2}\beta^{\rm I}_{\lambda_{\phi H}} = \frac{1}{16\pi^2}\Big\{12\lambda_H\lambda_{\phi H} + \lambda_\phi\lambda_{\phi H} + 4\lambda^2_{\phi H} + 6y_t^2\lambda_{\phi H} - \frac{3}{2}g_1^2\lambda_{\phi H} - \frac{9}{2}g_2^2\lambda_{\chi H} + 2\mathrm{Tr}[Y_\nu^\dagger Y_\nu]\lambda_{\phi H}\Big\}, \tag{4.23}$$

$$\frac{d\lambda_\phi}{dt} = \frac{1}{16\pi^2}\beta^{\rm I}_{\lambda_\phi} = \frac{1}{16\pi^2}\Big\{3\lambda^2_\phi + 12\lambda^2_{\phi H}\Big\}. \tag{4.24}$$

From the additional term $\beta^{\rm II}_{\lambda_H}$, we expect that the involvement of DM would affect the EW vacuum stability in a positive way (*i.e.* pushing the vacuum more toward the stability) as shown in [65, 68, 69, 71, 73, 342] whereas we noted in the previous subsection that the Yukawa coupling (if sizable) has a negative impact on it.

The interplay between the neutrino Yukawa coupling and Higgs portal coupling with DM is shown in Fig. 4.12, left and right panels (top and bottom). For the purpose of comparison, we have kept the same set of choices of parameters as in Fig.4.10, (left and right panels). For the top panels, we consider mass of the dark matter to be $m_{\rm DM} = 300$ GeV and for the bottom set, $m_{\rm DM} = 920$ GeV is taken. The choice of $m_{\rm DM}$ could in turn fix the $\lambda_{\phi H}$ coupling from the relic density plot of Fig.1.7. For example with $m_{\rm DM} = 300$ GeV $\lambda_{\phi H}$ is 0.075 and for $m_{\rm DM} = 920$ GeV, $\lambda_{\phi H}$ is given by 0.286 value. It is evident that the presence of Higgs portal coupling only has a mild effect as compared to the impact created by the neutrino Yukawa coupling. Finally in Fig.4.13 we provide the region plot in $\rm Tr[Y_\nu^\dagger Y_\nu]$ - m_t plane where the stable and instable regions are indicated by green and pink patches. This plot while compared with Fig.4.11, indicates that there is no such noticeable improvement except the mild enhancement of the metastable region due to the involvement of singlet scalar (DM) with Higgs portal coupling. With an aim to accommodate both the massive neutrinos and a relatively light dark matter (< 500 GeV), we move on to the next section where the χ field is included.

4.5.3 EW vacuum stability in extended Higgs portal DM and RH neutrinos

Turning into the discussion on vacuum stability in our framework of extended Higgs portal having three RH neutrinos, DM and the χ fields, we first put together the relevant RG equations (for $\mu > m_{\rm DM}, m_{H_2}$) as given by,

$$\frac{d\lambda_H}{dt} = \frac{1}{16\pi^2}\{\beta^{SM}_{\lambda_H} + \beta^{\rm I}_{\lambda_H} + \beta^{\rm II}_{\lambda_H} + \frac{\lambda^2_{\chi H}}{2}\}, \tag{4.25}$$

$$\frac{d\lambda_{\phi H}}{dt} = \frac{1}{16\pi^2}\{\beta^{\rm I}_{\lambda_{\phi H}} + \lambda_{\chi\phi}\lambda_{\chi H}\}, \tag{4.26}$$

$$\frac{d\lambda_{\phi}}{dt} = \frac{1}{16\pi^2}\{\beta^{\rm I}_{\lambda_{\phi}} + 3\lambda^2_{\chi\phi}\}, \tag{4.27}$$

$$\begin{aligned}
\frac{d\lambda_{\chi H}}{dt} &= \frac{1}{16\pi^2}\Big\{12\lambda_H\lambda_{\chi H} + \lambda_\chi\lambda_{\chi H} + 4\lambda^2_{\chi H} + 6y_t^2\lambda_{\chi H} - \frac{3}{2}g_1^2\lambda_{\chi H} - \frac{9}{2}g_2^2\lambda_{\chi H} + \lambda_{\chi\phi}\lambda_{\phi H} + 2{\rm Tr}[Y_\nu^\dagger Y_\nu]\lambda_{\chi H}\Big\}, \\
\frac{d\lambda_{\chi}}{dt} &= \frac{1}{16\pi^2}\Big\{3\lambda^2_\chi + 12\lambda^2_{\chi H} + 3\lambda^2_{\chi\phi}\Big\}, \\
\frac{d\lambda_{\chi\phi}}{dt} &= \frac{1}{16\pi^2}\Big\{4\lambda^2_{\chi\phi} + \lambda_{\chi\phi}(\lambda_\phi + \lambda_\chi) + 4\lambda_{\phi H}\lambda_{\chi H}\Big\}.
\end{aligned} \tag{4.28}$$

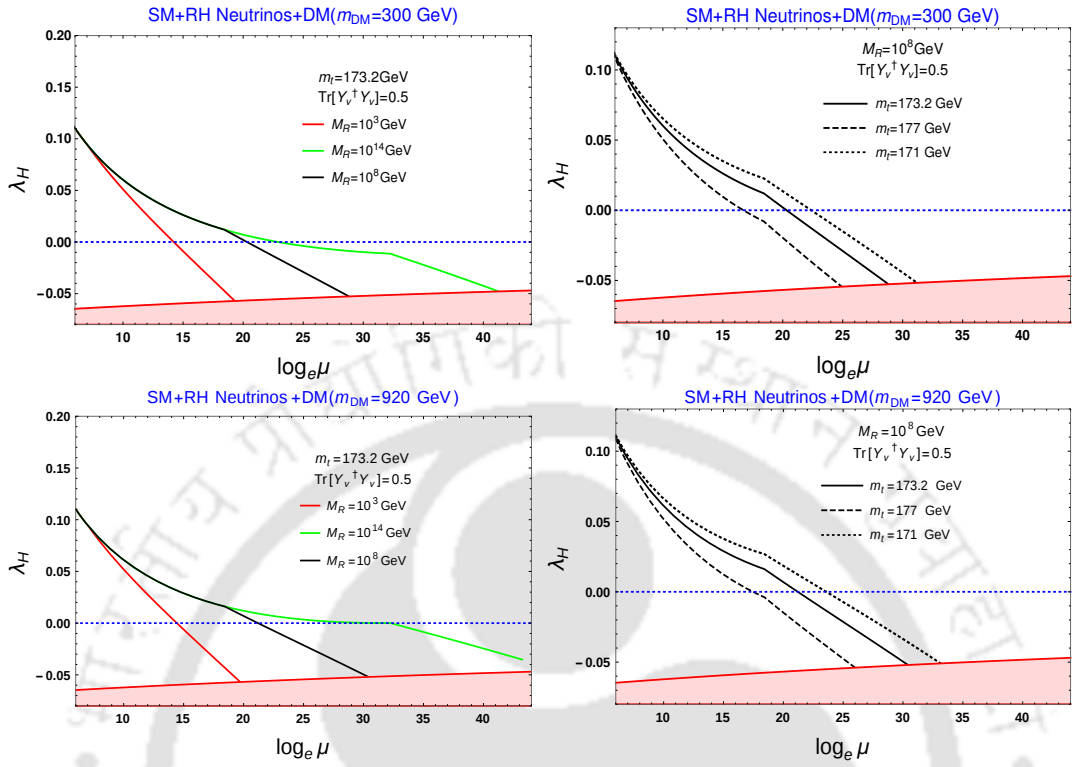

FIGURE 4.12: RG evolution of λ_H with energy scale μ with SM+DM+RH Neutrinos with $\lambda_\phi = 0.7$, $m_H = 125.09$ GeV and $\alpha_S(m_Z) = 0.1184$.: (a) [top panels]: $m_{\rm DM} = 300$ GeV, and (b) [bottom panels]: $m_{\rm DM} = 920$ GeV. In left panels m_t is fixed at 173.2 GeV and plots are there with different M_R while in right panel M_R is fixed at 10^8 GeV and different m_t values are considered.

We note that the couplings $\lambda_{\chi\phi}, \lambda_{\phi H}$ and $\lambda_{\chi H}$ which played important role in DM phenomenology, are involved in the running of couplings as well. From the discussion of the DM section, we have estimated these parameters in a range so as to satisfy the appropriate relic density and be within the direct search limits for a specific choice of other parameters at their reference values: $m_{H_2} = 300$ GeV and $v_\chi = 800$ GeV, $\sin\theta = 0.2$ (henceforth we describe this set as A). In particular an estimate for $\lambda_{\chi\phi}, \lambda_{\phi H}$ are obtained from Fig.4.3 (for 150 GeV$< m_{\rm DM} <$ 500 GeV) and from Fig. 4.8 (for $m_{\rm DM} <$ 150 GeV) having different choices of $m_{\rm DM}$ and $\sin\theta$. The parameter $\lambda_{\chi H}$ dependence is mostly realized through $\sin\theta$ following Eq.(6.21), where $m_{H_2}, \tan\beta$ are fixed from set A. This $\sin\theta$ is the most crucial parameter which control both the DM phenomenology and the vacuum stability. We have already seen that it allows the scalar singlet DM to be viable for the low mass window by relaxing $\lambda_{\phi H}$ from its sole role in case of single scalar singlet DM. On the other hand, a non-zero $\sin\theta$ provides a positive shift (it is effectively the threshold effect in the small θ limit as seen from Eq. (6.19)) to the Higgs quartic coupling and hence guides the λ_H toward more stability. Hence $\sin\theta$ would be a crucial parameter in this study. Note that the

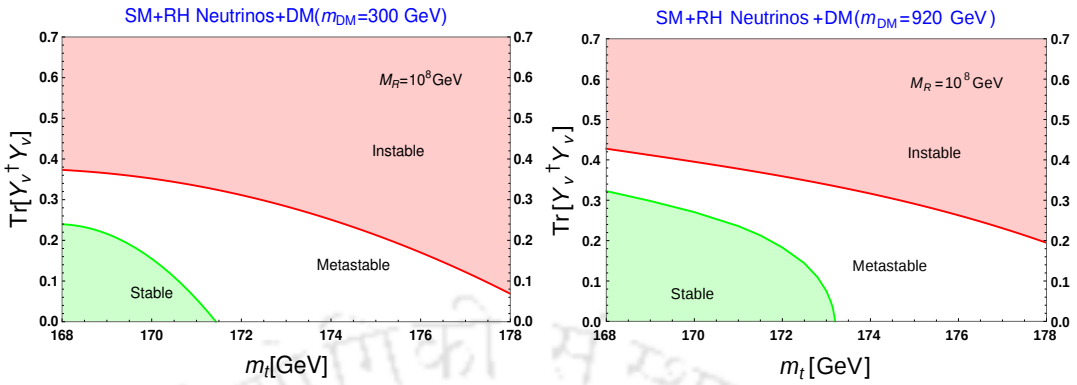

FIGURE 4.13: Regions of Stability, metastability and instability in SM+DM+RH neutrinos case in the $\mathrm{Tr}[Y_\nu^\dagger Y_\nu]$ -m_t plane for $m_{\rm DM} = 300$ GeV (left panel) and 920 GeV (right panel). We consider $\lambda_\phi = 0.7$, $m_H = 125.09$ GeV and $\alpha_S(m_Z) = 0.1184$ for both the figures.

RH neutrinos being relatively heavy as compared to the DM, neutrino Yukawa coupling does not play much role in DM phenomenology.

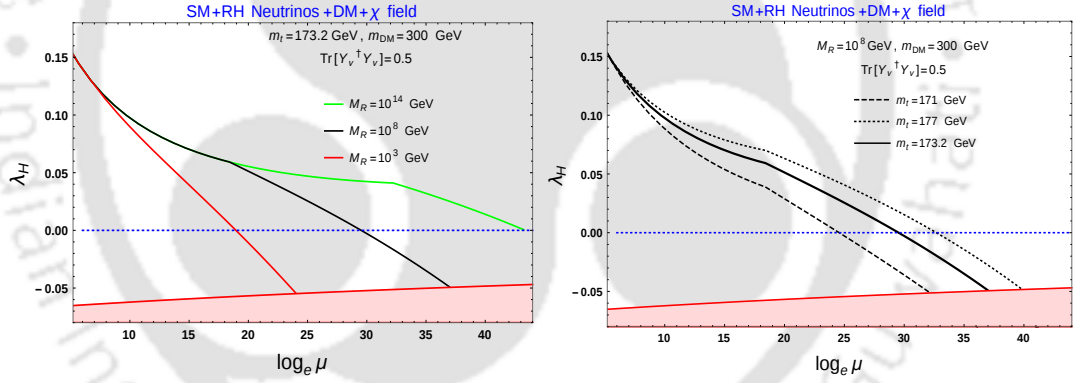

FIGURE 4.14: RG running of λ_H vs μ in the combined scenario of SM+RH Neutrinos+DM+χ field with $m_{\rm DM} = 300$ GeV, $\sin\theta = 0.2$ and $m_{H_2} = 300$ GeV. In [left pannel] m_t (~ 173.2 GeV) is kept fixed, M_R is varied, and in [right panel] M_R ($\sim 10^8$ GeV) is fixed, m_t has been varied. Point X ($\lambda_{\phi H} = 0.06$, $\lambda_{\chi\phi} = 0.135$) from Fig.4.7 and $\lambda_\phi = 0.7$ have been used as benchmark points.

Assuming the validity of this extended SM (with three RH neutrinos and two singlets, ϕ, χ) upto the Planck scale, we study the running of the Higgs quartic coupling λ_H from EW scale to M_P as shown in Fig.4.14. In obtaining the running, we have considered $m_{H_2} = 300$ GeV, $\sin\theta = 0.2$ and $m_{\rm DM}$ is considered to be 300 GeV. The values of $\lambda_{\chi\phi}$ and $\lambda_{\phi H}$ are fixed at 0.135 and 0.06 respectively (this particular point is denoted by a blue dot, named X, on Fig.4.7). It turns out that any other set of $\lambda_{\chi\phi}$ and $\lambda_{\phi H}$ other than this blue dot from Fig. (while $m_{\rm DM} = 300$ GeV is fixed) would not change our conclusion significantly as long as $\sin\theta$ is

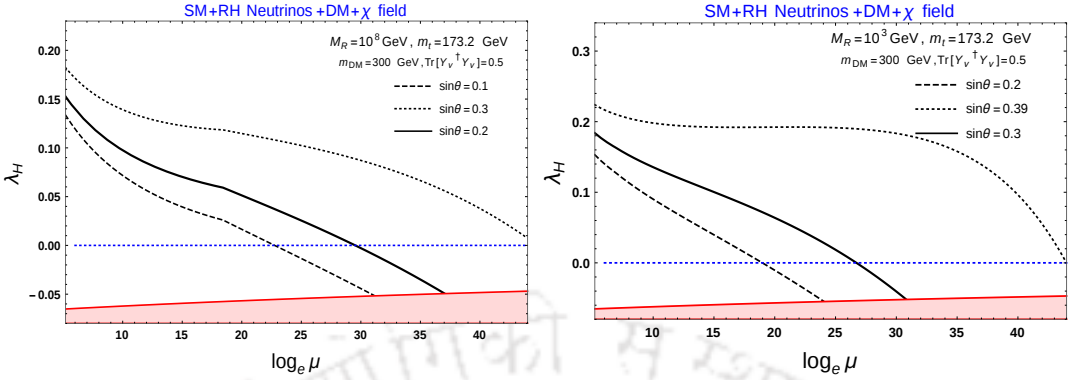

FIGURE 4.15: RG running of λ_H with energy scale μ for different values of $\sin\theta$ in the combined set up of SM+DM+RH neutrinos+χ field where in [left panel] $M_R = 10^8$ GeV and in [right panel] $M_R = 10^3$ GeV. Other reference values: $m_{\rm DM} = 300$ GeV, $m_{H_2} = 300$ GeV, $\mathrm{Tr}[Y_\nu^\dagger Y_\nu] = 0.5$ and $\lambda_{\phi H} = 0.06$ and $\lambda_{\chi\phi} = 0.135$.

considered at 0.2. In order to compare the effect of the extra scalar χ in the theory, we keep the neutrino parameters $\mathrm{Tr}[Y_\nu^\dagger Y_\nu]$ and M_R at their respective values considered in Figs.4.10, 4.12.

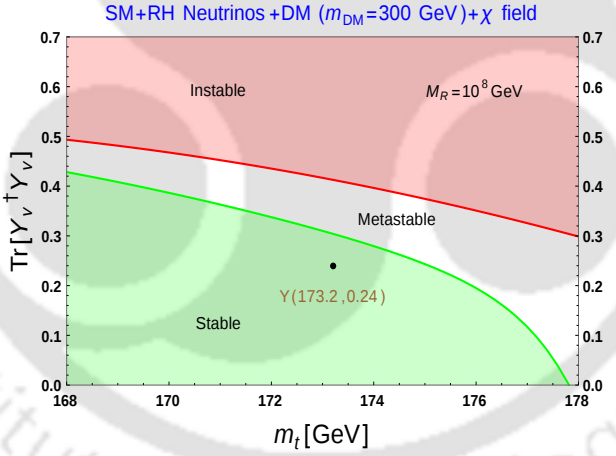

FIGURE 4.16: Stability, metastability and instability region on $\mathrm{Tr}[Y_\nu^\dagger Y_\nu]$ -m_t plane for $M_R = 10^8$ GeV in the extended scenario of the SM with 3 RH neutrinos, DM and χ. We have used point X ($\lambda_{\phi H} = 0.06$, $\lambda_{\chi\phi} = 0.135$) from Fig.4.7, $\sin\theta = 0.2$, $m_{H_2} = 300$ GeV, $v_\chi = 800$ GeV, $m_{\rm DM} = 300$ GeV and $\lambda_\phi = 0.7$ as benchmark points.

In the left panel of Fig.4.14, the running is performed for three different choices of M_R, specifically at 1 TeV, 10^8 GeV and 10^{14} GeV while top mass is fixed at 173.2 GeV. A similar plot is exercised in right panel of Fig.4.14 where three different choices of $m_t = (171, 173.2, 177)$ GeV are considered while M_R is fixed at 10^8 GeV. Contrary to our previous finding in section (see Fig.4.10, 4.12), we clearly see here that with $M_R = 10^{14}$ GeV and $m_t = 171$ GeV, λ_H remains positive upto M_P even in presence of large $\mathrm{Tr}[Y_\nu^\dagger Y_\nu] \sim \mathcal{O}(1)$. Hence EW vacuum turns

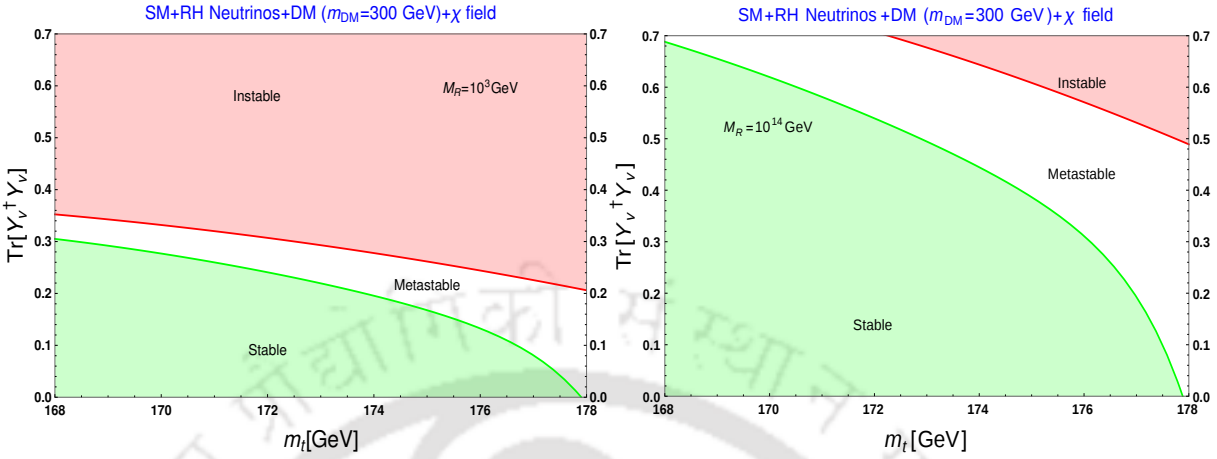

FIGURE 4.17: Stability, metastability and instability region on $\mathrm{Tr}[Y_\nu^\dagger Y_\nu]$ -m_t plane in the extended scenario of the SM with 3 RH neutrinos, DM and χ for (right panel) $M_R = 10^3$ GeV and (left panel) $M_R = 10^{14}$ GeV. We have used Point X ($\lambda_{\phi H} = 0.06$, $\lambda_{\chi\phi} = 0.135$) from Fig.4.7, $\sin\theta = 0.2$, $m_{H_2} = 300$ GeV, $v_\chi = 800$ GeV, $m_{\rm DM} = 300$ GeV and $\lambda_\phi = 0.7$ as benchmark points.

out to be absolutely stable. Although there exists other values of M_R and/or m_t, for which EW vacuum still remains unstable, the scale at which λ_H enters into the instable region is getting delayed with a noticeable change from earlier cases (Figs.4.10, 4.12). This becomes possible due to the introduction of the χ field having contribution mostly from the $\sin\theta$ parameter. In order to show its impact on stability, in Fig.4.15 (left panel), we plot λ_H running with different choices of $\sin\theta = 0.1, 0.2, 0.3$ for $M_R = 10^8$ GeV, $m_t = 173.2$ GeV and $m_{\rm DM} = 300$ GeV while keeping $\mathrm{Tr}[Y_\nu Y_\nu^\dagger] = 0.5$ (same as in Fig.4.14, left panel, black solid line). It shows that while $\sin\theta = 0.2$ (black solid line) can not make the EW vacuum absolutely stable till M_P, an increase of $\sin\theta$ value ~ 0.3 can do it (dotted line). Similarly in Fig. 4.15 (right panel), we consider a lowerer M_R as 1 TeV. We have already noticed that such a low M_R with large $\mathrm{Tr}[Y_\nu^\dagger Y_\nu] = 0.5$ pushes EW vacuum toward instability at a much lower scale $\sim 10^6$ GeV. In order to make the EW vacuum stable with such an M_R and $\mathrm{Tr}[Y_\nu^\dagger Y_\nu]$, one requires $\sin\theta \sim 0.4$ as seen from the right panel of Fig.4.15 (dotted line). However such a large $\sin\theta$ is ruled out from the experimental constraints [371]. For representative purpose, we also include study with other $\sin\theta = 0.2, 0.3$ denoted by dashed and solid lines.

We provide Fig.4.16 where the regions with stability, meta-stability and instability are marked green, white and pink patches in the plane containing $\mathrm{Tr}[Y_\nu^\dagger Y_\nu]$ and m_t. With $M_R = 10^3$ GeV and $M_R = 10^{14}$ GeV, similar plots are shown in Fig.4.17, left and right panels. Finally in Fig.4.18, we have shown the RG evolution of all the stability conditions in Eq.(4.11) from m_t to

M_P to check their validity all the way upto M_P. For this purpose, we have considered the initial values of the parameters involved in the following way. For values of $\lambda_{\phi H}$ and $\lambda_{\chi\phi}$ corresponding to $\sin\theta = 0.2, v_\chi = 800$ GeV and $m_{\rm DM} = 300$ GeV, we have considered the benchmark point values as indicated by a blue dot named X in Fig.4.7 . The value of λ_χ is then followed from Eq.(4.9) and λ_ϕ is chosen to be at 0.7. Values of $\mathrm{Tr}[Y_\nu^\dagger Y_\nu] = 0.24$ and $m_t = 173.2$ GeV are chosen for this purpose from Fig.4.16 (here the benchmark values are denoted by a black dot Y). We conclude that all the stability criteria are fulfilled within the framework. Lastly we comment that instead of picking up the point X from relic density contour with $\sin\theta \sim 0.2$ in Fig.4.7 to study vacuum stability in our model, we could have chosen any other point from that curve. As the stability of Higgs vacuum primarily depends on the value of θ, our conclusion would not change much. However choice of any point having large $\lambda_{\chi\phi}$ could make it reaching Landau pole well before M_P in its RG running through Eq.(4.28). To avoid that one can reduce the value of $\lambda_\phi \sim \mathcal{O}(10^{-2})$ or less (earlier it was 0.7) which has no direct connection or impact on DM phenomenology and vacuum stability analysis in the proposed set up. In Fig.4.19, we have shown the running of all parameters from M_R to M_P involved in perturbative unitarity bound for the benchmark point: $m_{H_2} = 300$ GeV, $\tan\beta = 0.30$, $\sin\theta = 0.2$, $m_{\rm DM} = 300$ GeV, $\lambda_{\phi H}$=0.06, $\lambda_{\chi\phi} = 0.135$, $M_R = 10^8$ GeV and $\mathrm{Tr}[Y_\nu^\dagger Y_\nu] = 0.24$ with $m_t = 173.2$ GeV. The parameters never exceed the upper limits coming from the unitarity bound. We have also confirmed that any other benchmark points wherever mentioned in our analysis satisfy the perturbativity unitarity limit.

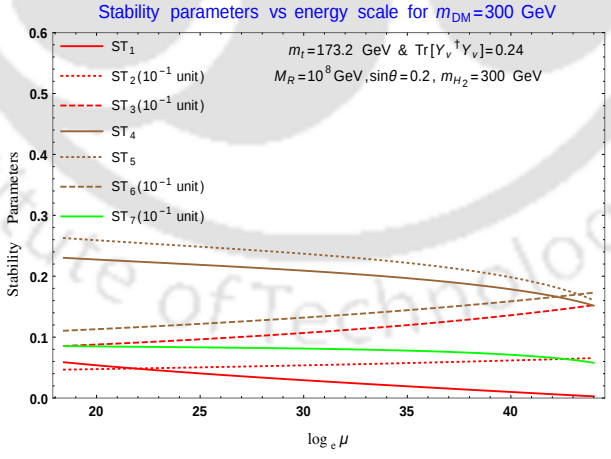

FIGURE 4.18: Evolution of stability parameters (Eq.4.11) for the point Y ($m_t = 173.2$ GeV, $\mathrm{Tr}[Y_\nu^\dagger Y_\nu] = 0.24$) from Fig.4.17 (top right panel). Benchmark points: Point X ($\lambda_{\phi H} = 0.06$, $\lambda_{\chi\phi} = 0.135$) from Fig.4.7, $M_R = 10^8$ GeV, $\sin\theta = 0.2$, $m_{H_2} = 300$ GeV, $v_\chi = 800$ GeV, $m_{\rm DM} = 300$ GeV and $\lambda_\phi = 0.7$ have been used.

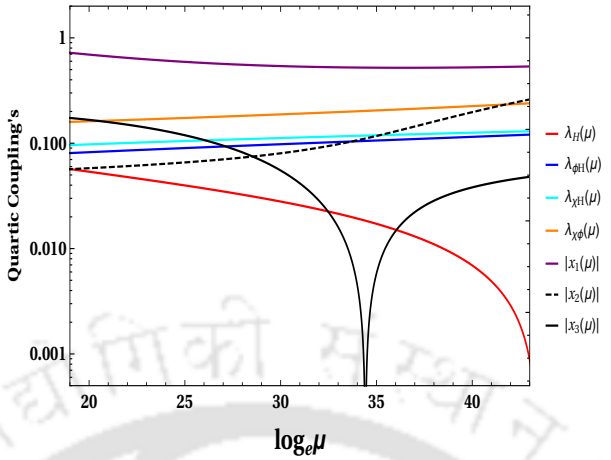

FIGURE 4.19: Evolution of parameters required to satisfy the perturbativity unitarity limit (Eq.(4.12)) for the point Y ($m_t = 173.2$ GeV, $\mathrm{Tr}[Y_\nu^\dagger Y_\nu] = 0.24$) from Fig.4.17 (top right panel). Benchmark points: Point X ($\lambda_{\phi H} = 0.06$, $\lambda_{\chi\phi} = 0.135$) from Fig.4.7, $M_R = 10^8$ GeV, $\sin\theta = 0.2$, $m_{H_2} = 300$ GeV, $v_\chi = 800$ GeV, $m_{\rm DM} = 300$ GeV and $\lambda_\phi = 0.7$ have been considered.

We end this section by comparing the results of vacuum stability in presence of (i) only RH neutrinos, (ii) RH neutrinos + DM and (iii) RH neutrinos + DM + extra scalar with non-zero vev, where in each cases neutrino Yukawa coupling Y_ν has sizeable contributions. For this purpose, we consider $m_t = 173.2$ GeV and $M_R = 10^8$ GeV. From Fig.4.11, for SM + RH neutrinos, we see that stability can not be achieved. The metastability scenario is still valid in this case upto $\mathrm{Tr}[Y_\nu^\dagger Y_\nu] < 0.26$. Next we add a singlet scalar DM candidate with nonzero Higgs portal coupling to SM with RH neutrinos. Fig.4.13 (left panel) shows, for $m_{\rm DM} = 300$ GeV, stability of EW vacuum still remains elusive. On the other hand the metastability bound on $\mathrm{Tr}[Y_\nu^\dagger Y_\nu]$ increases slightly from previous limit to 0.28. So DM with mass 300 GeV has mild impact on study of vacuum stability. Finally we add the extra scalar singlet with non zero vev to the SM with RH neutrinos and scalar DM. We have fixed the heavier Higgs mass $m_{H_2} = 300$ GeV and $\sin\theta = 0.2$. Now in the combined set up of the SM, scalar DM, scalar with non zero vev and RH neutrinos, the situation changes drastically from previous case as seen in Fig.4.16. For the same top and RH neutrino masses, we can now achieve absolute stability upto $\mathrm{Tr}[Y_\nu^\dagger Y_\nu] < 0.3$ and the metastability bound on $\mathrm{Tr}[Y_\nu^\dagger Y_\nu]$ further improved to 0.41. Overall notable enhancement in the stability and metastability region has been observed in $\mathrm{Tr}[Y_\nu^\dagger Y_\nu] - m_t$ plane compared to the earlier cases. Hence, the numerical comparison clearly shows that the extra scalar having non zero mixing with the SM Higgs effectively plays the leading role to get absolute vacuum stability in our model.

4.6 Connection with other observables

In this section, we first discuss in brief the constraints on the parameters of the model that may arise from lepton flavor violating (LFV) decays. The most stringent limit follows from $\mu \to e\gamma$ decay process. The branching ratio of such decay process in our set-up is given by [385–387]

$$\mathrm{Br}(\mu \to e\gamma) = \frac{3\alpha_e v^4}{16\pi M_R^4} |Y^\dagger_{\nu_{ei}} Y_{\nu_{i\mu}}|^2 |f(x)|^2, \tag{4.29}$$

where $\alpha_e = \frac{e^2}{4\pi}$ is the fine sructure constant, i runs from 1 to 3, $x = \frac{M_R^2}{m_W^2}$ and

$$f(x) = \frac{x\left(2x^3 + 3x^2 - 6x - 6x^2 \ln x + 1\right)}{2(1-x)^4}. \tag{4.30}$$

The current experimental limit on LFV branching ratio is [293]

$$\mathrm{Br}(\mu \to e\gamma) < 5.7 \times 10^{-13}. \tag{4.31}$$

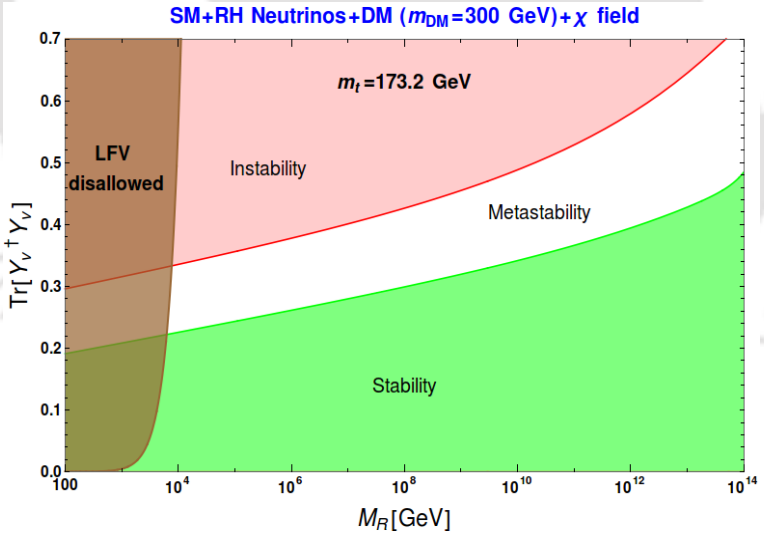

FIGURE 4.20: LFV and absolute vacuum stability constraint on $\mathrm{Tr}[Y_\nu^\dagger Y_\nu] - M_R$ in the combined set up of SM+DM+RH neutrinos+χ field where $m_{\mathrm{DM}} = 300$ GeV, $m_{H_2} = 300$ GeV, $\sin\theta = 0.2$, $\lambda_{\phi H} = 0.06$ and $\lambda_{\chi\phi} = 0.135$.

Using this limit, we therefore obtain bounds on $|(Y_\nu^\dagger Y_\nu)_{e\mu}|$ corresponding to a fixed M_R value which can be converted to constrain $\mathrm{Tr}[Y_\nu^\dagger Y_\nu]$ in our set up. In obtaining limits on $\mathrm{Tr}[Y_\nu^\dagger Y_\nu]$ (for fixed M_R), first note that $Y_\nu^\dagger Y_\nu$ remains function of M_R and parameter a only (see Eq.(4.17) with $O = \mathbb{I}$), once the best fit values of neutrino mixing angles [383, 384] are used to evaluate

$U_{\rm PMNS}$. Hence LFV limit basically constrains the parameter a which in turn is used to obtain $\mathrm{Tr}[Y_\nu^\dagger Y_\nu]$. This limit is shown on Fig.4.20 by the brown solid line, the left side of which is the disallowed region by LFV.

In the same plane of Fig.4.20 we also include the region of the parameter space allowed by both stability and metastability criteria. The green shaded region denotes the absolute stability of Higgs vacuum while the white region satisfies the metastability condition. We also indicate the instability region by pink patch in the same figure under discussion. For this purpose we have used $m_t = 173.2$ GeV and $m_{\rm DM} = 300$ GeV, $\sin\theta = 0.2$, $\lambda_{\phi H} = 0.06$ and $\lambda_{\chi\phi} = 0.135$ (corresponding to the benchmark point indicated by X in Fig.4.7). The brown shaded region is disfavored by the LFV constraint. Hence from Fig.4.20 we infer that for low M_R, LFV constraints turn out to be stronger one and for high M_R values, $\mathrm{Tr}[Y_\nu^\dagger Y_\nu]$ is mostly restricted by the stability issue.

It turns out that the proposed scenario does not provide any significant contribution to neutrinoless double beta decay [388–393] even for relatively low RH neutrino mass ($\sim 10^3$ GeV). This is in line with the observation made in [344]. Before concluding the section, it is perhaps important to comment on the possibility of explaining the baryon asymmetry of the Universe (BAU). The involvement of RH neutrinos would make the leptogenesis natural candidate to explain BAU from the completion point of view. However with the exactly degenerate RH neutrinos (we consider this for simplicity though), it is not possible. Once a small mass-splitting ΔM_R between two heavy RH neutrinos can be introduced (for example by radiative effect [394–396]), resonant leptogenesis mechanism [397–399] can be succesfully implemented [400]. Apart from this, provided one can extend our vacuum stability analysis in presence of non-degenerate RH neutrinos [346] with DM and χ field, usual thermal leptogenesis can also be employed to explain the BAU of the universe.

4.7 Chapter Summary

We have considered an extension of the SM by three RH neutrinos and two scalar singlets with an aim to study the EW vacuum stability in a framework that can incorporate a stable light DM within the reach of collider experiments and to explain the light neutrino mass. A $Z_2 \times Z_2'$ symmetry is imposed of which Z_2' is broken from the vev of one of the scalars. It is known that with a real scalar singlet DM model, present experimental limits by LUX 2016 and XENON 1T rule out DM mass below $m_{\rm DM} = 500$ GeV. Also its presence does not modify the fate of EW vacuum much and hence keep it metastable only. Although metastability is acceptable, it

however leaves some unwanted questions if we include primordial inflation in the picture. So an absolute stability of the EW vacuum is more favourable. On the other hand, introduction of RH neutrinos would have large impact on the running of the Higgs quartic coupling due to the neutrino Yukawa interaction. Provided the neutrino Yukawa coupling is as large as $\mathcal{O}(1)$ or more, it can actually destabilize the EW vacuum. Hence we have tried here achieving the stability of the EW vacuum in presence of RH neutrinos and DM. We also plan to find the possibility of a light scalar DM below 500 GeV. For this purpose, we have introduced additional scalar field which gets a vev. The other scalar among the two introduced does not get a vev and thereby is a good candidate for being a dark matter. The presence of the singlet with non-zero vev helps achieving the vacuum stability through a threshold like correction to λ_H. So in this particular scenario *i.e.* the SM extended by DM, three RH neutrinos plus one extra scalar, we have studied the Higgs vacuum stability issue considering large Yukawa coupling and variation of m_t within 2σ range of uncertainty. We have found the stability region in the $\mathrm{Tr}[Y_\nu^\dagger Y_\nu] - m_t$ plane has been significantly increased in presence of χ. Simultaneously mixing of this extra scalar with the SM Higgs doublet ensures its involvement in the DM annihilations. This mixing is effectively controlled by the Higgs portal coupling of the scalar which also enters into the running of the Higgs quartic coupling. Hence an interplay between the two conditions: one is to achieve the EW vacuum stability and the other is to find a viable DM below 500 GeV, can actually constrain the parameters involved to some extent. Since the set-up involves several new particles, finding their existence in future and ongoing experiments would be an interesting possibility to search for. Here we have assumed the physical Higgs other than the SM one is heavier. The other situation where the second physical Higgs is lighter than the Higgs discovered at 125 GeV. However this case is not of very interest in the present study as following from Eq.(6.19), it can be seen that the effective Higgs quartic coupling becomes less than the SM one in this case and this would not help making EW vacuum stable. Also the $\sin\theta$ allowed region for $m_{H_2} < m_{H_1}/2$ is almost excluded from the decay of $H_2 \to H_1 H_1$. Hence we discard this possibility. One interesting extension of our work could be the study of a SM gauge extension where the involvement of gauges bosons can modify our result. We keep it for a future study.

Chapter 5

Searching for a common origin of dark matter and inflation

5.1 Introduction

In the previous chapter we have done a detailed analysis of scalar DM in view of recent experimental bounds. However we have not predicted any specific origin of the DM. According to the inflationary hypothesis that at the end of inflation reheating occurs and after reheating all the particle species including DM remain in thermal equilibrium. It would be interesting to argue whether DM in the Universe has any connection with the inflation. This chapter (based on [401]) provides such kind of a unified BSM framework of inflation and scalar DM in a supersymmetric framework. Specifically we consider the existence of a different sector other than the SM, which can address primordial inflation and at the same time provides a suitable DM candidate. Earlier in [139], such an attempt to connect between primordial inflation and DM successfully has been made.

An inflation model embedded in a supersymmetric framework (for *e.g.*, supersymmetric hybrid inflation models) usually contains one or more mass scales that are quite large compared to the electroweak scale, although smaller than the Planck scale as indicated by Planck [39] and WMAP data [402]. In a remarkable attempt to address the issue [279], it was shown that the inclusion of a hidden sector in the form of supersymmetric QCD (SQCD) can dynamically generate the scale of inflation, or relate it to the heavy quark mass of the electric theory (*i.e.* the theory at scales above the strong coupling scale). Inflation based on strongly coupled supersymmetric gauge theories has been studied in [289, 290, 306, 403–406]. The properties of inflation

in the SQCD framework are determined by the number of colors (N_C) and number of flavors (N_f) in the model. If one initially chooses $N_f = N_C + 1$ [256, 259, 269], and then introduces a deformation of this pure $SU(N_C)$ gauge theory by assuming the presence of one massive quark, then, upon integrating our this heavy quark, one obtains an effective superpotential of exactly the type used in smooth hybrid inflation [407, 408]. Therefore, the theory naturally embeds two mass scales: one, the strong-coupling scale, is generated dynamically, while the other is related to the heavy quark mass. Hence a salient feature of such SQCD-embedded inflation model lies in the existence of a UV completion of the theory. Although in its original form the framework of smooth hybrid inflation embedded in supergravity is not consistent with all observational constraints, this can be corrected by considering a modified Kähler potential as shown in [409–412].

In this work, we demonstrate that DM candidates can arise from the same SQCD sector. We first note that at the end of the smooth hybrid inflation, one field from the inflation system gets a vacuum expectation value (VEV) and therefore breaks the associated global symmetry of the SQCD sector yielding a number of Nambu-Goldstone bosons (NGBs), whose interactions with the SM are suppressed by the spontaneous symmetry breaking scale, which is large, being related to the scale of inflation. Nambu-Goldstone bosons as DM has already been studied in some other contexts, see for example, [139–148].

We then assume a small deformation of the UV theory by providing small masses (small compared to one heavy quark mass already present in the construction with $N_f = N_c + 1$ gauge theory) to the SQCD fermions; this generates the masses of NGBs through Dashen's formula [413, 414]. Even with this deformation the NGBs are naturally stable and therefore serve as weakly interacting massive DM candidates; we will discuss this possibility in detail for various mass configurations. In the non-degenerate case, we show that DM-DM interactions play a crucial role in the thermal freeze-out, and therefore in relic density, and also impose the spin-independent (SI) direct search constraints from the XENON 1T.

We will assume that visible matter is included in a supersymmetric sector that is well described by the minimal supersymmetric Standard Model (MSSM) [239, 245, 248, 415, 416] at low energies. In this case the lightest supersymmetric particle (LSP) also serves as DM candidate in this framework. The case where this LSP contributes an important share of the relic density has been explored in various publications [158, 159, 161, 417] within the MSSM. Here we consider an alternative scenario where the LSP relic abundance is small, while NGB-LSP interaction plays a crucial role in surviving the direct search constraints, particularly for degenerate NGB DM scenario.

The chapter is organized as follows. In section 5.2, we discuss the basic SQCD framework, which leads to the smooth hybrid inflation. We point out the prediction of such smooth hybrid inflation model in view of Planck result [39]. Then in section 5.3, NGBs are identified as DM and a strategy for introducing DM masses are discussed. We indicate here on the superpotential that would be responsible for generating DM interaction with the SM particles. Parameter space scan for relic density and direct search constraints on the model is elaborated in section 5.4 and we finally conclude in section 5.5.

5.2 Smooth Hybrid Inflation in SQCD

We start with a brief introduction to the SQCD framework that leads to a smooth hybrid inflation as was proposed in [279]. We consider the existence of a strongly coupled supersymmetric $SU(N)$ gauge sector having N_f flavors of quark superfields denoted by Q_i and $\bar{Q}_i$ $(i = 1, ..., N_f)$ transforming as fundamental (N) and anti-fundamental $(\bar{N})$ representation of the gauge group $SU(N)$ respectively. This theory also has a global symmetry: $SU(N_f)_L \times SU(N_f)_R \times U(1)_B \times U(1)_R$, where the first $U(1)$ is proportional to the baryon number and the second one is related to the anomaly-free R-symmetry. We are particularly interested in $N_f = N$ case, where in the electric (or UV) theory, the following gauge invariant (but unnormalized) operators can be constructed: $M_{ij} = Q_i\bar{Q}_j$, $b = \epsilon_{i_1 i_2 ... i_N}\epsilon_{a_1 a_2 ... a_N} Q^{a_1}_{i_1} ....Q^{a_N}_{i_N}$ and $\bar{b} = \epsilon_{i_1 i_2 ... i_N}\epsilon_{a_1 a_2 ... a_N} \bar{Q}^{a_1}_{i_1} ....\bar{Q}^{a_N}_{i_N}$. Here a_i correspond to the color indices and i_j denote the flavor indices.

Classically, in absence of any superpotential, these invariant operators are required to satisfy the gauge and flavor-invariant constraint $\det M - b\bar{b} = 0$. As explained in [256, 259, 269], this constraint is modified by nonperturbative quantum contribution and becomes

$$\det M - b\bar{b} = \Lambda^{2N}, \tag{5.1}$$

where Λ is a dynamically-generated scale. The corresponding quantum superpotential can be constructed by introducing a Lagrange multiplier field X, carrying R charge of 2 units, and is given by

$$W = X\Big(\det M - b\bar{b} - \Lambda^{2N}\Big). \tag{5.2}$$

The necessity of introducing X follows from the fact that the expression of the quantum constraint does not carry any R charge and the superpotential W should have a R charge of 2 units.

With $N_f = N = 2$, it was shown in [280, 418] that such a superpotential results into a low energy effective superpotential that is very much similar to the one responsible for supersymmetric hybrid inflation. However, since in this case the predictions of the supersymmetric hybrid inflation are not in accordance with the results of WMAP and Planck, we use [279] instead $N_f = N = 4$, for which the corresponding effective superpotential still resembles the one in the smooth hybrid inflation scenario. In this case, the low energy (or IR) theory below the strong coupling scale Λ_0 of the $SU(N = 4)$ gauge theory, can be described in terms of meson fields T_{ij}, baryon B and antibaryon $\bar{B}$ superfields fields [1]

$$T_{ij} = \frac{Q_i \bar{Q}_j}{\Lambda_0}, \quad B = \frac{1}{\Lambda_0^3}\epsilon_{abcd} Q_1^a Q_2^b Q_3^c Q_4^d, \quad \text{and} \quad \bar{B} = \frac{1}{\Lambda_0^3}\epsilon_{ijkl}\epsilon_{abcd} \bar{Q}_1^a \bar{Q}_2^b \bar{Q}_3^c \bar{Q}_4^d, \tag{5.3}$$

having the superpotential

$$W = S\Big(\frac{\det T}{\Lambda_0^2} - B\bar{B} - \Lambda_{\rm eff}^2\Big). \tag{5.4}$$

(the relation to Eq.(5.2) is, $T = M/\Lambda_0$, $B = b/\Lambda_0^3$ where Λ_0 is the strong coupling scale of the $N_f = N = 4$ theory; then S can be identified with $\frac{X}{\Lambda_0^6}$ and $\Lambda_{\rm eff}^2$ with $\frac{\Lambda^8}{\Lambda_0^6}$) The effective mass scale $\Lambda_{\rm eff}$ can be interpreted in terms of holomorphic decoupling of one heavy flavor of quark (heavier than Λ_0) from a $SU(N)$ SQCD theory with $N_f = N + 1$ flavors as we discuss below.

5.2.1 Realization of the effective superpotential from $N_f = N + 1$ SQCD

The low energy version of the supersymmetric $SU(N)$ gauge theory with $N_f = N + 1$ (where $N = 4$) flavors is associated with mesons and baryons which are defined analogously to Eq. (5.3), but due to the presence of an extra flavor ($i = 1, 2, ...5$), the baryons carry a free flavor index ($\hat{B}^i \propto \epsilon^{ijklm}\epsilon_{abcd} Q_j^a Q_k^b Q_l^c Q_m^d$) and the meson matrix ($\hat{T}_{ij}$) becomes correspondingly larger. Hence the baryons $\hat{B}^i$ and $\bar{\hat{B}}^i$ transform under the global group, $SU(N_f) \times SU(N_f)$, as $(N_f, 1)$ and $(1, \bar{N_f})$ respectively. Following Seiberg's [256, 259] prescription, the system can then be represented by the superpotential,

$$\hat{W}_m = \hat{B}^i \hat{T}_{ij} \bar{\hat{B}}^j - \frac{1}{\Lambda_0^2}\det\hat{T}, \tag{5.5}$$

where Λ_0 is the strong coupling scale of $SU(N = 4)$ SQCD. Note that the superpotential will have an R charge 2 if we assign only the $\hat{T}_{N_f N_f} (= t)$ meson to carry $R = 2$.

[1] Here the Q denote the $SU(4)$ quark super-fields.

Next we introduce a tree level quark mass term in the superpotential,

$$\hat{W}_{N_f=N_c+1} = \hat{B}\hat{T}\bar{\hat{B}} - \frac{1}{\Lambda_0^2}\mathrm{det}\hat{T} + \Lambda_0\mathrm{Tr}(\hat{m}\hat{T}). \;, \quad \text{with} \;\; \hat{m} = \mathrm{diag}\{m_1, m_2, m_3, m_4, m_Q\}. \tag{5.6}$$

where we assume $m_Q >> m_{1,2,3,4}$.

Considering first the case $m_Q > \hat{\Lambda}_0$ and $m_{i=1,2,3,4} = 0$ (later we will discuss the effect of having nonzero $m_i << m_Q$), the F-flatness conditions for $\hat{T}_{iN_f}$, $\hat{T}_{N_f i}, \hat{B}^i, \bar{\hat{B}}^i$ (for $i < 5$) implies

$$\hat{B} = \begin{pmatrix} 0 & B^5 \end{pmatrix}, \quad \bar{\hat{B}} = \begin{pmatrix} 0 \\ \bar{B}^5 \end{pmatrix}, \quad \text{and} \quad \hat{T} = \begin{pmatrix} T & 0 \\ 0 & t \end{pmatrix}, \tag{5.7}$$

where we define the meson matrix $T_{ij} = \hat{T}_{ij}$ with $i, j = 1, 2, 3, 4$ and $T_{55} = t$. Hence after integrating out the heavy N_fth (the 5th) flavor of quark, we are left with the following effective superpotential for $N_f = N = 4$ SQCD

$$W_{N_f=N_c} = t\Big(B_5\bar{B}_5 - \frac{\mathrm{det}T}{\Lambda_0^2} + m_Q\Lambda_0\Big). \tag{5.8}$$

Comparing the above expression with Eq.(5.4), we can now identify $B = \hat{B}^5, \bar{B} = \bar{\hat{B}}^5$ and $S = t$. Hence the effective mass parameter involved in Eq.(5.4) is determined by the relation, $\Lambda_{\mathrm{eff}}^2 = m_Q\Lambda_0$ and the Lagrange multiplier field turns out to be proportional to the N_fth meson of the $N_f = N + 1$ theory.

We now turn our attention to the superpotential in Eq.(5.4) of $N_f = N(= 4)$ SQCD or equivalently to Eq.(5.8) and discuss the vacua of the theory. Different points on the quantum moduli space associated with this $N_f = N(= 4)$ SQCD theory exhibits different patterns of the chiral symmetry breaking [256, 259, 269] . Here we are interested in the specific point on the quantum moduli space (*a la* Eq.(5.4)) where $B = \bar{B} = 0$, and $T^{ij} = (\Lambda_0\Lambda_{\mathrm{eff}})^{1/2}\delta_{ij}$, which is the global vacuum of the theory. The corresponding chiral symmetry breaking pattern is then given by,

$$SU(4)_L \times SU(4)_R \times U(1)_B \times U(1)_R \to SU(4)_V \times U(1)_B \times U(1)_R. \tag{5.9}$$

Hence along the direction $B = \bar{B} = 0$ (the so-called meson branch of the theory), the superpotential reduces to

$$W_{\mathrm{Inf}} = S\Big(\frac{\chi^4}{\Lambda_0^2} - \Lambda_{\mathrm{eff}}^2\Big), \tag{5.10}$$

with $\mathrm{det}T = \chi^4$ and $S = -t$; this superpotential is the same as the one used in the smooth hybrid inflationary scenario [407, 408]. The SQCD construction of the superpotential serves

as a UV completed theory and also the scales associated are generated dynamically. Below we discuss in brief the inflationary predictions derived from this superpotential which can constrain the scales involved, $\Lambda_0, \Lambda_{\rm eff}$.

5.2.2 Inflationary predictions

The scalar potential obtained from Eq.(5.10) is given by

$$V(\sigma,\phi) = \Big(\frac{\phi^4}{4\Lambda_0^2} - \Lambda_{\rm eff}^2\Big)^2 + \frac{\phi^6\sigma^2}{\Lambda_0^4}, \tag{5.11}$$

where the real, normalized fields are defined as $\phi = \sqrt{2}\chi$ and $\sigma = \sqrt{2}S$ (we use the same letters to denote the superfields and their scalar components). As was found in [407, 408], the scalar potential has a local maximum at $\phi = 0$ for any value of the inflaton σ and there are two symmetric valleys of minima denoted by $\langle\phi\rangle = \pm\Lambda_0\Lambda_{\rm eff}/(\sqrt{3}\sigma)$. These valleys contain the global supersymmetric minimum

$$\langle\phi\rangle = (2\Lambda_{\rm eff}\Lambda_0)^{1/2},\ \langle\sigma\rangle = 0, \tag{5.12}$$

which is consistent with our chosen point on the quantum moduli space given by $\det T = \Lambda_0^2\Lambda_{\rm eff}^2$. At the end of inflation σ and ϕ will roll down to this (global) minimum During inflation $\sigma^2 >> \Lambda_{\rm eff}\Lambda_0$ and ϕ is stabilized at the local minimum $\langle\phi\rangle = \pm\Lambda_0\Lambda_{\rm eff}/(\sqrt{3}\sigma)$. The inflationary potential along this valley is given by

$$V(\sigma) \simeq \Lambda_{\rm eff}^4\Big(1 - \frac{1}{54}\frac{\Lambda_{\rm eff}^2\Lambda_0^2}{\sigma^4}\Big), \tag{5.13}$$

for $\sigma^2 >> \Lambda_{\rm eff}\Lambda_0$.

Within the slow-roll approximation, the amplitude of curvature perturbation Δ_R, spectral index n_s, and the tensor to scalar ratio r are given by

$$\Delta_R^2 = \frac{1}{24\pi^2 M_P^4}\Big(\frac{V(\sigma)}{\epsilon}\Big), \tag{5.14}$$

$$n_s \simeq 1 + 2\eta - 6\epsilon = 1 - \frac{5}{3N_e}, \tag{5.15}$$

$$r = 16\epsilon = \frac{8(2\pi\Delta_R)^{2/5}}{27N_e^2} \tag{5.16}$$

where ϵ and η are the usual slow roll parameters. Assuming $\langle\phi\rangle = M_{\rm GUT} = 2.86\times10^{16}$ GeV, then $\Delta_R = 2.2\times10^{-9}$ [39] implies $\Lambda_0 \simeq 4.3\times10^{17}$ GeV and $\Lambda_{\rm eff} \simeq 1.8\times10^{15}$ GeV. When the

number of e-folds is $N_e = 57$, smooth hybrid inflation predicts $n_s \simeq 0.967$ [419] and the very small value $r \simeq 3 \times 10^{-6}$ [419] that are in good agreement with Planck 2016 data [39].

However, supergravity corrections to inflationary potential in Eq.(5.13) have important contributions. With minimal Kähler potential, previously obtained values of n_s and r change to 0.99 and 1×10^{-6} respectively [419]. Particularly the value of $n_s \sim 0.99$ is in tension with observations [39]. To circumvent the problem one may use non-minimal Kähler potential as suggested in [412] to bring back the value of n_s within the desired range. On the other hand, to increase r to a detectable limit, further modification in Kähler potential may be required, as shown in [409, 411].

5.3 NGB as dark matter in SQCD

Once the inflation ends, the inflaton system slowly relaxes into its supersymmetric ground state specified by Eq.(5.12). This however spontaneously breaks the associated flavor symmetry from $SU(4)_L \times SU(4)_R$ to the diagonal $SU(4)_V$ subgroup. This would generate fifteen Nambu-Goldstone bosons (NBGs) those are the lightest excitations in the model. The Lagrangian so far considered has only the usual derivative couplings among the NGBs, which are suppressed by inverse powers of $\langle\chi\rangle$; in particular, they have no interactions with the SM sector, and they are stable over cosmological time scale. In the following we will introduce additional interactions that will modify this picture.

At the global minimum we can write

$$T = \chi \exp\Big(\frac{iG_S^a \lambda^a}{\langle\chi\rangle}\Big), \tag{5.17}$$

where G^a, $(a = 1, \ldots, 15)$ denote the NGBs, and λ_a are the generators of $SU(4)$. This expression also identifies $\langle\chi\rangle$ as the equivalent of the pion decay constant. Up to this point the NGBs are massless, which can be traced back to the choice of $m_{i=1,2,3,4} = 0$ in Eq. (5.6). If we relax this assumption (while maintianing $m_i << m_Q$) the chiral symmetry is broken (explicitly) and, as a consequence, the NGBs acquire a mass that can be calculated using Dashen's formula [413, 414]:

$$\begin{aligned} \langle\chi\rangle^2 (m_{G_S}^a)^2 &= \langle 0|[\tilde{\mathcal{Q}}_a, [\tilde{\mathcal{Q}}_a, H]]|0\rangle \qquad \text{(no summation over } a\text{)} \\ &= \bar{\psi}\Big[\frac{\lambda_a}{2}, \Big[\frac{\lambda_a}{2}, m_{\text{diag}}\Big]_+\Big]_+ \psi\,; \qquad m_{\text{diag}} = \text{diag}\{m_1, m_2, m_3, m_4\} \end{aligned} \tag{5.18}$$

where, as noted above, $\langle\chi\rangle$ corresponds to the decay constant, the "+" subscript denotes the anticommutation, and $\tilde{\mathcal{Q}}_a = \frac{1}{2}\int d^3x \psi^\dagger \gamma_5 \lambda_a \psi$ are the $SU(4)_A$ axial charges with the quark

state $\psi = (Q_1, Q_2, Q_3, Q_4)^T$; λ_a are the $SU(4)$ generators normalized such that $\mathrm{Tr}[\lambda_a \lambda_b] = \frac{\delta_{ab}}{2}$ ($a, b, \ldots$ denote generator indices with $a = 1, 2, ..., 15$). The details of the mass spectrum of these pseduo-NGBs (pNGB's) are provided in Appendix C.1.

The pNGB spectrum is determined by the light-mass hierarchy. Among several possibilities, we will concentrate on the following two cases:

- The simplest choice is to take $m_{1,2,3,4} = m$ in $m_{\rm diag}$ (see Eq.(5.6)). In this case all the fifteen pNGBs will be degenerate, having mass $m_{G_S}^2 = 2m\Lambda^3/\langle\chi\rangle^2$, where $\Lambda^3 = \langle\bar{Q}_i Q_i\rangle$.
- A split spectrum can be generated if one assumes $m_1 = m_2 = m_3 = m_\gamma$ and $m_4 >> m_\gamma$. Then we find three different sets of pNGB with different masses: *(i)* eight pNGBs will have mass $m_A^2 = 2m_\gamma\Lambda^3/\langle\chi\rangle^2$; *(ii)* six pNGBs with mass $m_B^2 = (m_4 + m_\gamma)\Lambda^3/\langle\chi\rangle^2$; and *(iii)* one pNGB with mass $m_C^2 = \Big(3m_4 + m_\gamma\Big)\Lambda^3/2\langle\chi\rangle^2$ (see Appendix C.1 for details).

We now turn to the discussion of the interactions of these pNGBs with the SM in this set-up. As noted in the introduction, we assume that at low energies the SM is contained in the MSSM. In this case, the S field (being neutral) serves as a mediator between the MSSM and SQCD sectors which then leads to the following modified superpotential

$$W_{\rm T} = S\Big(\frac{\det T}{\Lambda_0^2} - \Lambda_{\rm eff}^2\Big) + \kappa_1 S\Big\{\mathrm{Tr}(T^2) - \frac{(\mathrm{Tr}\ T)^2}{N_f}\Big\} + \kappa_2 S H_u H_d, \tag{5.19}$$

where H_u and H_d are the two Higgs (superfield) doublets in MSSM, and $\kappa_{1,2}$ are phenomenological constants that can be taken positive.

The terms within the curly brackets are phenomenologically motivated additions. Note that while the first (as in Eq. 5.10) and last terms in $W_{\rm Inf}$ respect the full $SU(N_f)_L \times SU(N_f)_R \times U(1)_B \times U(1)_R$ chiral symmetry, the middle term only respects the diagonal subgroup [**?**]. The inclusion of such terms hence naturally lead to additional interactions of pNGBs. It is important to note that during inflation T is proportional to the unit matrix, so the term proportional to κ_1 vanishes and does not affect the smooth hybrid inflation scenario described before. Below we will see how incorporation of such terms can lead to the desired DM properties.

The term in $W_{\rm T}$ proportional to κ_2 provides a connection between the SQCD sector and the minimal supersymmetric Standard model (MSSM). Inclusion of this term in the superpotential will have a significant effect on reheating after inflation[279]; it can address the so-called μ-problem in the MSSM [420–422], provided S acquires a small, $\sim \mathcal{O}$(TeV), vacuum expectation value. We will see that it also provides a useful annihilation channel for DM.

The linearity on S in these new contributions to the superpotential is motivated from R symmetry point of view. We note that any dimensionless coupling multiplying the first term in $W_{\rm Inf}$ can be absorbed in a redefinition of $\Lambda_{0,\rm eff}$; in contrast, the couplings $\kappa_{1,2}$ (assumed real) are physical and, as we show below, are constrained by observations such as the dark matter relic abundance and direct detection limits.

The scalar potential can now be obtained from $V_{\rm scalar} = |\partial W_{\rm T}/\partial S|^2 + |\partial W_{\rm T}/\partial T|^2$. At the supersymmetric minimum, it is given by

$$V_{\rm s} = \frac{\kappa_1^2}{4}\sum_{a,b}(G_S^a)^2(G_S^b)^2 + \kappa_2^2|H_u|^2|H_d|^2 - \frac{\kappa_1\kappa_2}{2}\sum_a (G_S^a)^2 H_u H_d + \text{h.c.} + \cdots \tag{5.20}$$

In obtaining this, we expanded T in powers of the NGBs:

$$T = \chi\Big\{1 + \frac{iG_S^a\lambda^a}{\langle\chi\rangle} - \frac{G_S^aG_S^b\lambda^a\lambda^b}{2\langle\chi\rangle^2} + ...\Big\}, \tag{5.21}$$

and χ is developed around its expectation value: $\chi = \langle\chi\rangle + \cdots$.

Note that the first term in $V_{\rm s}$ is of interest only when the pNGBs are not degenerate as otherwise it would not contribute to number changing process. In such a case with non-degenerate pNGBs, the heavier Gs can annihilate into the lighter ones. Hence in such a situation, κ_1 can also play a significant role in our DM phenomenology along with $\kappa_1\kappa_2/2$. In fact, we will show that the annihilation of the heavier ones to the lighter components will aid in freeze-out of the heavier component. This helps in evading the direct search bounds as the coupling κ_1 alone will not contribute to direct search cross section, thereby allowing a larger parameter space viable to our DM scenario. It is important to note here that even if we assume that the masses of the heavier pNGBs are very large, their annihilation cross-sections to the SM will be small enough for an early freeze-out, which leads to an unacceptably large relic abundance unless a large enough κ_1 allows them to annihilate to lighter ones. Note that the interactions among the G generated by $\text{Tr}(\partial_\mu T^\dagger\,\partial^\mu T)$ are negligible since they are suppressed by powers of $\langle\chi\rangle$.

The interaction of the pNGBs with the MSSM sector (the last term in Eq.(6.2.2)), is Higgs-portal like:

$$V_{\rm Int} = -\lambda\sum_{a=1}^{15}(G_S^a)^2(H_u^+H_d^- - H_u^0H_d^0)\,, \quad \text{where} \qquad \lambda = \frac{\kappa_1\kappa_2}{2}. \tag{5.22}$$

In terms of the physical mass eigenstates, the two Higgs doublets in MSSM can be written as follows [239, 245, 248, 415]:

$$H_u = \begin{bmatrix} H_u^- \\ H_u^0 \end{bmatrix} = \frac{1}{\sqrt{2}} \begin{bmatrix} \sqrt{2}(H^- \sin\beta - X^- \cos\beta) \\ v_u + (H\cos\alpha - h\sin\alpha) + i(A\sin\beta + X^0\cos\beta) \end{bmatrix}, \tag{5.23}$$

$$H_d = \begin{bmatrix} H_d^0 \\ H_d^+ \end{bmatrix} = \frac{1}{\sqrt{2}} \begin{bmatrix} v_d + (H\sin\alpha + h\cos\alpha) + i(A\cos\beta - X^0\sin\beta) \\ \sqrt{2}(H^+\cos\beta + X^+\sin\beta) \end{bmatrix}, \tag{5.24}$$

where h and H denote the light and heavy CP-even eigenstates respectively; $H^\pm$ and A are the charged and CP-odd physical scalars respectively, and $X^{0,\pm}$ are the would-be Goldstone bosons. As usual, h plays the role of the SM Higgs, and the vacuum expectation values of H_u^0, H_d^0 (denoted by v_u and v_d respectively) are related by

$$\tan\beta = \frac{v_u}{v_d}, \qquad v = \sqrt{v_u^2 + v_d^2} \simeq 246 \text{ GeV}. \tag{5.25}$$

The other mixing angle α appears as a result of the diagonalization of the CP-even Higgs mass-squared matrix (in the $H_u^0 - H_d^0$ basis) leading to the physical Higgses, h and H. The mixing angle α can be expressed in terms of β and the pseudoscalar A mass as

$$\tan 2\alpha = \tan 2\beta \, \frac{M_A^2 + M_Z^2}{M_A^2 - M_Z^2}. \tag{5.26}$$

We can now write the coupling of the pNBGs with the SM Higgs from Eq.(5.22) as follows:

$$V \supset -\left(\lambda^{'} h^2 + \lambda^{''} h v_d\right) \sum_a (G_S^a)^2, \tag{5.27}$$

where

$$\lambda^{'} = \frac{1}{2}\lambda \sin\alpha\cos\alpha, \quad \lambda^{''} = \frac{1}{2}\lambda\left(\sin\alpha - \frac{v_u}{v_d}\cos\alpha\right) = \frac{1}{2}\lambda\cos\alpha(\tan\alpha - \tan\beta). \tag{5.28}$$

On the other hand, the couplings of the SM Higgs h to the vector fields and fermions are given by

$$hWW : \frac{2m_W^2}{v}\sin(\beta-\alpha), \quad hZZ : \frac{2m_Z^2}{v}\sin(\beta-\alpha), \quad hf\bar{f} : \frac{m_f}{v}\frac{\sin\alpha}{\cos\beta}. \tag{5.29}$$

In view of Eq. (5.26), it can be noted that in the large pseudoscalar Higgs mass limit $M_A >> M_Z$, $\tan 2\beta \simeq \tan 2\alpha$, that has two solutions. One possibility is $\alpha \simeq \beta$, in which case couplings of the SM Higgs with W and Z vanish (see Eq.(5.29)) and $\lambda^{''} \sim \cos\alpha(\tan\beta - \tan\alpha) \to 0$ (see Eq.(6.47)), and hence is of limited interest. There is, however, a second solution: $\alpha \simeq \beta + \pi/2$, so that $\tan\beta \simeq -\cot\alpha$ (see Fig.5.1) in which case the lightest CP-even scalar h will be SM-like and Eq.(5.27) closely resembles a Higgs-portal coupling[54–56]. In the following we will continue

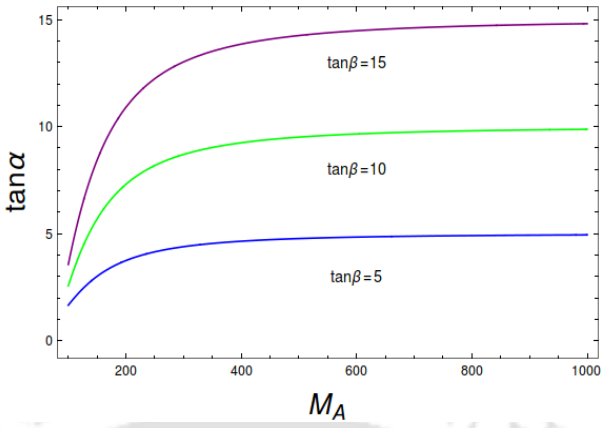

FIGURE 5.1: $\tan\alpha$ versus M_A where $\alpha = \frac{\pi}{2} + \beta$.

to assume $\alpha = \beta + \pi/2$. It is easy to show that with such a choice, λ', λ'' and λ are related with β as (using Eq.(5.27)

$$\frac{\lambda''}{\lambda} = \frac{1}{2\cos\beta}\,, \quad \frac{\lambda'}{\lambda} = -\frac{1}{4}\sin 2\beta\,; \qquad (\alpha = \beta + \pi/2). \tag{5.30}$$

These couplings are plotted in Fig.5.2 as functions of $\tan\beta$ (note that v_d is a monotonically decreasing function of $\tan\beta$).

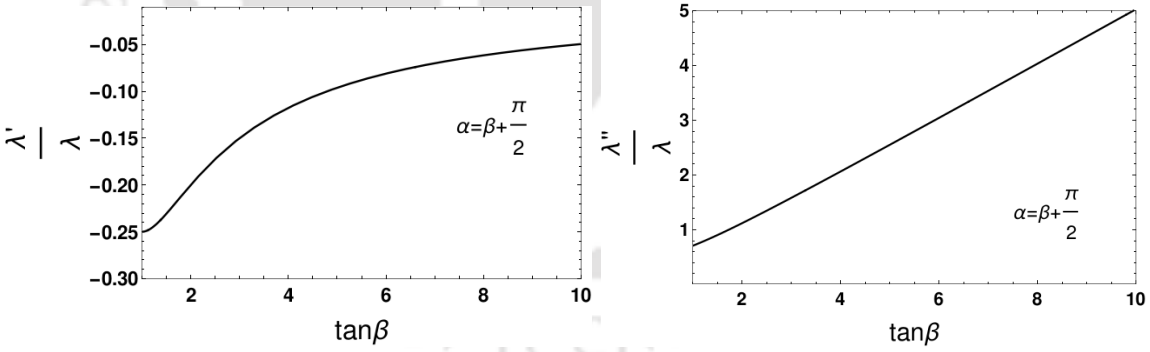

FIGURE 5.2: Variation of λ' and λ'' (scaled by λ) with $\tan\beta$. We assume $\alpha = \beta + \pi/2$ for both the cases.

5.4 Relic density and direct search of pNBG DM

We now turn to the determination of the regions of parameter space where our DM candidates, the pNGB's, satisfy the relic density and direct detection constraints. The pNBGs interact with

the SM through the Higgs portal as described in Eq.(5.27), so the behavior of the pNBG sector is similar to that of a scalar singlet Higgs portal. In view of our consideration, $\alpha = \beta + \pi/2$, the parameters for this sector are then effectively

$$m_{G_s}, \lambda, \tan\beta. \tag{5.31}$$

The other factor which determines the relic density of pNGB's is their mass spectrum; we will show that depending on the choice of mass parameters employed in the Dashen formula, we can have several phenomenologically viable situations where one or more of the G contribute to the relic density.

We hasten to note, however, that this model also contains an additional particle in the dark sector: the lightest supersymmetric particle (LSP), that we assume to be the lightest neutralino (χ_0), which is stable due to R parity conservation. The MSSM neutralino χ_0 has been studied as a DM candidate in various contexts [158, 159, 161, 417], and can annihilate to SM and supersymmetric particles through many different but known channels, depending on the composition of Bino-Wino-Higgsino admixture. In this work we will concentrate on the case where the pNBGs dominate the DM abundance. We still must incorporate neutralino and MSSM phenomenology to some extent as the pNBGs interact with the neutralino DM through the Higgs portal coupling. This is because, there is a Wino-Higgsino-Higgs ($\tilde{W} - \tilde{H}_{u/d} - H_{u/d}$) or Bino-Higgsino-Higgs ($\tilde{B} - \tilde{H}_{u/d} - H_{u/d}$) coupling in the MSSM through which the pNBGs can annihilate into a pair of neutralinos (or vice versa, depending on the mass hierarchy of the pNGBs and LSP). The strength of the pNBG-LSP interaction of course depends on the composition of neutralino and we consider two different situations of phenomenological interest: *(i)* when the pNBG-LSP interactions can be completely neglected and the DM relic density is solely composed of pNBGs, and *(ii)* when the pNBG-LSP interaction is weak but non-vanishing.

In general, the coupled Boltzmann equations that determine the relic density for our two-component DM model (considering the presence of a single pNGB having mass m_{G_s} and LSP with mass m_χ) can be written as follows:

$$\begin{aligned} \dot{n_{G_S}} + 3Hn_{G_S} &= -\langle\sigma v\rangle_{G_SG_S\to SM}(n_{G_S}^2 - n_{G_S}^{eq\ 2}) - \langle\sigma v\rangle_{G_SG_S\to\chi\chi}(n_{G_S}^2 - n_\chi^2), \\ \dot{n_\chi} + 3Hn_\chi &= -\langle\sigma v\rangle_{\chi\chi\to SM}(n_\chi^2 - n_\chi^{eq2}) + \langle\sigma v\rangle_{G_SG_S\to\chi\chi}(n_{G_S}^2 - n_\chi^2), \end{aligned} \tag{5.32}$$

where we assume $m_{G_s} > m_\chi$. Here n_{G_S} and n_χ denote the number density for the pNBG and LSP, respectively. Corresponding equilibrium distributions are given by

$$n_i^{eq} = \int \frac{\xi_i d^3p}{(2\pi)^3} \tilde{f}_i^{eq}, \quad \text{with} \quad \tilde{f}_i^{eq} = \frac{1}{e^{E/k_BT} - 1}\,. \tag{5.33}$$

where the index represents either of the DM species $i = \{G_s, \chi\}$ and ξ_i denotes the degrees of freedom for the corresponding DM species, and we assume zero chemical potential for all particle species. In principle annihilations of the pNBGs occur to both SM and supersymmetric particles. However, assuming that the supersymmetric particles are heavier (as searches at LHC have not been able to find them yet), the dominant annihilation of the pNBGs occurs to SM particles. After freeze out, relic density of the DM system is described by

$$\Omega = \Omega_{G_S} + \Omega_{\chi}, \tag{5.34}$$

where the individual densities are determined by the freeze-out conditions of the respective DM components; which, in turn, are governed by the annihilation of these DM components to the SM, and as well as by the interactions amongst themselves.

One can clearly see from Eq. (5.32) that the Boltzmann equations for the two dark sector components, LSP and pNGBs, are coupled due to the presence of the terms containing $\langle\sigma v\rangle_{G_S G_S \to \chi\chi}$; when this is of the same order as $\langle\sigma v\rangle_{G_S G_S \to SM}$ the individual abundances will differ significantly from those obtained when $\langle\sigma v\rangle_{G_S G_S \to \chi\chi} \simeq 0$. For example, consider the case where the LSP is dominated by the wino component. Then $\langle\sigma v\rangle_{\chi\chi \to SM}$ is significant because of the large coupling of the wino to the Z, and from the co-annihilation channel involving the lightest chargino. Because of this large cross section we expect that the LSP relic density will be small: $\Omega_{\chi} << 0.1$ and the relic density will be composed almost solely of pNBGs: $\Omega_{G_S} h^2 \sim \Omega h^2 \sim 0.1$. In the following we will consider separately the cases where the LSP-pNBG interactions are negligible and when they are significant.

As stated earlier, our scenario allows for 15 pNBGs which can be degenerate. Hence their total contribution to Ω will be 15 times that of a single boson. However, the degeneracy of the pNBGs follow from making the simplifying assumption $m_1 = m_2 = m_3 = m_4$ in Eq.(C.3)(see discussions of Dashen's formula in Appendix C.1). Other choices generate different patterns of the dark sector mass hierarchy, which in turn govern the phenomenology of the pNBG as DM candidates.

5.4.1 Negligible pNBG-LSP interaction limit

5.4.1.1 Degenerate pNBG DM

The simplest case we consider is that of completely degenerate pNGBs (which corresponds to $m_1 = m_2 = m_3 = m_4$); in this case the 15 G_S contribute to DM relic density equally. In

the absence of pNGB-neutralino interactions the individual abundance by the single-component Boltzmann equation

$$\dot{n}_{G_S} + 3Hn_{G_S} = -\langle\sigma v\rangle_{G_SG_S\to SM}(n^2_{G_S} - n^2_{eq}). \tag{5.35}$$

where the interactions between different pNBGs are also ignored because of the degeneracy. Therefore, total relic abundance can be obtained by adding all of the single component contributions. Now the relic density for a single component pNGB is given by[11]

$$\Omega^1_{G_S} = \frac{m_{G_S} n^{x\to\infty}_{G_S}}{\rho_c}\ \text{GeV}^{-2}, \tag{5.36}$$

where $\rho_c = 1.05\times10^{-5}h^2\frac{\text{GeV}}{c^2}\text{cm}^{-3}$[25] is the critical density of the universe. Eq.(5.36) can be translated to

$$\Omega^1_{G_S}h^2 = \frac{8.51\times10^{-12}x_f}{\langle\sigma v\rangle}\ \text{GeV}^{-2}, \tag{5.37}$$

where $x_f = \frac{m_{G_S}}{T_f}$ with the freeze-out temperature T_f. Next if one considers[2] $x_f = 22$, the total relic density turns out to be

$$\Omega h^2 = 15\ \Omega^1_{G_S}h^2 \simeq 15\times\left[\frac{2.0\times10^{-10}\ \text{GeV}^{-2}}{\langle\sigma v\rangle_{G_SG_S\to SM}}\right] \tag{5.38}$$

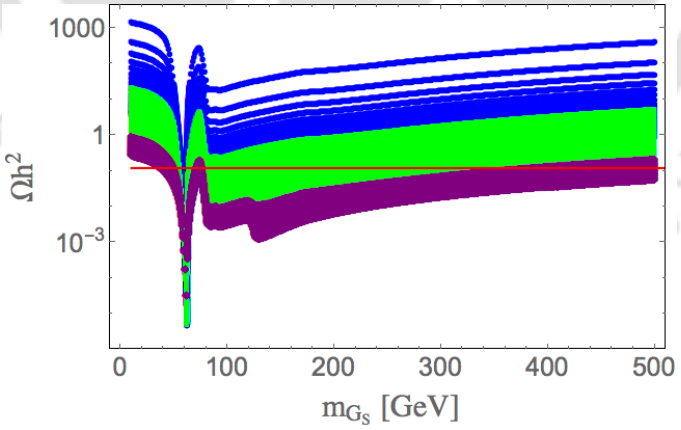

FIGURE 5.3: DM relic density as a function of the DM mass for the case of 15 degenerate pNBGs with $\tan\beta = 10$. The coupling λ is varied between $0.01-0.25$ (blue), $0.25-0.5$ (green) and $0.5-1.0$ (purple); The horizontal band shows the correct density by Planck. For the scan, we chose: $\alpha = \beta + \pi/2$.

[2]We show in Appendix C.3 that actual numerical solution to Boltzman equation, matches to approximate analytical solution for such values of x_f.

As mentioned earlier, the annihilation of pNBGs to SM states is controlled by two couplings $\lambda^{'}$ and $\lambda^{''}$ through Eq.(5.27). This situation is similar to the usual Higgs portal coupling with a singlet scalar, stabilized under a Z_2 symmetry [54–56] , with the important difference that the model we consider has two independent couplings, determined by λ and the angles α and β (cf. Eq. 6.47). In the limit where the psudoscalar mass is large, which we assume, the number of parameters is reduced by one because of the relation $\tan 2\alpha = \tan 2\beta$. This results into the phenomenologically acceptable relation involving α and β as $\alpha = \beta + \pi/2$.

The important cross sections contributing to Eq. (5.38) are:

$$\begin{aligned}
(\sigma v)_{G_sG_s\to f\bar{f}} &= \frac{m_f^2}{\pi v^2}\frac{\lambda''^2 v_d^2}{(s-m_h^2)^2+m_h^2\Gamma_h^2}\Big(1-\frac{4m_f^2}{s}\Big)^{\frac{3}{2}},\\
(\sigma v)_{G_sG_s\to W^+W^-} &= \frac{\lambda''^2 v_d^2}{2\pi v^2}\frac{s}{(s-m_h^2)^2+m_h^2\Gamma_h^2}(1+\frac{12m_W^4}{s^2}-\frac{4m_W^2}{s})\Big(1-\frac{4m_W^2}{s}\Big)^{\frac{1}{2}},\\
(\sigma v)_{G_sG_s\to ZZ} &= \frac{\lambda''^2 v_d^2}{4\pi v^2}\frac{s}{(s-m_h^2)^2+m_h^2\Gamma_h^2}(1+\frac{12m_Z^4}{s^2}-\frac{4m_Z^2}{s})\Big(1-\frac{4m_Z^2}{s}\Big)^{\frac{1}{2}},\\
(\sigma v)_{G_sG_s\to hh} &= \frac{1}{16\pi s}\Big[4\lambda'+\frac{6\lambda'' v_d m_h^2}{v(s-m_h^2)}-\frac{16\lambda''^2 v_d^2}{(s-2m_h^2)}\Big]^2\Big(1-\frac{4m_h^2}{s}\Big)^{\frac{1}{2}}.
\end{aligned} \tag{5.39}$$

The relic density Ω will be a function of the pNBG mass m_{G_s}, the coupling λ and the angles α, β. In Fig. 5.3 we evaluate Ω as a function of m_{G_s} for $0.05 < \lambda < 1.0$ and for $\tan\beta = 10$ when $\alpha = \beta + \pi/2$; the evaluation is obtained using `MicrOmegas` [423]. Note here, that the dominant annihilation of pNBG DM comes through $\lambda^{''}$. But the change in $\lambda^{''}$ due to change in $\tan\beta$ is neatly balanced by the change in v_d accompanying $\lambda^{''}$ in all vertices making the relic density invariant under $\tan\beta$. The results exhibit the usual resonant effect when $m_{G_s} \sim m_h/2 \sim 62.5$ GeV. We can also see that as λ increases Ω drops, a consequence of having larger cross sections.

The allowed region in the $m_{G_S} - \lambda$ plane by the DM relic density constraint is presented shown in Fig. 5.4 for $\tan\beta = 10$ when all 15 pNBGs are degenerate. The allowed parameter space is similar to that of a Higgs portal scalar singlet DM. The difference is mainly due to our having 15 particles: we requires larger cross section, corresponding to a larger value of λ, to compensate for the factor of 15 in Eq. 5.38.

The non-observation of DM in direct search experiments imposes a very strong constraint on DM models, ruling out or severely constraining most of the simplest single-component frameworks. It is therefore very important to study the constraints imposed on the pNBG parameter space by direct search data. Direct search reaction for the pNBG DM is mediated by Higgs boson in $t-$ channel as in Higgs portal scalar singlet DM. Spin-independent direct search cross-section

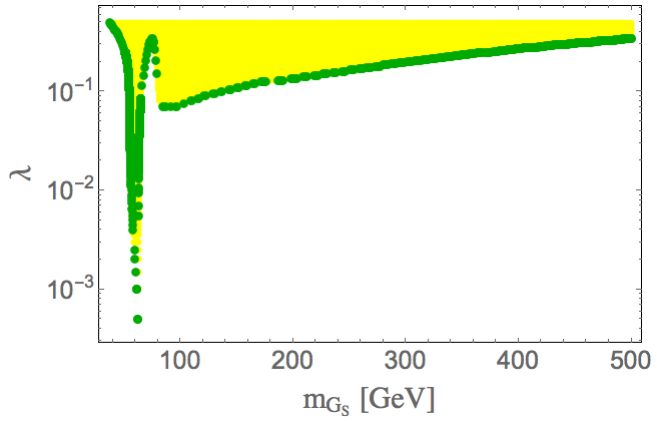

FIGURE 5.4: Regions of the $m_{G_S} - \lambda$ plane allowed by the relic density constraint by Planck[39] when all 15 pNBGs are degenerate is shown in green. Under abundant region is shown in yellow. We choose $\tan\beta = 10$ with $\alpha = \beta + \pi/2$.

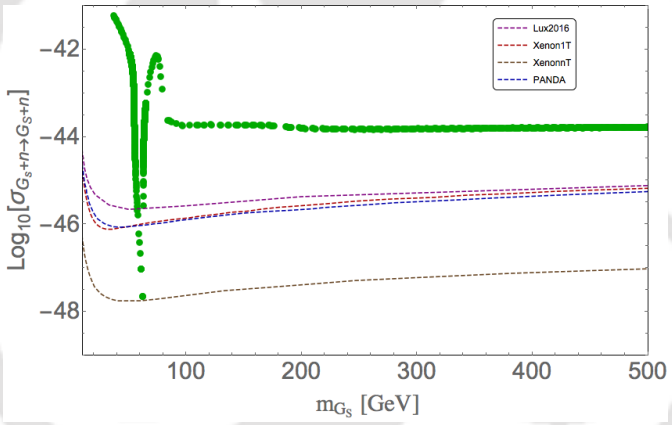

FIGURE 5.5: Spin-independent DM-nucleon cross section as a function of the DM mass, for $\tan\beta = 10$ for the case of 15 degenerate pNBG DM. Bounds from LUX 2016 [185], Xenon1T [183] and PANDA X [186] are shown with the expected sensitivity from XENONnT [379].

for pNBG DM is given by:

$$\sigma^{SI}_{pNBG} = \frac{\alpha_n^2 \mu_n^2}{4\pi m_{G_S}^2}, \quad \mu_n = \frac{m_n m_{G_S}}{m_n + m_{G_S}}, \tag{5.40}$$

where

$$\begin{aligned} \alpha_n &= m_n \sum_{u,d,s} f^{(n)}_{T_q} \frac{\alpha_q}{m_q} + \frac{2}{27} f^{(n)}_{T_g} \sum_{q=c,t,b} \frac{\alpha_q}{m_q}, \\ &= \frac{m_n \lambda''}{m_h^2} [(f^{(n)}_{T_u} + f^{(n)}_{T_d} + f^{(n)}_{T_s}) + \frac{2}{9}(f^{(n)}_{T_u} + f^{(n)}_{T_d} + f^{(n)}_{T_s})]. \end{aligned} \tag{5.41}$$

The subindex n refers to the nucleon (proton or neutron). We use default form factors for proton for calculating direct search cross-section: $f^p_{T_u} = 0.0153$, $f^p_{T_d} = 0.0191$, $f^p_{T_s} = 0.0447$ [377, 378]. In Fig. 5.5, we show the spin-independent nucleon-pNBG DM cross-section for the chosen benchmark point, plotted as a function of DM mass m_{G_S} . The green points in this figure also meet the relic density constraint. Bounds from LUX 2016 [185], Xenon1T [183] and PANDA X [186] and future predictions from XENONnT [379] are also in the figure. Clearly, the figure shows that the degenerate case is excluded by the direct search bound except in the Higgs resonance region. This is simply because for 15 degenerate DM particles, the values of λ'' required to satisfy relic density constraint correspond to a direct detection cross section large enough to be excluded by the data (except in the resonance region).

5.4.1.2 Non-degenerate pNBGs

We next consider the model when the pNGBs are not degenerate; we will see that in this case the allowed parameter space is considerably enlarged. For this it is sufficient to consider cases where there is a single lightest pNGB, and the simplest situaiont in which this occurs is when $m_1 = m_2 = m_3 = m$ and $m_4 \neq m$.

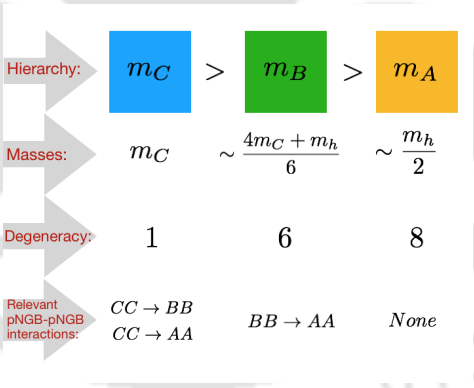

FIGURE 5.6: Masses, degeneracies and possible interactions of pNGB DMs in phenomenologically viable non-degenrate case, illustrated in this analysis.

In this case the pNGB spectrum is

type	# of degenerate pNGBs	mass
A	8	$m_A = 2m$
B	6	$m_B = m + m_4$
C	1	$m_C = (3m_4 + m)/2$

(5.42)

and there are two cases:

$$\begin{aligned} I: \ m > m_4: \quad &\Rightarrow \quad m_A > m_B > m_C \\ II: \ m < m_4: \quad &\Rightarrow \quad m_A < m_B < m_C \end{aligned} \tag{5.43}$$

In the first case there is a single lightest pNGB (type C), while in the second there are 8 lightest states (type A).

Note that due to the presence of three types of pNGBs, the total relic density should be written as $\Omega_T = n_A\Omega_A + n_B\Omega_B + n_C\Omega_C$, where $n_{A/B/C}$ are the number of degeneracies of the respective species. Compared to the case with all degenerate pNGBs, here the coupling κ_1 also comes into play along with λ. In case of all degenerate pNGBs, we have seen that the relic density satisfied region was ruled out by the direct detection cross-section limits excepting for Higgs resonance. This is because a large λ, as required to satisfy relic density, makes the direct detection cross section significantly higher than the experimental limits. Here we can make λ relatively free as κ_1 also enters in the game. which does not affect the direct detection cross section. We can allow a further smaller value of λ in this non-degenerate case, provided not all 15 pNGBs may not effectively contribute to the relic density. This can happen once we put mass of one type of pNGBs (out of A,B and C) near the resonance region $\sim m_h/2$ where the annihilation cross-section is large to make the corresponding relic density very small. In this case, the total relic density gets contribution from the two remaining types of pNGBs, therby a smaller λ (compared to all degenerate case) can be chosen. Note that case II would be more promising compared to case I from this point of view as by putting $m_A \simeq m_h/2$, we effectively have remaining 7 pNGBs to contribute to relic. In Fig.5.9, we demonstrate the masses, number of degeneracies and possible interactions among the pNGB DM candidates for the this case II. In this case $m_B \simeq (4m_C + m_h)/6$ and $m_C > m_h/2$ and the relic density reads (since $\Omega_A \simeq 0$),

$$\Omega_T \simeq \Omega_C + 6\Omega_B, \tag{5.44}$$

with $0.1175 < \Omega_T < 0.1219$ following Planck data[39].

In order to obtain $\Omega_{C,B}$ we consider the set of coupled Boltzmann equations for the C, B_i and A_i number densities (the last included for completeness):

$$\begin{aligned} \frac{dn_C}{dt} + 3Hn_C = &-\langle\sigma v\rangle_{G_CG_C\to \mathrm{SM}}\left(n_C^2 - n_C^{\mathrm{eq}2}\right) - 6\langle\sigma v\rangle_{G_CG_C\to G_BG_B}\left(n_C^2 - \frac{n_C^{\mathrm{eq}2}}{n_B^{\mathrm{eq}2}}n_B^2\right) \\ &- 8\langle\sigma v\rangle_{G_CG_C\to G_AG_A}\left(n_C^2 - \frac{n_C^{\mathrm{eq}2}}{n_A^{\mathrm{eq}2}}n_A^2\right), \end{aligned}$$

$$\frac{dn_{B_i}}{dt}+3Hn_{B_i}=-\langle\sigma v\rangle_{G_{B_i}G_{B_i}\to\mathrm{SM}}\left(n_{B_i}^2-n_{B_i}^{\mathrm{eq}2}\right)-8\langle\sigma v\rangle_{G_{B_i}G_{B_i}\to G_{A_i}G_{A_i}}\left(n_{B_i}^2-\frac{n_{B_i}^{\mathrm{eq}2}}{n_{A_i}^{\mathrm{eq}2}}n_{A_i}^2\right)$$
$$+\langle\sigma v\rangle_{G_CG_C\to G_{B_i}G_{B_i}}\left(n_C^2-\frac{n_C^{\mathrm{eq}2}}{n_{B_i}^{\mathrm{eq}2}}n_{B_i}^2\right),$$
$$\frac{dn_{A_i}}{dt}+3Hn_{A_i}=-\langle\sigma v\rangle_{G_{A_i}G_{A_i}\to\mathrm{SM}}\left(n_{A_i}^2-n_{A_i}^{\mathrm{eq}2}\right)+\langle\sigma v\rangle_{G_CG_C\to G_{A_i}G_{A_i}}\left(n_C^2-\frac{n_C^{\mathrm{eq}2}}{n_{A_i}^{\mathrm{eq}2}}n_{A_i}^2\right)+$$
$$\langle\sigma v\rangle_{G_BG_B\to G_{A_i}G_{A_i}}\left(n_B^2-\frac{n_B^{\mathrm{eq}2}}{n_{A_i}^{\mathrm{eq}2}}n_{A_i}^2\right). \tag{5.45}$$

In above we have ignored the interactions with the LSP. The numerical factors correspond to the number of final state particles each pNBG species can annihilate to. As is evident, a crucial role is played by the DM-DM contact interactions generated by (see Eq. 6.2.2)

$$V_{\mathrm{pNBG}}^{\mathrm{Int}}=\frac{\kappa_1^2}{4}\sum_{a,b}(G_S^a)^2(G_S^b)^2. \tag{5.46}$$

Since we assume that the A mass lies in the Higgs resonance region, $\langle\sigma v\rangle_{G_AG_A\to\mathrm{SM}}$ is very large, and produces very small relic density which we neglect in the following estimates; one can easily calculate that with $m_A\sim m_h/2$, the A contributes less than 1% to the total relic if $\lambda^{''}>10^{-3}$. We will use this value of $\lambda^{''}$ as a lower limit in our analysis.

Even if we neglect contributions from A type, pNBG, Eqs.(5.45) are coupled and must be solved numerically to find the freeze-out of the individual components. However, as it is shown in [339], for interacting multicomponent DM scenario [424, 425], annihilation of heavier components to lighter ones are crucial in determining the relics of only heavier components, while for lighter components it has mild effect. Hence we can derive an approximate analytic expressions for the individual relic densities by considering the annihilation of one pNGB kind to the lighter species. In this case we find

$$\Omega_Ch^2\sim\frac{2.0\times10^{-10}\ \mathrm{GeV}^{-2}}{\langle\sigma v\rangle_{G_CG_C\to\mathrm{SM}}+6\langle\sigma v\rangle_{G_CG_C\to G_BG_B}+8\langle\sigma v\rangle_{G_CG_C\to G_AG_A}},$$
$$\Omega_Bh^2\sim\frac{2.0\times10^{-10}\ \mathrm{GeV}^{-2}}{\langle\sigma v\rangle_{G_BG_B\to\mathrm{SM}}+8\langle\sigma v\rangle_{G_BG_B\to G_AG_A}},$$
$$\Omega_T=\Omega_C+6\Omega_B. \tag{5.47}$$

These approximate analytical results are in reasonably good agreement with the numerical solutions, as we show in Appendix C.3.

The DM phenomenology here crucially depends on the couplings λ and κ_1, which we have varied freely for the scan. In Fig. 5.7 [top panel], we show the allowed parameter space in the $\lambda - m_C$ (left) and $\lambda - m_B$ (right) planes for κ_1 varying between $0.01 - 0.25$ (blue), $0.25 - 0.45$ (green), $0.45 - 1$ (purple), that satisfies individually $\Omega_C < \Omega_T$ (left) and $\Omega_B < \Omega_T$ (right). It is observed that larger values of κ_1 requires also larger DM masses to produce the required annihilation cross-section. In Fig. 5.7 [bottom panel] we show the relative contributions to total relic density by individual components in $\lambda - m_C$ (left) plane and $\lambda - m_B$ (right) plane for varying κ_1 from 0.01 to 1.

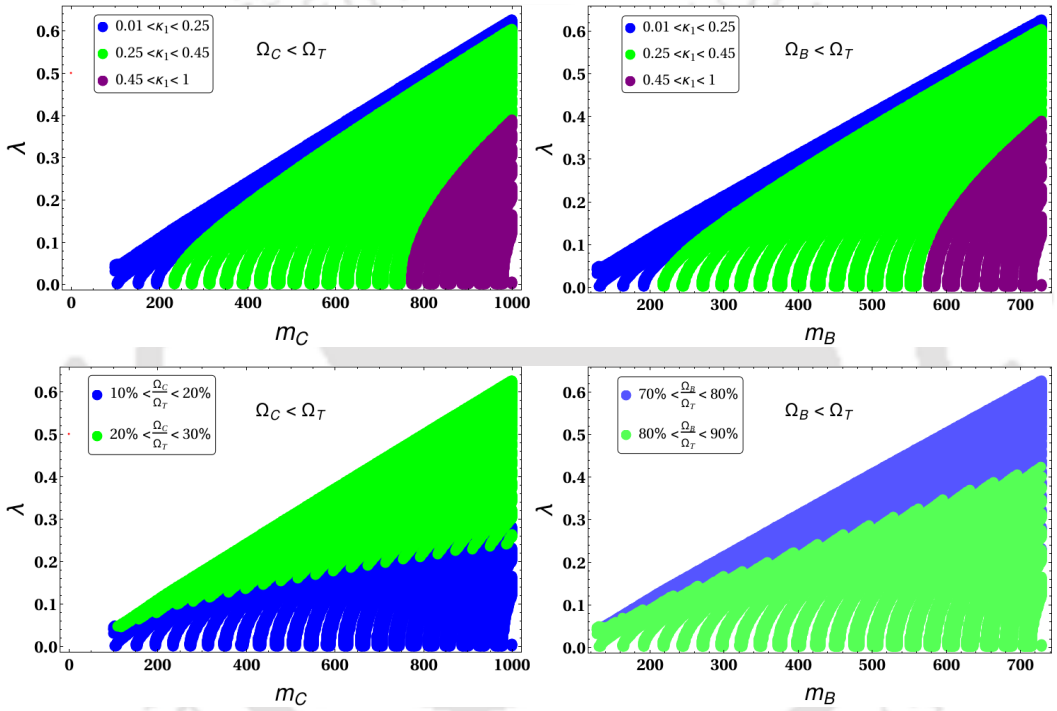

FIGURE 5.7: λ vs m_C (left) and λ vs m_B (right) for satisfying relic density $0.1175 < \Omega_T < 0.1219$.[Top panel:] Different choices of κ_1 are shown in different colours: $0.01 - 0.25$ (blue), $0.25 - 0.45$ (green), $0.45 - 1.0$ (purple). [Bottom panel:] Relative contributions of individual DM candidates to totla relic abundance have been shown in different colors.

In Fig. 5.8, we also show the relative contribution of relic density of one type of DM for a fixed κ_1; on the left (right) side, we choose $\kappa_1 = 0.35$ ($\kappa_1 = 0.45$). Contributions from different values of λ are shown in different colours. We note that Ω_C yields the dominant contribution to Ω_T, which occurs because C annihilation cross section is larger than for the B, by the contribution from the $CC \to BB$ process and also due to the larger degeneracy (6) of B component. We also see that with larger κ_1, the regions of larger λ disappear (*i.e.* are inconsistent with the constraints).

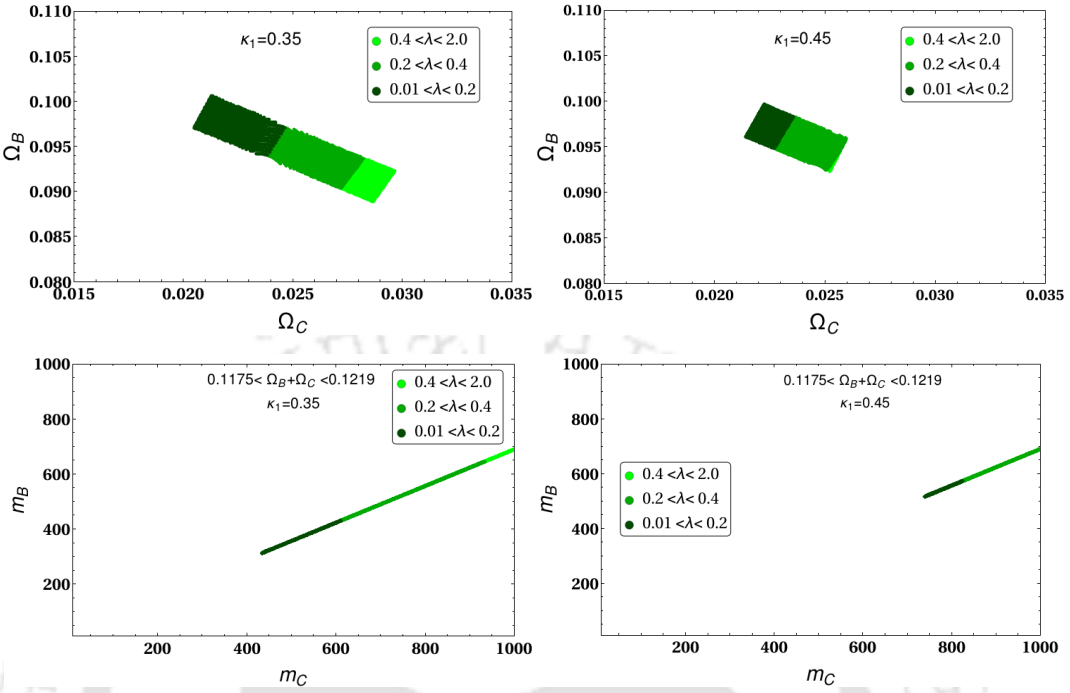

FIGURE 5.8: [Top panel:] Contribution to Ω_T from Ω_C and Ω_B for different choices of $\kappa_1 = 0.35$ (left) and 0.45 (right). Different ranges of λ are indicated $\lambda = \{0.01 - 0.2\}$ (dark green), $\{0.2 - 0.4\}$ (green) and $\{0.4 - 2.0\}$ (lighter green) respectively. [Bottom panel:] Mass correlation $(m_B - m_C)$ in allowed relic density parameter space. Color codes remain the same as in top panel.

Finally we show spin independent direct search cross section of C and B-types of DM in Fig 5.9. A large region of parameter space is allowed by the LUX limit; this is because the DM-DM conversion allows different pNBG species meet the required relic density, without contributing to direct search cross sections. Clearly depending on how large one can choose κ_1, the mass of the DM gets heavier to satisfy relic density and direct search constraints. Also due to the larger DM-DM conversion cross-section, the direct-detection probability for the C type of pNBG is smaller than for the B type.

We conclude the section by discussing a specific region of parameter space of the MSSM where the LSP is dominated by the wino/wino-Higgsino component, and also contributes negligibly to relic density. The LSP has four different contributions from the two Higgsinos ($\tilde{H}_{u,d}$), wino ($\tilde{W}$) and bino ($\tilde{B}$): [239, 245, 248, 415]

$$\chi_0 = Z_{11}\tilde{B} + Z_{12}\tilde{W} + Z_{13}\tilde{H}_u + Z_{14}\tilde{H}_d \tag{5.48}$$

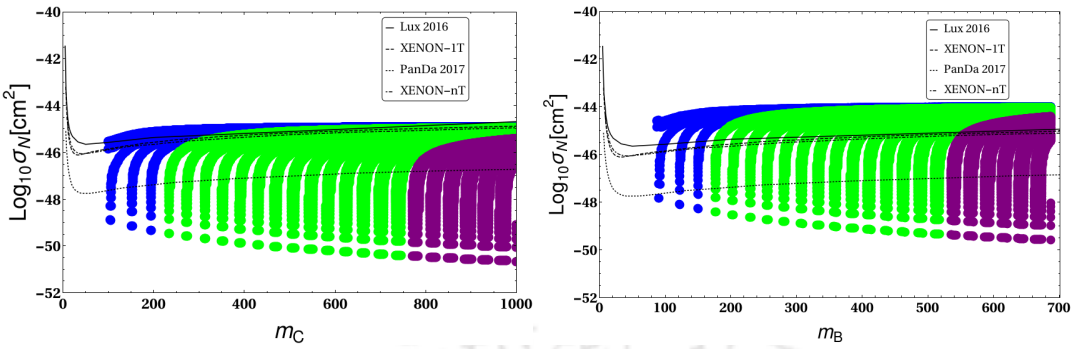

FIGURE 5.9: Spin independent direct detection cross section for C (left) and B (right) for relic density satisfied region have been compared with LUX 2016[185] and XENON 1T[183], Panda X[186] experimental constraints and with expected sensitivity from XENONnT[379]. Different choices of κ_1 are shown in different colours: $0.01 - 0.25$ (blue), $0.25 - 0.45$ (green), $0.45 - 1.0$ (purple)

μ	M_1	M_2	Z_{11}	Z_{12}	Z_{13}	Z_{14}	m_{χ_0}	$\Omega_{\chi_0}h^2$	$\sigma^{\mathrm{SI}}_{\chi_0\chi_0\to NN}$
250	3000	200	0.009	0.672	0.568	0.475	250	2×10^{-4}	1.2×10^{-46}
700	3000	400	0.003	0.976	0.178	0.124	400	5.6×10^{-3}	5.4×10^{-46}

TABLE 5.1: Relic density and corresponding SI direct detection cross section for wino/wino-Higgsino dominated neutralino with $\tan\beta = 5$. The input parameters in terms Bino (M_1), Wino (M_2) and Higgsino (μ) masses and the output in terms of neutralino mass and mixing parameters are indicated. All the masses are in GeVs. Spin independent direct search cross section is in cm^2.

where the Z_{1j} represent mixing angles. Now, since we are interested in the case where the DM density is dominated by the pNBGs, the relic density of neutralino (Ω_{χ_0}) has to be very small. This is possible when the neutralino is generally dominated by the wino component or wino Higgsino components [426]. We tabulize two such examples (Table 5.1) where we assume squarks, sleptons and gluinos of the order of 2 TeV, $\tan\beta = 5$ and all trilinear couplings at zero, excepting $A_t = -1000$ to yield correct Higgs mass. We find that the contribution of the LSP (neutralino) to the relic density is small and also the spin independent direct detection cross section $\sigma^{\mathrm{SI}}_{\chi_0\chi_0\to NN}$ is well below the PANDA X [186] experimental limit.

5.4.2 Non-negligible pNBG-LSP interaction limit

In this section we will consider some of the effects of the pNGB-LSP couplings; for simplicity we will assume that the fifteen pNGBs are degenerate (it is straightforward to relax this assumption). As noted above, there are cases where the LSP receives a non-negligible contribution from the Higgsinos, in which case the LSP-pNGB interactions cannot be ignored, even though

the DM relic density is still dominated by the pNBGs. In this case the evolution of the pNBG density is described by

$$\begin{aligned} \dot{n_{G_S}} + 3Hn_{G_S} &= -\langle\sigma v\rangle_{G_SG_S\to SM}(n_{G_S}^2 - n_\chi^{\rm eq2}) - \langle\sigma v\rangle_{G_SG_S\to\chi\chi}(n_{G_S}^2 - n_\chi^{\rm eq2}), \\ &= -\left[\langle\sigma v\rangle_{G_SG_S\to SM} + \langle\sigma v\rangle_{G_SG_S\to\chi\chi}\right](n_{G_S}^2 - n_\chi^{\rm eq2}). \end{aligned} \tag{5.49}$$

where in the last term, we used $n_{\chi_0} = n_{\chi_0}^{\rm eq}$ for the neutralinos since in the parameter region being considered they interact sufficiently strongly with the standard model to ensure they are in equilibrium; the decoupling of the LSP from the SM occurs much later than the decoupling of the pNBGs. We also assumed here that pNGBs are heavier than MSSM neutralino. Using then standard techniques[54] we find that the DM relic abundance is given approximately by

$$\Omega_T h^2 = 15 \times \frac{2.0\times10^{-10}{\rm GeV}^{-2}}{\langle\sigma v\rangle_{G_SG_S\to SM} + \langle\sigma v\rangle_{G_SG_S\to\chi_0\chi_0}}, \tag{5.50}$$

where the presence of the second term in the dominator will be instrumental in accommodating the direct detection constraints and the numerical factor 15 to take care of fifteen degenerate pNGB species.

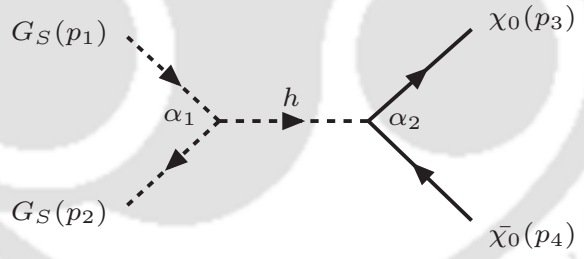

FIGURE 5.10: Feynman graph for Neutralino-pNBG interaction

The Feynman graph responsible for the pNBG-LSP interactions is presented in Fig. 5.10. The two vertex factors are named as $\alpha_1 = 2\lambda'' v_d$ and α_2 (elaborated below). This leads to the following annihilation cross section evaluated at threshold $s = 4m_{G_s}^2$:

$$(\sigma v)_{G_sG_s\to\chi\chi}|_{s=4m_{G_s}^2} = \frac{|\lambda''\ v_d\ \alpha_2\ C|^2}{8\pi}\frac{2-(m_{\chi_0}/m_{G_s})^2}{(4m_{G_s}^2 - m_h^2)^2}\left\{2 - \frac{m_{\chi_0}^2}{m_{G_s}^2}\left[1 + {\rm Re}\left(\frac{C^2}{|C|^2}\right)\right]\right\}, \tag{5.51}$$

where m_{χ_0} is the neutralino mass and

$$\lambda'' v_d = \frac{\lambda v_d}{2\cos\beta},$$
$$C = (Z_{14}\sin\beta - Z_{13}\cos\beta)\,(Z_{12} - \tan\theta_W Z_{11})\,. \tag{5.52}$$

The vertex containing α_2 is generated by the Higgs-neutralino interaction[248]:

$$-ig_2\bar{\chi}_0(C^* P_L + C P_R)\chi_0 h, \tag{5.53}$$

where g_2 is the $SU(2)_L$ gauge coupling constant; as previously, we assumed $\alpha = \beta + \pi/2$. The detailed calculation of cross-section is illustrated in Appendix C.2.

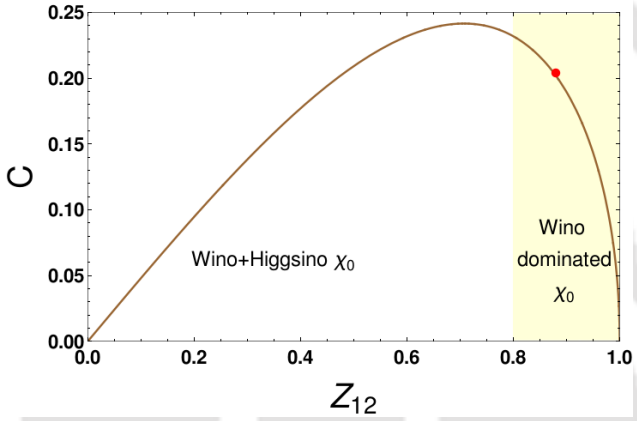

FIGURE 5.11: A plot between C and Z_{12} for $\tan\beta = 5$ assuming wino or wino-Higgsino dominated neutralino with $Z_{11} = 0$ and $Z_{13} = Z_{14}$. Our choice ($Z_{12} = 0.88$ and $C = 0.2$) has been denoted by a red dot.

We perform a scan of the pNBG DM parameter space by varying DM mass and coupling of pNGB with SM (proportional to λ) with pNBG DM-Neutralino annihilations into account. For that we choose two benchmark points by fixing $\tan\beta = 5$ and using $\alpha = \beta + \frac{\pi}{2}$ as mentioned in Table 5.2. This is following from what we obtained from Table 5.1, where neutralino has minimal relic density, but sizeable pNGB-neutralino interaction. The two interaction coefficients (λ' and λ'') in this approximation turns out to be:

$$\lambda' = \frac{\lambda}{2}\,\sin\alpha\,\cos\alpha = \frac{0.195}{2}\,\lambda,$$
$$\lambda'' = \frac{\lambda}{2}\,v_d\,\cos\alpha\,(\tan\alpha - \tan\beta) = -\frac{247}{2}\,\lambda. \tag{5.54}$$

M_A (GeV)	M_{χ_0} (GeV)	C	Z_{11}	Z_{12}	Z_{13}	Z_{14}
400	200	0.2	0	0.33	0.33	0.88
600	400	0.2	0	0.33	0.33	0.88

TABLE 5.2: Benchmark points used to find out the relic density and SI direct detection cross section of pNGB DM using pNGB-LSP interaction. We mention physical masses of neutralino (χ_0) and pseudoscalar Higgs A and mixing pattern of neutralinos.

Now as we are working with the wino or wino-Higgsino dominated neutralino, it is safe to consider $Z_{11} = 0$. For simplification purpose we also assume $Z_{13} = Z_{14}$. Next we employ the constraint $|Z_{11}|^2 + |Z_{12}|^2 + |Z_{13}|^2 + |Z_{14}|^2 = 1$. In that case C in Eq.(5.52) turns out to be a function of only Z_{12}. In Fig. 5.11 a line plot has been presented to show the variation of C with Z_{12}. For our analysis, we choose $C = 0.2$ and $Z_{12} = 0.88$ (wino dominated LSP) which has been denoted by a red dot in Fig. 5.11.

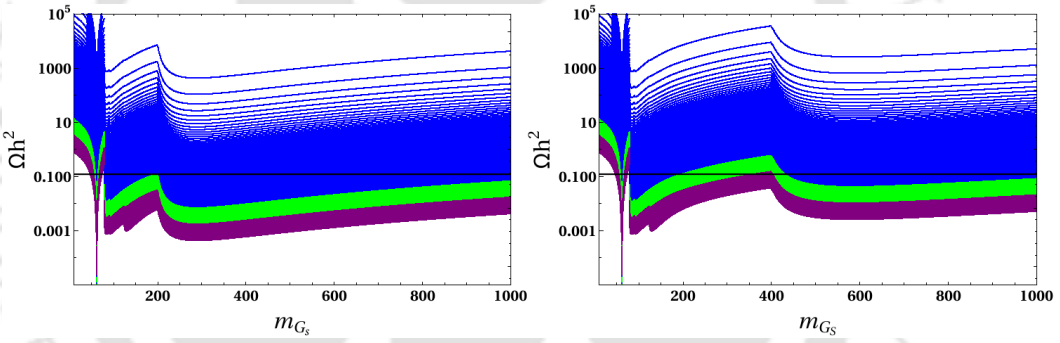

FIGURE 5.12: Relic density as a function of m_{G_S} for $\lambda = 0.005 - 0.25$ (blue), $0.25 - 0.5$ (green) and $0.5 - 2$ (purple). We assumed all 15 pNBGs are degenerate and included the effects of the pNBG-LSP interaction with $\tan\beta = 5$, $C = 0.2$, and a neutralino mass of $m_\chi = 200$ GeV (left) or $m_\chi = 400$ GeV (right).

The relic density for the case of 15 degenerate pNBGs as a function of pNBG DM mass is shown in Fig. 5.12, which takes into account the effects of the pNBG-LSP interaction. This is scanned for $\lambda = 0.005 - 0.25$ (blue), $0.25 - 0.5$ (green) and $0.5 - 2$ (purple). The graph clearly shows flattening of relic density lines (which corresponds to fixed values of λ) for $m_{G_S} \geq m_\chi$, when the pNBG→LSP annihilation channel becomes kinematically allowed. The allowed parameter space for the pNBGs in mass-coupling plane is shown in Fig. 5.13.

In addition to predicting the expected relic density, the model should also comply with the constraints from direct detection experiments. The restrictions imposed by the LUX 2017 [185], XENON1T [183] and PANDA X [186] experiments are presented in Fig. 5.14 for the cases of

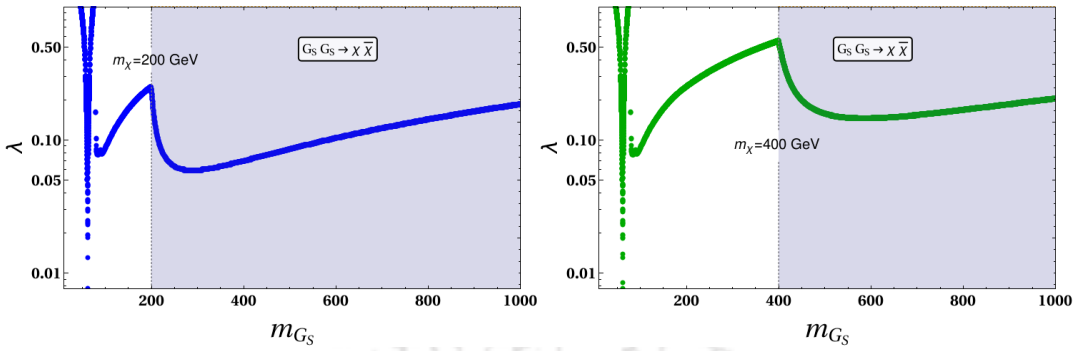

FIGURE 5.13: Region in the $m_{G_S} - \lambda$ space allowed by the relic density constraint. We assumed all 15 pNBGs are degenerate and included the effects of the pNBG-LSP interaction with $\tan\beta = 5$, $C = 0.2$, and a neutralino mass of $m_\chi = 200$ GeV (left) or $m_\chi = 400$ GeV (right).

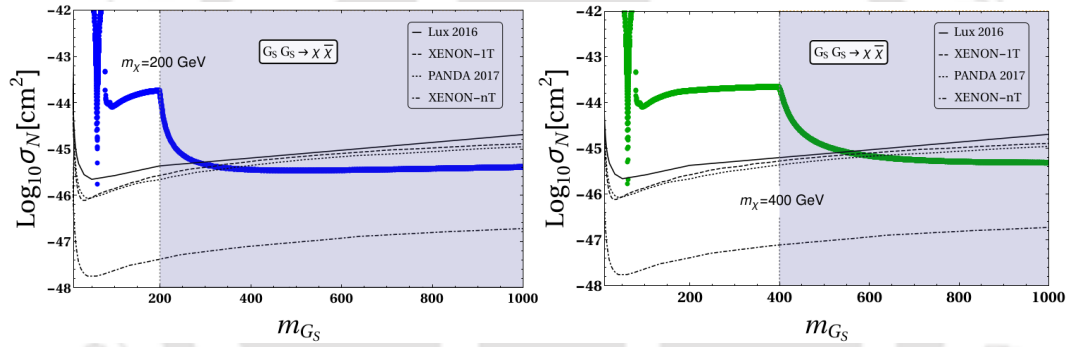

FIGURE 5.14: Direct search constraints for pNBG DMs from LUX 2016[185], XENON 1T[183], PANDA X[186] and future prediction of XENONnT[379] for the case of 15 degenerate pNBGs where the effects of the pNBG-LSP interaction is considered with $\tan\beta = 5$, $C = 0.2$ and neutralino mass $m_\chi = 200$ GeV (left), $m_\chi = 400$ GeV (right).

15 degenerate pNBGs with sizeable interaction with neutralinos. The results clearly indicate that in the presence of pNBG-LSP interactions the direct detection impose milder restrictions on parameter space compared to those cases where this coupling is negligible (compare figures 5.5 and 5.14). In particular, the fully degenerate pNGB case can now comply with the direct search constraints. It is again worth emphasizing the role played by the neutralino: it provides a new channel through which the pNBGs can annihilate (pNBG→LSP) that does not affect the direct detection cross section, this allows smaller values of λ (thus relaxing direct detection constraints), while keeping a large enough annihilation cross section, needed to meet the relic abundance requirements. As noted earlier, this occurs in the region where the LSP is wino/wino Higgsino dominated and in this reigon of parameter space $\Omega_{\mathrm{LSP}} << \Omega_{\mathrm{pNBG}} \simeq \Omega$.

5.5 Chapter Summary

DM as pNGB, arising out of breaking of a continuous symmetry has been studied in literature. Similar ideas have also been exploited to realize composite DM, which indeed appeal to a lot of astrophysical observations like non-cuspy halo profile etc. (see for example, [149–157]). Relating this type of DM to a consistent inflationary picture where the existence of pNGB is an artifact of the breaking of the continuous symmetry at the end of inflation, is the most interesting feature of our study. In this work, we have made use of the pNBGs, which are part of an SQCD framework in realizing early Universe inflation, as dark matter candidates. Due to the non-abelian nature of the chiral symmetry which was broken spontaneously at the end of inflation, a multiple such pNBGs as dark matter follow in the set-up. We have shown that depending on the explicit chiral symmetry breaking term, there could be different degree of degeneracy among the masses of these pNBGs. In addition, the presence of R-symmetry preserving supersymmetric Standard Model induces in general another candidate of DM, called the neutralino (being LSP). Hence we end up having a multi-particle DM scenario, which eventually is considered to be dominated by the pNBGs only as far as the contribution to relic density is concerned. We then divide our analysis into two parts; one is when the interaction between LSP and pNBGs is completely neglected and the other one is with non-zero but small LSP-pNBGs interaction. We find that the case with all degenerate pNBGs can not lead to a successful situation consistent with the recent direct detection limit in the first case. On the other hand, the case with non-degenerate pNBGs without any effective contribution of the LSP toward relic density can be consistent with direct search bound. In case of small but non-zero LSP-pNBG interaction, we have found that this possibility alters our previous conclusions significantly. For example, the case of fifteen degenrate pNBG DM now becomes a possibility. Therefore our model provides an interesting possibility of pNBG dark matter scenario.

Chapter 6

Study of Higgs vacuum stability in a scalar extended singlet doublet dark matter model

6.1 Introduction

In chapter 4, we have proposed a framework to realize EW vacuum stability in presence of scalar DM. In that set up, the SM is extended with two SM singlet scalars, one is with zero and other has non-zero vacuum expectation value (vev). We have shown that the presence of singlet scalar with non-zero vev has two fold impact: (i) the scalar DM having mass $\sim$ 200 GeV and onward can satisfy the relic density and direct search constraints from LUX [185], XENON-1T [183], Panda 2018 [186] and XENON-nT [379]. (ii) it can indeed make the electroweak vacuum absolutely stable [67] with the help of threshold effect [58, 59, 427].

In this chapter (based on [428]), we study the phenomenology of fermionic DM in presence of an additional scalar field. The role of the scalar field is to achieve the EW vacuum stability till M_P energy scale in the scenario. This will be more clear as we proceed. For the purpose we start with the singlet doublet fermionic dark matter (SDDM) DM model. In a typical SDDM model [429–444], the dark sector is made up with two Weyl fermion doublets and one Weyl singlet fermion. The Yukawa interactions of them with the SM Higgs result three neutral fermion states, the lightest of which becomes a viable candidate for DM provided the stability is guaranteed by some symmetry argument. Unlike Higgs portal dark matter models, singlet doublet dark matter scenario directly couples the mass and dynamics of dark sector with the

SM gauge sector. This is analogous to the case of supersymmetric extensions [445] where the supersymmetry breaking scale provides mass of dark matter [435]. Singlet doublet dark matter models also induce considerable co-annihilation effect which is absent in usual Higgs portal DM scenarios. Another interesting feature of SDDM model is related to evading the direct detection bound with some specified "blind spots" of the model [435].

The SDDM carries different phenomenology from the usual extension of dark sector with vector-like fermion doublet and singlet [446–451] due to the involvement of three neutral Majorana fermions in SDDM as compared to two vector like neutral fermions in [446–449, 451]. In case of vector like singlet doublet models, it is possible to have interaction with Z boson which can enhance the spin independent dark matter nucleon cross-section considerably. On the other hand, in case of SDDM, such interaction is suppressed [435]. Although in SDDM, spin dependent interaction (i.e. axial vector interaction) survives, the bounds on spin dependent dark matter nucleon cross-section [452] is not that stringent compared to spin independent limits and hence remain well below the projected upper limits. Therefore it relaxes the bounds on model parameters in the singlet doublet model allowing the model to encompass a large range of parameter space.

Although the SDDM has many promising features as mentioned above, it also has some serious issues with the Higgs vacuum stability. The model involves new fermions, which can affect the running of Higgs quartic coupling leading to instability at high energy scale [453]. In an attempt to solve the Higgs vacuum stability where the DM is part of the SDDM model, we propose an extension of the SDDM with a SM singlet scalar. We employ a Z_4 symmetry under which all the beyond SM fields carry non-trivial charges while the SM fields are not transforming. The salient features of our model are the followings:

- There exists a coupling between the additional scalar and the singlet Weyl fermion which eventually contributes to the mass matrix involving three neutral Weyl fermions. After the SM Higgs doublet and the scalar get vevs, mixing between neutral singlet fermion and doublet Weyl fermions occur and the lightest neutral fermion can serve as a stable Majorana dark matter protected by the residual Z_2 symmetry. In this way, the vev of the additional scalar contributes to the mass of the DM as well as the mixing.

- Due to the mixing between this new scalar and the SM Higgs doublet, two physical Higgses will result in this set-up. One of these would be identified with the Higgs discovered at LHC. This set-up therefore introduces a rich DM phenomenology (and different as compared to usual SDDM model) as the second Higgs would also contribute to DM annihilation and the direct detection cross-section.

- The presence of the singlet scalar with non-zero vev helps in achieving the absolute stability of the EW vacuum. Here the mixing between singlet doublet scalars (we call it scalar mixing) plays an important role. Hence the combined analysis of DM phenomenology (where this scalar mixing also participates) and vacuum stability results in constraining this scalar mixing at a level which is even stronger than the existing limits on it from experiments.

The Chapter is organized as follows. In Sec. 6.2, we describe the singlet scalar extended SDDM model. Various theoretical and observational limits on the specified model are presented in Sec. 6.3. In the next section, we present our strategy, the related expressions including Feynman diagrams for studying dark matter phenomenology of this model. The discussion on the allowed parameter space of the model in terms of satisfying the DM relic density and direct detection limits are also mentioned in this Sec. 6.4. In Sec. 6.5, the strategy to achieve vacuum stability of the scalar enhanced singlet doublet model is presented. In Sec. 6.6, we elaborate on how to constrain parameters of the model while having a successful DM candidate with absolute vacuum stability within the framework. Finally the work is concluded with conclusive remarks in Sec. 6.7.

6.2 The Model

Like the usual singlet doublet dark matter model[430–433], here also we extend the SM framework by introducing two doublet Weyl fermions, ψ_{D_1}, ψ_{D_2} and a singlet Weyl fermion field ψ_S. The doublets are carrying equal and opposite hypercharges ($Y = \frac{1}{2}(-\frac{1}{2})$ for $\psi_{D_1(D_2)}$) as required from gauge anomaly cancellation. Additionally the scalar sector is extended by including a SM real singlet scalar field, ϕ. There exists a Z_4 symmetry, under which only these additional fields are charged which are tabulated in Table 6.1. The purpose of introducing this Z_4 is two fold: firstly it avoids a bare mass term for the ψ_S field. Secondly, although the Z_4 is broken by the vev of the ϕ field, there prevails a residual Z_2 under which all the extra fermions are odd. Hence the lightest combination of them is essentially stable. Note that with this construction, not only the DM mass involves vev of ϕ but also the dark matter phenomenology becomes rich due to the involvement of two physical Higgs (as a result of mixing between ϕ and the SM Higgs doublet H). Apart from these, ϕ is also playing a crucial role in achieving electroweak vacuum stability. The purpose of ϕ will be unfolded as we proceed. For the moment, we split our discussion into two parts first as extended fermion and next as scalar sectors of the model.

Symmetry	ψ_{D_1}	ψ_{D_2}	ψ_S	ϕ
Z_4	-i	i	i	-1

TABLE 6.1: Particle multiplets and their transformation properties under Z_4 symmetry.

6.2.1 Extended fermion sector

The dark sector fermions ψ_{D_1}, ψ_{D_2} and ψ_S are represented as,

$$\psi_{D_1} = \begin{pmatrix} \psi_1^0 \\ \psi_1^- \end{pmatrix} : [2, \frac{1}{2}] \ , \qquad \psi_{D_2} = \begin{pmatrix} \psi_2^+ \\ \psi_2^0 \end{pmatrix} : [2, -\frac{1}{2}] \ , \qquad \psi_S : [1, 0] \ . \tag{6.1}$$

Here field transformation properties under the SM $(SU(2)_L \times U(1)_Y)$ are represented within square brackets. The additional fermionic Lagrangian in the present framework is therefore given as

$$\begin{aligned} \mathcal{L}_{Dark} = & \, i\psi_{D_1}^\dagger \bar{\sigma}^\mu D_\mu \psi_{D_1} + i\psi_{D_2}^\dagger \bar{\sigma}^\mu D_\mu \psi_{D_2} + \\ & i\psi_S^\dagger \bar{\sigma}^\mu \partial_\mu \psi_S - (m_\psi \epsilon^{ab} \psi_{D_1 a} \psi_{D_2 b} + \frac{1}{2} c\phi \psi_S \psi_S + h.c.) \ , \end{aligned} \tag{6.2}$$

where D_μ is the gauge covariant derivative in the Standard Model, $D_\mu = \partial_\mu - igW_\mu^a \frac{\sigma_a}{2} - ig'YB_\mu$. From Eq.(6.2) it can be easily observed that after ϕ gets a vev, the singlet fermion ψ_S in the present model receives a Majorana mass, $m_{\psi_S} = c\langle\phi\rangle$.

Apart from the interaction with the singlet scalar ϕ, the dark sector doublet ψ_{D_1} and singlet ψ_S can also have Yukawa interactions with the Standard Model Higgs doublet, H. This Yukawa interaction term is given as

$$-\mathcal{L}_Y = \lambda \psi_S \psi_{D_1} H + h.c. \ . \tag{6.3}$$

Note that due to Z_4 charge assignment, ψ_{D_2} does not have such Yukawa coupling in this present scenario. Once ϕ gets a vev v_ϕ and the electroweak symmetry is broken (with H acquires a vev $v/\sqrt{2}$, with $v = 246$ GeV), Eq.(6.3) generates a Dirac mass term for the additional neutral fermions. Hence including Eq.(6.2) and Eq.(6.3), the following mass matrix (involving the neutral fermions only) results

$$\mathcal{M} = \begin{pmatrix} m_{\psi_S} & \frac{1}{\sqrt{2}}\lambda v & 0 \\ \frac{1}{\sqrt{2}}\lambda v & 0 & m_\psi \\ 0 & m_\psi & 0 \end{pmatrix} . \tag{6.4}$$

The matrix is constructed with the basis $\mathcal{X}^T = (\psi_S,\ \psi_1^0,\ \psi_2^0)$. On the other hand, the charged components have a Dirac mass term, $m_\psi \psi_1^- \psi_2^+ + h.c.$.

In general the mass matrix $\mathcal{M}$ could be complex. However for simplicity, we consider the parameters m_{ψ_S}, λ and m_ψ to be real. By diagonalizing this neutral fermion mass matrix, we obtain $V^T \mathcal{M} V = diag(m_{\chi_1}, m_{\chi_2}, m_{\chi_3})$, where the three physical states $\mathcal{P}^T = (\chi_1, \chi_2, \chi_3)$ are related to $\mathcal{X}$ by,

$$\mathcal{X}_i = V_{ij} \mathcal{P}_j, \tag{6.5}$$

where V is diagonalizing matrix of $\mathcal{M}$. Then the corresponding real mass eigenvalues obtained at the tree level are given as [432, 454]

$$m_{\chi_1} = -\frac{B}{3A} - \frac{2}{3A}\Big(\frac{R}{2}\Big)^{1/3} \cos\theta_m\,, \tag{6.6}$$

$$m_{\chi_2} = -\frac{B}{3A} + \frac{1}{3A}\Big(\frac{R}{2}\Big)^{1/3} (\cos\theta_m - \sqrt{3}\sin\theta_m)\,, \tag{6.7}$$

$$m_{\chi_3} = -\frac{B}{3A} + \frac{1}{3A}\Big(\frac{R}{2}\Big)^{1/3} (\cos\theta_m + \sqrt{3}\sin\theta_m)\,, \tag{6.8}$$

where $A = 1,\ B = -m_{\psi_S},\ C = -(m_\psi^2 + \frac{\lambda^2 v^2}{2}),\ D = m_\psi^2 m_{\psi_S}$ (provided the discriminant (Δ) of $\mathcal{M}$ is positive). Now R and the angle θ_m can be expressed as

$$R = \sqrt{P^2 + Q^2}, \qquad \tan 3\theta_m = \frac{Q}{P}\,, \tag{6.9}$$

where $P = 2B^3 - 9ABC + 27A^2D$ and $Q = 3\sqrt{3\Delta}A$, $\Delta = 18ABCD - 4B^3D + B^2C^2 - 4AC^3 - 27A^2D^2$ is the discriminant of the matrix $\mathcal{M}$. The lightest neutral fermion, protected by the unbroken Z_2, can serve as a potential candidate for dark matter.

At this stage, one can form usual four component spinors out of these physical fields [430–433]. Below we define the Dirac fermion (F^+) and three neutral Majorana fermions ($F_{i=1,2,3}$) as,

$$F^+ = \begin{pmatrix} {\psi^+}_\alpha \\ (\psi^-)^{\dagger\dot{\alpha}} \end{pmatrix}, \quad F_i = \begin{pmatrix} \chi_{i\alpha} \\ (\chi_i)^{\dagger\dot{\alpha}} \end{pmatrix}\,, \tag{6.10}$$

where ψ_1^- and ψ_2^+ are identified with ψ^- and ψ^+ respectively. In the above expressions of F^+ and F_i, $\alpha(\dot{\alpha}) = 1, 2$ refers to upper (lower) two components of the Dirac spinor that distinguishes the left handed Weyl spinor from the right handed Weyl spinor [248]. Hence $m_{F^+} = -m_\psi$ corresponds to the tree level Dirac mass for the charged fermion. Masses of the neutral fermions are then denoted as $m_{F_i} = m_{\chi_i}$. As we have discussed earlier, although the Z_4 symmetry is broken by $\langle\phi\rangle$, a remnant Z_2 symmetry prevails in the dark sector which prevents dark sector

fermions to have direct interaction with the SM fermions. This can be understood later from the Lagrangian of Eq.(6.22) which remains invariant if the dark sector fermions are odd under the remnant Z_2 symmetry.

Now we need to proceed for finding out various interaction terms involving these fields which will be crucial in evaluating DM relic density and finding direct detection cross-sections. However as in our model, there exists an extra singlet scalar, ϕ with non-zero vev, its mixing with the SM Higgs doublet also requires to be included. For that purpose, we now discuss the scalar sector of our framework.

6.2.2 Scalar sector

As mentioned earlier, we introduce an additional real singlet scalar ϕ that carries Z_4 charge as given in Table 6.1. The most general potential involving the SM Higgs doublet and the newly introduced scalar is given as

$$\mathcal{L}_{\text{scalar}}(H,\phi) = -\mu_H^2|H|^2 + \lambda_H|H|^4 - \frac{\mu_\phi^2}{2}\phi^2 + \frac{\lambda_\phi}{4}\phi^4 + \frac{\lambda_{\phi H}}{2}|H|^2\phi^2. \tag{6.11}$$

After electroweak symmetry is broken and ϕ gets vev, these scalar fields can be expressed as

$$H = \begin{pmatrix} 0 \\ \frac{1}{\sqrt{2}}(v + H_0) \end{pmatrix}, \qquad \phi = v_\phi + \phi_0 \ . \tag{6.12}$$

Minimization of the scalar potential leads to the following vevs of ϕ and H given by

$$v_\phi^2 = \frac{4\mu_\phi^2\lambda_H - 2\mu_H^2\lambda_{\phi H}}{4\lambda_H\lambda_\phi - \lambda_{\phi H}^2}, \tag{6.13}$$

$$v^2 = \frac{4\mu_H^2\lambda_\phi - 2\mu_\phi^2\lambda_{\phi H}}{4\lambda_H\lambda_\phi - \lambda_{\phi H}^2}. \tag{6.14}$$

Therefore, after ϕ gets the vev and electroweak symmetry is broken, the mixing between the neutral component of H and ϕ will take place (the mixing is parametrized by angle θ) and new mass or physical eigenstates will be formed. The two physical eigenstates (H_1 and H_2) can be obtained in terms of H_0 and ϕ_0 as

$$\begin{aligned} H_1 &= H_0\cos\theta - \phi_0\sin\theta, \\ H_2 &= H_0\sin\theta + \phi_0\cos\theta, \end{aligned} \tag{6.15}$$

where θ is the scalar mixing angle defined by

$$\tan 2\theta = \frac{\lambda_{\phi H} v v_\phi}{-\lambda_H v^2 + \lambda_\phi v_\phi^2}. \tag{6.16}$$

Similarly the mass eigenvalues of these physical scalars at tree level are found to be

$$m_{H_1}^2 = \lambda_\phi v_\phi^2 (1 - \sec 2\theta) + \lambda_H v^2 (1 + \sec 2\theta), \tag{6.17}$$

$$m_{H_2}^2 = \lambda_\phi v_\phi^2 (1 + \sec 2\theta) + \lambda_H v^2 (1 - \sec 2\theta). \tag{6.18}$$

Using Eqs.(6.16-6.18), the couplings λ_H, λ_ϕ and $\lambda_{\phi H}$ can be expressed in terms of the masses of the physical eigenstates H_1 and H_2, the vevs (v, v_ϕ) and the mixing angle θ as

$$\lambda_H = \frac{m_{H_1}^2}{4v^2}(1 + \cos 2\theta) + \frac{m_{H_2}^2}{4v^2}(1 - \cos 2\theta), \tag{6.19}$$

$$\lambda_\phi = \frac{m_{H_1}^2}{4v_\phi^2}(1 - \cos 2\theta) + \frac{m_{H_2}^2}{4v_\phi^2}(1 + \cos 2\theta), \tag{6.20}$$

$$\lambda_{\phi H} = \sin 2\theta \Big(\frac{m_{H_2}^2 - m_{H_1}^2}{2 v v_\phi} \Big). \tag{6.21}$$

Note that with H_1 as the SM Higgs, second term in Eq. (6.19) serves as the threshold correction to the SM Higgs quartic coupling. This would help λ_H to maintain its positivity at high scale. Before proceeding for discussion of how this model works in order to provide a successful DM scenario and the status of electroweak vacuum stability, we first summarize relevant part of the interaction Lagrangian and the various vertices relevant for DM phenomenology and study of our model.

6.2.3 Interactions in the model

Substituting the singlet and doublet fermion fields of Eqs.(6.2-6.3) in terms of their mass eigenstates following Eq.(6.5) and using the redefinition of fields given in Eq.(6.10), gauge and Yukawa

interaction terms can be obtained as

$$\begin{aligned}
\mathcal{L}_{int} &= eA_\mu \bar{F^+}\gamma^\mu F^+ + \frac{g}{2c_W}(c_W^2 - s_W^2) Z_\mu \bar{F^+}\gamma^\mu F^+ + \frac{g}{\sqrt{2}}\sum_i W_\mu^- (V_{3i}^* \bar{F}_i \gamma^\mu P_L F^+ - V_{2i}\bar{F}_i\gamma^\mu P_R F^+) \\
&+ \frac{g}{\sqrt{2}}\sum_i W_\mu^+ (V_{3i}\bar{F^+}\gamma^\mu P_L F_i - V_{2i}^*\bar{F^+}\gamma^\mu P_R F_i) - \frac{1}{2}\sum_{ij} \mathrm{Re}X_{ij} Z_\mu \bar{F}_i\gamma^\mu\gamma^5 F_j + \frac{1}{2}\sum_{ij}\mathrm{Im}X_{ij} Z_\mu \bar{F}_i\gamma^\mu F_j \\
&- \frac{1}{2}\sum_i \bar{F}_i F_i [\mathrm{Re}Y_{ii}\cos\theta - \mathrm{Re}(cV_{1i}^2)\sin\theta] H_1 - \frac{1}{2}\sum_{i\neq j}\bar{F}_i F_j [\mathrm{Re}(Y_{ij}+Y_{ji})\cos\theta - \mathrm{Re}(cV_{1i}V_{1j})\sin\theta] H_1 \\
&- \frac{1}{2}\sum_i \bar{F}_i F_i [\mathrm{Re}Y_{ii}\sin\theta + \mathrm{Re}(cV_{1i}^2)\cos\theta] H_2 - \frac{1}{2}\sum_{i\neq j}\bar{F}_i F_j [\mathrm{Re}(Y_{ij}+Y_{ji})\sin\theta + \mathrm{Re}(cV_{1i}V_{1j})\cos\theta] H_2 \\
&+ \frac{1}{2}\sum_i \bar{F}_i i\gamma^5 F_i [\mathrm{Im}Y_{ii}\cos\theta - \mathrm{Im}(cV_{1i}^2)\sin\theta] H_1 + \frac{1}{2}\sum_i \bar{F}_i i\gamma^5 F_i [\mathrm{Im}Y_{ii}\sin\theta + \mathrm{Im}(cV_{1i}^2)\cos\theta] H_2 \\
&+ \frac{1}{2}\sum_{i\neq j}\bar{F}_i i\gamma^5 F_j [\mathrm{Im}(Y_{ij}+Y_{ji})\cos\theta - \mathrm{Im}(cV_{1i}V_{1j})\sin\theta] H_1 \\
&+ \frac{1}{2}\sum_{i\neq j}\bar{F}_i i\gamma^5 F_j [\mathrm{Im}(Y_{ij}+Y_{ji})\sin\theta + \mathrm{Im}(cV_{1i}V_{1j})\cos\theta] H_2 \ . \qquad (6.22)
\end{aligned}$$

Here the expressions of different couplings are given as

$$X_{ij} = \frac{g}{2c_W}(V_{2i}^* V_{2j} - V_{3i}^* V_{3j}), \qquad (6.23)$$

$$Y_{ii} = \sqrt{2}\ \lambda V_{1i} V_{2i}, \quad Y_{ij} + Y_{ji} = \sqrt{2}\ \lambda (V_{1i}V_{2j} + V_{1j}V_{2i}). \qquad (6.24)$$

With the consideration that all the couplings involved in $\mathcal{M}$ are real, the elements of diagonalizing matrix V in Eq.(6.5) become real[454] and hence the interactions proportional to the imaginary parts in Eq.(6.22) will disappear. Only real parts of X_{ij}, Y_{ij} will survive. From Eq.(6.22) we observe that the Largrangian remains invariant if a Z_2 symmetry is imposed on the fermions. Therefore this residual Z_2 stabilises the lightest fermion that serves as our dark matter candidate.

The various vertex factors involved in DM phenomenology, generated from the scalar Lagrangian, are

$$\begin{aligned}
H_1 f\bar{f}, H_2 f\bar{f} &: \frac{m_f}{v}\cos\theta, \frac{m_f}{v}\sin\theta \\
H_1 ZZ, H_2 ZZ &: \frac{2m_Z^2}{v}\cos\theta g^{\mu\nu}, \frac{2m_Z^2}{v}\sin\theta g^{\mu\nu} \\
H_1 W^+W^-, H_2 W^+W^- &: \frac{2m_Z^2}{v}\cos\theta g^{\mu\nu}, \frac{2m_Z^2}{v}\sin\theta g^{\mu\nu} \\
H_1 H_1 H_1 &: [6v\lambda_H \cos^3\theta - 3v_\phi\lambda_{\phi H}\cos^2\theta\sin\theta + 3v\lambda_{\phi H}\cos\theta\sin^2\theta - 6v_\phi\lambda_\phi\sin^3\theta] \\
H_2 H_2 H_2 &: [6v\lambda_H \sin^3\theta + 3v_\phi\lambda_{\phi H}\cos\theta\sin^2\theta + 3v\lambda_{\phi H}\cos^2\theta\sin\theta + 6v_\phi\lambda_\phi\cos^3\theta]
\end{aligned}$$

$$
\begin{aligned}
H_1H_1H_2 \quad &: \quad [2v(3\lambda_H - \lambda_{\phi H})\cos^2\theta\sin\theta + v\lambda_{\phi H}\sin^3\theta + v_\phi(6\lambda_\phi - 2\lambda_{\phi H})\cos\theta\sin^2\theta \\
&\quad +v_\phi\lambda_{\phi H}\cos^3\theta] \\
H_1H_2H_2 \quad &: \quad [2v(3\lambda_H - \lambda_{\phi H})\cos\theta\sin^2\theta + v\lambda_{\phi H}\cos^3\theta - v_\phi(6\lambda_\phi - 2\lambda_{\phi H})\cos^2\theta\sin\theta \\
&\quad -v_\phi\lambda_{\phi H}\sin^3\theta],
\end{aligned}
\tag{6.25}
$$

where m_f represents mass of the SM fermion(s) (f) and m_Z corresponds to the mass of the Z boson (at tree level).

6.3 Constraints

In this section we illustrate important theoretical and experimental bounds that can constrain the parameter space of the proposed model. Note that among H_1 and H_2, one of them would be the Higgs discovered at LHC (say the SM Higgs). The other Higgs can be heavier or lighter than the SM Higgs. In this analysis, we consider the lightest scalar state H_1 as the Higgs with mass $m_{H_1} = 125.09$ GeV [25]. We argue at the end of this section why such a choice is phenomenologically favoured from DM and vacuum stability issues with respect to the case with additional Higgs being lighter than the SM one. Now from the discussion of Secs. 6.2.1 and 6.2.2, it turns out that there are six independent parameters in the set up: three (m_{H_2}, $\sin\theta$ and v_ϕ) from the scalar sector and other three (λ, m_ψ, c) from the fermionic sector. These parameters can be constrained using the limits from perturbativity, perturbative unitarity, electroweak precision data and the singlet induced NLO correction to the W boson mass [371, 373, 455]. In addition, constraints from DM experiments, LHC and LEP will also be applicable. We discuss these constraints below.

[A] Theoretical Constraints:

- The scalar potential should be bounded from below in any field direction. This poses some constraints[360, 361] on the scalar couplings of the model which we will discuss in Sec. 6.5 in detail. The conditions must be satisfied at any energy scales till M_P in order to ensure the stability of the entire scalar potential in any field direction.

- One should also consider the the perturbative unitarity bound associated with the S matrix corresponding to scattering processes involving all two-particle initial and final states. In the specific model under study, there are five neutral (W^+W^-, ZZ, H_0H_0, $H_0\phi_0$, $\phi_0\phi_0$)

and three singly charged (W^+H_0, $W^+\phi_0$, W^+Z) combinations of two-particle initial and final states [362, 363, 456]. The perturbative unitarity limit can be derived by implementing the bound on the scattering amplitude $\mathcal{M}$ [362, 363, 456]

$$\mathcal{M} < 8\pi. \tag{6.26}$$

The unitarity constraints are obtained as [362, 363, 456]

$$\lambda_H < 4\pi, \quad \lambda_{\phi H} < 8\pi, \text{ and } \frac{1}{4}\{12\lambda_H + \lambda_\phi \pm \sqrt{16\lambda_{\phi H}^2 + (\lambda_\phi - 12\lambda_H)^2}\} < 8\pi. \tag{6.27}$$

- In addition, all relevant couplings in the framework should maintain the perturbativity limit. Perturbative conditions of relevant couplings in our set up appear as [354] [1]

$$\lambda_H < \frac{2}{3}\pi,\ \lambda_\phi < \frac{2}{3}\pi,\ \lambda_{\phi H} < 4\pi,\ \lambda < \sqrt{4\pi}, \text{ and } c < \sqrt{4\pi}. \tag{6.28}$$

We will ensure the perturbativity of the couplings present in the model till M_P energy scale by employing the renormalization group equations.

[B] Experimental Constraints:

- In the present singlet doublet dark matter model, dark matter candidate χ_1 has coupling with the Standard Model Higgs H_1 and neutral gauge boson Z. Therefore, if kinematically allowed, the gauge boson and Higgs can decay into pair of dark matter particles. Hence we should take into account the bound on invisible decay width of Higgs and Z boson from LHC and LEP. The corresponding tree level decay widths of Higgs boson H_1 and Z into DM is given as

$$\Gamma_{H_1}^{inv} = \frac{\lambda_{H_1\chi_1\chi_1}^2}{16\pi} m_{H_1} \left(1 - \frac{4m_{\chi_1}^2}{m_{H_1}^2}\right)^{3/2}$$
$$\Gamma_{Z}^{inv} = \frac{\lambda_{Z\chi_1\chi_1}^2}{24\pi} m_{Z} \left(1 - \frac{4m_{\chi_1}^2}{m_{Z}^2}\right)^{3/2}, \tag{6.29}$$

where the couplings, $\lambda_{H_1\chi_1\chi_1}$ and $\lambda_{Z\chi_1\chi_1}$ can be obtained from Eq.(6.22). The bound on Z invisible decay width from LEP is $\Gamma_Z^{inv} \leq 2$ MeV at 95% C.L. [457] while LHC provides

[1] With a Lagrangian term like $\lambda\phi_i\phi_j\phi_k\phi_l$, the perturbative expansion parameter for a $2 \to 2$ process involving different scalars $\phi_{i,j,k,l}$ turns out to be λ. Hence the limit is $\lambda < 4\pi$ [354]. Similarly with a term $yS f_i f_j$ involving scalar S and fermions $f(i \neq j)$, the corresponding expansion parameter is restricted by $y^2 < 4\pi$ [354]. Considering the associated symmetry factors (due to the presence of identical fields), we arrive at the limits mentioned at Eq.(6.28).

bound on Higgs invisible decay and invisible decay branching fraction $\Gamma^{inv}_{H_1}/\Gamma_{H_1}$ is 23% [458].

- The mass of the SM gauge boson W gets correction from the scalar induced one loop diagram[364]. This poses stronger limit on the scalar mixing angle $\sin\theta \lesssim (0.3 - 0.2)$ for 300 GeV $< m_{H_2} <$ 800 GeV [371].

- Moreover, the Higgs production cross-section also gets modified in the present model due to mixing with the real scalar singlet. As a result, Higgs production cross-section at LHC is scaled by a factor $\cos^2\theta$ and the corresponding Higgs signal strength is given as $R = \frac{\sigma_{H_1}}{\sigma_{SM}} \frac{Br(H_1 \to XX)}{Br_{SM}}$ [370], where σ_{SM} is the SM Higgs production cross-section and Br_{SM} is the measure of the SM Higgs branching ratio to final state particles X. The simplified expression for the signal strength is given as [365–371, 459]

$$R = \cos^4\theta \frac{\Gamma_1}{\Gamma^{Tot}_{H_1}} \ , \tag{6.30}$$

where Γ_1 is the decay width of H_1 in the SM. In absence of any invisible decay (when $m_{\chi_1} > m_{H_1}/2$), the signal strength is simply given as $R = \cos^2\theta$. Since H_1 is the SM like Higgs with mass 125.09 GeV, $R \simeq 1$. Hence, this restricts the mixing between the scalars. The ATLAS [457] and CMS [458] combined result provides

$$R = 1.09^{+0.11}_{-0.10}. \tag{6.31}$$

This can be translated into an upper bound on $\sin\theta \lesssim 0.36$ at 3σ.

Similarly, one can also obtain signal strength of the other scalar involved in the model expressed as $R^{'} = \sin^4\theta \frac{\Gamma_2}{\Gamma^{Tot}_{H_2}}$, where Γ_2 being the decay with of H_2 with mass m_{H_2} in the SM and $\Gamma^{Tot}_{H_2}$ is the total decay width of the scalar H_2 given as $\Gamma^{Tot}_{H_2} = \sin^2\theta\ \Gamma_2 + \Gamma^{inv}_{H_2} + \Gamma_{H_2 \to H_1 H_1}$. The additional term $\Gamma_{H_2 \to H_1 H_1}$ appears when $m_{H_2} \geq 2m_{H_1}$ and is expressed as $\Gamma_{H_2 \to H_1 H_1} = \frac{\lambda^2_{H_1 H_1 H_2}}{32\pi m_{H_2}} \sqrt{1 - \frac{4m^2_{H_1}}{m^2_{H_2}}}$, where $\lambda_{H_1 H_1 H_2}$ can be obtained from Eq.(6.25). However due to small mixing with the SM Higgs H_1, $R^{'}$ is very small to provide any significant signal to be detected at LHC [371].

- In addition, we include the LEP bound on the charged fermions involved in the singlet doublet model. The present limit from LEP excludes a singly charged fermion having mass below 100 GeV [460]. Therefore we consider $m_\psi \gtrsim 100$ GeV. The LEP bound on the heavy Higgs state (having mass above 250 GeV) turns out to be weaker compared to the limit obtained from W boson mass correction [371].

- The presence of fermions in the dark sector and the additional scalar ϕ will affect the oblique parameters [461] S, T and U through changes in gauge boson propagators. However only T parameter could have a relevant contributions from the newly introduced fields. Contributions to the T parameter by the additional scalar field ϕ can be found in [462]. However in the small mixing case, this turns out to be negligible [463] and can be safely ignored [432]. When we consider fermions, the corresponding T parameter in our model is obtained as [431, 464]

$$\Delta T = \sum_{i=1}^{3}\left[\frac{1}{2}(V_{3i}-V_{2i})^2\mathcal{A}(m_\psi,m_i)+\frac{1}{2}(V_{3i}+V_{2i})^2\mathcal{A}(m_\psi,-m_i)\right] - \sum_{i,j=1}^{3}\frac{1}{4}(V_{2i}V_{2j}-V_{3i}V_{3j})^2\mathcal{A}(m_i,-m_j), \tag{6.32}$$

where $\mathcal{A}(m_i,m_j) = \frac{1}{32\alpha_{\rm em}\pi v^2}\left[(m_i-m_j)^2\ln\frac{\Lambda^4}{m_i^2m_j^2} - 2m_im_j + \frac{2m_im_j(m_i^2+m_j^2)-m_i^4-m_j^4}{m_i^2-m_j^2}\ln\frac{m_i^2}{m_j^2}\right]$ and Λ is the cut off of the loop integral which vanishes during the numerical estimation.

- Furthermore, we also use the measured value of DM relic abundance by Planck experiment [39] and apply limits on DM direct detection cross-sections from LUX [185], XENON-1T [183], Panda 2018 [186] and XENON-nT [379] experiments to constrain the parameter space of the model. Detailed discussions on direct searches of dark matter have been presented later in Sec. 6.4.

In the above discussion, we infer that the scalar mixing angle $\sin\theta$ is restricted by $\sin\theta \lesssim 0.3$, provided the mass of additional Higgs (m_{H_2}) is around 300 GeV. For further heavier m_{H_2}, $\sin\theta$ is even more restricted, *e.g.* $\sin\theta \lesssim 0.2$ for m_{H_2} around 800 GeV. On the other hand, if we consider H_1 to be lighter than the Higgs discovered at LHC, we need to identify H_2 as the SM Higgs as per Eqs.(6.15,6.17-6.18) (where $\sin\theta \to 1$ is the decoupling limit). In this case, the limit turns out to be $\sin\theta \gtrsim 0.87$ for $m_{H_1} \lesssim 100$ GeV [371]. Note that this case is not interesting from vacuum stability point of view in this work for the following reason. From Eq. (6.19), we find the first term in right hand side serves as the threshold correction to the SM Higgs quartic coupling (contrary to the case with H_1 as the SM Higgs and H_2 as the heavier one, where the threshold correction is provided by the second term). However with $m_{H_1} < m_{H_2} \equiv$ SM Higgs and $\sin\theta \gtrsim 0.87$, the contribution of the first term is much less compared to the second term. Hence in this case, the SM Higgs quartic coupling λ_H cannot be enhanced significantly such

that its positivity till very high scale can be ensured[2]. Therefore we mainly focus on the case with $m_{H_2} > m_{H_1} (\equiv$ SM Higgs) for the rest of our analysis.

6.4 Dark matter phenomenology

In the present model, apart from the SM particles we have three neutral Majorana fermions, one charged Dirac fermion and one additional Higgs (other than the SM one). Out of these, the lightest neutral Majorana (χ_1) plays the role of dark matter. Being odd under residual Z_2, stability of the DM is ensured. As observed through Eq.(6.4), masses of these neutral Majorana fermions depend effectively on three parameters m_{ψ_S}, λ and m_ψ. However in our present scenario, m_{ψ_S} actually involves two parameters; c and v_ϕ, the individual roles of which are present in DM annihilation and vacuum stability. For the case when coupling λ is small ($\lambda < 1$), with $m_\psi > m_{\psi_S}$ (with $\lambda v/\sqrt{2} < m_\psi$), our DM candidate remains singlet dominated and for $m_\psi < m_{\psi_S}$, this becomes doublet like [439]. In the present work we will investigate the characteristics of the dark matter candidate irrespective of its singlet or doublet like nature.

6.4.1 Dark Matter relic Density

Dark matter relic density is obtained by solving the Boltzmann equation. The expression for dark matter relic density is given as [54, 465]

$$\Omega_{\chi_1} h^2 = \frac{2.17 \times 10^8 \text{ GeV}^{-1}}{g_\star^{1/2} M_P} \frac{1}{J(x_f)} \ , \tag{6.33}$$

where M_P denotes the reduced Planck mass (2.435×10^{18} GeV) and the factor $J(x_f)$ is expressed as

$$J(x_f) = \int_{x_f}^{\infty} \frac{\langle \sigma |v| \rangle}{x^2} dx \ , \tag{6.34}$$

where $x_f = m_{\chi_1}/T_f$, with T_f denoting freeze out temperature and $g_\star$ is the total number of degrees of freedom of particles. In the above expression, $\langle \sigma |v| \rangle$ is the measure of thermally averaged annihilation cross-section of dark matter χ_1 into different SM final state particles. It is to be noted that annihilation of dark matter in the present model also includes co-annihilation channels due to the presence of other dark sector particles. Different Feynmann diagrams

[2]With $m_{H_2} > m_{H_1} \equiv$ SM Higgs and $\sin\theta \sim 0.1 - 0.3$, the second term can definitely contribute to a large extent toward the positivity of λ_H.

for dark matter annihilations and co-annihilations are shown in Fig. 6.1 and Figs. 6.2,6.3,6.4 respectively.

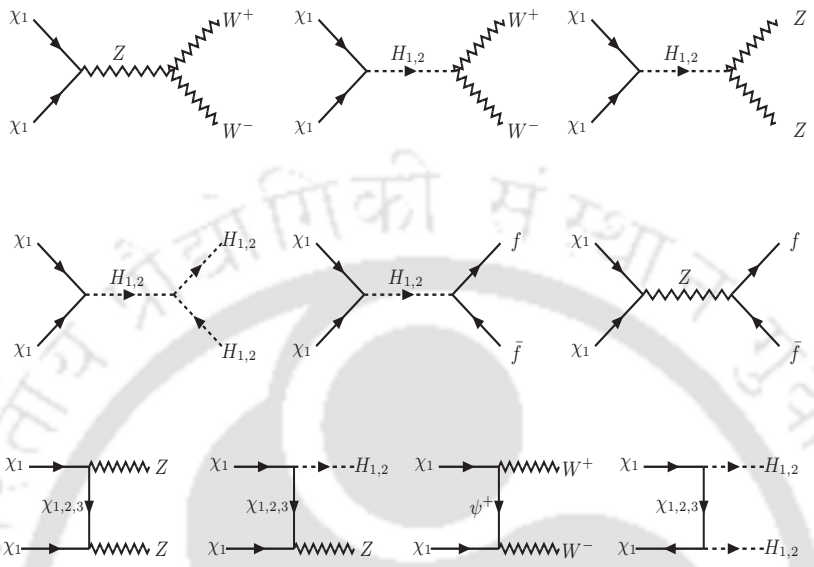

FIGURE 6.1: The dominant annihilation channels of DM to SM fields and heavy Higgs in the final states.

The thermally averaged dark matter annihilation cross-section $\langle\sigma|v|\rangle$ is expressed as

$$\begin{aligned}\langle\sigma|v|\rangle =& \frac{g_1^{'2}}{g_{eff}^2}\sigma(\chi_1\chi_1) + 2\frac{g_1'g_2'}{g_{eff}^2}\sigma(\chi_1\chi_2)(1+\Delta_{21})^{3/2}exp(-x\Delta_{21}) + 2\frac{g_1'g_3'}{g_{eff}^2}\sigma(\chi_1\chi_3)(1+\Delta_{31})^{3/2}exp(-x\Delta_{31}) \\ &+ 2\frac{g_2'g_3'}{g_{eff}^2}\sigma(\chi_2\chi_3)(1+\Delta_{21})^{3/2}(1+\Delta_{31})^{3/2}exp(-x(\Delta_{21}+\Delta_{31})) \\ &+ 2\frac{g_1'g_+'}{g_{eff}^2}\sigma(\chi_1\psi^+)(1+\Delta_{+1})^{3/2}exp(-x\Delta_{+1}) + \frac{g_+^{'2}}{g_{eff}^2}\sigma(\psi^+\psi^-)(1+\Delta_{+1})^{3}exp(-2x\Delta_{+1}) \\ &+ 2\frac{g_2'g_+'}{g_{eff}^2}\sigma(\chi_2\psi^+)(1+\Delta_{+1})^{3/2}(1+\Delta_{21})^{3/2}exp(-x(\Delta_{+1}+\Delta_{21})) \\ &+ 2\frac{g_3'g_+'}{g_{eff}^2}\sigma(\chi_3\psi^+)(1+\Delta_{+1})^{3/2}(1+\Delta_{31})^{3/2}exp(-x(\Delta_{+1}+\Delta_{31}) \\ &+ \frac{g_2^{'2}}{g_{eff}^2}\sigma(\chi_2\chi_2)(1+\Delta_{21})^{3}exp(-2x\Delta_{21}) + \frac{g_3^{'2}}{g_{eff}^2}\sigma(\chi_3\chi_3)(1+\Delta_{31})^{3}exp(-2x\Delta_{31}) \ ,\end{aligned} \tag{6.35}$$

where $\Delta_{i1} = \frac{m_{\chi_i}-m_{\chi_1}}{m_{\chi_1}}$ and $\Delta_{+1} = \frac{m_{\psi}-m_{\chi_1}}{m_{\chi_1}}$ are the corresponding mass splitting ratios. Therefore it can be easily concluded that for smaller values of mass splitting co-annihilation effects

will enhance the final dark matter annihilation cross-section significantly. The effective degrees of freedom g_{eff}

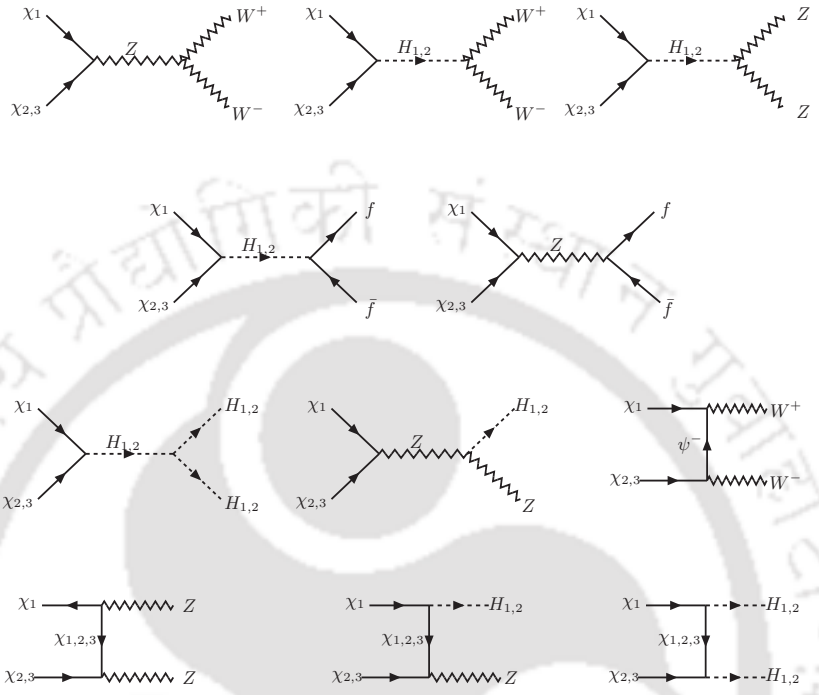

FIGURE 6.2: The dominant co-annihilation channels of DM (χ_1) with neutral fermions $\chi_{2,3}$.

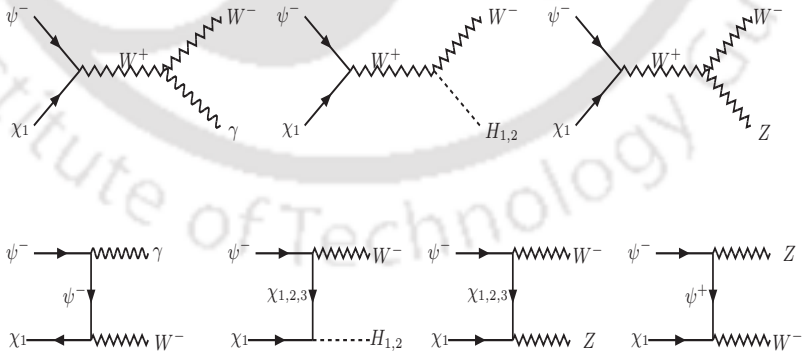

FIGURE 6.3: The dominant co-annihilation channels of DM (χ_1) with charged fermion ψ^-.

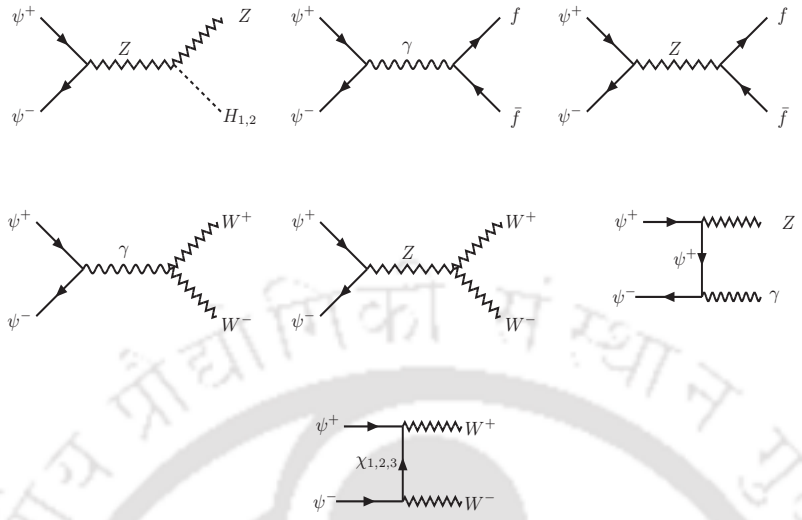

FIGURE 6.4: The dominant co-annihilation channels of the charged fermion pair ψ^+ and ψ^-.

is denoted as

$$g_{eff} = g_1' + g_2'(1+\Delta_{21})^{3/2} exp(-x\Delta_{21}) + g_3'(1+\Delta_{31})^{3/2} exp(-x\Delta_{31}) + g_+'(1+\Delta_{+1})^{3/2} exp(-x\Delta_{+1}). \quad (6.36)$$

In the above expression $g_i', i = 1-3$ are spin degrees of freedom of particles. Using Eqs.(6.33-**??**), relic density of the dark matter χ_1 can be obtained for the model parameters. The relic density of the dark matter candidate must satisfy the bounds from Planck [39] with 1σ uncertainty is given as

$$0.1175 \leq \Omega_{DM} h^2 \leq 0.1219 \ . \quad (6.37)$$

6.4.2 Direct searches for dark matter

Direct detection of dark matter is based on the scattering of the incoming dark matter particle with detector nucleus. In the present scenario, the dark matter candidate χ_1 can have both spin independent (SI) and spin dependent (SD) scatterings with the detector. In view of Eq.(6.22), spin independent interactions are mediated by scalars H_1 and H_2 while spin dependent scattering is mediated via neutral gauge boson Z as shown in Fig. 6.5.

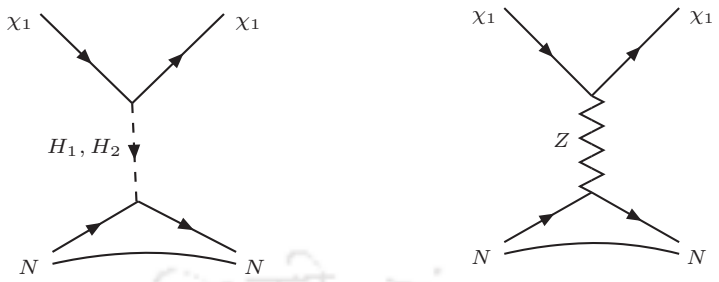

FIGURE 6.5: Schematic diagrams for dark matter direct detection processes: left panel: spin independent and right panel: spin dependent processes (N is the nucleon).

The expression for spin independent direct detection cross-section in the present singlet doublet model is given as [66]

$$\sigma_{SI} \simeq \frac{m_r^2}{8\pi}\left(\frac{\lambda_{H_1\chi_1\chi_1}\cos\theta}{m_{H_1}^2} - \frac{\lambda_{H_2\chi_1\chi_1}\sin\theta}{m_{H_2}^2}\right)^2 \lambda_p^2 \tag{6.38}$$

where $\lambda_{H_i\chi_1\chi_1}$, $i = 1, 2$ denotes the coupling of dark matter χ_1 with the scalar H_1 and H_2 as given in the Eq.(6.22). In the above expression of direct detection cross-section, m_r is the reduced mass for the dark matter-nucleon scattering, $m_r = \frac{m_{\chi_1} m_p}{m_{\chi_1}+m_p}$, m_p being the proton mass. The scattering factor λ_p is expressed as [**?**]

$$\lambda_p = \frac{m_p}{v}\left[\sum_q f_q + \frac{2}{9}\left(1 - \sum_q f_q\right)\right] \simeq 1.3 \times 10^{-3}\ , \tag{6.39}$$

where f_q is the atomic form factor[377, 378].

As we have mentioned earlier, following the interaction Lagrangian described in Eq.(6.22), we have an axial vector interaction of the neutral Majorana fermions with the SM gauge boson Z. This will infer spin dependent dark matter nucleon scattering with the detector nuclei. The expression for the spin dependent cross-section is given as [466]

$$\sigma_{SD} = \frac{16 m_r^2}{\pi}\left[\sum_{q=u,d,s} d_q \lambda_q\right]^2 J_N(J_N+1). \tag{6.40}$$

where $d_q \sim \frac{g^2}{2c_W m_Z^2} ReX_{11}$ (following Eq.(6.22)) and λ_q depends on the nucleus considering χ_1 as the dark matter candidate.

6.4.3 Results

In this section we present the dark matter phenomenology involving different model parameters and constrain the parameter space with theoretical and experimentally observed bounds discussed in Sec. 6.4. As mentioned earlier, the dark matter candidate is a thermal WIMP (Weakly Interacting Massive Particle) in nature. The dark matter phenomenology is controlled by the following parameters [3],

$$\{c,\ v_\phi,\ \lambda,\ \sin\theta,\ m_\psi\ ,\ m_{H_2}\}.$$

We have used LanHEP (version 3.2) [467] to extract the model files and use MicrOmegas (version 3.5.5) [372] to perform the numerical analysis. The model in general consists of three neutral fermions $\chi_i,\ i = 1-3$ and one charged fermion ψ^+ which take part in this analysis. The lightest fermion χ_1 is the dark matter candidate that annihilates into the SM particles and freeze out to provide the required dark matter relic density. The heavier neutral particles in the dark sector $\chi_{2,3}$ and the charged particle ψ annihilates into the lightest particle χ_1. Also $\chi_{2,3}$ co-annihilation contributes to the dark matter relic abundance (when the mass differences are small). Different possible annihilation and co-annihilation channels of the dark matter particle is shown in Figs. 6.1, 6.2, 6.3, 6.4 .

We have kept the mass of the heavier Higgs m_{H_2} below 1 TeV from the viewpoint of future experimental search at LHC. In particular, unless otherwise stated, for discussion purpose we have kept the heavy Higgs at 300 GeV. Also note that in this regime, $\sin\theta$ is bounded by $\sin\theta \lesssim 0.3$ [371], so we could exploit maximum amount of variation for $\sin\theta$ as otherwise with heavier H_2 $\sin\theta$ will be more restrictive. In the small $\sin\theta$ approximation, λ_ϕ almost coincides with the second term in Eq.(6.20). Now it is quite natural to keep the magnitude of a coupling below unity to maintain the perturbativity at all energy scales (including its running). Hence with the demand $\lambda_\phi < 1$, from Eq.(6.20) one finds $v_\phi > \sqrt{3}m_{H_2}$.

6.4.3.1 Study of importance of individual parameters

Now we would like to investigate how the relic density and direct detection cross-section depend on different parameters of the set-up. For this purpose, in Fig. 6.6 (left panel) we plot the variation of DM mass m_{χ_1} with relic density for four different values of Yukawa coupling λ

[3] Note that although c and v_ϕ together forms m_{ψ_S} appearing in neutral fermion mass eigenvalues (see Eq. (6.6-6.8)), the parameter c alone (*i.e.* without v_ϕ) is involved in DM-annihilation processes (see Eq. (6.22)). Hence we treat both c and v_ϕ as independent parameters.

while m_ψ is taken to be 500 GeV. The vev of the singlet scalar ϕ is varied from 500 GeV to 10 TeV. Fig. 6.6 (right panel) corresponds to a different $m_\psi = 1000$ GeV. Other parameters $m_{H_2}, \sin\theta$ and c are kept fixed at 300 GeV, 0.1 and 0.1 respectively as indicated on top of each figures. Note that $c = 0.1$ is a natural choice from the viewpoint that it remains non-perturbative even at very high scale. The horizontal black lines in both the figures denote the required dark matter relic abundance. In producing Fig. 6.6, dark matter direct detection limits from both spin independent and spin dependent searches are included. The solid (colored) portion of a curve correspond to the range of m_{χ_1} which satisfies the SI direct detection (DD) bounds while the dotted portion exhibits the disallowed range using DD limits.

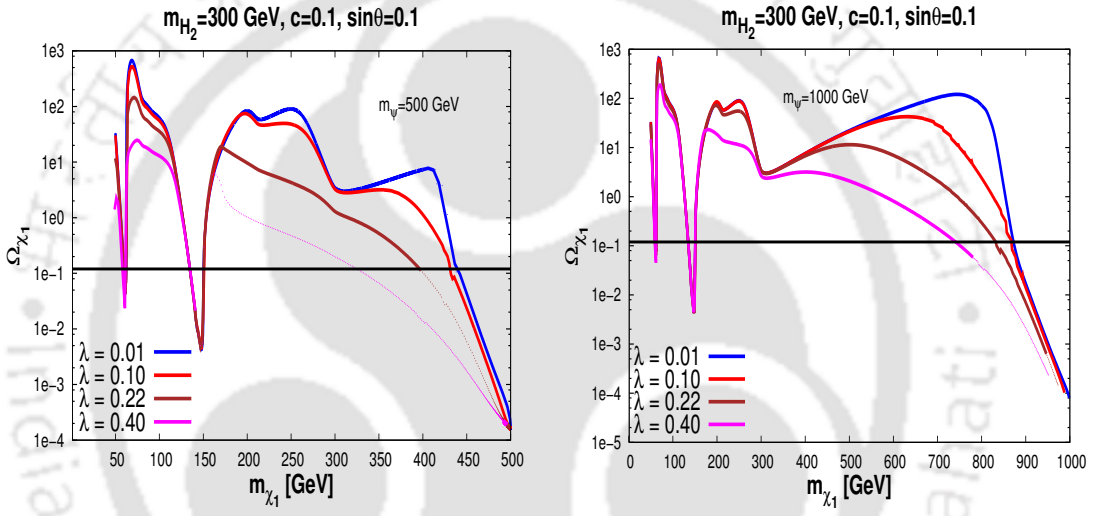

FIGURE 6.6: DM relic density as a function of DM mass for [left panel:] $m_\psi = 500$ GeV and [right panel:] $m_\psi = 1000$ GeV with different choices of $\lambda = 0.01$ (blue), 0.1 (red), 0.25 (brown) and 0.4 (pink). Values of heavy Higgs mass, scalar mixing angle and c have been kept fixed at $m_{H_2} = 300$ GeV, $\sin\theta = 0.1$ and $c = 0.1$. Dotted portions indicate the disallowed part from SI direct detection cross-section limit.

From Fig. 6.6, we also observe that apart from the two resonances, one for the SM Higgs and other for the heavy Higgs, the dark matter candidate satisfies the required relic density in another region with large value of m_{χ_1}. For example, with $\lambda = 0.22$, the relic density and DD cross-section is marginally satisfied by $m_{\chi_1} \sim 400$ GeV. The presence of this allowed value of dark matter mass is due to the fact that the co-annihilation processes turn on (they become effective when $\Delta_{i1}/m_{\chi_1} \sim 0.1$ or less) which increases the effective annihilation cross-section $\langle\sigma|v|\rangle$ and hence a sharp fall in relic density results. Since both annihilation and co-annihilations are proportional to λ (see Eq.(6.22)), an increase in λ (from pink to red lines) leads to decrease in relic density (for a fixed dark matter mass) and this would correspond to smaller value of

m_{χ_1} for the satisfaction of the relic density apart from resonance regions. For example, with $\lambda = 0.1$ or 0.01, relic density and DD satisfied value of m_{χ_1} is shifted to ~ 440 GeV compared to $m_{\chi_1} \sim 400$ GeV with $\lambda = 0.22$. It can also be traced that there exist couple of small drops of relic density near $m_{\chi_1} \sim 212$ GeV and 300 GeV. This is mostly prominent for the line with small λ (=0.1 (red line) and 0.01 (blue line)). While the first drop indicates the opening of the final states H_1H_2, the next one is due to the appearance of H_2H_2 final states.

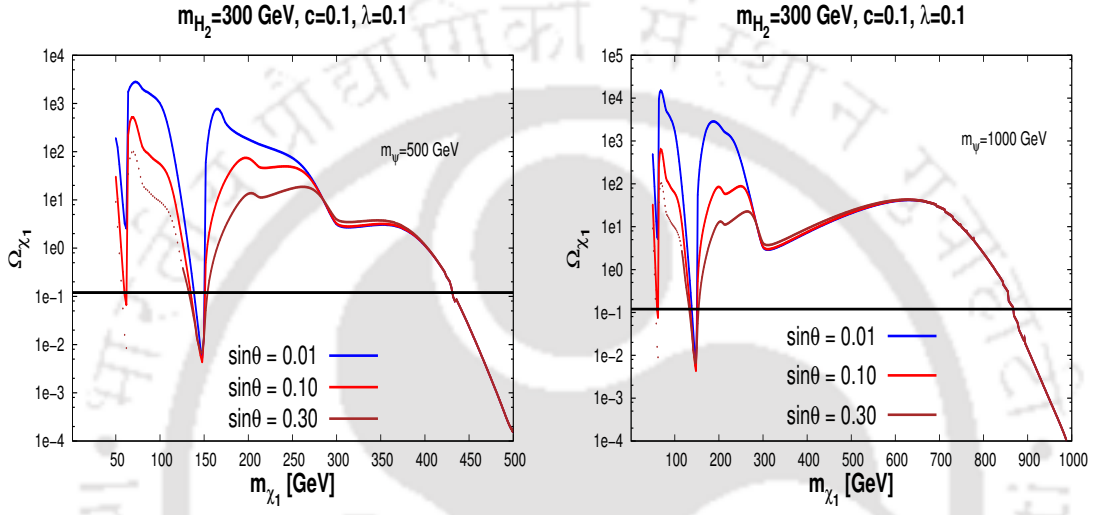

FIGURE 6.7: DM relic density as a function of DM mass considering [left panel:] $m_\psi = 500$ GeV and [right panel:] $m_\psi = 1000$ GeV for different choices of scalar mixing angle $\sin\theta \sim 0.01$ (blue), 0.1 (red) and 0.3 (brown). Values of other parameters have been fixed at $m_{H_2} = 300$ GeV, $\lambda = 0.1$ and $c = 0.1$. Dotted portions indicate the disallowed part from SI direct detection cross-section limit.

In the present dark matter model, we found that the regions that satisfy dark matter relic density has spin dependent cross-section $\sim 10^{-42} - 10^{-44}$ cm^2 which is well below the present limit obtained from spin dependent bounds (for the specific mass range of dark matter we are interested in) from direct search experiments [452]. Therefore, it turns out that the spin independent scattering of dark matter candidate is mostly applicable in restricting the parameter space of the present model.

In Fig. 6.7, we depict the effect of scalar mixing in dark matter phenomenology keeping parameters c and λ both fixed at 0.1 along with the same values of m_ψ and m_{H_2} used in Fig. 6.6. The vev v_ϕ is varied within the range 500 GeV $\leq v_\phi \leq 10$ TeV. Similar to Fig. 6.6 (there with λ), here also we notice a scaling with respect to different values of $\sin\theta$ as the dark matter annihilations depend upon it and there exist two resonances. However beyond $m_{\chi_1} \sim 250$ GeV,

dependence on $\sin\theta$ mostly disappears as seen from the Fig. 6.7 as we observe all three lines merge into a single one. Note that this is also the region where co-annihilations start to become effective as explained in the context of Fig. 6.6. It turns out that due to the presence of axial type of coupling in the Lagrangian (see Eq.(6.22)), the co-annihilation processes with final state particles including $W^{\pm}$ and Z bosons are most significant and they are independent of the scalar mixing θ. It therefore explains the behavior of the red (with $\sin\theta = 0.01$), green (with $\sin\theta = 0.1$) and blue (with $\sin\theta = 0.2$) lines in Fig. 6.7.

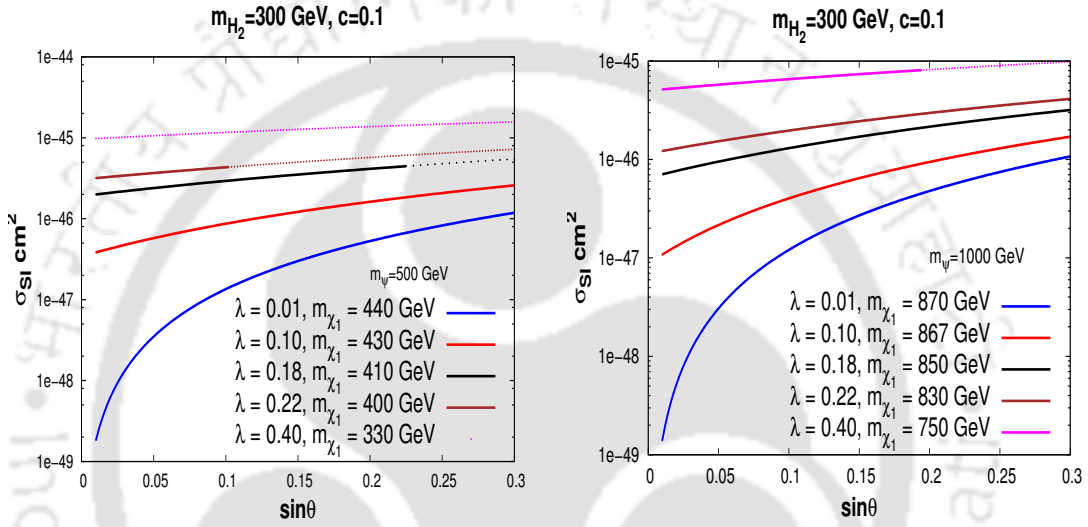

FIGURE 6.8: Effects of scalar mixing angle for different values of $\lambda \sim 0.01$ (blue), 0.1 (red), 0.18 (black), 0.22 (brown), 0.4 (pink) on dark matter spin independent direct detection cross-section for [left panel:] $m_\psi = 500$ GeV and [right panel:] $m_\psi = 1000$ GeV. Values of other parameters have been fixed at $m_{H_2} = 300$ GeV and $c = 0.1$. Dotted portions indicate the disallowed part from SI direct detection cross-section limit.

From Fig. 6.7, it is observed that scalar mixing has not much role to play in the co-annihilation region. However the scalar mixing has significant effect in the direct detection (DD) of dark matter. To investigate the impact of $\sin\theta$ on DD cross-section of DM, we choose few benchmark points (set of λ, m_{χ_1} values) in our model that satisfy DM relic density excluding the resonance regions ($m_{\chi_1} \simeq m_{H_1}/2$ resonance regime is highly constrained from invisible Higgs decay limits from LHC). Here we vary scalar mixing from 0.01 to 0.3.

In Fig. 6.8, we show the variation of spin independent dark matter direct detection cross-section (σ_{SI}) against $\sin\theta$ for those chosen benchmark values of dark matter mass. Keeping parameters c and m_{H_2} fixed at values 0.1 and 300 GeV respectively, m_ψ is considered at 500 GeV for the left panel and at 1000 GeV for the right panel of Fig. 6.8. Among these five

benchmark sets, four of them (except $\lambda = 0.18$, $m_{\chi_1} = 410$ GeV) were already present in the of Fig. 6.6 (corresponding to $\sin\theta = 0.1$). Five lines (blue, red, black, brown and pink colored ones corresponding to different sets of values of λ and m_{χ_1}) describe the DD cross-section dependence with $\sin\theta$. It is interesting to observe that with higher λ, there exists an increasing dotted portion on the curves (*e.g.* in brown colored line for $m_\psi = 500$ GeV, it starts from $\sin\theta > 0.1$, which stands for the non-satisfaction of the parameter space by the DD limits. This behaviour can be understood in the following way. From Eq.(6.38), it is clear that the first term dominates and hence an increase of SI DD cross-section with respect to larger $\sin\theta$ value (keeping other parameters fixed) is expected as also evident in the figures. We do not include the spin dependent cross-section here; however checked that it remains well within the observed limits.

In Fig. 6.9, we plot the dark matter relic density against dark matter mass for different values of c keeping other parameters fixed and using the same range of v_ϕ (500 GeV - 10 TeV) as considered in earlier plots. The top (bottom) left panel of Fig. 6.9 corresponds to $m_\psi = 500$ GeV and top (bottom) right panel are plotted for $m_\psi = 1000$ GeV. Curves with higher value of c start with larger initial value of dark matter mass. This can be understood easily from mass matrix $\mathcal{M}$ of Eq.(6.4), as large

m_ψ with small v_ϕ and λ, dark matter mass $\sim cv_\phi$. Hence as c increases, the DM mass starts from a higher value. The upper panel of figures is for $\lambda = 0.1$ and the lower panel stands for $\lambda = 0.25$.

We observe from Fig. 6.9 that enhancing c reduces DM relic density particularly for the region where DM annihilation processes are important. At some stage co-annihilation, in particular, processes with final states including the SM gauge fields takes over which is mostly insensitive to c. Hence all different curves join together. This is in line with observation in Fig. 6.7 as well. Here also

we notice that all the curves have fall around 212 GeV and 300 GeV where DM DM $\rightarrow H_1, H_2$ and DM DM $\rightarrow H_2, H_2$ channels open up respectively. We observe that with a higher value of c, for example with $c = 0.5$ in Fig. 6.9 (top left panel), the $DMDM \rightarrow H_2H_2$ annihilation becomes too large and also disallowed by the DD bounds as indicated by dotted lines. We therefore infer that the satisfaction of the DD bounds and the DM relic density prefer a lower value of c which is also consistent with the perturbativity point of view. Increasing the Yukawa coupling λ will change the above scenario, as depicted in lower panel of Fig. 6.9. We found that such effect is prominent for smaller values of m_ψ while compared top and bottom left panels of Fig. 6.9.

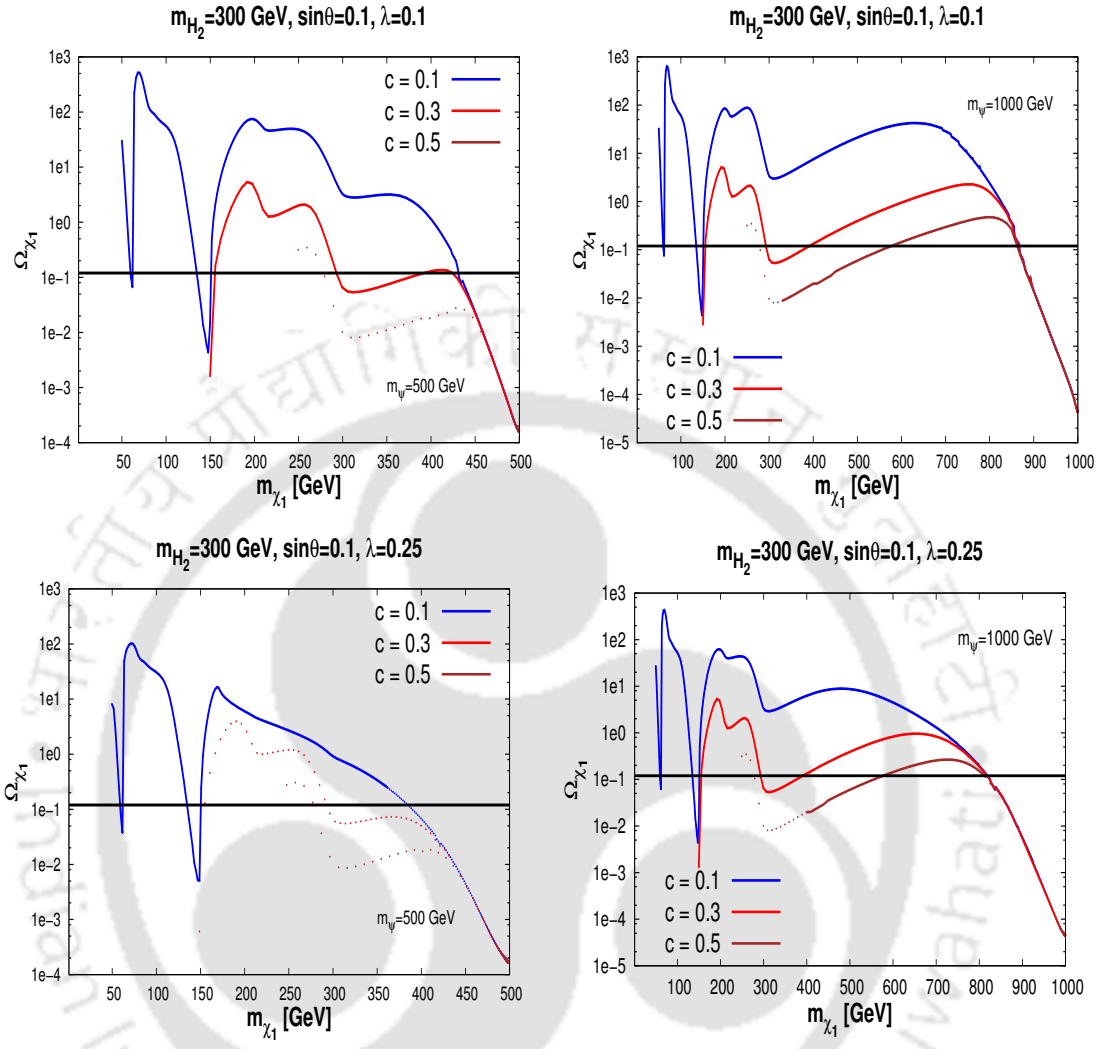

FIGURE 6.9: Dark matter relic density as a function of DM mass with different choices of $c \sim 0.1$ (blue), 0.3 (red), 0.5 (brown) for [top left:] $m_\psi = 500$ GeV, $\lambda = 0.1$, [top right:] $m_\psi = 1000$ GeV, $\lambda = 0.1$, [bottom left:] $m_\psi = 500$ GeV, $\lambda = 0.0.25$ and [bottom right:] $m_\psi = 1000$ GeV, $\lambda = 0.25$. Values of other parameters have been kept fixed at $m_{H_2} = 300$ GeV and $\sin\theta = 0.3$. Dotted portions indicate the disallowed part from SI direct detection cross-section limit.

So far, in Figs. 6.6-6.9, we have presented the variations of DM relic density with DM mass keeping the mass of heavy scalar H_2 fixed. In Fig. 6.10 (left panel), we show the variation of DM relic density against m_{χ_1} for three different values of $m_{H_2} = 300, 500, 1000$ GeV with fixed values of c, λ, $\sin\theta$ (all set to the value 0.1) with $m_\psi = 500$ GeV. The vev v_ϕ is varied from 1 TeV to 10 TeV. From Fig. 6.10 (left panel), we note that each plot for a specific m_{H_2} follow the same pattern as in previous figures. Here we notice that with different m_{H_2}, the heavy Higgs resonance place ($m_{\chi_1} \sim m_{H_2}/2$)

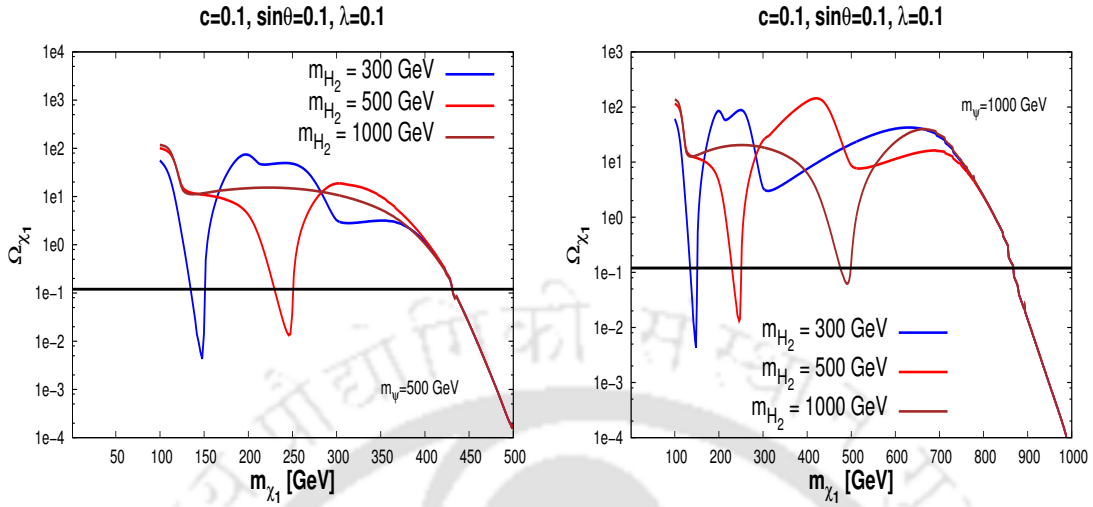

FIGURE 6.10: Relic density of dark matter as a function of DM mass for different values of $m_{H_2} = 300$ GeV (blue), 500 GeV (red) and 1000 GeV (brown) with [left panel:] $m_\psi = 500$ GeV and [right panel:] $m_\psi = 1000$ GeV. The other parameters c, λ and $\sin\theta$ are kept fixed at 0.1.

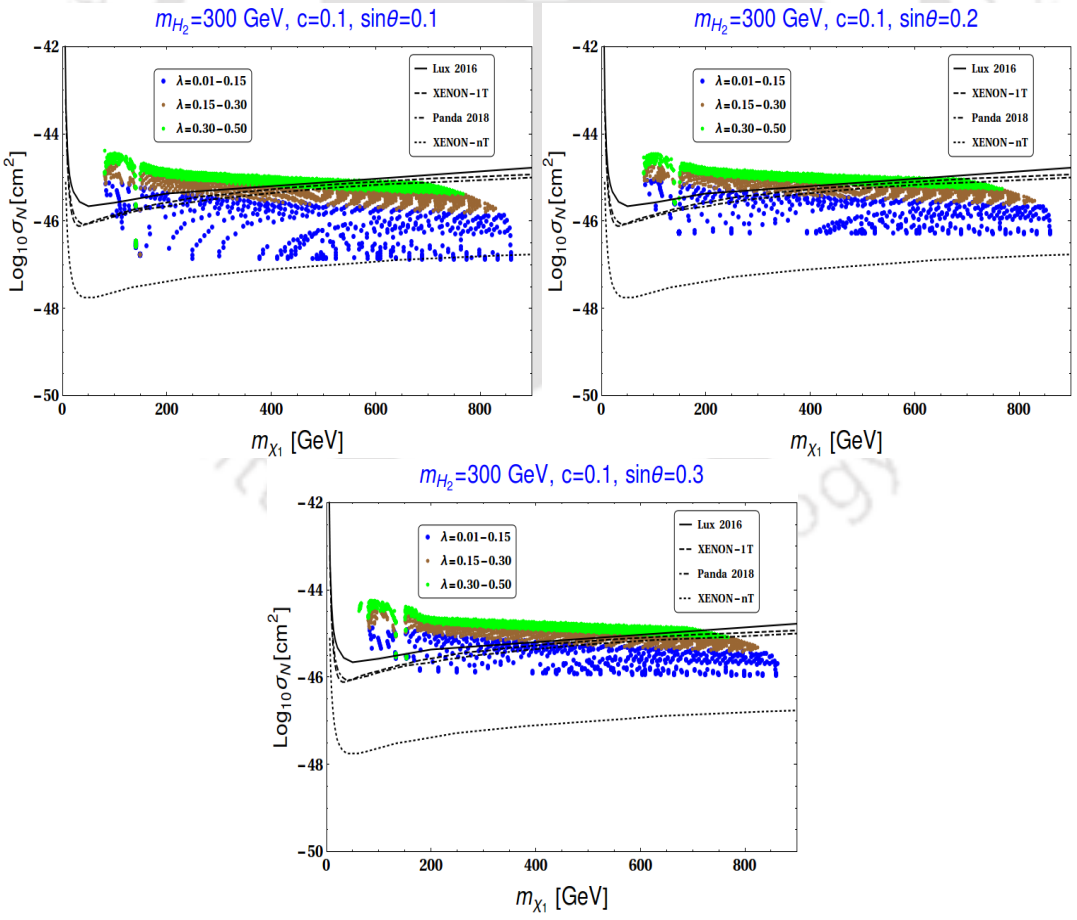

FIGURE 6.11: SI direct detection cross-section is plotted against DM mass for relic density satisfied points for [top left:] $\sin\theta = 0.1$, [top right:] $\sin\theta = 0.2$ and [bottom:] $\sin\theta = 0.3$. The other parameters $c = 0.1$ and $m_{H_2} = 300$ GeV have been kept fixed. Bounds from LUX 2016, XENON 1T, PANDA 2018, XENON-nT are also included in the plot.

is only affected. For large m_{H_2} (say for 1000 GeV), the resonance point disappears as it falls within the co-annihilation dominated region. A similar plot using the same set of parameters and value of m_{H_2} but with $m_\psi = 1000$ GeV in Fig. 6.10 (right panel) clearly shows this. In this case, we have a prominent resonance region for $m_{H_2} = 1000$ GeV as the co-annihilation takes place at a higher value of dark matter mass with the increase in m_ψ. It is to be mentioned once again that in all the above plots (Figs. 6.6-6.10), solid regions indicate the satisfied region and dotted region indicates the disallowed region for DM mass by spin independent direct detection cross-section bounds.

6.4.3.2 Constraining $\lambda - \sin\theta$ from a combined scan of parameters

A more general result for the present dark matter model can be obtained by varying the mass of charged fermion m_ψ, vev v_ϕ of the heavy singlet scalar field and the Yukawa coupling λ. We use the LEP bound on chargino mass to set the lower limit on the mass of charged fermion $m_\psi \gtrsim 100$ GeV [460]. Using this limit on charged fermion mass, we scan the parameter space of the model with the following set of parameters

$$100 \text{ GeV} \lesssim m_\psi \lesssim 1000 \text{ GeV};\ 500 \text{ GeV} \lesssim v_\phi \lesssim 10 \text{ TeV};\ 0.01 \lesssim \lambda \lesssim 0.5;$$
$$\sin\theta = 0.1, 0.2, 0.3;\ c = 0.1;\ \ m_{H_2} = 300 \text{ GeV}. \qquad (6.41)$$

In Fig. 6.11 (top left panel) we plot the values of DM mass against dark matter spin independent cross-section for the above mentioned ranges of parameters with $\sin\theta = 0.1$ which already satisfy DM relic abundance obtained from Planck [39]. Different ranges of the Yukawa coupling λ are shown in blue (0.01-0.15), brown (0.15-0.30) and green (0.30-0.50) shaded regions.

The bounds on DM mass and SI direct detection scattering cross-section from LUX [185], XENON-1T [183], Panda 2018 [186] and XENON-nT [379] are also shown for comparison. The spin dependent scattering cross-section for the allowed parameter space is found to be in agreement with the present limits from Panda 2018 [186] and does not provide any new constraint on the present phenomenology. From Fig. 6.11 (top left panel) it can also be observed that increasing λ reduces the region allowed by the most stringent Panda 2018 limit. This is due to the fact that an increase in λ enhances the dark matter direct detection cross-section as we have clearly seen from previous plots (see Fig. 6.6). Here we observe that with the specified set of parameters, dark matter with mass above 100 GeV is consistent with DD limits with $\lambda = 0.01 - 0.15$ (see the blue shaded region). For the brown region, we conclude that with $\lambda = 0.15 - 0.30$, DM mass above 400 GeV is allowed and with high $\lambda = 0.30 - 0.50$, DM with

mass 600 GeV or more is only allowed. We also note that a large region of the allowed parameter space is ruled out when XENON-nT [379] direct detection limit is taken into account.

Similar plots for the same range of parameters given in Eq.(6.41) for $\sin\theta = 0.2$ and 0.3 are shown in top right panel and bottom panel of Fig. 6.11 respectively. These plots depict the same nature as observed in top left panel of Fig. 6.11. In all these plots, the low mass region ($m_{\chi_1} \lesssim 62.5$ GeV) is excluded due to invisible decay bounds on Higgs and Z. It can be observed comparing all three plots in Fig. 6.11, that the allowed region of DM satisfying relic density and DD limits by Panda 2018 becomes shortened with the increase $\sin\theta$. In other words, it prefers a larger value of DM mass with the increase of $\sin\theta$. This is also expected as the increase of $\sin\theta$ is associated with larger DD cross-section (due to H_1, H_2 mediated diagram). Hence overall we conclude from this DM phenomenology that increase of both λ and $\sin\theta$ push the allowed value of DM mass toward a high value. In terms of vacuum stability, these two parameters, the Yukawa coupling λ and the scalar mixing $\sin\theta$, affect the Higgs vacuum stability differently. The Yukawa coupling destabilizes the Higgs vacuum while the scalar mixing $\sin\theta$ makes the vacuum more stable. Detailed discussion on the Higgs vacuum stability is presented in the next section.

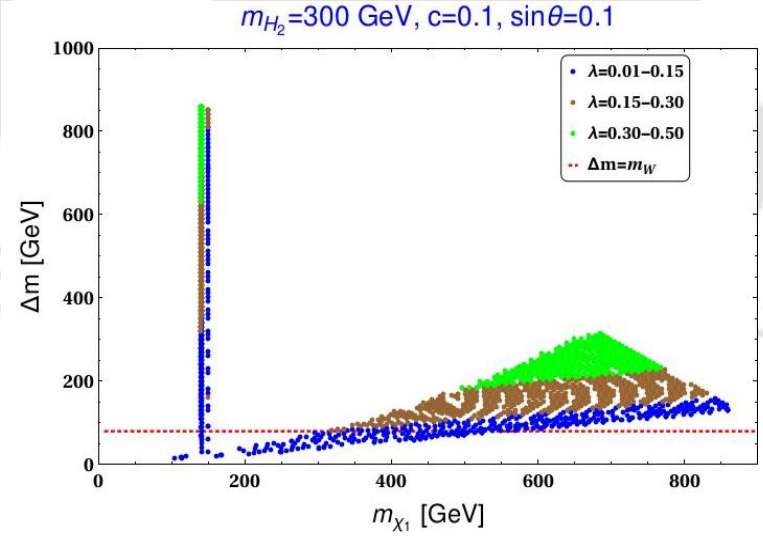

FIGURE 6.12: Mass difference between DM and the charged fermion Δm is plotted against m_{χ_1} for different sets of $\lambda \sim 0.01$-0.15 (blue), 0.15-0.30 (brown) and 0.30-0.50 (green) with $\sin\theta = 0.1$. All points satisfy the relic density direct detection cross-section bound from PANDA 2018. The other parameters are kept fixed at $c = 0.1$ and $m_{H_2} = 300$ GeV. The red line indicates the W boson mass (m_W).

A general feature of the singlet doublet model is the existence of two other neutral fermions, $\chi_{2,3}$ and a charged fermion, ψ^+. All these participate in the co-annihilation process which

contributes to the relic density of the dark matter candidate, χ_1. The charged fermion ψ^+ can decay into W^+ and χ_1, when the mass splitting $\Delta m = m_\psi - m_{\chi_1}$ is larger than W^+ mass. However, for mass splitting Δm between χ_1 and ψ^+ smaller than the mass of gauge boson W^+, the three body decay of charged fermion, ψ^+ into χ_1 associated with lepton and neutrino becomes plausible. This three body decay must occur before χ_1 freezes out, otherwise it would contribute to the relic. Therefore, the decay lifetime of ψ^+ should be smaller compared to the freeze out time of χ_1. The freeze out of the dark matter candidate χ_1 takes place at temperature $T_f = m_{\chi_1}/20$. Therefore, the corresponding freeze out time can be expressed as

$$t = 1.508 g_\star^{-\frac{1}{2}} M_P / T_f^2 \ , \tag{6.42}$$

where M_P is the reduced Planck mass $M_P = 2.435 \times 10^{18}$ GeV and $g_\star$ is effective number of degrees of freedom. The decay lifetime of the charged fermion ψ^+ is given as $\tau_{\psi^+} = \frac{1}{\Gamma_{\psi^+}}$, where Γ_{ψ^+} is the decay width for the decay $\psi^+ \to \chi_1 l^+ \bar{\nu}_l$, is of the form

$$\begin{aligned}\Gamma_{\psi^+} = \frac{G_F^2}{12\pi^3} \big[& (V_{31}^2 + V_{21}^2)\{-2 m_\psi m_{\chi_1}^2 I_1 + 3(m_\psi^2 + m_{\chi_1}^2) I_2 - 4 m_\psi I_3\} \\ & + 12 V_{31} V_{21} \{ m_{\chi_1}(m_\psi^2 + m_{\chi_1}^2) I_1 - 2 m_\psi m_{\chi_1} I_2 \} \big] \ . \end{aligned} \tag{6.43}$$

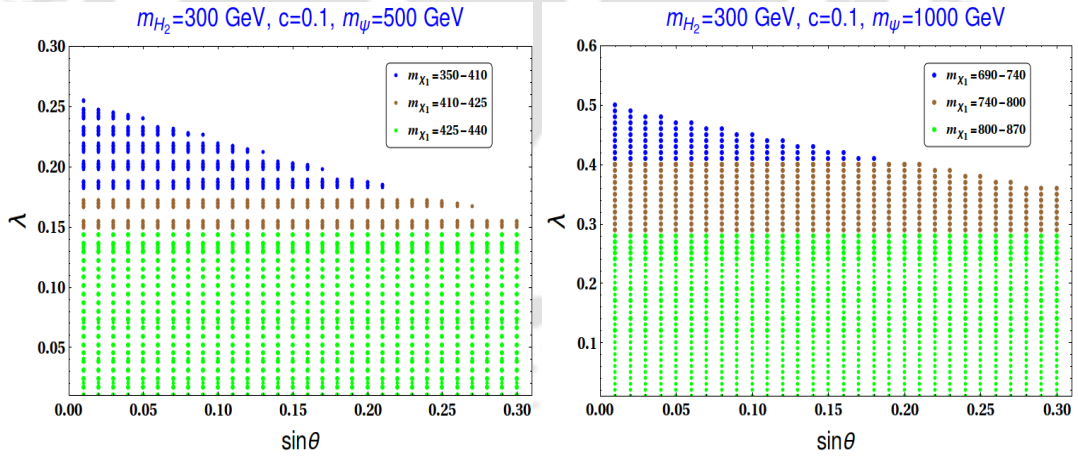

FIGURE 6.13: Correlation between λ and $\sin\theta$ for both relic and direct detection cross-section satisfied points with [left panel:] $m_\psi = 500$ GeV and [right panel:] $m_\psi = 1000$ GeV. The other parameters are kept fixed at $c = 0.1$, $m_{H_2} = 300$ GeV. Different ranges of m_{χ_1} (in GeV) are shown with color codes as mentioned in the inset.

In the above expression, G_F is the Fermi constant and the terms $I_{1,2,3}$ is expressed as

$$I_1 = \int \sqrt{x^2 - a^2}dx, \quad I_2 = \int x\sqrt{x^2 - a^2}dx, \quad I_3 = \int x^2\sqrt{x^2 - a^2}dx \tag{6.44}$$

where $x = E_{\chi_1}$ and $a = m_{\chi_1}$, E_{χ_1} being the total energy of χ_1.

In order to satisfy the condition that ψ^+ decays before the freeze out of χ_1, one must have $\tau_{\psi_+} \leq t$. The integrals $I_{1,2,3}$ in Eq.(6.44) are functions of mass splitting Δm and so is the total decay width Γ_{ψ^+}. To show the dependence on Δm, we present a correlation plot m_{χ_1} against Δm in Fig. 6.12. Fig. 6.12 is plotted for the case $\sin\theta = 0.1$ (consistent with Fig. 6.11 having the region allowed by the DD bound from Panda 2018). We use the same color code for λ as shown in Fig. 6.11. The horizontal red line indicates the the region where $\Delta m = m_W$. From Fig. 6.12 we observe that for smaller values of λ (0.01-0.15), $\Delta m < m_W$ is satisfied upto $m_{\chi_1} \sim 500$ GeV. The mass splitting increases for larger λ values. We find that for the chosen range of model parameters (Eq.(6.41)), the decay life time τ_{ψ^+} is several order of magnitudes smaller than the freeze out time of χ_1.

We end this section by estimating the value of T parameter in Table 6.2 for two sets of relic satisfied points (with $\lambda = 0.4$ and 0.18) as we mentioned before that among the S, T and U, only T would be relevant in this scenario. With further smaller λ, T parameter comes out to be

c	$m_\psi(GeV)$	v_ϕ (TeV)	m_{χ_1} (GeV)	λ	T$\times 10^{-4}$
0.1	1000	7.55	750	0.4	1
0.1	500	4.20	410	0.28	0.1

TABLE 6.2: Values of T-parameter induced by extra fermions in the set up for two sets of relic density satisfied points (see Fig. 6.8).

very small and hence it does not pose any stringent constraint on the relic satisfied parameter space. However with large $\lambda \sim 1$, the situation may alter.

In our scenario, we have also seen in Fig. 6.6 that for value of λ larger than 0.4, the direct detection cross-section of dark matter candidate also increases significantly and are thereby excluded by present limits on dark matter direct detection cross-section. To make this clear, here we present a plot, Fig. 6.13 (left panel), of relic density and DD satisfied points in the $\sin\theta - \lambda$ plane, where the other parameters are fixed at $c = 0.1, m_\psi = 500$ GeV, $m_{H_2} = 300$ GeV. As before, v_ϕ is varied between 500 GeV and 10 TeV. Similar plot with same set of c, m_{H_2} but with $m_\psi = 1000$ GeV is depicted in right panel of Fig. 6.13. Different ranges of dark matter masses are specified with different colors as mentioned in the caption of Fig. 6.13. From Fig. 6.13 we observe that allowed range of λ reduces with the increase of scalar mixing due to the DD

bounds. From Fig. 6.13 (left panel) we get a maximum allowed $\lambda \sim 0.25$ while the same for the $m_\psi = 1000$ GeV (right panel) turns out to be $\lambda = 0.5$. Furthermore as we will see the study of vacuum stability, discussed in Sec. 6.5, indicates that the Yukawa coupling λ should not be large in order to maintain the electroweak vacuum absolutely stable till Planck scale. Therefore, larger values of λ (close to 1) is not favoured in the present scenario.

6.5 EW vacuum stability

In the present work consisting of singlet doublet dark matter model with additional scalar, we have already analysed (in previous section) the parameter space of the set-up using the relic density and direct detection bounds. Here we extend the analysis by examining the Higgs vacuum stability within the framework. It is particularly interesting as the framework contains two important parameters, (i) coupling of dark sector fermions with the SM Higgs doublet (λ) and (ii) mixing (parametrized by angle θ) between the singlet scalar and the SM Higgs doublet. The presence of these two will modify the stability of the EW vacuum. First one makes the situation worse than in the SM by driving the Higgs quartic coupling λ_H negative earlier than $\Lambda_I^{\rm SM}$. The second one, if sufficiently large, can negate the effect of first and make the Higgs vacuum stable. Thus the stability of Higgs vacuum depends on the interplay between these two. Moreover, as we have seen, the scalar singlet also enriches the dark sector with several new interactions that significantly contribute to DM phenomenology satisfying the observed relic abundance and direct detection constraint. Also the scalar mixing angle is bounded by experimental constraints ($\sin\theta \lesssim 0.3$) as we have discussed in Sec. 6.3.

The proposed set up has two additional mass scales: the DM mass (m_{χ_1}) and heavy Higgs (m_{H_2}). Although the dark sector has four physical fermions (three neutral and one charged), we can safely ignore the mass differences between them when we consider our DM to fall outside the two resonance regions (Figs. 6.6-6.10). As we have seen in this region (see Fig. 6.12), co-annihilation becomes dominant, all the masses in the dark sector fermions are close enough ($\sim m_{\chi_1}$, see Figs. 6.6-6.10). Hence the renormalisation group (RG) equations will be modified accordingly from the SM ones with the relevant couplings entering at different mass scales. Here we combine the RG equations (for the relevant couplings only) [468] together in the following

(provided $\mu > m_\phi, m_{\chi_1}$),

$$\frac{dg_1}{dt} = \beta_{g_1}^{\rm SM} + \frac{1}{16\pi^2}\frac{2}{3}g_1^3, \tag{6.45}$$

$$\frac{dg_2}{dt} = \beta_{g_2}^{\rm SM} + \frac{1}{16\pi^2}\frac{2}{3}g_2^3, \tag{6.46}$$

$$\frac{d\lambda_H}{dt} = \beta_{\lambda_H}^{\rm SM} + \frac{1}{16\pi^2}\Big\{\frac{\lambda_{\phi H}^2}{2}\Big\} + \frac{1}{16\pi^2}\Big\{-2\lambda^4 + 4\lambda_H\lambda\Big\}, \tag{6.47}$$

$$\frac{dy_t}{dt} = \beta_{y_t}^{\rm SM} + \frac{1}{16\pi^2}\Big\{\lambda^2 y_t\Big\}, \tag{6.48}$$

$$\frac{d\lambda}{dt} = \frac{1}{16\pi^2}\Big\{\lambda(3y_t^2 - \frac{3}{4}g_1^2 - \frac{9}{4}g_2^2) + \frac{5}{2}\lambda^3\Big\}, \tag{6.49}$$

$$\frac{d\lambda_{\phi H}}{dt} = \frac{1}{16\pi^2}\Big\{12\lambda_H\lambda_{\phi H} + 6\lambda_\phi\lambda_{\phi H} + 4\lambda_{\phi H}^2 + 6y_t^2\lambda_{\phi H} - \frac{3}{2}g_1^2\lambda_{\phi H} - \frac{9}{2}g_2^2\lambda_{\phi H} + 2\lambda^2\lambda_{\phi H} + 2c^2\lambda_{\phi H}\Big\},$$

$$\frac{d\lambda_\phi}{dt} = \frac{1}{16\pi^2}\Big\{18\lambda_\phi^2 + 2\lambda_{\phi H}^2 - \frac{1}{2}c^4 + 4\lambda_\phi c^2\Big\}, \tag{6.50}$$

$$\frac{dc}{dt} = \frac{1}{16\pi^2}\Big\{6c^3\Big\}, \tag{6.51}$$

where $\beta^{\rm SM}$ is the SM β function (in three loop) of respective couplings [34, 225, 469, 470].

In this section our aim is to see whether we can achieve the SM Higgs vacuum stability till Planck mass (M_P). However we have two scalars (SM Higgs doublet and one gauge singlet ϕ) in the model. Therefore we should ensure the boundedness or stability of the entire scalar potential in any field direction. In that case the following matrix

$$\begin{pmatrix} \lambda_H & \frac{\lambda_{\phi H}}{2} \\ \frac{\lambda_{\phi H}}{2} & \lambda_\phi \end{pmatrix}, \tag{6.52}$$

has to be co-positive. The conditions of co-positivity [360, 361] of such a matrix is provided by

$$\lambda_H(\mu) > 0,\ \lambda_\phi(\mu) > 0,\ \text{and}\ \lambda_{\phi H}(\mu) + 2\sqrt{\lambda_H(\mu)\lambda_\phi(\mu)} > 0. \tag{6.53}$$

Violation of $\lambda_H > 0$ could lead to unbounded potential or existence of another deeper minimum along the Higgs direction. The second condition ($\lambda_\phi(\mu) > 0$) restricts the scalar potential from having any runway direction along ϕ. Finally, $\lambda_{\phi H}(\mu) + 2\sqrt{\lambda_H(\mu)\lambda_\phi(\mu)} > 0$ ensures the potential to be bounded from below or non-existence of another deeper minimum somewhere between ϕ or H direction.

On the other hand, if there exists another deeper minimum other than the EW one, the estimate of the tunneling probability P_T of the EW vacuum to the second minimum is essential. The Universe will be in metastable state only, provided the decay time of the EW vacuum is

longer than the age of the Universe. The tunneling probability is given by [30, 34],

$$P_T = T_U^4 \mu_B^4 e^{-\frac{8\pi^2}{3|\lambda_H(\mu_B)|}}. \tag{6.54}$$

where T_U is the age of the Universe, μ_B is the scale at which probability is maximized, determined from $\beta_{\lambda_H} = 0$. Hence metastable Universe requires [30, 34]

$$\lambda_H(\mu_B) \; > \; \frac{-0.065}{1 - \ln\left(\frac{v}{\mu_B}\right)}. \tag{6.55}$$

As noted in [34], for $\mu_B > M_P$, one can safely consider $\lambda_H(\mu_B) = \lambda_H(M_P)$.

The RG improved effective Higgs potential (at high energies $H_0 >> v$) can be written as [35, 219]

$$V_H^{\rm eff} = \frac{\lambda_H^{\rm eff}(\mu)}{4} H_0^4, \tag{6.56}$$

with $\lambda_H^{\rm eff}(\mu) = \lambda_H^{\rm SM,\ eff}(\mu) + \lambda_H^{\phi,{\rm eff}}(\mu) + \lambda_H^{(\psi_{D_1},\psi_S,){\rm eff}}(\mu)$ where $\lambda_H^{\rm SM,\ eff}$ is the Standard Model contribution to λ_H. The other two contributions $\lambda_H^{\phi,{\rm eff}}$ and $\lambda^{(\psi_{D_1},\chi),{\rm eff}}$ are due to the newly added fields in the present model as provided below.

$$\lambda_H^{\phi,{\rm eff}}(\mu) = e^{4\Gamma(H_0=\mu)}\Big[\frac{\lambda_{\phi H}^2}{64\pi^2}\Big(\ln\frac{\lambda_{\phi H}}{2} - \frac{3}{2}\Big)\Big], \tag{6.57}$$

$$\lambda_H^{(\psi_{D_1},\chi),{\rm eff}}(\mu) = e^{4\Gamma(H_0=\mu)}\Big[\frac{\lambda^4}{16\pi^2}\Big(\ln\frac{\lambda}{2} - \frac{3}{2}\Big)\Big]. \tag{6.58}$$

Here $\Gamma(H_0) = \int_{m_t}^{H_0} \gamma(\mu) d\ln\mu$, $\gamma(\mu)$ is the anomalous dimension of the Higgs field [34].

In the SM, the top quark Yukawa coupling (y_t) drives the Higgs quartic coupling to negative values. In our set up, the coupling λ has very similar effect on λ_H in Eq.(6.47). So combination of both y_t and λ make the situation worse (by driving Higgs vacuum more towards instability) than in the SM. However due to the presence of extra singlet scalar, λ_H gets a positive threshold shift (second term in Eq.(6.19) at energy scale m_{H_2}. Also the RG equation of λ_H is aided by a positive contribution from the interaction of the SM Higgs with the extra scalar ($\lambda_{\phi H}$). Here we study whether these two together can negate the combined effect of y_t and λ leading to $\lambda_H^{\rm eff} > 0$ for all energy scale running from m_t to M_P. Note that the threshold shift (second term in Eq.(6.19)) in λ_H is function of m_{H_2} and $\sin\theta$. On the other hand, other new couplings relevant for study of EW vacuum stability are λ_ϕ and $\lambda_{\phi H}$ which can be evaluated from the values of m_{H_2}, v_ϕ and $\sin\theta$ through Eq.(6.20) and Eq.(6.21). Hence once we fix m_{H_2} and use the SM values of Higgs and top mass, the stability analysis effectively depends on λ, $\sin\theta$ and v_ϕ. We

run the three loop RG equations for all the SM couplings and one loop RG equations for the other relevant couplings in the model from $\mu = m_t$ to M_P. We use the boundary conditions of the SM couplings as provided in Table 6.3. The boundary values have been evaluated in [34] by taking various threshold corrections at m_t and mismatch between top pole mass and $M\bar{S}$ renormalised couplings into account.

Scale	y_t	g_1	g_2	g_3	λ_H
$\mu = m_t$	0.93610	0.357606	0.648216	1.16655	0.125932

TABLE 6.3: Values of the relevant SM couplings (top-quark Yukawa y_t, gauge couplings g_i and λ_H) at energy scale $\mu = m_t = 173.2$ GeV with m_h (m_{H_1}) = 125.09 GeV and $\alpha_S(m_Z) = 0.1184$.

6.6 Phenomenological implications from DM analysis and EW vacuum stability

We have already found the correlation between λ and $\sin\theta$ to satisfy the relic abundance and spin independent DD cross-section limits on DM mass as displayed in Fig. 6.13. It clearly shows that for comparatively larger value of λ, upper limit on $\sin\theta$ from DD cross-section is more restrictive. On the other hand, a relatively large value of λ affects the EW vacuum stability adversely. In this regard, a judicious choice of reference points from Fig. 6.13 is made in fixing benchmark points (BP-I of Table 6.4, corresponding to left panel of Fig. 6.13 and BP-II of Table 6.4 corresponding to right panel of Fig. 6.13). BP-I and BP-II involve moderate values of λ for which DD-limits starts constraining $\sin\theta$ (more than the existing constraints as per Sec. 3) and λ_H gets significant running. These points would then indeed test the viability of the model. Note that the benchmark points (BP-I and II) are also present in Fig. 6.13 in which restrictions on $\sin\theta$ from DD limits are explicitly shown.

Benchmark points	m_{χ_1} (GeV)	m_ψ (GeV)	m_{H_2} (GeV)	c	v_ϕ (TeV)	λ
BP-I	410	500	300	0.1	4.2	0.18
BP-II	750	1000	300	0.1	7.55	0.4

TABLE 6.4: Initial values of the relevant mass scales (DM mass m_{χ_1} and heavy Higgs mass m_{H_2}), v_ϕ and the couplings (c and λ) of the dark sector used to study the Higgs vacuum stability.

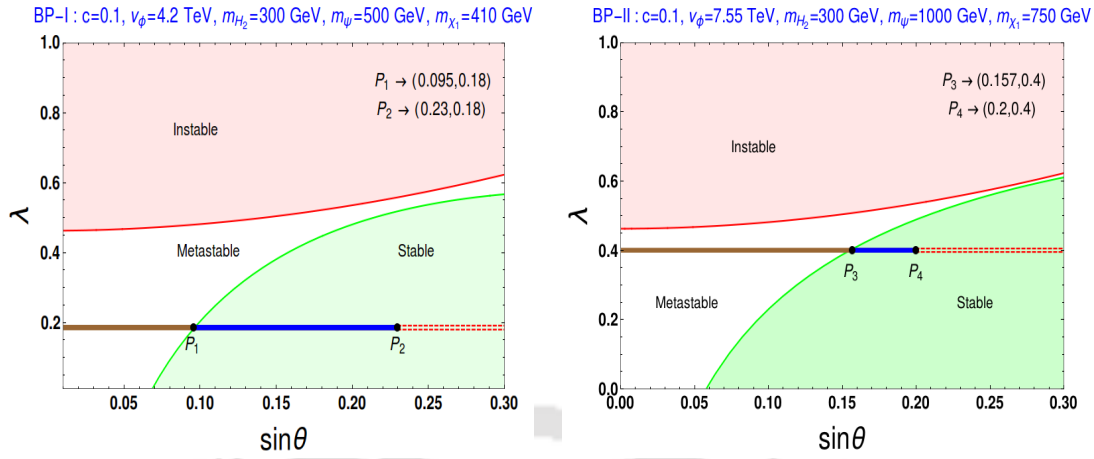

FIGURE 6.14: Vacuum stability (green), metastable (white) and instability (pink) region in $\sin\theta - \lambda$ plane for BP-I [left panel] and BP-II [right panel]. The horizontal lines describe correct relic density contours for BP-I and BP-II. The red dashed portion of these horizontal lines represent the disallowed regions from direct detection limit. The blue section of each relic contour satisfies both vacuum stability criteria as well as the direct detection bound while the brown portion is excluded by vacuum stability condition only. The points P_1 and P_2 in left panel and P_3 and P_4 from right panel will be used to show the evolution of λ_H as a function of energy scale μ in Fig. 6.15.

In Fig.6.14, we constrain the $\sin\theta - \lambda$ parameter space using the absolute stability criteria ($\lambda_H^{\rm eff}(\mu) > 0$ for $\mu = m_t$ to M_P) for the EW vacuum for BP-I and BP-II as values of parameters given in Table 6.4. The solid green line in Fig. 6.14 indicates the boundary line in $\sin\theta - \lambda$ plane beyond which the stability criteria of the SM Higgs vacuum violates. Hence all points in the green shaded region satisfies the absolute stability of the EW vacuum. Similarly the solid red line indicates the boundary of the metastable-instable region as obtained through Eq.(6.55). The pink shaded region therefore indicates instability of the EW vacuum with $m_t = 173.2$ GeV and $m_h = 125.09$ GeV. Here we use the upper limit on the scalar mixing as 0.3 so as to be consistent with experimental limits on it. The DD cross-section corresponding to these particular dark matter masses (410 GeV and 750 GeV) with specific choices of λ ($\lambda = 0.18$ in left plot while $\lambda = 0.4$ in right plot in Fig. 6.14) against $\sin\theta$ along with the same values of other parameters $(c, v_\phi, m_\psi, m_{H_2})$ are already provided in Fig. 6.8 (also in Fig. 6.13). Using Fig. 6.8, we identify here the relic density satisfied contour (horizontal solid line) in the $\sin\theta - \lambda$ plane on Fig.6.14. We note that DD sets an upper bound on $\sin\theta$, due to which the excluded region of $\sin\theta$ is marked in red within the horizontal line(s) in both the figures. The brown portion of the $\lambda = 0.18(0.4)$ line corresponds to the relic and DD allowed range of $\sin\theta$ in left(right) plot; however this falls in a region where EW vacuum is metastable. In Fig. 6.14 (left panel), the blue portion of the constant λ line indicates that with this restricted region of $\sin\theta$, we have a dark matter of mass 410 GeV which satisfy the relic density and DD bounds and on the other

hand, the EW vacuum remains absolutely stable all the way till M_P.

The outcome of this combined analysis of relic and DD satisfied value of a DM mass and stability of the EW vacuum in presence of two new scales, DM mass and heavy Higgs, seems to be interesting. It can significantly restrict the scalar mixing angle. For example with $m_{\chi_1} = 410$ GeV in Fig. 6.8 (left panel) and $m_{H_2} = 300$ GeV, we find $\lambda = 0.18$ restricts $\sin\theta \lesssim 0.23$ which is more stringent than the existing experimental one. This set of $(\sin\theta, \lambda)$ values is denoted by P_2 in left panel of

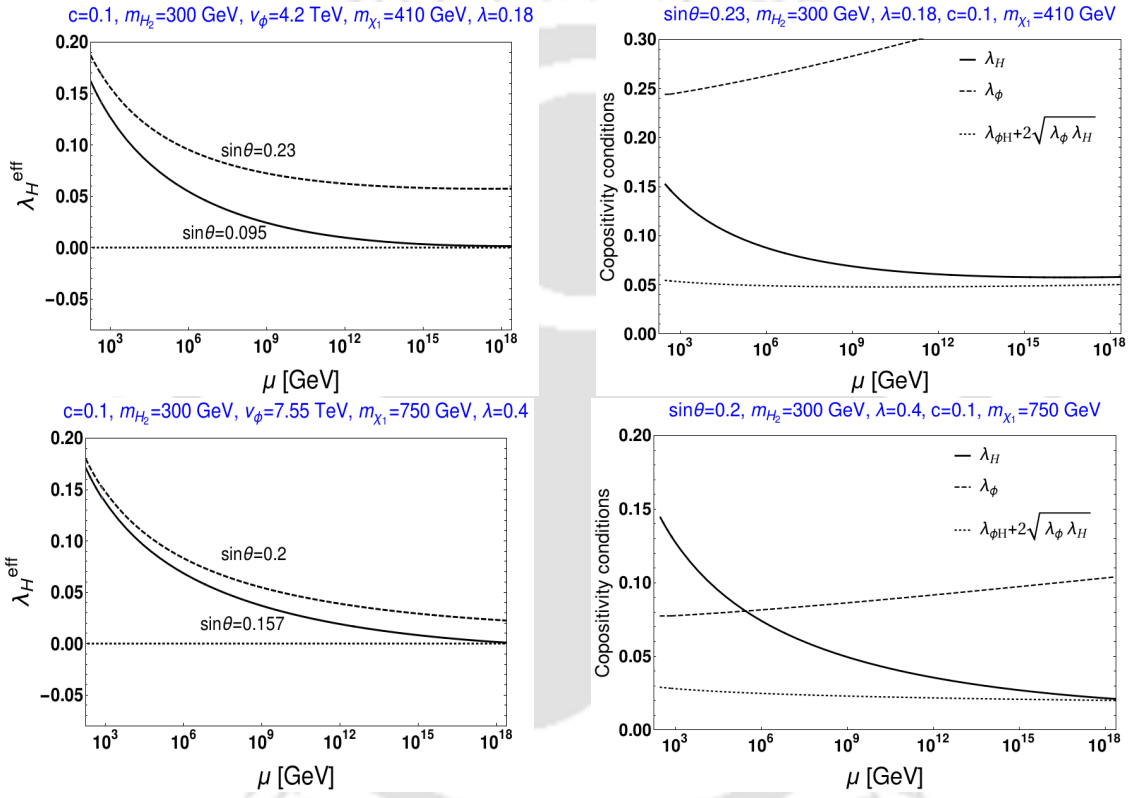

FIGURE 6.15: Evolution of $\lambda_H^{\rm eff}$ from $\mu = m_t$ to M_P for P_1, P_2 [top left] and P_3, P_4 [bottom left] points of Fig.6.14. In right panels, copositivity criterias are shown as a function of μ for P_2 [top] and P_4 [bottom] points.

Fig. 6.13. On top of this, if the EW vacuum needs to be absolutely stable, we note that we can obtain a lower limit on $\sin\theta$ as 0.095. The corresponding set of $(\sin\theta, \lambda)$ values is denoted by P_1 which follows from the intersection of relic density contour ($\lambda = 0.18$ line) with boundary line of the absolute stability region (solid green line). Combining these we obtain: $0.095 \lesssim \sin\theta \lesssim 0.23$. A similar criteria with $m_{\chi_1} = 750$ GeV restricts $\sin\theta$ to be within 0.157 (point P_3) $\lesssim \sin\theta \lesssim 0.2$ (point P_4). Therefore, from this analysis we are able to draw

both upper and lower limits on $\sin\theta$ for the two benchmark points. This turns out to be the most interesting and key feature of the proposed model. The vacuum stability analysis can be extended for any other points in Fig. 6.13. However if we go for higher value of λ, the simultaneous satisfied region of DM relic abundance, DD cross-section bound and stability of EW vacuum will be reduced as seen while comparing the left with right panel of Fig. 6.14.

Finally one may wonder about the nature of evolution of $\lambda_H^{\rm eff}$ and the co-positivity conditions for any points within EW vacuum stability satisfied region of Fig. 6.14. Hence, in Fig.6.15, running of $\lambda_H^{\rm eff}$ is shown against the energy scale μ for P_1 and P_2 (in top left panel of Fig. 6.15); P_3 and P_4 (in bottom left panel of Fig. 6.15). Note that these two points also satisfy the relic density and DD cross-section bounds. We find for $\sin\theta = 0.2$, $\lambda_H^{\rm eff}$ remains positive starting from $\mu = m_t$ to M_P energy scale and for $\sin\theta = 0.157$, although $\lambda_H^{\rm eff}$ stays positive throughout its evolution, it marginally reaches zero at M_P. Hence this point appears as the boundary point in $\sin\theta - \lambda$ plane of Fig. 6.14 (right panel) beyond which the SM Higgs vacuum becomes unstable. In top and bottom right panel of Fig. 6.15, we show the evolution of all the co-positivity conditions from $\mu = m_t$ to M_P corresponding to P_2 and P_4 points respectively.

6.7 Chapter Summary

We have explored a dark matter model by extending the Standard Model of particle physics with a singlet scalar and a dark sector comprised of two Weyl doublets and a Weyl singlet fermions. The scalar singlet acquires a vev and contributes to the mass the dark sector particles consisting of three neutral Majorana fermions and one charged Dirac fermion. The lightest Majorana particle is stable due to the presence of a residual Z_2 symmetry and hence we study whether this can account for the dark matter relic density and also satisfy the direct detection bounds. There exists a mixing of the singlet scalar with the SM Higgs doublet in the model which results in two physical scalars, which in turn affect the DM phenomenology. We have found that apart from the region of two resonances, there exists a large available region of parameter space satisfying various theoretical and experimental bounds particularly due to large co-annihilations effects present. On the other hand, inclusion of new fermions in the model affects the Higgs vacuum stability adversely by leading it more toward instability at high scale due to new Yukawa like coupling. This issue however can be resolved by the involvement of extra scalar singlet. We find that with the demand of having a dark matter mass $\sim$ few hundred GeV to 1 TeV consistent with appropriate relic density and DD limits and simultaneously to make the EW vacuum absolutely stable upto the Planck scale, we can restrict the scalar mixing angle significantly. The result is carrying a strong correlation with the dark sector Yukawa

coupling, λ. It turns out that, with higher dark matter mass, the allowed range of $\sin\theta$ becomes more stringent from this point of view. Hence future limits of $\sin\theta$ will have the potential to allow or rule out the model under consideration.

Chapter 7

Summary and Conclusions

Despite the impressive success of both the SM of particle physics and Big Bang Cosmology, there exist plenty of long standing unresolved theoretical and observational puzzles. In brief, the SM of particle physics fails to explain non-zero mass of neutrino, dark matter hypothesis, naturalness issue, matter-antimatter asymmetry of the Universe *etc.* Furthermore, stability of the EW vacuum is not assured within the SM framework. On the other hand, horizontal and flatness problems have no satisfactory explanation in Big bang cosmology. Although, the "inflation" hypothesis during very early phase of the Universe could cure the flatness and homogeneous problem, the SM of particle physics does not accommodate any potential candidate for inflation. Therefore it seems that the extension of the SM with new sets of field is inevitable. In this regard, we argue whether inclusion of additional scalars in the extended framework could be useful in alleviating some the above mentioned puzzles associated with the SM and Big bang cosmology. Motivated by this, in the current thesis, we investigate the role of "*additional scalar fields*" in an effort to circumvent some of the unsolved mysteries of the Universe. Additionally, we have also attempted to develop some correlations between two or more such issues in a unified manner. Below we briefly state the brief summary of the respective chapters.

In Chapter 1, we provide brief introductions of the SM of particle physics and Big bang cosmology. We have also mentioned the problems associated with these standard theories in detail. Subsequently, we discuss the possibilities where additional scalar fields can play important roles in solving these issues individually. We point out that it would be interesting to investigate the importance of scalar fields while two or more problems are taken together. This serves the purpose of motivation part of the thesis works.

In Chapter 2, we consider the sneutrino chaotic inflation model where the role of inflaton field is played by the scalar partner of RH neutrino superfield. This kind of model does not produce consistent results (for n_s and r values) with Planck data. We therefore we couple the inflation sector with a SUSY breaking sector which is identified with a strongly gauged (in form of SQCD) sector having a UV complete theory. This interaction results in providing correct values of n_S and r allowed by Planck constraint. Simultaneously, we also realize supersymmetry breaking at the end of inflation. Some aspects of neutrino physics within the proposed set up are also discussed.

Then in Chapter 3, we study the fate of EW vacuum in presence of the standard chaotic inflation (SCI) having quadratic potential (non-supersymmetric). The inflation sector consists of a single scalar field having zero vev which play the role of inflaton. We then extend the set up with an additional SM gauge singlet scalar field with non zero vev. This scalar field interacts with both the inflaton and SM Higgs doublet. The interaction of the additional scalar field with the inflaton results in correcting the predictions of standard chaotic inflation to be consistent with Planck 2015 results which was otherwise ruled out. The same scalar field also makes the SM Higgs vacuum absolutely stable till M_P energy scale during and after inflation.

In next two chapters, we investigate the role of scalar field as a potential DM candidate. In this regard, in Chapter 4, we focus on the fact that low mass range of scalar DM ($m_{\rm DM} < 500$ GeV) is ruled out from experimental bounds. We also look at the EW vacuum stability issue in presence of both scalar DM and RH neutrinos in a Type-I seesaw framework. With an aim to revive the scalar DM of low mass and making EW vacuum absolutely stable, we extend the combined framework of SM+scalar DM+RH neutrinos by a SM gauge singlet scalar field. The additional gauge singlet scalar having non zero vacuum expectation value couples to both the DM and SM Higgs. The presence of the extra scalar has two fold impact: (i) it helps the scalar DM in evading the strong direct detection limit from XENON 1T and (ii) affects the evolution of Higgs quartic coupling in such a way that the SM electroweak vacuum becomes stable till M_P even after including the effect of large Yukawa coupling in the neutrino sector.

In Chapter 5, we investigate whether scalar DM in the Universe has any possible connection with the primordial inflation. We begin with an inflation model governed by a supersymmetric gauged theory (in form of a SQCD sector). The chosen inflationary model is well favored by the Planck experiment. In the set up, at the end of inflation, the associated global symmetry breaks down spontaneously and Nambu Goldstones result. We identify these Nambu Goldstone bosons as potential DM candidates. We discuss the DM phenomenology in detail in context of the present experimental bounds (XENON 1T and PANDA X) to have a consistent scenario.

In Chapter 6 of the thesis, we extend the minimal framework of SDDM model with a gauge singlet scalar field. The additional scalar singlet provides the mass to the Majorona singlet fermion. The primary motivation to include the gauge singlet scalar field is to achieve the absolute vacuum stability in presence of large Yukawa coupling of additional fermions with the SM Higgs doublet within the set up. In the construction after electroweak symmetry breaking, the lightest Majorona fermion serves the role of DM. Note that the scalar field also enriches the dark sector with several new interactions that significantly contribute to DM phenomenology. We find the relevant parameter space which satisfies both DM constraints and make the EW absolutely stable.

To sum up, we have explored few possible roles of scalar field in the Universe to address some of the important issues which requires knowledge beyond the SM of particle physics and Big bang cosmology. We have mainly concentrated on few specific topics: inflation, supersymmetry breaking, dark matter, Higgs vacuum stability and neutrino physics. We showed that an extra scalar could successfully revive the minimal set up of chaotic inflation model in both supersymmetric and non-supersymmetric framework provided it has non zero interaction with the inflaton. The fate of the proposed inflation models will be decided by the future predictions from Planck experiment. In addition, we also found that simple extension of scalar DM sector by another scalar field is sufficient to save the model in view of DM experimental bounds. Besides, we also establish that the same scalar field which corrects the chaotic inflation can guarantee the stability of EW vacuum in an inflatonary Universe. In a similar way absolute vacuum stability could also be realized in presence of DM (scalar or fermionic) and RH neutrinos. We have also discussed the possibility of having a common origin of inflation and scalar DM. Thus the thesis also offers some sorts of possible correlations between two or more issues in a single framework by utilizing the presence of additional scalar fields.

To conclude, our study in the thesis shows that indeed the extension of the SM of particle physics by scalar fields could be a powerful and well motivated possibility for being the guiding theory of the Universe. We end this chapter by pointing out some new directions one can work in continuation of the thesis. In the thesis we have discussed inflationary models within both supersymmetric and non-supersymmetric framework. It might be possible to study inflation and its dynamics in some of the well known scalar extended multi-Higgs models like 2HDM, IDM etc.. We have also offered possibility of having a common origin for scalar WIMP-type scalar DM and inflation. As the experimental constraints are getting stringent for WIMP, use of an alternative type of DM *i.e.* FIMP or SIMP could be interesting to explore the connection with the inflation. Moreover, we have studied Higgs vacuum stability in presence of singlet

component scalar DM. It might be exciting to extend the study in multi component (scalar-scalar, scalar-fermion) DM framework.

Appendix A

Appendix related to Chapter 2

A.1 Finding the root of σ.

Setting $\frac{\partial V_{\rm Inf}(\tilde{\chi},\tilde{\sigma})}{\partial\tilde{\sigma}} = 0$, we get a fifth order polynomial equation in $\tilde{\sigma}$ of the form,

$$\frac{\tilde{\sigma}^5}{2} + \tilde{\sigma}^3 + k_1\Big[1 - \frac{6(1-p)}{\tilde{\chi}^2} + \tilde{\sigma}^2\Big\{\frac{1}{4} - \frac{6(1-p)}{\tilde{\chi}^2}\Big\} - \frac{\tilde{\sigma}^4}{4}\Big] + k_2\tilde{\sigma} = 0, \tag{A.1}$$

where $k_1 = -\frac{2A}{\tilde{m}^2}\tilde{\chi}^{5-6p}$ and $k_2 = \frac{4}{\tilde{\chi}^2}\Big[1 + \tilde{\chi}^{10-12p}\frac{A^2}{2\tilde{m}^4}\Big\{9(1-p)^2 - \frac{\tilde{\chi}^2}{4}\Big\}\Big]$. Here we disregard the first and third terms from the coefficient of $\tilde{\sigma}^3$ in Eq.(2.35) as $\tilde{\chi}$ being greater than one during inflation, $\frac{\tilde{m}^2\tilde{\chi}^2}{4}$ is the dominant contribution. We now try to solve the Eq.(A.1) to express $\langle\tilde{\sigma}\rangle$ in terms of $\tilde{\chi}$. In doing so, note that $\tilde{\chi}$ being inflaton is super-Planckian while $\tilde{\sigma}$ remains sub-Planckian ($\tilde{\sigma} < 1$) during inflation. Also the parameters involved, $\tilde{\Lambda}$ and $\tilde{m}$, are considered to be much less than one (in M_P unit), $\tilde{\Lambda}$, $\tilde{m} << 1$ with $\tilde{\Lambda}\tilde{\chi} << 1$. We have also taken $\tilde{\Lambda} \geq \tilde{m}$. Since the added contribution via $W_{\rm Int}$ is expected to provide modification only on the minimal chaotic inflation, it is natural that m should be close to 10^{13} GeV (also $\tilde{\chi}$ is expected of order $\mathcal{O}(10)$). These consideration keeps k_1 to be less than one ($k_1 < 1$) although k_2 can be somewhat larger.

With $p = 4/7$, we find $\tilde{\sigma}^4$ can be neglected and the Eq.(A.1) then reduces to the form

$$\frac{\tilde{\sigma}^5}{2} + \Big(\tilde{\sigma}^3 + c_1\tilde{\sigma}^2 + k_2\tilde{\sigma} + c_3\Big) = 0, \tag{A.2}$$

where $c_1 = k_1\Big(\frac{1}{4} - \frac{18}{7\tilde{\chi}^2}\Big)$ and $c_3 = k_1\Big(1 - \frac{18}{7\tilde{\chi}^2}\Big)$. The coefficient of $\tilde{\sigma}^5$ being 1/2, the $\tilde{\sigma}^5$ term can be considered as a perturbation over the cubic equation in $\tilde{\sigma}$, as indicated by the first brackets

in Eq.(A.2). Let $\tilde{\sigma_0}$ be the solution of this cubic part of Eq.(A.2) and the analytic form of it can easily be obtained (for real root). Then we consider the solution of Eq.(A.2) as

$$\tilde{\sigma} = \tilde{\sigma}_0 + \epsilon\tilde{\sigma}_1 + \epsilon^2\tilde{\sigma}_2 + \epsilon^3\tilde{\sigma}_3, \tag{A.3}$$

with $\epsilon = 1/2$ (coefficient of $\tilde{\sigma}_5$ term) as a perturbation parameter. Finally we get

$$\tilde{\sigma}_1 = \frac{-\tilde{\sigma}_0^5}{k_2 + 2c_1\tilde{\sigma}_0 + 3\tilde{\sigma}_0^2}, \tag{A.4}$$

$$\tilde{\sigma}_2 = \frac{-5\tilde{\sigma}_0^4\tilde{\sigma}_1 - 3\tilde{\sigma}_0\tilde{\sigma}_1^2 - c_1\tilde{\sigma}_1^2}{k_2 + 2c_1\tilde{\sigma}_0 + 3\tilde{\sigma}_0^2}, \tag{A.5}$$

$$\tilde{\sigma}_3 = \frac{-5\tilde{\sigma}_0^4\tilde{\sigma}_2 - 10\tilde{\sigma}_0^3\tilde{\sigma}_1^2 - 6\tilde{\sigma}_0\tilde{\sigma}_1\tilde{\sigma}_2 - \tilde{\sigma}_1^3 - 2c_1\tilde{\sigma}_1\tilde{\sigma}_2}{k_2 + 2c_1\tilde{\sigma}_0 + 3\tilde{\sigma}_0^2}. \tag{A.6}$$

We have checked numerically (using mathematica) that this perturbation method for solving the fifth order polynomial equation as in Eq.(A.1) works reasonably well. For comparison, we have included Fig. A.1 where $\langle\tilde{\sigma}\rangle$ is depicted against the variation of $\tilde{\chi}$ (particularly during inflation when χ acquires super-Planckian value). The solid line represents the VEV of $\tilde{\sigma}$ as obtained from our perturbation method and the dashed line gives the exact numerical estimate of $\langle\tilde{\sigma}\rangle$ from Eq.(A.1). In order to get $V_{\rm Inf}$ in terms of $\tilde{\chi}$, we have used the analytic form of $\langle\tilde{\sigma}\rangle$ obtained through this perturbation method.

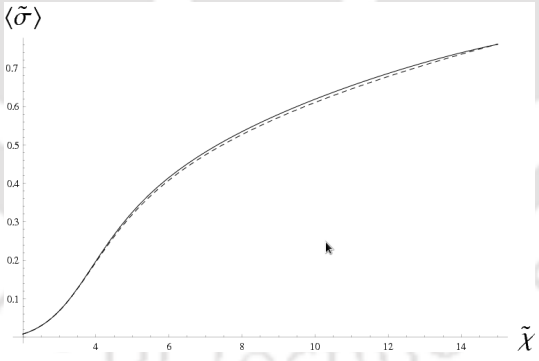

FIGURE A.1: Comparison of $\langle\tilde{\sigma}\rangle$ with $\tilde{\chi}$ using perturbation (solid line) and exact numerical result (dashed line).

A.2 R charges of various fields

Here we discuss the R-charge assignments for the various fields involved in our construction. Firstly in Table A.1, we include various $U(1)$ global charges associated with massless SQCD

theory ($N_f = 9$, $N_c = 7$) following [259]. However once the term $m_Q \mathrm{Tr} Q\tilde{Q}$ is included in the

Fields	$U(1)_B$	$U(1)_A$	$U(1)_{R'}$
Q	1	1	$\frac{2}{9}$
$\tilde{Q}$	-1	1	$\frac{2}{9}$
Λ	0	$\frac{3}{2}$	0
W	0	0	2
q	$\frac{7}{2}$	$-\frac{1}{4}$	$\frac{7}{9}$
$\tilde{q}$	$-\frac{7}{2}$	$-\frac{1}{4}$	$\frac{7}{9}$
Φ	0	$\frac{1}{2}$	$\frac{4}{9}$

TABLE A.1: Global charges of various fields in a massless SQCD theory [259].

UV description and a baryonic deformation (through $m_q qq$ term in Eq.(2.47)) is considered as well in the magnetic description, there exists a residual $U(1)_R$ symmetry only. The charges of the fields in the magnetic description can be obtained [471] from

$$R = \frac{2}{7}B + \frac{28}{9}A + R'. \tag{A.7}$$

This redefined R-charges are mentioned in Table 2.3. The superpotential in Eq.(2.48) respects this $U(1)_R$ symmetry. From $\Phi = \mathrm{Tr}(Q\tilde{Q})/\Lambda$, the $Q\tilde{Q}$ combination has two units of R charges.

Appendix B

Appendix related to Chapter 4

B.1 Unitarity Constraints

In this section we draw the perturbative unitarity limits on quartic couplings present in our model. Scattering amplitude for any $2 \to 2$ process can be expressed in terms of Legendre polynomial as[362, 363]

$$\mathcal{M}^{2\to 2} = 16\pi \sum_{l=0}^{\infty} a_l (2l+1) P_l(\cos\theta),$$

where, θ is the scattering angle and $P_l(\cos\theta)$ is the Legendre polynomial of order l. In high energy limit only s wave ($l = 0$) partial amplitude a_0 will determine the leading energy dependence of the scattering processes[362, 363]. The unitarity constraint says

$$|\text{Re } a_0| < 1/2. \tag{B.1}$$

This constraint Eq.(B.1) can be further translated to a bound on the scattering amplitude $\mathcal{M}$[362, 363].

$$|\mathcal{M}| < 8\pi. \tag{B.2}$$

In our proposed model we have multiple possible $2 \to 2$ scattering processes. Therefore we need to construct a matrix ($M^{2\to 2}_{i,j} = \mathcal{M}_{i\to j}$) considering all possible two particle states. Finally we need to calculate the eigenvalues of M and employ the bound as in Eq.(B.2).

In the high energy limit we express the SM Higgs doublet as $H^T = (w^+, \frac{H^0+iz}{2})$. Then the scalar potential (V) in Eq.(4.1) gives rise to eleven neutral combination of two particle states

$$w^+w^-,\ \frac{zz}{\sqrt{2}},\ \frac{H^0H^0}{\sqrt{2}},\ \frac{\chi\chi}{\sqrt{2}},\ \frac{\phi\ \phi}{\sqrt{2}},\ H^0\chi,\ H^0\ \phi,\ \chi\ \phi,\ z\ H^0,\ z\ \chi,\ z\ \phi), \tag{B.3}$$

and four singly charged two particle states

$$w^+H^0,\ w^+\chi,\ w^+z,\ w^+\phi. \tag{B.4}$$

Hence we can write the scattering amplitude matrix (M) in block diagonal form by decomposing it into neutral and singly charged sector as

$$M_{15\times15} = \begin{pmatrix} M^{\rm n}_{11\times11} & 0 \\ 0 & M^{sc}_{4\times4} \end{pmatrix}. \tag{B.5}$$

The submatrices are provided below :

$$M^n_{11\times11} = \begin{pmatrix}
4\lambda_H & \sqrt{2}\lambda_H & \sqrt{2}\lambda_H & \frac{\lambda_{\chi H}}{\sqrt{2}} & \frac{\lambda_{\phi H}}{\sqrt{2}} & 0 & 0 & 0 & 0 & 0 & 0 \\
\sqrt{2}\lambda_H & 3\lambda_H & \lambda_H & \frac{\lambda_{\chi H}}{2} & \frac{\lambda_{\phi H}}{2} & 0 & 0 & 0 & 0 & 0 & 0 \\
\sqrt{2}\lambda_H & \lambda_H & 3\lambda_H & \frac{\lambda_{\chi H}}{2} & \frac{\lambda_{\phi H}}{2} & 0 & 0 & 0 & 0 & 0 & 0 \\
\frac{\lambda_{\chi H}}{\sqrt{2}} & \frac{\lambda_{\chi H}}{2} & \frac{\lambda_{\chi H}}{2} & \frac{\lambda_{\chi}}{2} & \frac{\lambda_{\chi\phi}}{2} & 0 & 0 & 0 & 0 & 0 & 0 \\
\frac{\lambda_{\phi H}}{\sqrt{2}} & \frac{\lambda_{\phi H}}{2} & \frac{\lambda_{\phi H}}{2} & \frac{\lambda_{\chi\phi}}{2} & \frac{\lambda_{\phi}}{2} & 0 & 0 & 0 & 0 & 0 & 0 \\
0 & 0 & 0 & 0 & 0 & \lambda_{\chi H} & 0 & 0 & 0 & 0 & 0 \\
0 & 0 & 0 & 0 & 0 & 0 & \lambda_{\phi H} & 0 & 0 & 0 & 0 \\
0 & 0 & 0 & 0 & 0 & 0 & 0 & \lambda_{\chi\phi} & 0 & 0 & 0 \\
0 & 0 & 0 & 0 & 0 & 0 & 0 & 0 & 2\lambda_H & 0 & 0 \\
0 & 0 & 0 & 0 & 0 & 0 & 0 & 0 & 0 & \lambda_{\chi H} & 0 \\
0 & 0 & 0 & 0 & 0 & 0 & 0 & 0 & 0 & 0 & \lambda_{\phi H}
\end{pmatrix}. \tag{B.6}$$

$$M^{sc}_{4\times4} = \begin{pmatrix}
2\lambda_H & 0 & 0 & 0 \\
0 & \lambda_{\chi H} & 0 & 0 \\
0 & 0 & 2\lambda_H & 0 \\
0 & 0 & 0 & \lambda_{\phi H}
\end{pmatrix}. \tag{B.7}$$

The distinct eigen values of matrix Eq.(B.6) and Eq.(B.7) are following :

$$2\lambda_H,\ \lambda_{\chi H},\ \lambda_{\phi H},\ \lambda_{\chi\phi} \text{ and } x_{1,2,3},$$

where $x_{1,2,3}$ are the roots of the following polynomial equation,

$$x^3 + x^2(-12\lambda_H - \lambda\chi - \lambda\phi) + x\left(12\lambda_H\lambda_\chi + 12\lambda_H\lambda_\phi - 4\lambda^2_{\chi H} - \lambda^2_{\chi_\phi} + \lambda_\chi\lambda_\phi - 4\lambda^2_{\phi H}\right) + 12\lambda_H\lambda^2_{\chi\phi} - 12\lambda_H\lambda_\chi\lambda_\phi + 4\lambda^2_{\chi H}\lambda_\phi + 4\lambda_\chi\lambda^2_{\phi H} - 8\lambda_{\chi H}\lambda_{\chi\phi}\lambda_{\phi H} = 0. \quad \text{(B.8)}$$

Therefore the unitarity constraints in the proposed set up are following:

$$\lambda_H < 4\pi, \quad \lambda_{\phi H} < 8\pi, \quad \lambda_{\chi H} < 8\pi, \quad \lambda_{\chi\phi} < 8\pi \quad \text{and} \quad x_{1,2,3} < 16\pi \ . \quad \text{(B.9)}$$

Appendix C

Appendix related to Chapter 5

C.1 Dashen Formula

Dashen formula for pNGB reads as

$$\langle\chi\rangle^2(m^a_{G_s})^2 = \langle 0|[\tilde{\mathcal{Q}}_i,[\tilde{\mathcal{Q}}_i,H]]|0\rangle \tag{C.1}$$

$$= \bar{\psi}\Big[\frac{\lambda_a}{2},\Big[\frac{\lambda_a}{2},m_{\rm diag}\Big]_+\Big]_+\psi \tag{C.2}$$

where $i = 1, 2, ..4$ and

$$m_{\rm diag} = \begin{pmatrix} m_1 & 0 & 0 & 0 \\ 0 & m_2 & 0 & 0 \\ 0 & 0 & m_3 & 0 \\ 0 & 0 & 0 & m_4 \end{pmatrix} \tag{C.3}$$

and $\psi = \{Q_1, Q_2, Q_3, Q_4\}$ is the quark state. $\tilde{\mathcal{Q}}_i = \int d^3x\psi^\dagger(x)\gamma_5\frac{\lambda_a}{2}\psi(x)$ is the axial charge of the broken $SU(4)$. $H = \bar{\psi}M\psi$ λ_a are the generators of broken $SU(4)_A$ with $a = 1, 2, ...15$. When quark condensates like in form of $\langle\bar{Q}Q\rangle = \Lambda^3$, we find for a=1,

$$\lambda_1 = \begin{pmatrix} 0 & 1 & 0 & 0 \\ 1 & 0 & 0 & 0 \\ 0 & 0 & 0 & 0 \\ 0 & 0 & 0 & 0 \end{pmatrix} \tag{C.4}$$

$$\text{Correspondingly, } (m^1_{G_s})^2 = (m_1+m_2)\langle\psi\bar{\psi}\rangle = (m_1+m_2)\frac{\Lambda^3}{\langle\chi\rangle^2} \tag{C.5}$$

Similarly using other λ^a's for SU(4), we find ($\zeta = \Lambda/\langle\chi\rangle$)

$$m_{G_s}^{2,3} = \zeta\sqrt{(m_1+m_2)\Lambda}\,, \quad m_{G_s}^{4,5} = \zeta\sqrt{(m_1+m_3)\Lambda}\,, \quad m_{G_s}^{6,7} = \zeta\sqrt{(m_2+m_3)\Lambda} \tag{C.6}$$

$$m_{G_s}^{9,10} = \zeta\sqrt{(m_1+m_4)\Lambda}\,, \quad m_{G_s}^{11,12} = \zeta\sqrt{(m_2+m_4)\Lambda}\,, \quad m_{G_s}^{13,14} = \zeta\sqrt{(m_3+m_4)\Lambda} \tag{C.7}$$

$$m_{G_s}^{8} = \zeta\sqrt{(m_1+m_2+4m_3)\Lambda^3/3}\,, \quad m_{G_s}^{15} = \zeta\sqrt{(m_1+m_2+m_3+9m_4)\Lambda^3/6} \tag{C.8}$$

C.2 pNBG annihilation cross-section to Neutralino

In MSSM, after electroweak symmetry breaking, neutral gauginos and Higgsinos mix to yield four physical fields called neutralinos. In the mass basis, the neutralino can be written as a combination of wino, bino and two Higgssions. For example, the lightest one can be written as

$$\chi_0 = Z_{11}\tilde{B} + Z_{12}\tilde{W} + Z_{13}\tilde{H}_u + Z_{14}\tilde{H}_d, \tag{C.9}$$

where the coefficients Z_{ij} are the elements of the diagonalizing mass matrix and crucially control its interaction to other MSSM and SM particles. In our analysis, we have considered that the pNBG's can only annihilate to lightest neutralino by assuming the rest to be heavier than the pNBGs. The interaction lagrangian of $\chi_0\bar{\chi}_0 h$ vertex is $\mathcal{L} = -ig_2\bar{\chi}_0(C_{L1}P_L + C_{R1}P_R)\chi_0 h$. Our aim is to calculate the cross section for $G_S G_S \to \bar{\chi_0}\chi_0$ annihilation process that has been used in the estimation of pNGB DM relic density. It is a two body scattering process and the differential scattering cross section in centre of mass frame is given by

$$\frac{d\sigma}{d\Omega} = \frac{1}{16\pi^2|v_1 - v_2|}\frac{p_f}{s^{3/2}}\overline{|M|^2}\,, \quad p_f = \frac{\sqrt{\{s-(m_3+m_4)^2\}\{s-(m_3-m_4)^2\}}}{2\sqrt{s}} \tag{C.10}$$

(p_f is the final state momentum). The Feynman amplitude for the process is

$$-iM = -i\alpha_2\Big\{C_{L1}v_3\frac{1-\gamma_5}{2}\bar{u_4} + C_{L2}v_3\frac{1+\gamma_5}{2}\bar{u_4}\Big\}\frac{\alpha_1}{(p_2-p_1)^2 - m_h^2} \tag{C.11}$$

where $\alpha_2 = g_2(C_L P_L + C_R P_R)$ and $\alpha_1 = 2\lambda'' v_d$ are two vertex factors in Fig.5.10 as obtained from Eq.(5.27). Using standard procedure, we find

$$\overline{|M|^2} = \frac{2\alpha_2^2\alpha_1^2}{(s-m_h^2)^2}\Big[(|C_L|^2 + |C_R|^2)\frac{(s-2m_3^2)}{2} - (C_L^* C_{R1} + C_R^* C_L)m_3^2\Big] \tag{C.12}$$

Finally from Eq.(C.10) we obtain the s-wave contribution to the annihilation cross-section as,

$$\sigma v_{rel} = \frac{1}{4\pi}\frac{\sqrt{s-4m_\chi^2}}{s^{3/2}}\frac{\alpha_1^2\alpha_2^2}{(s-m_h^2)^2}\Big[(|C_L|^2+|C_R|^2)\frac{(s-2m_\chi^2)}{2} - (C_L^*C_R + C_R^*C_L)m_\chi^2\Big], \quad \text{(C.13)}$$

where

$$\begin{aligned}
C_L &= -Q_{11}''^{*}\sin\alpha - S_{11}''^{*}\cos\alpha,\\
C_R &= -Q_{11}''\sin\alpha - S_{11}''\cos\alpha,\\
Q_{11}'' &= \frac{1}{2}\Big[Z_{13}(Z_{12}-\tan\theta_W Z_{11}) + Z_{13}(Z_{12}-\tan\theta_W Z_{11})\Big],\\
S_{11}'' &= \frac{1}{2}\Big[Z_{14}(Z_{12}-\tan\theta_W Z_{11}) + Z_{14}(Z_{12}-\tan\theta_W Z_{11})\Big],\\
m_1 &= m_2 = m_{G_S},\\
m_3 &= m_4 = m_\chi,\\
\sqrt{s} &= E_1+E_2 = 2E_1 = 2m_{G_S}.
\end{aligned} \quad \text{(C.14)}$$

For simplification, we have assumed $C_L = C_R$ in our analysis.

C.3 Numerical estimate of Boltzmann equations

Relic density allowed parameter space of non-degenerate multipartite DM components of the model (Section 4.1.2 and Section 4.2) has been obtained by using approximate analytic solution (Eq. (5.45)). Here we will explicitly demonstrate the viability of such analytic solution to the exact numerical solution of the coupled Boltzmann equations (BEQ) that defines the freeze-out of such non-degenerate DMs. We will illustrate the case of non-degenerate pNGBs, with negligible interactions to LSP (Section 4.1.2).

Let us define $Y = n_i/s$, where n_i is the number density of i'th DM candidate and s is the entropy density of the universe. The BEQ is rewritten as a function of $x = m/T$, where m is the mass of DM particle and T is the temperature of the thermal bath. As we have three DM candidates of type A, B and C, we use instead a common variable $x = \mu/T$ where $1/\mu = 1/m_A + 1/m_B + 1/m_C$ and $1/x = T/\mu = 1/x_1 + 1/x_2 + 1/x_3$. Assuming $m_C > m_B > m_A$,

the coupled BEQ then reads

$$\begin{aligned}
\frac{dY_C}{dx} =& -0.264 M_P \sqrt{g_*}\frac{\mu}{x^2}\Big[\langle\sigma v\rangle_{CC\to SM}(Y_C^2 - Y_C^{\rm eq2}) + 6\langle\sigma v\rangle_{CC\to B_iB_i}\Big(Y_C^2 - \frac{Y_C^{\rm eq2}}{Y_{B_i}^{\rm eq2}}Y_{B_i}^2\Big) \\
&+8\langle\sigma v\rangle_{CC\to A_iA_i}\Big(Y_C^2 - \frac{Y_C^{\rm eq2}}{Y_{A_i}^{\rm eq2}}Y_{A_i}^2\Big)\Big] \\
\frac{dY_{B_i}}{dx} =& -0.264 M_P \sqrt{g_*}\frac{\mu}{x^2}\Big[\langle\sigma v\rangle_{B_iB_i\to SM}(Y_{B_i}^2 - Y_{B_i}^{\rm eq2}) - \langle\sigma v\rangle_{CC\to B_iB_i}\Big(Y_C^2 - \frac{Y_C^{\rm eq2}}{Y_{B_i}^{\rm eq2}}Y_{B_i}^2\Big) \\
&+8\langle\sigma v\rangle_{B_iB_i\to A_iA_i}\Big(Y_{B_i}^2 - \frac{Y_{B_i}^{\rm eq2}}{Y_{A_i}^{\rm eq2}}Y_{A_i}^2\Big)\Big], \\
\frac{dY_{A_i}}{dx} =& -0.264 M_P \sqrt{g_*}\frac{\mu}{x^2}\Big[\langle\sigma v\rangle_{A_iA_i\to SM}(Y_{A_i}^2 - Y_{A_i}^{\rm eq2}) - \langle\sigma v\rangle_{CC\to A_iA_i}\Big(Y_C^2 - \frac{Y_C^{\rm eq2}}{Y_{A_i}^{\rm eq2}}Y_{A_i}^2\Big) \\
&- \langle\sigma v\rangle_{B_iB_i\to A_iA_i}\Big(Y_{B_i}^2 - \frac{Y_{B_i}^{\rm eq2}}{Y_{A_i}^{\rm eq2}}Y_{A_i}^2\Big)\Big],
\end{aligned} \tag{C.15}$$

where the equilibrium distribution has the form

$$Y_i^{\rm eq}(x) = 0.145\frac{g}{g_*}x^{3/2}\Big(\frac{m_i}{\mu}\Big)^{3/2}e^{-x\left(\frac{m_i}{\mu}\right)}. \tag{C.16}$$

We have already explained that the relic density of A-type DM having mass $\sim \frac{m_h}{2}$ is negligible due to resonance enhancement of annihilation cross-section. Therefore, it freezes out much later than B and C type DMs. During the freeze out of B and C type DM, we can then safely write $Y_A \simeq Y_A^{\rm eq}$ and ignore its contribution to the relic density. The coupled BEQ then effectively turns to

$$\begin{aligned}
\frac{dy_C}{dx} &= -\frac{1}{x^2}\Big\{(\langle\sigma v\rangle_{CC\to SM} + 8\langle\sigma v\rangle_{CC\to A_iA_i})(y_C^2 - y_C^{\rm eq^2}) + 6\langle\sigma v\rangle_{CC\to B_iB_i}(y_C^2 - \frac{y_C^{\rm eq^2}}{y_{B_i}^{\rm eq^2}}y_{B_i}^2)\Big\}, \\
\frac{dy_{B_i}}{dx} &= -\frac{1}{x^2}\Big\{(\langle\sigma v\rangle_{B_iB_i\to SM} + 8\langle\sigma v\rangle_{B_iB_i\to A_iA_i})(y_C^2 - y_C^{\rm eq^2}) - 6\langle\sigma v\rangle_{CC\to B_iB_i}(y_C^2 - \frac{y_C^{\rm eq^2}}{y_{B_i}^{\rm eq^2}}y_{B_i}^2)\Big\},
\end{aligned} \tag{C.17}$$

where

$$y_i = 0.264 M_P \sqrt{g_*}\mu Y_i, \tag{C.18}$$

$$y_i^{\rm eq} = 0.264 M_P \sqrt{g_*}\mu Y_i^{\rm eq}. \tag{C.19}$$

Once we obtain the freeze out temperature by solving the set of coupled equations (as in

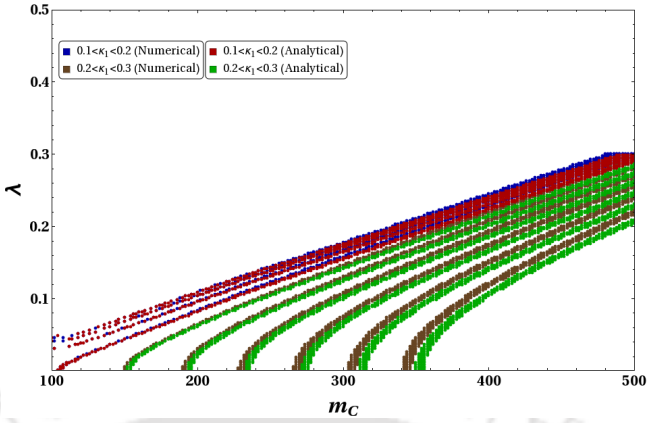

FIGURE C.1: Comparison between relic density found using numerical solution to coupled Boltzmann equation (Eq.(C.17)) and approximate analytical solutions as in Eq.(5.47) in m_C (GeV) -λ plane for $\kappa : \{0.1 - 0.3\}$.

Eq.(C.17) numerically, we can compute the relic density for each of the DM species by

$$\Omega_C h^2 = \frac{854.45 \times 10^{-13}}{\sqrt{g_*}} \frac{m_C}{\mu} y_C \Big[\frac{\mu}{m_C} x_\infty\Big],$$
$$\Omega_B h^2 = \frac{854.45 \times 10^{-13}}{\sqrt{g_*}} \frac{m_B}{\mu} y_B \Big[\frac{\mu}{m_C} x_\infty\Big], \tag{C.20}$$
$$\Omega_T \simeq \Omega_C + 6\Omega_B. \tag{C.21}$$

$y_i\Big[\frac{\mu}{m_i} x_\infty\Big]$ indicates the value of y_i evaluated at $\frac{\mu}{m_i} x_\infty$, where x_∞ denotes a very large value of x after decoupling. For numerical analysis we have taken $x = 500$ which is a legitimate choice. We scan for $\kappa_1 \sim 0.1 - 0.3$ and $m_C = 100 - 500$ GeV to find out relic density allowed points. We have shown it in terms of $\lambda - m_C$ in Fig.C.1. $\kappa : \{0.1 - 0.2\}$. Analytical solutions (Eq. (5.47)) for relic density is plotted in the same graph for comparative purpose. We see for low values of $\kappa : \{0.1 - 0.2\}$ the numerical solution (in blue) and approximated analytical solution (in red) falls on top of each other with very good agreement. With larger $\kappa : \{0.2 - 0.3\}$, the separation between numerical (in grey) and approximate analytical solution (in green) increases mildly within $\Delta m_{DM} \sim 10$ GeV.

Bibliography

[1] E. S. Abers and B. W. Lee, Phys. Rept. **9**, 1 (1973). doi:10.1016/0370-1573(73)90027-6

[2] J. E. Kim, P. Langacker, M. Levine and H. H. Williams, Rev. Mod. Phys. **53**, 211 (1981). doi:10.1103/RevModPhys.53.211

[3] P. Aurenche, hep-ph/9712342.

[4] G. ALTARELLI, hep-ph/0510281.

[5] J. Iliopoulos, doi:10.5170/CERN-2014-008.1, 10.5170/CERN-2016-005.1 arXiv:1305.6779 [hep-ph].

[6] M. K. Gaillard, P. D. Grannis and F. J. Sciulli, Rev. Mod. Phys. **71**, S96 (1999) doi:10.1103/RevModPhys.71.S96 [hep-ph/9812285].

[7] S. F. Novaes, In *Sao Paulo 1999, Particles and fields* 5-102 [hep-ph/0001283].

[8] M. Herrero, NATO Sci. Ser. C **534**, 1 (1999) doi:10.1007/978-94-011-4689-01 [hep-ph/9812242].

[9] G. Aad *et al.* [ATLAS Collaboration], Phys. Lett. B **716**, 1 (2012) [arXiv:1207.7214 [hep-ex]].

[10] S. Chatrchyan *et al.* [CMS Collaboration], Phys. Lett. B **716**, 30 (2012) [arXiv:1207.7235 [hep-ex]].

[11] E. W. Kolb and M. S. Turner, Front. Phys. **69**, 1 (1990).

[12] B. Pontecorvo, Sov. Phys. JETP **6**, 429 (1957) [Zh. Eksp. Teor. Fiz. **33**, 549 (1957)].

[13] S. M. Bilenky and S. T. Petcov, Rev. Mod. Phys. **59**, 671 (1987) Erratum: [Rev. Mod. Phys. **61**, 169 (1989)] Erratum: [Rev. Mod. Phys. **60**, 575 (1988)]. doi:10.1103/RevModPhys.59.671

[14] A. Bandyopadhyay, S. Choubey, R. Gandhi, S. Goswami and D. P. Roy, Phys. Lett. B **559**, 121 (2003) doi:10.1016/S0370-2693(03)00340-X [hep-ph/0212146].

[15] M. Maltoni and A. Y. Smirnov, Eur. Phys. J. A **52**, no. 4, 87 (2016) doi:10.1140/epja/i2016-16087-0 [arXiv:1507.05287 [hep-ph]].

[16] S. Fukuda *et al.* [Super-Kamiokande Collaboration], Phys. Lett. B **539**, 179 (2002) [hep-ex/0205075]; P. Adamson *et al.* [MINOS Collaboration], Phys. Rev. Lett. **106**, 181801 (2011) [arXiv:1103.0340 [hep-ex]]; T. Araki *et al.* [KamLAND Collaboration], Phys. Rev. Lett. **94**, 081801 (2005) [hep-ex/0406035].

[17] Y. Fukuda *et al.* [Super-Kamiokande Collaboration], Phys. Rev. Lett. **82**, 2430 (1999) doi:10.1103/PhysRevLett.82.2430 [hep-ex/9812011].

[18] J. Boger *et al.* [SNO Collaboration], Nucl. Instrum. Meth. A **449**, 172 (2000) doi:10.1016/S0168-9002(99)01469-2 [nucl-ex/9910016].

[19] M. H. Ahn *et al.* [K2K Collaboration], Phys. Rev. D **74**, 072003 (2006) doi:10.1103/PhysRevD.74.072003 [hep-ex/0606032].

[20] S. Abe *et al.* [KamLAND Collaboration], Phys. Rev. Lett. **100**, 221803 (2008) doi:10.1103/PhysRevLett.100.221803 [arXiv:0801.4589 [hep-ex]].

[21] R. N. Mohapatra and G. Senjanovic, Phys. Rev. Lett. **44**, 912 (1980). doi:10.1103/PhysRevLett.44.912

[22] G. Lazarides, Q. Shafi and C. Wetterich, Nucl. Phys. B **181**, 287 (1981). doi:10.1016/0550-3213(81)90354-0

[23] M. Magg and C. Wetterich, Phys. Lett. **94B**, 61 (1980). doi:10.1016/0370-2693(80)90825-4

[24] R. Foot, H. Lew, X. G. He and G. C. Joshi, Z. Phys. C **44**, 441 (1989). doi:10.1007/BF01415558

[25] C. Patrignani *et al.* [Particle Data Group], Chin. Phys. C **40**, no. 10, 100001 (2016). doi:10.1088/1674-1137/40/10/100001

[26] P. B. Arnold, Phys. Rev. D **40**, 613 (1989). doi:10.1103/PhysRevD.40.613

[27] M. Sher, Phys. Rept. **179**, 273 (1989). doi:10.1016/0370-1573(89)90061-6

[28] P. B. Arnold and S. Vokos, Phys. Rev. D **44**, 3620 (1991). doi:10.1103/PhysRevD.44.3620

[29] J. R. Espinosa and M. Quiros, Phys. Lett. B **353**, 257 (1995) doi:10.1016/0370-2693(95)00572-3 [hep-ph/9504241].

[30] G. Isidori, G. Ridolfi and A. Strumia, Nucl. Phys. B **609**, 387 (2001) doi:10.1016/S0550-3213(01)00302-9 [hep-ph/0104016].

[31] J. R. Espinosa, G. F. Giudice and A. Riotto, JCAP **0805**, 002 (2008) doi:10.1088/1475-7516/2008/05/002 [arXiv:0710.2484 [hep-ph]].

[32] J. Ellis, J. R. Espinosa, G. F. Giudice, A. Hoecker and A. Riotto, Phys. Lett. B **679**, 369 (2009) doi:10.1016/j.physletb.2009.07.054 [arXiv:0906.0954 [hep-ph]].

[33] F. Bezrukov and M. Shaposhnikov, JHEP **0907**, 089 (2009) doi:10.1088/1126-6708/2009/07/089 [arXiv:0904.1537 [hep-ph]].

[34] D. Buttazzo, G. Degrassi, P. P. Giardino, G. F. Giudice, F. Sala, A. Salvio and A. Strumia, JHEP **1312**, 089 (2013) doi:10.1007/JHEP12(2013)089 [arXiv:1307.3536 [hep-ph]].

[35] G. Degrassi, S. Di Vita, J. Elias-Miro, J. R. Espinosa, G. F. Giudice, G. Isidori and A. Strumia, JHEP **1208**, 098 (2012) doi:10.1007/JHEP08(2012)098 [arXiv:1205.6497 [hep-ph]].

[36] Y. Tang, Mod. Phys. Lett. A **28**, 1330002 (2013) doi:10.1142/S0217732313300024 [arXiv:1301.5812 [hep-ph]].

[37] S. Alekhin, A. Djouadi and S. Moch, Phys. Lett. B **716**, 214 (2012) doi:10.1016/j.physletb.2012.08.024 [arXiv:1207.0980 [hep-ph]].

[38] J. R. Espinosa, PoS TOP **2015**, 043 (2016) doi:10.22323/1.257.0043 [arXiv:1512.01222 [hep-ph]].

[39] P. A. R. Ade *et al.* [Planck Collaboration], Astron. Astrophys. **594**, A13 (2016) doi:10.1051/0004-6361/201525830 [arXiv:1502.01589 [astro-ph.CO]].

[40] N. Aghanim *et al.* [Planck Collaboration], arXiv:1807.06209 [astro-ph.CO].

[41] P. A. R. Ade *et al.* [Planck Collaboration], arXiv:1303.5076 [astro-ph.CO].

[42] J. C. Mather, D. J. Fixsen, R. A. Shafer, C. Mosier and D. T. Wilkinson, Astrophys. J. **512**, 511 (1999) doi:10.1086/306805 [astro-ph/9810373].

[43] A. H. Guth, Phys. Rev. D **23**, 347 (1981) [Adv. Ser. Astrophys. Cosmol. **3**, 139 (1987)]. doi:10.1103/PhysRevD.23.347

[44] A. D. Linde, Phys. Lett. **108B**, 389 (1982) [Adv. Ser. Astrophys. Cosmol. **3**, 149 (1987)]. doi:10.1016/0370-2693(82)91219-9

[45] A. D. Linde, Rept. Prog. Phys. **47**, 925 (1984). doi:10.1088/0034-4885/47/8/002

[46] G. Lazarides, hep-ph/0204294.

[47] A. R. Liddle, Class. Quant. Grav. **19**, 3391 (2002) doi:10.1088/0264-9381/19/13/301 [astro-ph/0109439].

[48] D. Baumann and H. V. Peiris, Adv. Sci. Lett. **2**, 105 (2009) doi:10.1166/asl.2009.1019 [arXiv:0810.3022 [astro-ph]].

[49] L. Kofman, A. D. Linde and V. F. Mukhanov, JHEP **0210**, 057 (2002) doi:10.1088/1126-6708/2002/10/057 [hep-th/0206088].

[50] D. Baumann, doi:10.1142/9789814327183-0010 arXiv:0907.5424 [hep-th].

[51] A. Linde, doi:10.1093/acprof:oso/9780198728856.003.0006 arXiv:1402.0526 [hep-th].

[52] A. D. Linde, Lect. Notes Phys. **738**, 1 (2008) doi:10.1007/978-3-540-74353-81 [arXiv:0705.0164 [hep-th]].

[53] S. Tsujikawa, hep-ph/0304257.

[54] J. McDonald, Phys. Rev. D **50**, 3637 (1994) doi:10.1103/PhysRevD.50.3637 [hep-ph/0702143 [HEP-PH]].

[55] W. L. Guo and Y. L. Wu, JHEP **1010**, 083 (2010) doi:10.1007/JHEP10(2010)083 [arXiv:1006.2518 [hep-ph]].

[56] A. Biswas and D. Majumdar, Pramana **80**, 539 (2013) doi:10.1007/s12043-012-0478-z [arXiv:1102.3024 [hep-ph]].

[57] W. Rodejohann and C. E. Yaguna, JCAP **1512**, no. 12, 032 (2015) doi:10.1088/1475-7516/2015/12/032 [arXiv:1509.04036 [hep-ph]].

[58] J. Elias-Miro, J. R. Espinosa, G. F. Giudice, H. M. Lee and A. Strumia, JHEP **1206**, 031 (2012) doi:10.1007/JHEP06(2012)031 [arXiv:1203.0237 [hep-ph]].

[59] O. Lebedev, Eur. Phys. J. C **72**, 2058 (2012) doi:10.1140/epjc/s10052-012-2058-2 [arXiv:1203.0156 [hep-ph]].

[60] C. N. Karahan and B. Korutlu, Phys. Lett. B **732**, 320 (2014) doi:10.1016/j.physletb.2014.03.063 [arXiv:1404.0175 [hep-ph]].

[61] G. B. Pivovarov and V. T. Kim, Phys. Rev. D **78**, 016001 (2008) doi:10.1103/PhysRevD.78.016001 [arXiv:0712.0402 [hep-ph]].

[62] R. Brustein and D. H. Oaknin, Phys. Rev. Lett. **82**, 2628 (1999) doi:10.1103/PhysRevLett.82.2628 [hep-ph/9809365].

[63] T. Moroi and H. Murayama, Phys. Lett. B **553**, 126 (2003) doi:10.1016/S0370-2693(02)03227-6 [hep-ph/0211019]. ——-

[64] J. Martin, C. Ringeval and V. Vennin, Phys. Dark Univ. **5-6**, 75 (2014) doi:10.1016/j.dark.2014.01.003 [arXiv:1303.3787 [astro-ph.CO]].

[65] V. V. Khoze, C. McCabe and G. Ro, JHEP **1408**, 026 (2014) doi:10.1007/JHEP08(2014)026 [arXiv:1403.4953 [hep-ph]].

[66] E. Gabrielli, M. Heikinheimo, K. Kannike, A. Racioppi, M. Raidal and C. Spethmann, Phys. Rev. D **89**, no. 1, 015017 (2014) doi:10.1103/PhysRevD.89.015017 [arXiv:1309.6632 [hep-ph]].

[67] P. Ghosh, A. K. Saha and A. Sil, Phys. Rev. D **97**, no. 7, 075034 (2018) doi:10.1103/PhysRevD.97.075034 [arXiv:1706.04931 [hep-ph]].

[68] M. Gonderinger, Y. Li, H. Patel and M. J. Ramsey-Musolf, JHEP **1001**, 053 (2010) doi:10.1007/JHEP01(2010)053 [arXiv:0910.3167 [hep-ph]].

[69] W. Chao, M. Gonderinger and M. J. Ramsey-Musolf, Phys. Rev. D **86**, 113017 (2012) doi:10.1103/PhysRevD.86.113017 [arXiv:1210.0491 [hep-ph]].

[70] S. Baek, P. Ko, W. I. Park and E. Senaha, JHEP **1211**, 116 (2012) doi:10.1007/JHEP11(2012)116 [arXiv:1209.4163 [hep-ph]].

[71] M. Gonderinger, H. Lim and M. J. Ramsey-Musolf, Phys. Rev. D **86**, 043511 (2012) doi:10.1103/PhysRevD.86.043511 [arXiv:1202.1316 [hep-ph]].

[72] I. Garg, S. Goswami, Vishnudath K.N. and N. Khan, Phys. Rev. D **96**, no. 5, 055020 (2017) doi:10.1103/PhysRevD.96.055020 [arXiv:1706.08851 [hep-ph]].

[73] N. Khan and S. Rakshit, Phys. Rev. D **90**, no. 11, 113008 (2014) doi:10.1103/PhysRevD.90.113008 [arXiv:1407.6015 [hep-ph]].

[74] N. Haba, H. Ishida, K. Kaneta and R. Takahashi, Phys. Rev. D **90**, 036006 (2014) doi:10.1103/PhysRevD.90.036006 [arXiv:1406.0158 [hep-ph]].

[75] A. Eichhorn and M. M. Scherer, Phys. Rev. D **90**, no. 2, 025023 (2014) doi:10.1103/PhysRevD.90.025023 [arXiv:1404.5962 [hep-ph]].

[76] C. S. Chen and Y. Tang, JHEP **1204**, 019 (2012) doi:10.1007/JHEP04(2012)019 [arXiv:1202.5717 [hep-ph]].

[77] J. Erler, In *Stock, R. (ed.): Encyclopedia of applied high energy and particle physics* 119-145

[78] G. Altarelli, hep-ph/9811456.

[79] A. Pich, arXiv:1201.0537 [hep-ph].

[80] C. Quigg, "Gauge Theories of the Strong, Weak, and Electromagnetic Interactions : Second Edition,"

[81] T. P. Cheng and L. F. Li, Oxford, Uk: Clarendon (1984) 536 P. (Oxford Science Publications)

[82] T. Muta, World Sci. Lect. Notes Phys. **57**, 1 (1998).

[83] A. V. Smilga, "Lectures on quantum chromodynamics,"

[84] A. Pich, In *Sorrento 1994, High energy physics* 157-207 [hep-ph/9505231].

[85] J. W. Moffat, arXiv:1203.1573 [hep-ph].

[86] I. J. R. Aitchison and A. J. G. Hey,

[87] S. L. Glashow, Nucl. Phys. **22**, 579 (1961). doi:10.1016/0029-5582(61)90469-2

[88] S. Weinberg, Phys. Rev. Lett. **19**, 1264 (1967). doi:10.1103/PhysRevLett.19.1264

[89] A. Santamaria, Phys. Lett. B **305**, 90 (1993) doi:10.1016/0370-2693(93)91110-9 [hep-ph/9302301].

[90] S. Dawson, hep-ph/9901280.

[91] S. Dawson, In *Boulder 1994, Proceedings, CP violation and the limits of the standard model* 445-505, and Brookhaven Nat. Lab. Upton - BNL-61012 (94/10,rec.Nov.) 43 p [hep-ph/9411325].

[92] R. S. Chivukula, hep-ph/9803219.

[93] M. Spira and P. M. Zerwas, Lect. Notes Phys. **512**, 161 (1998) doi:10.1007/BFb0106895 [hep-ph/9803257].

[94] R. H. Brandenberger, PoS ICFI **2010**, 001 (2010) doi:10.22323/1.124.0001 [arXiv:1103.2271 [astro-ph.CO]].

[95] J. L. Cervantes-Cota and G. Smoot, AIP Conf. Proc. **1396**, 28 (2011) doi:10.1063/1.3647524 [arXiv:1107.1789 [astro-ph.CO]].

[96] S. Dodelson, Amsterdam, Netherlands: Academic Pr. (2003) 440 p

[97] A. R. Liddle, Chichester, UK: Wiley (1998) 129 p

[98] E. W. Kolb, astro-ph/9403007.

[99] V. A. Rubakov, doi:10.5170/CERN-2014-003.151 arXiv:1504.03587 [astro-ph.CO].

[100] A. R. Liddle and D. H. Lyth, Cambridge, UK: Univ. Pr. (2000) 400 p

[101] H. V. Peiris *et al.* [WMAP Collaboration], Astrophys. J. Suppl. **148**, 213 (2003) doi:10.1086/377228 [astro-ph/0302225].

[102] P. A. R. Ade *et al.* [Planck Collaboration], arXiv:1502.02114 [astro-ph.CO].

[103] A. D. Linde, Phys. Lett. **129B**, 177 (1983). doi:10.1016/0370-2693(83)90837-7

[104] A. D. Linde, Phys. Lett. **162B**, 281 (1985). doi:10.1016/0370-2693(85)90923-2

[105] K. Garrett and G. Duda, Adv. Astron. **2011**, 968283 (2011) doi:10.1155/2011/968283 [arXiv:1006.2483 [hep-ph]].

[106] K. A. Olive, astro-ph/0301505.

[107] G. B. Gelmini, arXiv:1502.01320 [hep-ph].

[108] D. Hooper, arXiv:0901.4090 [hep-ph].

[109] T. Plehn, arXiv:1705.01987 [hep-ph].

[110] M. Lisanti, arXiv:1603.03797 [hep-ph].

[111] A. Borriello and P. Salucci, Mon. Not. Roy. Astron. Soc. **323**, 285 (2001) doi:10.1046/j.1365-8711.2001.04077.x [astro-ph/0001082].

[112] A. Burkert and J. Silk, Astrophys. J. **488**, L55 (1997) doi:10.1086/310935 [astro-ph/9707343].

[113] M. Persic, P. Salucci and F. Stel, Mon. Not. Roy. Astron. Soc. **281**, 27 (1996) doi:10.1093/mnras/281.1.27, 10.1093/mnras/278.1.27 [astro-ph/9506004].

[114] K. Freese, EAS Publ. Ser. **36**, 113 (2009) doi:10.1051/eas/0936016 [arXiv:0812.4005 [astro-ph]].

[115] H. Hoekstra, H. Yee and M. Gladders, New Astron. Rev. **46**, 767 (2002) [astro-ph/0205205].

[116] R. B. Metcalf, L. A. Moustakas, A. J. Bunker and I. R. Parry, Astrophys. J. **607**, 43 (2004) [astro-ph/0309738].

[117] L. A. Moustakas and R. B. Metcalf, Mon. Not. Roy. Astron. Soc. **339**, 607 (2003) [astro-ph/0206176].

[118] N. Kaiser and G. Squires, Astrophys. J. **404**, 441 (1993). doi:10.1086/172297

[119] P. Schneider, Mon. Not. Roy. Astron. Soc. **283**, 837 (1996) doi:10.1093/mnras/283.3.837 [astro-ph/9601039].

[120] R. Massey, T. Kitching and J. Richard, Rept. Prog. Phys. **73**, 086901 (2010) doi:10.1088/0034-4885/73/8/086901 [arXiv:1001.1739 [astro-ph.CO]].

[121] D. Clowe, M. Bradac, A. H. Gonzalez, M. Markevitch, S. W. Randall, C. Jones and D. Zaritsky, Astrophys. J. **648**, L109 (2006) doi:10.1086/508162 [astro-ph/0608407].

[122] A. G. Bergmann, V. Petrosian, and R. Lynds. Gravitational lens models of arcs in clusters. *Astrophys. J.*, **350**:2335, February 1990

[123] N. Aghanim *et al.* [Planck Collaboration], Astron. Astrophys. **594**, A11 (2016) doi:10.1051/0004-6361/201526926 [arXiv:1507.02704 [astro-ph.CO]].

[124] G. Hinshaw *et al.* Nine-Year Wilkinson Microwave Anisotropy Probe (WMAP) Observations: Cosmological Parameter Results. *Astrophys. J. Suppl.* **208**, (2013) 19.

[125] L. J. Hall, K. Jedamzik, J. March-Russell and S. M. West, JHEP **1003**, 080 (2010) doi:10.1007/JHEP03(2010)080 [arXiv:0911.1120 [hep-ph]].

[126] N. Bernal, M. Heikinheimo, T. Tenkanen, K. Tuominen and V. Vaskonen, Int. J. Mod. Phys. A **32**, no. 27, 1730023 (2017) doi:10.1142/S0217751X1730023X [arXiv:1706.07442 [hep-ph]].

[127] Y. Hochberg, E. Kuflik, T. Volansky and J. G. Wacker, Phys. Rev. Lett. **113**, 171301 (2014) doi:10.1103/PhysRevLett.113.171301 [arXiv:1402.5143 [hep-ph]].

[128] N. Bernal, C. Garcia-Cely and R. Rosenfeld, Nucl. Part. Phys. Proc. **267-269**, 353 (2015). doi:10.1016/j.nuclphysbps.2015.11.001

[129] N. Bernal, C. Garcia-Cely and R. Rosenfeld, JCAP **1504**, no. 04, 012 (2015) doi:10.1088/1475-7516/2015/04/012 [arXiv:1501.01973 [hep-ph]].

[130] H. M. Lee, New Phys. Sae Mulli **66**, no. 8, 993 (2016). doi:10.3938/NPSM.66.993

[131] S. M. Choi, H. M. Lee and M. S. Seo, EPJ Web Conf. **168**, 06009 (2018) doi:10.1051/epjconf/201816806009 [arXiv:1708.05953 [hep-ph]].

[132] S. M. Choi, Y. Hochberg, E. Kuflik, H. M. Lee, Y. Mambrini, H. Murayama and M. Pierre, JHEP **1710**, 162 (2017) doi:10.1007/JHEP10(2017)162 [arXiv:1707.01434 [hep-ph]].

[133] S. Bhattacharya, J. L. Diaz-Cruz, E. Ma and D. Wegman, Phys. Rev. D **85**, 055008 (2012) doi:10.1103/PhysRevD.85.055008 [arXiv:1107.2093 [hep-ph]].

[134] J. L. Diaz-Cruz and E. Ma, Phys. Lett. B **695**, 264 (2011) doi:10.1016/j.physletb.2010.11.039 [arXiv:1007.2631 [hep-ph]].

[135] Y. Farzan and A. R. Akbarieh, Phys. Lett. B **724**, 84 (2013) doi:10.1016/j.physletb.2013.06.004 [arXiv:1211.4685 [hep-ph]].

[136] Y. G. Kim and K. Y. Lee, Phys. Rev. D **75**, 115012 (2007) doi:10.1103/PhysRevD.75.115012 [hep-ph/0611069].

[137] Y. G. Kim, K. Y. Lee and S. Shin, JHEP **0805**, 100 (2008) doi:10.1088/1126-6708/2008/05/100 [arXiv:0803.2932 [hep-ph]].

[138] Y. G. Kim and S. Shin, JHEP **0905**, 036 (2009) doi:10.1088/1126-6708/2009/05/036 [arXiv:0901.2609 [hep-ph]].

[139] S. M. Boucenna, S. Morisi, Q. Shafi and J. W. F. Valle, Phys. Rev. D **90**, no. 5, 055023 (2014) doi:10.1103/PhysRevD.90.055023 [arXiv:1404.3198 [hep-ph]].

[140] V. Berezinsky and J. W. F. Valle, Phys. Lett. B **318**, 360 (1993) doi:10.1016/0370-2693(93)90140-D [hep-ph/9309214].

[141] S. Bhattacharya, B. Meli? and J. Wudka, JHEP **1402** (2014) 115 doi:10.1007/JHEP02(2014)115 [arXiv:1307.2647 [hep-ph]].

[142] Y. Ametani, M. Aoki, H. Goto and J. Kubo, Phys. Rev. D **91**, no. 11, 115007 (2015) doi:10.1103/PhysRevD.91.115007 [arXiv:1505.00128 [hep-ph]].

[143] G. Ballesteros, J. Redondo, A. Ringwald and C. Tamarit, Phys. Rev. Lett. **118**, no. 7, 071802 (2017) doi:10.1103/PhysRevLett.118.071802 [arXiv:1608.05414 [hep-ph]].

[144] M. Lattanzi, AIP Conf. Proc. **966**, 163 (2007) doi:10.1063/1.2836988 [arXiv:0802.3155 [astro-ph]].

[145] N. Rojas, R. A. Lineros and F. Gonzalez-Canales, arXiv:1703.03416 [hep-ph].

[146] P. H. Gu, E. Ma and U. Sarkar, Phys. Lett. B **690**, 145 (2010) doi:10.1016/j.physletb.2010.05.012 [arXiv:1004.1919 [hep-ph]].

[147] M. Frigerio, T. Hambye and E. Masso, Phys. Rev. X **1**, 021026 (2011) doi:10.1103/PhysRevX.1.021026 [arXiv:1107.4564 [hep-ph]].

[148] C. Garcia-Cely and J. Heeck, JHEP **1705**, 102 (2017) doi:10.1007/JHEP05(2017)102 [arXiv:1701.07209 [hep-ph]].

[149] J. M. Cline, Z. Liu, G. Moore and W. Xue, Phys. Rev. D **90** (2014) no.1, 015023 doi:10.1103/PhysRevD.90.015023 [arXiv:1312.3325 [hep-ph]].

[150] J. Kopp, J. Liu, T. R. Slatyer, X. P. Wang and W. Xue, JHEP **1612** (2016) 033 doi:10.1007/JHEP12(2016)033 [arXiv:1609.02147 [hep-ph]].

[151] Y. Wu, T. Ma, B. Zhang and G. Cacciapaglia, JHEP **1711**, 058 (2017) doi:10.1007/JHEP11(2017)058 [arXiv:1703.06903 [hep-ph]].

[152] G. Ballesteros, A. Carmona and M. Chala, Eur. Phys. J. C **77**, no. 7, 468 (2017) doi:10.1140/epjc/s10052-017-5040-1 [arXiv:1704.07388 [hep-ph]].

[153] R. Balkin, G. Perez and A. Weiler, Eur. Phys. J. C **78**, no. 2, 104 (2018) doi:10.1140/epjc/s10052-018-5552-3 [arXiv:1707.09980 [hep-ph]].

[154] M. Frigerio, A. Pomarol, F. Riva and A. Urbano, JHEP **1207**, 015 (2012) doi:10.1007/JHEP07(2012)015 [arXiv:1204.2808 [hep-ph]].

[155] O. Antipin, M. Redi, A. Strumia and E. Vigiani, JHEP **1507**, 039 (2015) doi:10.1007/JHEP07(2015)039 [arXiv:1503.08749 [hep-ph]].

[156] D. Marzocca and A. Urbano, JHEP **1407**, 107 (2014) doi:10.1007/JHEP07(2014)107 [arXiv:1404.7419 [hep-ph]].

[157] M. Y. Khlopov and C. Kouvaris, Phys. Rev. D **78**, 065040 (2008) doi:10.1103/PhysRevD.78.065040 [arXiv:0806.1191 [astro-ph]].

[158] K. A. Olive, hep-ph/0412054.

[159] F. D. Steffen, arXiv:0711.1240 [hep-ph].

[160] P. Gondolo and G. Gelmini, Nucl. Phys. B **360**, 145 (1991). doi:10.1016/0550-3213(91)90438-4

[161] J. Ellis and K. A. Olive, In *Bertone, G. (ed.): Particle dark matter* 142-163 [arXiv:1001.3651 [astro-ph.CO]].

[162] R. T. Co, L. J. Hall and K. Harigaya, Phys. Rev. Lett. **120**, no. 21, 211602 (2018) doi:10.1103/PhysRevLett.120.211602 [arXiv:1711.10486 [hep-ph]].

[163] J. C. Montero, A. Romero and B. L. Snchez-Vega, Phys. Rev. D **97**, no. 6, 063015 (2018) doi:10.1103/PhysRevD.97.063015 [arXiv:1709.04535 [hep-ph]].

[164] V. B. .Klaer and G. D. .Moore, JCAP **1711**, no. 11, 049 (2017) doi:10.1088/1475-7516/2017/11/049 [arXiv:1708.07521 [hep-ph]].

[165] H. Fukuda, M. Ibe and T. T. Yanagida, Phys. Rev. D **95**, no. 9, 095017 (2017) doi:10.1103/PhysRevD.95.095017 [arXiv:1702.00227 [hep-ph]].

[166] A. Ringwald, PoS NOW **2016**, 081 (2016) doi:10.22323/1.283.0081 [arXiv:1612.08933 [hep-ph]].

[167] A. Ringwald and K. Saikawa, Phys. Rev. D **93**, no. 8, 085031 (2016) Addendum: [Phys. Rev. D **94**, no. 4, 049908 (2016)] doi:10.1103/PhysRevD.93.085031, 10.1103/PhysRevD.94.049908 [arXiv:1512.06436 [hep-ph]].

[168] E. Di Valentino, E. Giusarma, M. Lattanzi, A. Melchiorri and O. Mena, Phys. Rev. D **90**, no. 4, 043534 (2014) doi:10.1103/PhysRevD.90.043534 [arXiv:1405.1860 [astro-ph.CO]].

[169] E. J. Chun, Phys. Lett. B **735**, 164 (2014) doi:10.1016/j.physletb.2014.06.017 [arXiv:1404.4284 [hep-ph]].

[170] L. Visinelli and P. Gondolo, Phys. Rev. Lett. **113**, 011802 (2014) doi:10.1103/PhysRevLett.113.011802 [arXiv:1403.4594 [hep-ph]].

[171] K. S. Jeong, M. Kawasaki and F. Takahashi, JCAP **1402**, 046 (2014) doi:10.1088/1475-7516/2014/02/046 [arXiv:1310.1774 [hep-ph]].

[172] O. Erken, P. Sikivie, H. Tam and Q. Yang, Phys. Rev. Lett. **108**, 061304 (2012) doi:10.1103/PhysRevLett.108.061304 [arXiv:1104.4507 [astro-ph.CO]].

[173] H. Baer, A. D. Box and H. Summy, JHEP **0908**, 080 (2009) doi:10.1088/1126-6708/2009/08/080 [arXiv:0906.2595 [hep-ph]].

[174] L. D. Duffy and K. van Bibber, New J. Phys. **11**, 105008 (2009) doi:10.1088/1367-2630/11/10/105008 [arXiv:0904.3346 [hep-ph]].

[175] L. Visinelli and P. Gondolo, Phys. Rev. D **80**, 035024 (2009) doi:10.1103/PhysRevD.80.035024 [arXiv:0903.4377 [astro-ph.CO]].

[176] J. c. Hwang and H. Noh, Phys. Lett. B **680**, 1 (2009) doi:10.1016/j.physletb.2009.08.031 [arXiv:0902.4738 [astro-ph.CO]].

[177] F. D. Steffen, Eur. Phys. J. C **59**, 557 (2009) doi:10.1140/epjc/s10052-008-0830-0 [arXiv:0811.3347 [hep-ph]].

[178] R. D. Peccei, Lect. Notes Phys. **741**, 3 (2008) doi:10.1007/978-3-540-73518-21 [hep-ph/0607268].

[179] J. E. Kim and G. Carosi, Rev. Mod. Phys. **82**, 557 (2010) doi:10.1103/RevModPhys.82.557 [arXiv:0807.3125 [hep-ph]].

[180] T. Marrodn Undagoitia and L. Rauch, J. Phys. G **43**, no. 1, 013001 (2016) doi:10.1088/0954-3899/43/1/013001 [arXiv:1509.08767 [physics.ins-det]].

[181] T. Li, Phys. Lett. B **782**, 497 (2018) doi:10.1016/j.physletb.2018.05.073 [arXiv:1804.02120 [hep-ph]].

[182] D. G. Cerdeno and A. M. Green, In *Bertone, G. (ed.): Particle dark matter* 347-369 [arXiv:1002.1912 [astro-ph.CO]].

[183] E. Aprile *et al.* [XENON Collaboration], Phys. Rev. Lett. **119**, no. 18, 181301 (2017) doi:10.1103/PhysRevLett.119.181301 [arXiv:1705.06655 [astro-ph.CO]].

[184] E. Aprile *et al.* [XENON Collaboration], Phys. Rev. Lett. **121**, 111302 (2018) doi:10.1103/PhysRevLett.121.111302 [arXiv:1805.12562 [astro-ph.CO]].

[185] D. S. Akerib *et al.* [LUX Collaboration], Phys. Rev. Lett. **118**, no. 2, 021303 (2017) doi:10.1103/PhysRevLett.118.021303 [arXiv:1608.07648 [astro-ph.CO]].

[186] X. Cui *et al.* [PandaX-II Collaboration], Phys. Rev. Lett. **119**, no. 18, 181302 (2017) doi:10.1103/PhysRevLett.119.181302 [arXiv:1708.06917 [astro-ph.CO]].

[187] J. M. Gaskins, Contemp. Phys. **57**, no. 4, 496 (2016) [arXiv:1604.00014 [astro-ph.HE]].

[188] J. Conrad, arXiv:1411.1925 [hep-ph].

[189] T. R. Slatyer, arXiv:1710.05137 [hep-ph].

[190] G. Altarelli and F. Feruglio, New J. Phys. **6**, 106 (2004) doi:10.1088/1367-2630/6/1/106 [hep-ph/0405048].

[191] H. Fritzsch and Z. z. Xing, Prog. Part. Nucl. Phys. **45**, 1 (2000) doi:10.1016/S0146-6410(00)00102-2 [hep-ph/9912358].

[192] V. Barger, D. Marfatia and K. Whisnant, Int. J. Mod. Phys. E **12**, 569 (2003) doi:10.1142/S0218301303001430 [hep-ph/0308123].

[193] O. Adriani *et al.* [PAMELA Collaboration], Nature **458**, 607 (2009) doi:10.1038/nature07942 [arXiv:0810.4995 [astro-ph]].

[194] M. Ackermann *et al.* [Fermi-LAT Collaboration], Phys. Rev. D **82**, 092004 (2010) doi:10.1103/PhysRevD.82.092004 [arXiv:1008.3999 [astro-ph.HE]].

[195] T. Yanagida, Prog. Theor. Phys. **64**, 1103 (1980). doi:10.1143/PTP.64.1103

[196] M. Gell-Mann, P. Ramond and R. Slansky, Conf. Proc. C **790927**, 315 (1979) [arXiv:1306.4669 [hep-th]].

[197] P. Minkowski, Phys. Lett. **67B**, 421 (1977). doi:10.1016/0370-2693(77)90435-X

[198] A. Zee, Phys. Lett. **93B**, 389 (1980) Erratum: [Phys. Lett. **95B**, 461 (1980)]. doi:10.1016/0370-2693(80)90349-4, 10.1016/0370-2693(80)90193-8

[199] M. C. Gonzalez-Garcia, M. Maltoni and T. Schwetz, JHEP **1411**, 052 (2014) doi:10.1007/JHEP11(2014)052 [arXiv:1409.5439 [hep-ph]].

[200] D. V. Forero, M. Tortola and J. W. F. Valle, Phys. Rev. D **90**, no. 9, 093006 (2014) doi:10.1103/PhysRevD.90.093006 [arXiv:1405.7540 [hep-ph]].

[201] F. Capozzi, G. L. Fogli, E. Lisi, A. Marrone, D. Montanino and A. Palazzo, Phys. Rev. D **89**, 093018 (2014) doi:10.1103/PhysRevD.89.093018 [arXiv:1312.2878 [hep-ph]].

[202] O. Lebedev and A. Westphal, Phys. Lett. B **719**, 415 (2013) doi:10.1016/j.physletb.2012.12.069 [arXiv:1210.6987 [hep-ph]].

[203] A. Kobakhidze and A. Spencer-Smith, Phys. Lett. B **722**, 130 (2013) doi:10.1016/j.physletb.2013.04.013 [arXiv:1301.2846 [hep-ph]].

[204] M. Fairbairn and R. Hogan, Phys. Rev. Lett. **112**, 201801 (2014) doi:10.1103/PhysRevLett.112.201801 [arXiv:1403.6786 [hep-ph]].

[205] A. Hook, J. Kearney, B. Shakya and K. M. Zurek, JHEP **1501**, 061 (2015) doi:10.1007/JHEP01(2015)061 [arXiv:1404.5953 [hep-ph]].

[206] M. Herranen, T. Markkanen, S. Nurmi and A. Rajantie, Phys. Rev. Lett. **113**, no. 21, 211102 (2014) doi:10.1103/PhysRevLett.113.211102 [arXiv:1407.3141 [hep-ph]].

[207] K. Kamada, Phys. Lett. B **742**, 126 (2015) doi:10.1016/j.physletb.2015.01.024 [arXiv:1409.5078 [hep-ph]].

[208] J. R. Espinosa, G. F. Giudice, E. Morgante, A. Riotto, L. Senatore, A. Strumia and N. Tetradis, JHEP **1509**, 174 (2015) doi:10.1007/JHEP09(2015)174 [arXiv:1505.04825 [hep-ph]].

[209] J. Kearney, H. Yoo and K. M. Zurek, Phys. Rev. D **91**, no. 12, 123537 (2015) doi:10.1103/PhysRevD.91.123537 [arXiv:1503.05193 [hep-th]].

[210] Y. Ema, K. Mukaida and K. Nakayama, JCAP **1610**, no. 10, 043 (2016) doi:10.1088/1475-7516/2016/10/043 [arXiv:1602.00483 [hep-ph]].

[211] M. Herranen, T. Markkanen, S. Nurmi and A. Rajantie, Phys. Rev. Lett. **115**, 241301 (2015) doi:10.1103/PhysRevLett.115.241301 [arXiv:1506.04065 [hep-ph]].

[212] K. Kohri and H. Matsui, Phys. Rev. D **94**, no. 10, 103509 (2016) doi:10.1103/PhysRevD.94.103509 [arXiv:1602.02100 [hep-ph]].

[213] K. Enqvist, T. Meriniemi and S. Nurmi, JCAP **1407**, 025 (2014) doi:10.1088/1475-7516/2014/07/025 [arXiv:1404.3699 [hep-ph]].

[214] A. Shkerin and S. Sibiryakov, Phys. Lett. B **746**, 257 (2015) doi:10.1016/j.physletb.2015.05.012 [arXiv:1503.02586 [hep-ph]].

[215] A. Joti, A. Katsis, D. Loupas, A. Salvio, A. Strumia, N. Tetradis and A. Urbano, JHEP **1707**, 058 (2017) doi:10.1007/JHEP07(2017)058 [arXiv:1706.00792 [hep-ph]].

[216] K. Enqvist, M. Karciauskas, O. Lebedev, S. Rusak and M. Zatta, JCAP **1611**, 025 (2016) doi:10.1088/1475-7516/2016/11/025 [arXiv:1608.08848 [hep-ph]].

[217] M. Postma and J. van de Vis, JCAP **1705**, no. 05, 004 (2017) doi:10.1088/1475-7516/2017/05/004 [arXiv:1702.07636 [hep-ph]].

[218] Y. Ema, K. Mukaida and K. Nakayama, JCAP **1712**, no. 12, 030 (2017) doi:10.1088/1475-7516/2017/12/030 [arXiv:1706.08920 [hep-ph]].

[219] J. A. Casas, J. R. Espinosa and M. Quiros, Phys. Lett. B **342**, 171 (1995) doi:10.1016/0370-2693(94)01404-Z [hep-ph/9409458].

[220] C. Ford, I. Jack and D. R. T. Jones, Nucl. Phys. B **387**, 373 (1992) Erratum: [Nucl. Phys. B **504**, 551 (1997)] doi:10.1016/0550-3213(92)90165-8, 10.1016/S0550-3213(97)00532-4 [hep-ph/0111190].

[221] M. B. Einhorn and D. R. T. Jones, JHEP **0704**, 051 (2007) doi:10.1088/1126-6708/2007/04/051 [hep-ph/0702295 [HEP-PH]].

[222] M. F. Zoller, Subnucl. Ser. **50**, 557 (2014) doi:10.1142/9789814603904-0034 [arXiv:1209.5609 [hep-ph]].

[223] M. Zoller, PoS EPS **-HEP2013**, 322 (2013) doi:10.22323/1.180.0322 [arXiv:1311.5085 [hep-ph]].

[224] K. G. Chetyrkin and M. F. Zoller, JHEP **1206**, 033 (2012) doi:10.1007/JHEP06(2012)033 [arXiv:1205.2892 [hep-ph]].

[225] L. N. Mihaila, J. Salomon and M. Steinhauser, Phys. Rev. Lett. **108**, 151602 (2012) doi:10.1103/PhysRevLett.108.151602 [arXiv:1201.5868 [hep-ph]].

[226] A. V. Bednyakov, A. F. Pikelner and V. N. Velizhanin, Phys. Lett. B **737**, 129 (2014) doi:10.1016/j.physletb.2014.08.049 [arXiv:1406.7171 [hep-ph]].

[227] C. Bonilla, R. M. Fonseca and J. W. F. Valle, Phys. Lett. B **756**, 345 (2016) doi:10.1016/j.physletb.2016.03.037 [arXiv:1506.04031 [hep-ph]].

[228] A. K. Saha and A. Sil, JHEP **1511**, 118 (2015) doi:10.1007/JHEP11(2015)118 [arXiv:1509.00218 [hep-ph]].

[229] H. Murayama, H. Suzuki, T. Yanagida and J. Yokoyama, Phys. Rev. Lett. **70**, 1912 (1993).

[230] J. R. Ellis, Nucl. Phys. Proc. Suppl. **137**, 190 (2004) [hep-ph/0403247].

[231] S. Khalil and A. Sil, Phys. Rev. D **84**, 103511 (2011) [arXiv:1108.1973 [hep-ph]].

[232] H. Murayama, K. Nakayama, F. Takahashi and T. T. Yanagida, Phys. Lett. B **738**, 196 (2014) [arXiv:1404.3857 [hep-ph]].

[233] J. L. Evans, T. Gherghetta and M. Peloso, Phys. Rev. D **92**, no. 2, 021303 (2015) [arXiv:1501.06560 [hep-ph]].

[234] S. Dimopoulos and S. Raby, Nucl. Phys. B **192**, 353 (1981). doi:10.1016/0550-3213(81)90430-2

[235] M. Dine, W. Fischler and M. Srednicki, Nucl. Phys. B **189**, 575 (1981). doi:10.1016/0550-3213(81)90582-4

[236] S. Dimopoulos and H. Georgi, Nucl. Phys. B **193**, 150 (1981). doi:10.1016/0550-3213(81)90522-8

[237] N. Sakai, Z. Phys. C **11**, 153 (1981). doi:10.1007/BF01573998

[238] R. K. Kaul and P. Majumdar, Nucl. Phys. B **199**, 36 (1982). doi:10.1016/0550-3213(82)90565-X

[239] J. Wess and J. Bagger, Princeton, USA: Univ. Pr. (1992) 259 p

[240] P. P. Srivastava, Bristol, Uk: Hilger (1986) 162 P. (Graduate Student Series In Physics)

[241] P. Ramond, Front. Phys. **101**, 1 (1999).

[242] R. N. Mohapatra, New York, USA: Springer (2003) 421 p. doi:10.1007/978-1-4757-1928-4

[243] I. L. Buchbinder and S. M. Kuzenko, Bristol, UK: IOP (1998) 656 p

[244] S. Weinberg,

[245] M. Drees, R. Godbole and P. Roy, Hackensack, USA: World Scientific (2004) 555 p

[246] N. Polonsky, Lect. Notes Phys. Monogr. **68**, 1 (2001) doi:10.1007/3-540-44642-7 [hep-ph/0108236].

[247] M. Dine, Cambridge, UK: Cambridge Univ. Pr. (2007) 515 p

[248] S. P. Martin, Adv. Ser. Direct. High Energy Phys. **21**, 1 (2010) [Adv. Ser. Direct. High Energy Phys. **18**, 1 (1998)] doi:10.1142/9789812839657-0001, 10.1142/9789814307505-0001 [hep-ph/9709356].

[249] L. O'Raifeartaigh, Nucl. Phys. B **96**, 331 (1975). doi:10.1016/0550-3213(75)90585-4

[250] A. E. Nelson and N. Seiberg, Nucl. Phys. B **416**, 46 (1994) doi:10.1016/0550-3213(94)90577-0 [hep-ph/9309299].

[251] J. R. Ellis, C. H. Llewellyn Smith and G. G. Ross, Phys. Lett. **114B**, 227 (1982). doi:10.1016/0370-2693(82)90482-8

[252] M. A. Luty and J. Terning, Phys. Rev. D **62**, 075006 (2000) doi:10.1103/PhysRevD.62.075006 [hep-ph/9812290].

[253] N. J. Craig, P. J. Fox and J. G. Wacker, Phys. Rev. D **75**, 085006 (2007) doi:10.1103/PhysRevD.75.085006 [hep-th/0611006].

[254] W. Fischler, V. Kaplunovsky, C. Krishnan, L. Mannelli and M. A. C. Torres, JHEP **0703**, 107 (2007) doi:10.1088/1126-6708/2007/03/107 [hep-th/0611018].

[255] S. A. Abel, C. S. Chu, J. Jaeckel and V. V. Khoze, JHEP **0701**, 089 (2007) doi:10.1088/1126-6708/2007/01/089 [hep-th/0610334].

[256] K. A. Intriligator, N. Seiberg and D. Shih, JHEP **0604**, 021 (2006) [hep-th/0602239].

[257] K. A. Intriligator, N. Seiberg and D. Shih, JHEP **0707**, 017 (2007) doi:10.1088/1126-6708/2007/07/017 [hep-th/0703281].

[258] S. A. Abel, J. Jaeckel and V. V. Khoze, JHEP **0701**, 015 (2007) doi:10.1088/1126-6708/2007/01/015 [hep-th/0611130].

[259] K. A. Intriligator and N. Seiberg, Class. Quant. Grav. **24**, S741 (2007) [hep-ph/0702069].

[260] E. Witten, Nucl. Phys. B **188**, 513 (1981). doi:10.1016/0550-3213(81)90006-7

[261] K. A. Intriligator, N. Seiberg and S. H. Shenker, Phys. Lett. B **342**, 152 (1995) doi:10.1016/0370-2693(94)01336-B [hep-ph/9410203].

[262] J. Bagger, E. Poppitz and L. Randall, Nucl. Phys. B **426**, 3 (1994) doi:10.1016/0550-3213(94)90123-6 [hep-ph/9405345].

[263] M. Kawasaki, M. Yamaguchi and T. Yanagida, Phys. Rev. Lett. **85**, 3572 (2000) [hep-ph/0004243].

[264] M. Kawasaki, M. Yamaguchi and T. Yanagida, Phys. Rev. D **63**, 103514 (2001) [hep-ph/0011104].

[265] K. Harigaya, M. Kawasaki and T. T. Yanagida, Phys. Lett. B **741**, 267 (2015) [arXiv:1410.7163 [hep-ph]].

[266] T. Li, Z. Li and D. V. Nanopoulos, JCAP **1402**, 028 (2014) [arXiv:1311.6770 [hep-ph]].

[267] K. Nakayama, F. Takahashi and T. T. Yanagida, JCAP **1308**, 038 (2013) [arXiv:1305.5099 [hep-ph]].

[268] K. Nakayama, F. Takahashi and T. T. Yanagida, Phys. Lett. B **737**, 151 (2014) [arXiv:1407.7082 [hep-ph]].

[269] M. E. Peskin, hep-th/9702094.

[270] M. A. Shifman, Prog. Part. Nucl. Phys. **39**, 1 (1997) doi:10.1016/S0146-6410(97)00042-2 [hep-th/9704114].

[271] M. J. Strassler, doi:10.1142/9789812702821-0011 hep-th/0309149.

[272] T. R. Taylor, G. Veneziano and S. Yankielowicz, Nucl. Phys. B **218**, 493 (1983). doi:10.1016/0550-3213(83)90377-2

[273] A. C. Davis, M. Dine and N. Seiberg, Phys. Lett. **125B**, 487 (1983). doi:10.1016/0370-2693(83)91332-1

[274] N. Seiberg, Nucl. Phys. B **435**, 129 (1995) doi:10.1016/0550-3213(94)00023-8 [hep-th/9411149].

[275] A. Giveon, A. Katz, Z. Komargodski and D. Shih, JHEP **0810**, 092 (2008) doi:10.1088/1126-6708/2008/10/092 [arXiv:0808.2901 [hep-th]].

[276] I. Affleck, M. Dine and N. Seiberg, Nucl. Phys. B **241**, 493 (1984). doi:10.1016/0550-3213(84)90058-0

[277] P. Brax, C. A. Savoy and A. Sil, Phys. Lett. B **671**, 374 (2009) [arXiv:0807.1569 [hep-ph]].

[278] C. A. Savoy and A. Sil, Phys. Lett. B **660**, 236 (2008) [arXiv:0709.1923 [hep-ph]].

[279] P. Brax, C. A. Savoy and A. Sil, JHEP **0904**, 092 (2009) [arXiv:0902.0972 [hep-ph]].

[280] N. J. Craig, JHEP **0802**, 059 (2008) [arXiv:0801.2157 [hep-th]].

[281] S. Abel, C. Durnford, J. Jaeckel and V. V. Khoze, Phys. Lett. B **661**, 201 (2008) [arXiv:0707.2958 [hep-ph]].

[282] G. ›t Hooft, in *Recent Developments in Gauge Theories*, edited by G. ›t Hooftet al. (Plenum, Carg′ese, 1980).

[283] K. Harigaya, M. Ibe, M. Kawasaki and T. T. Yanagida, arXiv:1506.05250 [hep-ph].

[284] C. Pallis, Phys. Rev. D **91**, no. 12, 123508 (2015) [arXiv:1503.05887 [hep-ph]].

[285] G. Barenboim and W. I. Park, arXiv:1504.02080 [astro-ph.CO].

[286] L. M. Carpenter and S. Raby, Phys. Lett. B **738**, 109 (2014) [arXiv:1405.6143 [hep-ph]].

[287] L. Heurtier, S. Khalil and A. Moursy, arXiv:1505.07366 [hep-ph].

[288] W. Buchmuller, E. Dudas, L. Heurtier and C. Wieck, JHEP **1409**, 053 (2014) [arXiv:1407.0253 [hep-th]].

[289] K. Harigaya, M. Ibe, K. Schmitz and T. T. Yanagida, Phys. Rev. D **90**, no. 12, 123524 (2014) [arXiv:1407.3084 [hep-ph]].

[290] K. Harigaya, M. Ibe, K. Schmitz and T. T. Yanagida, Phys. Lett. B **733**, 283 (2014) [arXiv:1403.4536 [hep-ph]].

[291] X. Gao, T. Li and P. Shukla, Phys. Lett. B **738**, 412 (2014) [arXiv:1404.5230 [hep-ph]].

[292] R. Barbieri, L. J. Hall, D. Tucker-Smith, A. Strumia and N. Weiner, JHEP **9812**, 017 (1998) [hep-ph/9807235].

[293] K. A. Olive *et al.* [Particle Data Group Collaboration], Chin. Phys. C **38**, 090001 (2014).

[294] K. S. Babu and R. N. Mohapatra, Phys. Lett. B **532**, 77 (2002) [hep-ph/0201176].

[295] B. Karmakar and A. Sil, arXiv:1509.07090 [hep-ph].

[296] M. Kawasaki, F. Takahashi and T. T. Yanagida, Phys. Rev. D **74**, 043519 (2006) [hep-ph/0605297].

[297] M. Kawasaki, F. Takahashi and T. T. Yanagida, Phys. Lett. B **638**, 8 (2006) [hep-ph/0603265].

[298] M. Kawasaki, K. Kohri, T. Moroi and A. Yotsuyanagi, Phys. Rev. D **78**, 065011 (2008) [arXiv:0804.3745 [hep-ph]].

[299] M. Viel, J. Lesgourgues, M. G. Haehnelt, S. Matarrese and A. Riotto, Phys. Rev. D **71**, 063534 (2005) [astro-ph/0501562].

[300] K. Kohri, M. Yamaguchi and J. Yokoyama, Phys. Rev. D **70**, 043522 (2004) [hep-ph/0403043].

[301] H. Fukushima and R. Kitano, JHEP **1401**, 081 (2014) [arXiv:1311.6228 [hep-ph]].

[302] W. Buchmuller and T. Yanagida, Phys. Lett. B **445**, 399 (1999) [hep-ph/9810308].

[303] E. E. Jenkins and A. V. Manohar, Phys. Lett. B **668**, 210 (2008) [arXiv:0807.4176 [hep-ph]].

[304] A. K. Saha and A. Sil, Phys. Lett. B **765**, 244 (2017) doi:10.1016/j.physletb.2016.12.031 [arXiv:1608.04919 [hep-ph]].

[305] R. Kallosh and A. Linde, JCAP **1011**, 011 (2010) doi:10.1088/1475-7516/2010/11/011 [arXiv:1008.3375 [hep-th]].

[306] K. Harigaya, M. Ibe, K. Schmitz and T. T. Yanagida, Phys. Lett. B **720**, 125 (2013) doi:10.1016/j.physletb.2013.01.058 [arXiv:1211.6241 [hep-ph]].

[307] K. Nakayama, F. Takahashi and T. T. Yanagida, Phys. Lett. B **725**, 111 (2013) doi:10.1016/j.physletb.2013.06.050 [arXiv:1303.7315 [hep-ph]].

[308] W. E. East, J. Kearney, B. Shakya, H. Yoo and K. M. Zurek, [arXiv:1607.00381 [hep-ph]].

[309] C. Gross, O. Lebedev and M. Zatta, Phys. Lett. B **753**, 178 (2016) doi:10.1016/j.physletb.2015.12.014 [arXiv:1506.05106 [hep-ph]].

[310] Y. Ema, K. Mukaida and K. Nakayama, arXiv:1605.07342 [hep-ph].

[311] L. A. Anchordoqui, I. Antoniadis, H. Goldberg, X. Huang, D. Lust, T. R. Taylor and B. Vlcek, JHEP **1302**, 074 (2013) doi:10.1007/JHEP02(2013)074 [arXiv:1208.2821 [hep-ph]].

[312] L. Basso, O. Fischer and J. J. van Der Bij, Phys. Lett. B **730**, 326 (2014) doi:10.1016/j.physletb.2014.01.064 [arXiv:1309.6086 [hep-ph]].

[313] O. Fischer, arXiv:1607.00282 [hep-ph].

[314] K. Bhattacharya, J. Chakrabortty, S. Das and T. Mondal, JCAP **1412**, no. 12, 001 (2014) doi:10.1088/1475-7516/2014/12/001 [arXiv:1408.3966 [hep-ph]].

[315] Y. Mambrini, N. Nagata, K. A. Olive and J. Zheng, arXiv:1602.05583 [hep-ph].

[316] S. Khan, S. Goswami and S. Roy, Phys. Rev. D **89**, no. 7, 073021 (2014) doi:10.1103/PhysRevD.89.073021 [arXiv:1212.3694 [hep-ph]].

[317] A. Datta, A. Elsayed, S. Khalil and A. Moursy, Phys. Rev. D **88**, no. 5, 053011 (2013) doi:10.1103/PhysRevD.88.053011 [arXiv:1308.0816 [hep-ph]].

[318] J. Chakrabortty, P. Konar and T. Mondal, Phys. Rev. D **89**, no. 5, 056014 (2014) doi:10.1103/PhysRevD.89.056014 [arXiv:1308.1291 [hep-ph]].

[319] A. Kobakhidze and A. Spencer-Smith, JHEP **1308**, 036 (2013) doi:10.1007/JHEP08(2013)036 [arXiv:1305.7283 [hep-ph]].

[320] S. Baek, H. Okada and T. Toma, JCAP **1406**, 027 (2014) doi:10.1088/1475-7516/2014/06/027 [arXiv:1312.3761 [hep-ph]].

[346] C. Coriano, L. Delle Rose and C. Marzo, Phys. Lett. B **738**, 13 (2014) doi:10.1016/j.physletb.2014.09.001 [arXiv:1407.8539 [hep-ph]].

[322] R. N. Mohapatra and Y. Zhang, JHEP **1406**, 072 (2014) doi:10.1007/JHEP06(2014)072 [arXiv:1401.6701 [hep-ph]].

[323] N. Haba and Y. Yamaguchi, PTEP **2015**, no. 9, 093B05 (2015) doi:10.1093/ptep/ptv121 [arXiv:1504.05669 [hep-ph]].

[324] L. Delle Rose, C. Marzo and A. Urbano, JHEP **1512**, 050 (2015) doi:10.1007/JHEP12(2015)050 [arXiv:1506.03360 [hep-ph]].

[325] A. Das, N. Okada and N. Papapietro, arXiv:1509.01466 [hep-ph].

[326] N. Haba, H. Ishida, N. Okada and Y. Yamaguchi, Eur. Phys. J. C **76**, no. 6, 333 (2016) doi:10.1140/epjc/s10052-016-4180-z [arXiv:1601.05217 [hep-ph]].

[347] J. N. Ng and A. de la Puente, Eur. Phys. J. C **76**, no. 3, 122 (2016) doi:10.1140/epjc/s10052-016-3981-4 [arXiv:1510.00742 [hep-ph]].

[328] K. Mukaida and K. Nakayama, JCAP **1408**, 062 (2014) doi:10.1088/1475-7516/2014/08/062 [arXiv:1404.1880 [hep-ph]].

[329] M. Fukugita and T. Yanagida, Phys. Lett. B **174**, 45 (1986). doi:10.1016/0370-2693(86)91126-3

[330] M. Flanz, E. A. Paschos and U. Sarkar, Phys. Lett. B **345**, 248 (1995) Erratum: [Phys. Lett. B **384**, 487 (1996)] Erratum: [Phys. Lett. B **382**, 447 (1996)] doi:10.1016/0370-2693(96)00866-0, 10.1016/0370-2693(96)00842-8, 10.1016/0370-2693(94)01555-Q [hep-ph/9411366].

[331] L. Covi, E. Roulet and F. Vissani, Phys. Lett. B **384**, 169 (1996) doi:10.1016/0370-2693(96)00817-9 [hep-ph/9605319].

[332] M. Plumacher, Z. Phys. C **74**, 549 (1997) doi:10.1007/s002880050418 [hep-ph/9604229].

[333] W. Buchmuller and M. Plumacher, Phys. Lett. B **431**, 354 (1998) doi:10.1016/S0370-2693(97)01548-7 [hep-ph/9710460].

[334] V. Silveira and A. Zee, Phys. Lett. **161B**, 136 (1985). doi:10.1016/0370-2693(85)90624-0

[335] J. M. Cline, K. Kainulainen, P. Scott and C. Weniger, Phys. Rev. D **88**, 055025 (2013) Erratum: [Phys. Rev. D **92**, no. 3, 039906 (2015)] doi:10.1103/PhysRevD.92.039906, 10.1103/PhysRevD.88.055025 [arXiv:1306.4710 [hep-ph]].

[336] F. S. Queiroz and K. Sinha, Phys. Lett. B **735**, 69 (2014) doi:10.1016/j.physletb.2014.06.016 [arXiv:1404.1400 [hep-ph]].

[337] K. Ghorbani and H. Ghorbani, Phys. Rev. D **93**, no. 5, 055012 (2016) doi:10.1103/PhysRevD.93.055012 [arXiv:1501.00206 [hep-ph]].

[338] S. Bhattacharya, S. Jana and S. Nandi, Phys. Rev. D **95**, no. 5, 055003 (2017) doi:10.1103/PhysRevD.95.055003 [arXiv:1609.03274 [hep-ph]].

[339] S. Bhattacharya, P. Poulose and P. Ghosh, arXiv:1607.08461 [hep-ph].

[340] J. A. Casas, D. G. Cerdeo, J. M. Moreno and J. Quilis, arXiv:1701.08134 [hep-ph].

[341] P. Athron *et al.* [GAMBIT Collaboration], arXiv:1705.07931 [hep-ph].

[342] N. Haba, K. Kaneta and R. Takahashi, JHEP **1404**, 029 (2014) doi:10.1007/JHEP04(2014)029 [arXiv:1312.2089 [hep-ph]].

[343] M. Lindner, H. H. Patel and B. Radovi, Phys. Rev. D **93**, no. 7, 073005 (2016) doi:10.1103/PhysRevD.93.073005 [arXiv:1511.06215 [hep-ph]].

[344] G. Bambhaniya, P. S. B. Dev, S. Goswami, S. Khan and W. Rodejohann, arXiv:1611.03827 [hep-ph].

[345] J. Chakrabortty, M. Das and S. Mohanty, Mod. Phys. Lett. A **28**, 1350032 (2013) doi:10.1142/S0217732313500326 [arXiv:1207.2027 [hep-ph]].

[346] C. Coriano, L. Delle Rose and C. Marzo, Phys. Lett. B **738**, 13 (2014) doi:10.1016/j.physletb.2014.09.001 [arXiv:1407.8539 [hep-ph]].

[347] J. N. Ng and A. de la Puente, Eur. Phys. J. C **76**, no. 3, 122 (2016) doi:10.1140/epjc/s10052-016-3981-4 [arXiv:1510.00742 [hep-ph]].

[348] W. Rodejohann and H. Zhang, JHEP **1206**, 022 (2012) doi:10.1007/JHEP06(2012)022 [arXiv:1203.3825 [hep-ph]].

[349] E. Ma, Phys. Rev. D **73**, 077301 (2006) doi:10.1103/PhysRevD.73.077301 [hep-ph/0601225].

[350] H. Davoudiasl and I. M. Lewis, Phys. Rev. D **90**, no. 3, 033003 (2014) doi:10.1103/PhysRevD.90.033003 [arXiv:1404.6260 [hep-ph]].

[351] N. Chakrabarty, D. K. Ghosh, B. Mukhopadhyaya and I. Saha, Phys. Rev. D **92**, no. 1, 015002 (2015) doi:10.1103/PhysRevD.92.015002 [arXiv:1501.03700 [hep-ph]].

[352] A. Abada and S. Nasri, Phys. Rev. D **88**, no. 1, 016006 (2013) doi:10.1103/PhysRevD.88.016006 [arXiv:1304.3917 [hep-ph]].

[353] A. Ahriche, A. Arhrib and S. Nasri, JHEP **1402**, 042 (2014) doi:10.1007/JHEP02(2014)042 [arXiv:1309.5615 [hep-ph]].

[354] N. Chakrabarty, U. K. Dey and B. Mukhopadhyaya, JHEP **1412**, 166 (2014) doi:10.1007/JHEP12(2014)166 [arXiv:1407.2145 [hep-ph]].

[355] D. Das and I. Saha, Phys. Rev. D **91**, no. 9, 095024 (2015) doi:10.1103/PhysRevD.91.095024 [arXiv:1503.02135 [hep-ph]].

[356] N. Chakrabarty and B. Mukhopadhyaya, Eur. Phys. J. C **77**, no. 3, 153 (2017) doi:10.1140/epjc/s10052-017-4705-0 [arXiv:1603.05883 [hep-ph]].

[357] G. Arcadi, M. Dutra, P. Ghosh, M. Lindner, Y. Mambrini, M. Pierre, S. Profumo and F. S. Queiroz, arXiv:1703.07364 [hep-ph].

[358] N. Okada and Q. Shafi, Phys. Lett. B **747**, 223 (2015) doi:10.1016/j.physletb.2015.06.001 [arXiv:1501.05375 [hep-ph]].

[359] G. R. Dvali, Z. Tavartkiladze and J. Nanobashvili, Phys. Lett. B **352**, 214 (1995) doi:10.1016/0370-2693(95)00511-I [hep-ph/9411387].

[360] K. Kannike, Eur. Phys. J. C **72**, 2093 (2012) doi:10.1140/epjc/s10052-012-2093-z [arXiv:1205.3781 [hep-ph]].

[361] J. Chakrabortty, P. Konar and T. Mondal, Phys. Rev. D **89**, no. 9, 095008 (2014) doi:10.1103/PhysRevD.89.095008 [arXiv:1311.5666 [hep-ph]].

[362] J. Horejsi and M. Kladiva, Eur. Phys. J. C **46**, 81 (2006) doi:10.1140/epjc/s2006-02472-3 [hep-ph/0510154].

[363] G. Bhattacharyya and D. Das, Pramana **87**, no. 3, 40 (2016) doi:10.1007/s12043-016-1252-4 [arXiv:1507.06424 [hep-ph]].

[364] D. Lpez-Val and T. Robens, Phys. Rev. D **90**, 114018 (2014) doi:10.1103/PhysRevD.90.114018 [arXiv:1406.1043 [hep-ph]].

[365] V. Khachatryan *et al.* [CMS Collaboration], JHEP **1510**, 144 (2015) doi:10.1007/JHEP10(2015)144 [arXiv:1504.00936 [hep-ex]].

[366] G. Aad *et al.* [ATLAS Collaboration], Eur. Phys. J. C **76**, no. 1, 45 (2016) doi:10.1140/epjc/s10052-015-3820-z [arXiv:1507.05930 [hep-ex]].

[367] S. Chatrchyan *et al.* [CMS Collaboration], Phys. Rev. D **89**, no. 9, 092007 (2014) doi:10.1103/PhysRevD.89.092007 [arXiv:1312.5353 [hep-ex]].

[368] CMS Collaboration (2012), CMS-PAS-HIG-12-045.

[369] CMS Collaboration (2013), CMS-PAS-HIG-13-003.

[370] M. J. Strassler and K. M. Zurek, Phys. Lett. B **661**, 263 (2008) doi:10.1016/j.physletb.2008.02.008 [hep-ph/0605193].

[371] T. Robens and T. Stefaniak, Eur. Phys. J. C **76**, no. 5, 268 (2016) doi:10.1140/epjc/s10052-016-4115-8 [arXiv:1601.07880 [hep-ph]].

[372] G. Belanger, F. Boudjema, A. Pukhov and A. Semenov, Comput. Phys. Commun. **185**, 960 (2014) doi:10.1016/j.cpc.2013.10.016 [arXiv:1305.0237 [hep-ph]].

[373] T. Robens and T. Stefaniak, Eur. Phys. J. C **75**, 104 (2015) doi:10.1140/epjc/s10052-015-3323-y [arXiv:1501.02234 [hep-ph]].

[374] G. Chalons, D. Lopez-Val, T. Robens and T. Stefaniak, PoS ICHEP **2016**, 1180 (2016) [arXiv:1611.03007 [hep-ph]].

[375] S. Dawson and I. M. Lewis, Phys. Rev. D **92**, no. 9, 094023 (2015) doi:10.1103/PhysRevD.92.094023 [arXiv:1508.05397 [hep-ph]].

[376] I. M. Lewis and M. Sullivan, arXiv:1701.08774 [hep-ph].

[377] J. M. Alarcon, J. Martin Camalich and J. A. Oller, Phys. Rev. D **85**, 051503 (2012) doi:10.1103/PhysRevD.85.051503 [arXiv:1110.3797 [hep-ph]].

[378] J. M. Alarcon, L. S. Geng, J. Martin Camalich and J. A. Oller, Phys. Lett. B **730**, 342 (2014) doi:10.1016/j.physletb.2014.01.065 [arXiv:1209.2870 [hep-ph]].

[379] E. Aprile *et al.* [XENON Collaboration], JCAP **1604**, no. 04, 027 (2016) doi:10.1088/1475-7516/2016/04/027 [arXiv:1512.07501 [physics.ins-det]].

[380] J. A. Casas and A. Ibarra, Nucl. Phys. B **618**, 171 (2001) doi:10.1016/S0550-3213(01)00475-8 [hep-ph/0103065].

[381] W. l. Guo, Z. z. Xing and S. Zhou, Int. J. Mod. Phys. E **16**, 1 (2007) doi:10.1142/S0218301307004898 [hep-ph/0612033].

[382] Y. F. Pirogov and O. V. Zenin, Eur. Phys. J. C **10**, 629 (1999) doi:10.1007/s100520050602, 10.1007/s100529900035 [hep-ph/9808396].

[383] I. Esteban, M. C. Gonzalez-Garcia, M. Maltoni, I. Martinez-Soler and T. Schwetz, JHEP **1701**, 087 (2017) doi:10.1007/JHEP01(2017)087 [arXiv:1611.01514 [hep-ph]].

[384] P. F. de Salas, D. V. Forero, C. A. Ternes, M. Tortola and J. W. F. Valle, arXiv:1708.01186 [hep-ph].

[385] A. Ilakovac and A. Pilaftsis, Nucl. Phys. B **437**, 491 (1995) doi:10.1016/0550-3213(94)00567-X [hep-ph/9403398].

[386] D. Tommasini, G. Barenboim, J. Bernabeu and C. Jarlskog, Nucl. Phys. B **444**, 451 (1995) doi:10.1016/0550-3213(95)00201-3 [hep-ph/9503228].

[387] D. N. Dinh, A. Ibarra, E. Molinaro and S. T. Petcov, JHEP **1208**, 125 (2012) Erratum: [JHEP **1309**, 023 (2013)] doi:10.1007/JHEP09(2013)023, 10.1007/JHEP08(2012)125 [arXiv:1205.4671 [hep-ph]].

[388] A. Ibarra, E. Molinaro and S. T. Petcov, JHEP **1009**, 108 (2010) doi:10.1007/JHEP09(2010)108 [arXiv:1007.2378 [hep-ph]].

[389] V. Tello, M. Nemevsek, F. Nesti, G. Senjanovic and F. Vissani, Phys. Rev. Lett. **106**, 151801 (2011) doi:10.1103/PhysRevLett.106.151801 [arXiv:1011.3522 [hep-ph]].

[390] M. Mitra, G. Senjanovic and F. Vissani, Nucl. Phys. B **856**, 26 (2012) doi:10.1016/j.nuclphysb.2011.10.035 [arXiv:1108.0004 [hep-ph]].

[391] J. Chakrabortty, H. Z. Devi, S. Goswami and S. Patra, JHEP **1208**, 008 (2012) doi:10.1007/JHEP08(2012)008 [arXiv:1204.2527 [hep-ph]].

[392] P. S. Bhupal Dev, S. Goswami and M. Mitra, Phys. Rev. D **91**, no. 11, 113004 (2015) doi:10.1103/PhysRevD.91.113004 [arXiv:1405.1399 [hep-ph]].

[393] P. S. Bhupal Dev, S. Goswami, M. Mitra and W. Rodejohann, Phys. Rev. D **88**, 091301 (2013) doi:10.1103/PhysRevD.88.091301 [arXiv:1305.0056 [hep-ph]].

[394] R. Gonzalez Felipe, F. R. Joaquim and B. M. Nobre, Phys. Rev. D **70**, 085009 (2004) doi:10.1103/PhysRevD.70.085009 [hep-ph/0311029].

[395] K. Turzynski, Phys. Lett. B **589**, 135 (2004) doi:10.1016/j.physletb.2004.03.071 [hep-ph/0401219].

[396] G. C. Branco, R. Gonzalez Felipe, F. R. Joaquim and B. M. Nobre, Phys. Lett. B **633**, 336 (2006) doi:10.1016/j.physletb.2005.11.070 [hep-ph/0507092].

[397] M. Flanz, E. A. Paschos, U. Sarkar and J. Weiss, Phys. Lett. B **389**, 693 (1996) doi:10.1016/S0370-2693(96)01337-8, 10.1016/S0370-2693(96)80011-6 [hep-ph/9607310].

[398] A. Pilaftsis, Phys. Rev. D **56**, 5431 (1997) doi:10.1103/PhysRevD.56.5431 [hep-ph/9707235].

[399] A. Pilaftsis and T. E. J. Underwood, Nucl. Phys. B **692**, 303 (2004) doi:10.1016/j.nuclphysb.2004.05.029 [hep-ph/0309342].

[400] G. C. Branco, R. Gonzalez Felipe, M. N. Rebelo and H. Serodio, Phys. Rev. D **79**, 093008 (2009) doi:10.1103/PhysRevD.79.093008 [arXiv:0904.3076 [hep-ph]].

[401] S. Bhattacharya, A. K. Saha, A. Sil and J. Wudka, arXiv:1805.03621 [hep-ph].

[402] D. N. Spergel *et al.* [WMAP Collaboration], Astrophys. J. Suppl. **170**, 377 (2007) doi:10.1086/513700 [astro-ph/0603449].

[403] V. Domcke and K. Schmitz, arXiv:1712.08121 [hep-ph].

[404] V. Domcke and K. Schmitz, Phys. Rev. D **95**, no. 7, 075020 (2017) doi:10.1103/PhysRevD.95.075020 [arXiv:1702.02173 [hep-ph]].

[405] K. Schmitz and T. T. Yanagida, Phys. Rev. D **94**, no. 7, 074021 (2016) doi:10.1103/PhysRevD.94.074021 [arXiv:1604.04911 [hep-ph]].

[406] K. Harigaya and K. Schmitz, Phys. Lett. B **773**, 320 (2017) doi:10.1016/j.physletb.2017.08.050 [arXiv:1707.03646 [hep-ph]].

[407] G. Lazarides and C. Panagiotakopoulos, Phys. Rev. D **52**, R559 (1995) doi:10.1103/PhysRevD.52.R559 [hep-ph/9506325].

[408] G. Lazarides, C. Panagiotakopoulos and N. D. Vlachos, Phys. Rev. D **54** (1996) 1369 doi:10.1103/PhysRevD.54.1369 [hep-ph/9606297].

[409] M. U. Rehman and U. Zubair, Phys. Rev. D **91**, 103523 (2015) doi:10.1103/PhysRevD.91.103523 [arXiv:1412.7619 [hep-ph]].

[410] M. ur Rehman, V. N. Senoguz and Q. Shafi, Phys. Rev. D **75**, 043522 (2007) doi:10.1103/PhysRevD.75.043522 [hep-ph/0612023].

[411] M. U. Rehman and Q. Shafi, Phys. Rev. D **86**, 027301 (2012) doi:10.1103/PhysRevD.86.027301 [arXiv:1202.0011 [hep-ph]].

[412] S. Khalil, Q. Shafi and A. Sil, Phys. Rev. D **86**, 073004 (2012) doi:10.1103/PhysRevD.86.073004 [arXiv:1208.0731 [hep-ph]].

[413] G. Veneziano, Phys. Lett. **128B**, 199 (1983). doi:10.1016/0370-2693(83)90390-8

[414] C. A. Dominguez and A. Zepeda, Phys. Rev. D **18**, 884 (1978). doi:10.1103/PhysRevD.18.884

[415] H. E. Haber and G. L. Kane, Phys. Rept. **117**, 75 (1985). doi:10.1016/0370-1573(85)90051-1

[416] H. P. Nilles, Phys. Rept. **110**, 1 (1984). doi:10.1016/0370-1573(84)90008-5

[417] G. Jungman, M. Kamionkowski and K. Griest, Phys. Rept. **267**, 195 (1996) doi:10.1016/0370-1573(95)00058-5 [hep-ph/9506380].

[418] S. Dimopoulos, G. R. Dvali and R. Rattazzi, Phys. Lett. B **410**, 119 (1997) doi:10.1016/S0370-2693(97)00970-2 [hep-ph/9705348].

[419] V. N. Senoguz and Q. Shafi, Phys. Lett. B **567**, 79 (2003) doi:10.1016/j.physletb.2003.06.030 [hep-ph/0305089].

[420] J. E. Kim and H. P. Nilles, Phys. Lett. **138B**, 150 (1984). doi:10.1016/0370-2693(84)91890-2

[421] G. R. Dvali, G. Lazarides and Q. Shafi, Phys. Lett. B **424**, 259 (1998) doi:10.1016/S0370-2693(98)00145-2 [hep-ph/9710314].

[422] G. R. Dvali, G. F. Giudice and A. Pomarol, Nucl. Phys. B **478**, 31 (1996) doi:10.1016/0550-3213(96)00404-X [hep-ph/9603238].

[423] G. Blanger, F. Boudjema, A. Pukhov and A. Semenov, Comput. Phys. Commun. **192**, 322 (2015) doi:10.1016/j.cpc.2015.03.003 [arXiv:1407.6129 [hep-ph]].

[424] S. Bhattacharya, A. Drozd, B. Grzadkowski and J. Wudka, JHEP **1310** (2013) 158 doi:10.1007/JHEP10(2013)158 [arXiv:1309.2986 [hep-ph]].

[425] A. Ahmed, M. Duch, B. Grzadkowski and M. Iglicki, arXiv:1710.01853 [hep-ph].

[426] S. Profumo, T. Stefaniak and L. Stephenson Haskins, Phys. Rev. D **96**, no. 5, 055018 (2017) doi:10.1103/PhysRevD.96.055018 [arXiv:1706.08537 [hep-ph]].

[427] I. Gogoladze, N. Okada and Q. Shafi, Phys. Rev. D **78**, 085005 (2008) doi:10.1103/PhysRevD.78.085005 [arXiv:0802.3257 [hep-ph]].

[428] A. Dutta Banik, A. K. Saha and A. Sil, arXiv:1806.08080 [hep-ph].

[429] C. Cai, Z. H. Yu and H. H. Zhang, Nucl. Phys. B **921**, 181 (2017) doi:10.1016/j.nuclphysb.2017.05.015 [arXiv:1611.02186 [hep-ph]].

[430] R. Mahbubani and L. Senatore, Phys. Rev. D **73**, 043510 (2006) doi:10.1103/PhysRevD.73.043510 [hep-ph/0510064].

[431] F. D'Eramo, Phys. Rev. D **76**, 083522 (2007) doi:10.1103/PhysRevD.76.083522 [arXiv:0705.4493 [hep-ph]].

[432] R. Enberg, P. J. Fox, L. J. Hall, A. Y. Papaioannou and M. Papucci, JHEP **0711**, 014 (2007) doi:10.1088/1126-6708/2007/11/014 [arXiv:0706.0918 [hep-ph]].

[433] T. Cohen, J. Kearney, A. Pierce and D. Tucker-Smith, Phys. Rev. D **85**, 075003 (2012) doi:10.1103/PhysRevD.85.075003 [arXiv:1109.2604 [hep-ph]].

[434] C. Cheung and D. Sanford, JCAP **1402**, 011 (2014) doi:10.1088/1475-7516/2014/02/011 [arXiv:1311.5896 [hep-ph]].

[435] L. Calibbi, A. Mariotti and P. Tziveloglou, JHEP **1510**, 116 (2015) doi:10.1007/JHEP10(2015)116 [arXiv:1505.03867 [hep-ph]].

[436] S. Horiuchi, O. Macias, D. Restrepo, A. Rivera, O. Zapata and H. Silverwood, JCAP **1603**, no. 03, 048 (2016) doi:10.1088/1475-7516/2016/03/048 [arXiv:1602.04788 [hep-ph]].

[437] S. Banerjee, S. Matsumoto, K. Mukaida and Y. L. S. Tsai, JHEP **1611**, 070 (2016) doi:10.1007/JHEP11(2016)070 [arXiv:1603.07387 [hep-ph]].

[438] T. Abe, Phys. Lett. B **771**, 125 (2017) doi:10.1016/j.physletb.2017.05.048 [arXiv:1702.07236 [hep-ph]].

[439] Q. F. Xiang, X. J. Bi, P. F. Yin and Z. H. Yu, Phys. Rev. D **97**, no. 5, 055004 (2018) doi:10.1103/PhysRevD.97.055004 [arXiv:1707.03094 [hep-ph]].

[440] N. Maru, T. Miyaji, N. Okada and S. Okada, JHEP **1707**, 048 (2017) doi:10.1007/JHEP07(2017)048 [arXiv:1704.04621 [hep-ph]].

[441] N. Maru, N. Okada and S. Okada, Phys. Rev. D **96**, no. 11, 115023 (2017) doi:10.1103/PhysRevD.96.115023 [arXiv:1801.00686 [hep-ph]].

[442] L. Calibbi, L. Lopez-Honorez, S. Lowette and A. Mariotti, arXiv:1805.04423 [hep-ph].

[443] S. Esch, M. Klasen and C. E. Yaguna, arXiv:1804.03384 [hep-ph].

[444] G. Arcadi, arXiv:1804.04930 [hep-ph].

[445] N. Arkani-Hamed, A. Delgado and G. F. Giudice, Nucl. Phys. B **741**, 108 (2006).

[446] S. Bhattacharya, B. Karmakar, N. Sahu and A. Sil, Phys. Rev. D **93**, no. 11, 115041 (2016) doi:10.1103/PhysRevD.93.115041 [arXiv:1603.04776 [hep-ph]].

[447] S. Bhattacharya, B. Karmakar, N. Sahu and A. Sil, JHEP **1705**, 068 (2017) doi:10.1007/JHEP05(2017)068 [arXiv:1611.07419 [hep-ph]].

[448] S. Bhattacharya, N. Sahoo and N. Sahu, Phys. Rev. D **96**, no. 3, 035010 (2017) doi:10.1103/PhysRevD.96.035010 [arXiv:1704.03417 [hep-ph]].

[449] S. Bhattacharya, N. Sahoo and N. Sahu, Phys. Rev. D **93**, no. 11, 115040 (2016) doi:10.1103/PhysRevD.93.115040 [arXiv:1510.02760 [hep-ph]].

[450] N. Narendra, N. Sahoo and N. Sahu, arXiv:1712.02960 [hep-ph].

[451] C. E. Yaguna, Phys. Rev. D **92**, no. 11, 115002 (2015) doi:10.1103/PhysRevD.92.115002 [arXiv:1510.06151 [hep-ph]].

[452] C. Fu *et al.* [PandaX-II Collaboration], Phys. Rev. Lett. **118**, no. 7, 071301 (2017) doi:10.1103/PhysRevLett.118.071301 [arXiv:1611.06553 [hep-ex]].

[453] D. Egana-Ugrinovic, JHEP **1712**, 064 (2017) doi:10.1007/JHEP12(2017)064 [arXiv:1707.02306 [hep-ph]].

[454] B. Adhikary, M. Chakraborty and A. Ghosal, JHEP **1310**, 043 (2013) Erratum: [JHEP **1409**, 180 (2014)] doi:10.1007/JHEP10(2013)043, 10.1007/JHEP09(2014)180 [arXiv:1307.0988 [hep-ph]].

[455] G. Chalons, D. Lopez-Val, T. Robens and T. Stefaniak, PoS DIS **2016**, 113 (2016) [arXiv:1606.07793 [hep-ph]].

[456] S. K. Kang and J. Park, JHEP **1504**, 009 (2015) doi:10.1007/JHEP04(2015)009 [arXiv:1306.6713 [hep-ph]].

[457] S. Schael *et al.* [ALEPH and DELPHI and L3 and OPAL and SLD Collaborations and LEP Electroweak Working Group and SLD Electroweak Group and SLD Heavy Flavour Group], Phys. Rept. **427**, 257 (2006) doi:10.1016/j.physrep.2005.12.006 [hep-ex/0509008].

[458] CMS Collaboration [CMS Collaboration], CMS-PAS-HIG-16-016.

[459] ATLAS and CMS Collaborations (2015), ATLAS-CONF-2015-044

[460] J. Abdallah *et al.* [DELPHI Collaboration], interpretation of the results within the MSSM," Eur. Phys. J. C **31**, 421 (2003) doi:10.1140/epjc/s2003-01355-5 [hep-ex/0311019].

[461] M. E. Peskin and T. Takeuchi, Phys. Rev. D **46**, 381 (1992). doi:10.1103/PhysRevD.46.381

[462] V. Barger, P. Langacker, M. McCaskey, M. J. Ramsey-Musolf and G. Shaughnessy, Phys. Rev. D **77**, 035005 (2008) doi:10.1103/PhysRevD.77.035005 [arXiv:0706.4311 [hep-ph]].

[463] S. Ghosh, A. Kundu and S. Ray, Phys. Rev. D **93**, no. 11, 115034 (2016) doi:10.1103/PhysRevD.93.115034 [arXiv:1512.05786 [hep-ph]].

[464] R. Barbieri, L. J. Hall, Y. Nomura and V. S. Rychkov, Phys. Rev. D **75**, 035007 (2007) doi:10.1103/PhysRevD.75.035007 [hep-ph/0607332].

[465] G. Cynolter and E. Lendvai, Eur. Phys. J. C **58**, 463 (2008)

[466] P. Agrawal, Z. Chacko, C. Kilic and R. K. Mishra, arXiv:1003.1912 [hep-ph].

[467] A. Semenov, Comput. Phys. Commun. **201**, 167 (2016) doi:10.1016/j.cpc.2016.01.003 [arXiv:1412.5016 [physics.comp-ph]].

[468] Q. Lu, D. E. Morrissey and A. M. Wijangco, JHEP **1706**, 138 (2017) doi:10.1007/JHEP06(2017)138 [arXiv:1705.08896 [hep-ph]].

[469] L. Mihaila, J. Salomon and M. Steinhauser, PoS LL **2012**, 043 (2012) [PoS LL **2012**, 043 (2012)] [arXiv:1209.5497 [hep-ph]].

[470] A. V. Bednyakov, A. F. Pikelner and V. N. Velizhanin, Phys. Lett. B **722**, 336 (2013) doi:10.1016/j.physletb.2013.04.038 [arXiv:1212.6829 [hep-ph]].

[471] C. Durnford, "Duality and Models of Supersymmetry Breaking."